



An integrative approach towards unraveling the activation of oncogenic FLT3

Erwin Pannecoucke

Promotor: Prof. Dr. Savvas Savvides

Thesis submitted in partial fulfilment of the requirements for the degree of
Doctor of Sciences: biochemistry and biotechnology

Academic year 2018-2019

Dutch translation of the title:

Een multidisciplinaire benadering voor het verkrijgen van inzichten in oncogene FLT3 activatie

Front cover illustration

The cover shows a photo taken inside the Swiss Light Source, a third-generation synchrotron light source located at the Paul Scherrer Institute, Switzerland. Allowing to perform X-ray crystallographic experiments at such centers of state-of-the-art technology always felt like an exciting privilege, regardless the number of visits. Overlaid are sections of the first article that describes a titration calorimeter allowing thermodynamic characterization of protein interactions in solution. Although this publication already dates from the wonderful year 1989, it is surprising to see how little the setup of this machine has changed: the incredible technologic advances of the past 30 years notwithstanding, last generation machines still feature a similar, if not identical architecture. Together, X-ray crystallography and ITC embody the backbone of this dissertation.

Wiseman, T., Williston, S., Brandts, J. F. & Lin, L. N. Rapid measurement of binding constants and heats of binding using a new titration calorimeter. *Anal. Biochem.* 179, 131–137 (1989).

Funding

This research was financially supported by a personal pre-doctoral fellowship granted by the Vlaams Agentschap Innoveren & Ondernemen (VLAIO), formerly known as Instituut voor Wetenschap en Technologie (IWT), and was further funded by the Vlaams Instituut for Biotechnology (VIB) and Ghent University.

Disclaimer

No part of this thesis may be reproduced or used in any way without prior written permission of the author.

Board of Examiners

Prof. Dr. Xavier Saelens (Chairman)

Department of Biochemistry and microbiology, Ghent University
VIB-UGent Center for Medical Biotechnology

Prof. Dr. Bart Devreese (Secretary)

Department of Biochemistry and microbiology, Ghent University

Prof. Dr. Savvas Savvides (Promotor)

Department of Biochemistry and microbiology, Ghent University
VIB Center for Inflammation Research

Prof. Dr. Frank Peelman

Faculty of Medicine and Health Sciences, Ghent University
VIB-UGent Center for Medical Biotechnology

Prof. Dr. Pieter Van Vlierberghe

Faculty of Medicine and Health Sciences, Ghent University
VIB-UGent Center for Medical Biotechnology

Dr. Ignace Lasters

Complix NV

Dr. Md. Simon Tavernier

Faculty of Medicine and Health Sciences, Ghent University
VIB-UGent Center for Medical Biotechnology

Dr. Jan Félix

Institut de Biologie Structurale, Grenoble, France

Acknowledgements

Six years. Or, more precisely, 6 years, 4 months and 14 days. That is how long I've been on this PhD adventure, and that is how long the list of people that I owe my gratitude, was allowed to grow.

Above all, I want to express my gratitude towards my promotor **Prof. Dr. Savvas Savvides**. He was the first to provide a taste of the ever-fascinating world of protein crystallography, by arranging an opportunity for Master-1 students to perform experiments at the DESY synchrotron. I can honestly say that my affinity towards X-ray crystallography to date, can still be traced back to that long day in Hamburg. It also exemplifies Savvas as a person: above all, he is a tutor willing to give everything within his potential to transfer knowledge to whoever is interested. Even though it seemed like every one of his days at least 24 hours too short, Savvas' door has literally always been open for questions and issues, both from a professional as well as a personal level. The past years made it increasingly clear that the academic world is tough one, in which everyone is expected to play the game hard. Savvas' success to excel in this world notwithstanding, there hasn't been a single moment in which he canalized the toughness he experienced, to us. Even at the very last part of my PhD trajectory, he kept on surprising me with how much humanism he is leading this lab. I know who to take an example from when I ever become in a mentoring position myself. Therefore, Savvas: thank you!

Next, I would like to thank all Members of the Examination Board for taking the time to critically evaluate my dissertation, provide constructive remarks and stimulate discussions. Together, they have not only improved the manuscript but also my personal scientific insights and knowledge. Thank you **Prof. Dr. Xavier Saelens, Prof. Dr. Bart Devreese, Prof. Dr. Pieter Van Vlierberghe, Prof. Dr. Frank Peelman, Dr. Ignace Lasters, Dr. Md. Simon Tavernier and Dr. Jan Félix**.

I furthermore would like to express my gratitude to every (ex-) member of USSa. Saying I'm not the easiest person when I'm under stress or when things are not going as planned, is a severe understatement. And things haven't gone as planned... a lot. Therefore: **Steven, Sammy, Julie, Tatjana, Koen, Ann, Maria, Danielle, Kenneth, Yehudi, Romain, Ola, Steven, Jan, Kasia and Wouter**; thanks for coping with me, and helping me out when needed. A special thanks should go to **Steven**, my RTK partner in crime, and to **Jan**, who guided me during my master thesis. Also **Laurens** should be thanked: I've set the bar quite high for a master thesis student, but you performed excellent. I should probably also thank **Bjorn**, although I'm not quite sure why – possibly because he taught me to be as critical as possible towards my own data, just to prevent him taking pleasure in bringing down my scientific conclusions.

I would also like to thank all IRC Research Groups and VIB Core Facilities I had the honors to work with. The way **Prof. Dr. Bart Lambrecht** leads the IRC, is truly price worthy. This UGent-VIB research building really excels at stimulating collaborations and knowledge transfers between groups, and does an amazing job in providing technical support. Coming from a Tower of Isolation at the Ledeganck, I was baffled with the amount of science one can perform just by being part of this department. And if it wasn't for this open environment in which I was allowed, or even stimulated to use UBl's

infrastructure (and, I should admit, his extensive library of antibodies), I would never have been able to perform the flow cytometry experiments that I'm so fond of. In that regard, it goes without saying that these experiments would not have been possible without the help of **Simon, Kim and Gert**, who are always willing to help where they can, and make you feel more than comfortable in the FACS room. The same holds true for the **Microscopy core facility**: although none of the experiments made it in this dissertation, **Eef** never seemed reluctant to perform yet another (miserably failing) experiment. I would also like to thank **Marnik** for the time we've spend in performing a statistical analysis of the ITC data. It wasn't trivial, but that analysis has arguably elevated this dissertation to a higher level. Marnik furthermore showed that a statistic analysis doesn't have to be performed in colorless environment soaked with mathematics – it was truly refreshing to interact with him. I would also like to thank **Marita** and **Ruth** for all the nice chats and their support, both on a professional and personal level. I'm furthermore grateful for all the interactions with everyone from the **Connecting People**, you guys are really a pleasure to work with. Finally, I would like to thank **Ann, Carine, Kurt, Charly, Geert, Natalie, Nancy, TC Core, Didier and his team, Chantal, Veerle, Myriam, Eline** and all other technical personnel for their support.

Ik ben ook dankbaar voor het begrip dat mijn familie steeds maar bleef opbrengen wanneer ik laat thuis was, slecht gezind was of opnieuw een familiefeest miste omdat ik "in een synchrotron op kristallen aan het schieten was". Merci **Mama, Papa, Malaika** en **Gwen** – ik hoop dat deze doctoraatsverdediging het laatste examen van me is waaronder jullie te lijden hebben. **Monique, René, Ine, Ronald, Lore** en **Geert**, dit geldt ook voor jullie: vanaf nu teken ik zonder uitzondering present op al jullie Limburgse taartfestijn.

Ook mijn vrienden mag ik dankbaar zijn: het zijn 6 jaren van hard labeur geweest, en dit is ten koste gegaan van mijn aanwezigheid en sociaal engagement. En toch zijn jullie er steeds voor mij gebleven, niet in het minste wanneer ik van het verre Aalst terug naar Gent kwam. **Jonathan, Anton, Jan, Katrijn, Basil, Bernard, Ben, Bert, Lise, Line** en alle andere Geitenwollensokken en Ouwe Stamleden: bedankt. Finaal zijn ook **Julie** en **Charles** bedankt voor alle (veel te lange) aperitieven, (veel te lekkere) maaltijden en (veel te lastige) toertochten.

Last but far from least, I want to thank **Nele**. You are by far the best thing that came into my life, and undoubtedly will keep that title for the rest of my life. If it wasn't for your support, help and amazing personality, this dissertation would not be here in its current representation. You were always there when results demotivated me, you always understood when I was home late and you always stimulated me to keep going to the lab if necessary - even if it meant spending again a free day at work. And yet, regardless of all these moments you motivated me to continue working, you have always been the sole reason why I wanted to go home early. I hope that I can always be there for you, just as you've been here for me during the past years.

Nele, de laatste maanden zijn niet de gemakkelijkste geweest, om het zachtjes te zeggen. En er zullen ongetwijfeld nog lastige momenten komen in de (vele!) jaren die voor ons liggen. Maar hoe serieus die problemen ook mogen zijn en hoe onoverkomelijk ze op die moment ook mogen lijken: zolang jij naast me staat, ga ik ze met een glimlach tegemoet. We denken op dezelfde manier, we

oordelen op dezelfde manier en we genieten op dezelfde manier. Wij, Nele, zijn een fantastisch team – nu, en in de toekomst. En laat die toekomst nu maar komen!

Table of content

| | |
|--|-------------|
| <u>List of Abbreviations</u> | <u>VIII</u> |
| <u>Samenvatting</u> | <u>XII</u> |
| <u>Summary</u> | <u>XVI</u> |
| | |
| <u>Chapter A – Introduction</u> | <u>1</u> |
| 1. FLT3 plays a guiding role in hematopoiesis | 2 |
| 2. Leukemia: hematopoiesis in overdrive | 11 |
| 3. Clinical targeting of FLT3-mutated AML | 17 |
| 4. Outlook | 24 |
| 5. References | 26 |
| | |
| <u>Problem definition and research aims</u> | <u>39</u> |
| | |
| <u>Chapter B - Biophysical and structural characterization of wild-type and oncogenic FLT3</u> | <u>40</u> |
| 1. Ligand-binding of FLT3 is a cooperative event | 41 |
| 2. Unraveling mechanistic principles underlying oncogenic driver mutations in the extracellular domain of FLT3 | 73 |
| 3. Discussion | 85 |
| 4. Outlook | 91 |
| 5. Experimental procedures | 97 |
| 6. Author contributions | 103 |
| 7. References | 104 |
| | |
| <u>Chapter C - Towards unraveling the mechanism of ligand-mediated TKI resistance in AML</u> | <u>110</u> |
| 1. Introduction | 111 |
| 2. Results | 112 |
| 3. Discussion | 115 |
| 4. Outlook | 120 |
| 5. Experimental procedures | 123 |
| 6. Author contributions | 124 |
| 7. References | 125 |
| | |
| <u>Curriculum Vitae</u> | <u>129</u> |

List of abbreviations

A

| | |
|-----------|--|
| Akt | Protein kinase B |
| ALL | Acute lymphoblastic leukemia |
| ALL | Acute lymphocytic leukemia |
| allo-HSCT | Allogenic hematopoietic stem cell transplantation |
| AML | Acute myeloid leukemia |
| AML1-ETO | A cotranslational fusion between acute myeloid leukemia 1 protein and eight-twenty one oncoprotein |
| APC | In context of an FACS experiment: allophycocyanin |
| APC | In an immunology context: antigen-presenting cell |
| ATP | Adenosine triphosphate |
| AXL | AXL receptor tyrosine kinase |

B

| | |
|------|-------------------------|
| BCL2 | B-cell lymphoma 2 |
| BLI | Bi-layer interferometry |
| BM | Bone marrow |

C

| | |
|--------------------|--|
| CBF β -SMMHC | A cotranslational fusion between core-binding factor beta and smooth muscle myosin heavy chain |
| cDC1 | Conventional dendritic cell type 1 |
| cDC2 | Conventional dendritic cell type 2 |
| CDP | Common dendritic cell progenitor |
| CEPBA | CCAAT/enhancer-binding protein |
| CL | Confidence level |
| CLL | Chronic lymphocytic leukemia |
| CLP | common lymphoid progenitor |
| CML | Chronic myeloid leukemia |
| cMoP | Common monocyte progenitor |
| CMP | Common myeloid progenitor |
| COSMIC | Catalogue of somatic mutations in cancer |
| CSF-1 | Colony-stimulating factor-1 |
| CSF-1R | Colony-stimulating factor-1 receptor |

D

| | |
|--------|--|
| DC | Dendritic cell |
| DDxpY | Aspartate-aspartate-[any-residue]-phosphotyrosine protein sequence |
| DFG | Aspartate-Phenylalanine-Glycine |
| DMEM | Dulbecco's Modified Eagle Medium |
| DNMT3A | DNA methyltransferase 3 alpha |

E

| | |
|------------------|--|
| <i>E. coli</i> | <i>Escherichia coli</i> |
| EC ₅₀ | The half maximal effective concentration |
| ECD | Extracellular domain |

| | |
|---------|--|
| ELN | European LeukemiaNet |
| EndoH/T | Endoglycosidase H or T |
| ERK | Extracellular signal-regulated kinase |
| ETP | Early T-cell progenitor |
| ETP-ALL | Early T-cell progenitor acute lymphocytic leukemia |
| EZH2 | Zeste 2 polycomb repressive complex 2 subunit |

F

| | |
|------|--|
| Fab | Antigen-binding antibody fragment |
| FCS | Fetal calf serum |
| FDA | Food and Drug Administration |
| FL | Fms-like tyrosine kinase receptor 3 ligand |
| FLT3 | Fms-like tyrosine kinase receptor 3 |

G

| | |
|------|-----------------------------------|
| GIST | Gastrointestinal stromal tumor |
| GMP | Granulocyte-macrophage progenitor |
| GOF | Gain-of-function |

H

| | |
|-------|--|
| HBS | HEPES buffered saline |
| HEK | Human embryonic kidney |
| HEPES | 4-(2-hydroxyethyl)-1-piperazineethanesulfonic acid |
| HGLMM | Hierarchical Generalized Linear Models |
| HSC | Hematopoietic stem cell |
| HSCT | Hematopoietic stem cell transplantation |

I

| | |
|------------------|---|
| IC ₅₀ | The half maximal inhibitory concentration |
| IDH1 | Isocitrate dehydrogenase-1 |
| IDH2 | Isocitrate dehydrogenase-2 |
| IFN- α | Type-1 interferon |
| Ig | Immunoglobuline |
| IL-34 | Interleukin-34 |
| IMAC | Immobilized metal affinity chromatography |
| IPTG | Isopropylthio-beta-galactoside |
| ITC | Isothermal titration calorimetry |
| ITD | Internal tandem duplication |

J

| | |
|-----------|----------------------|
| JAK2 | Janus kinase 2 |
| JM domain | Juxtamembrane domain |

K

| | |
|----------------|-----------------------------------|
| k _a | Association rate constant |
| k _d | Dissociation rate constant |
| K _D | Equilibrium dissociation constant |

M

| | |
|-------|--|
| MALLS | Multi-angle laser light scattering |
| MDP | Macrophage-dendritic cell progenitor |
| MEK | Mitogen-activated protein kinase kinase |
| MEP | Megakaryocyte-erythrocyte progenitor |
| MES | 2-(N-morpholino)ethanesulfonic acid |
| MGAT | Alpha-1,3-mannosyl-glycoprotein 2-beta-N-acetylglucosaminyltransferase |
| MHCII | Major histocompatibility complex type 2 |
| MHCII | Major histocompatibility complex type 1 |
| Mo-DC | Monocyte-derived dendritic cell |
| Mono | Monocyte |
| MPAL | Mixed phenotype acute leukemia |
| MPP | Multipotent progenitor |
| mTOR | Mechanistic target of rapamycin |
| MW | Molecular weight |

N

| | |
|------|--|
| NAE | Neural-precursor-cell-expressed developmentally down-regulated 8 activating enzyme |
| NCCN | National Comprehensive Cancer Network |
| NIH | National institute of health |
| NK | Natural killer T-cells |
| NKP | Nature killer progenitor |
| NPM1 | Nucleophosmin |
| NRAS | Neuroblastoma proto-oncogene protein p21 |

O

| | |
|----|------------------|
| OS | Overall survival |
|----|------------------|

P

| | |
|----------------|--|
| PDB | Protein databank |
| pDC | Plasmacytoid dendritic cell |
| PDGF | Platelet derived growth factor |
| PDGFR | Platelet-derived growth factor receptor |
| PDGFR α | Platelet-derived growth factor receptor alpha |
| PDGFR β | Platelet-derived growth factor receptor beta |
| PEG | Polyethylene glycol |
| PEI | Polyethylenimine |
| PI3K | Phosphoinositide 3-kinase |
| PIA | Plasma inhibitory activity |
| PML-RARA | A cotranslational fusion between promyelocytic leukemia protein and Retinoic Acid Receptor Alpha |
| PNP | Peripheral neuropathic pain |
| PPR | Pattern recognition receptors |

R

| | |
|------------|---|
| R.M.S.D. | Root-mean-square deviation |
| RAF kinase | Rapidly Accelerated Fibrosarcoma kinase |

| | |
|---------|---|
| RATIFY | Randomized AML trial in FLT3 in patients less than 60 years old |
| RET | Neurotrophic factor receptor |
| Rhyd | Hydrodynamic radius |
| RKT | Receptor tyrosine kinase |
| RTK-III | Receptor tyrosine kinase Class 3 |
| RTK-V | Receptor tyrosine kinase Class 5 |

S

| | |
|----------|--|
| S451F | Serine-451 to phenylalanine substitution |
| SAXS | Small angle X-ray scattering |
| SCF | Stem cell factor |
| SDS-PAGE | Sodium dodecyl sulfate poly-acrylamide gel electrophoresis |
| SEC | Size-exclusion chromatography |
| STAT3 | Signal transducer and activator of transcription 3 |
| ST-HSTC | Short-term hematopoietic stem cell |
| SUZ12 | Polycomb repressive complex 2 Subunit |

T

| | |
|-------|---|
| T343I | Threonine-343 to isoleucin substitution |
| TAM | Tyro3-Axl-MER receptor tyrosine kinase |
| TET2 | Ten-eleven translocation methylcytosine dioxygenase 2 |
| TF | Transcription factor |
| TKD | Tyrosine kinase domain |
| TKI | Tyrosine kinase inhibitor |
| TM | Transmembrane domain |
| TP53 | Tumor protein 53 |
| TR | Tetracycline repressor protein |
| TrKA | Tropomyosin receptor kinase A |

U

| | |
|------|---------------------------------------|
| UCLA | University of California, Los Angeles |
|------|---------------------------------------|

V

| | |
|-------|---|
| VEGFR | Vascular endothelial growth factor receptor |
| VPRGS | Valine-proline-arginine-glycine-serine protein sequence |

W

| | |
|-----|---------------------------|
| WHO | World Health Organisation |
| WT | Wild-type |

Samenvatting

Stichting tegen Kanker (<https://www.kanker.be>) schat dat tegen het einde van 2018, wereldwijd ongeveer 18 miljoen individuen een kankerdiagnose zullen gekregen hebben. Cijfers uit de Verenigde Staten geven aan dat meer dan 21.000 van deze nieuwe patiënten getroffen zullen zijn door acute myeloïde leukemie (AML), de meest voorkomende kanker van de bloedcellen. Bijna de helft van deze nieuwe kankerpatiënten zullen 65-plussers zijn, en hoewel de kans op genezing bij jongere patiënten de afgelopen jaren sterk is vooruitgegaan, blijft de prognose in net deze leeftijdsgroep dramatisch: 2 jaar na diagnose zal slechts 15% van hen nog in leven zijn.

Studies tonen aan dat het constitutieve proliferatiesignaal van de AML-kankercellen, de zogenaamde blasten, in 20-30% van alle nieuwe patiënten afkomstig is van een FLT3 variant met intracellulaire carcinogene mutaties. Aanwezigheid van dergelijke mutaties is gecorreleerd met een ongunstige prognose, waarbij een verhoogd risico op herval na initiële remissie zich vertaalt in een grotere kans op sterfte. De hoge prevalentie van FLT3-mutaties in AML-patiënten, heeft dit membraaneiwit de afgelopen twee decennia in het middelpunt van de farmaceutische belangstelling geplaatst. Ondanks hoge verwachtingen, bleken klinische studies echter vooral aan te tonen dat de zogenaamde tyrosine-kinase-inhibitoren (TKIs) wel snel leidden tot remissie, maar deze nooit lang konden aanhouden. De goedkeuring van midostaurine voor de behandeling van nieuw-gediagnostiseerde AML-patiënten met mutaties in FLT3, midden 2017, beloofde het verhoopte keerpunt te worden in de gerichte behandeling van deze patiënten. De observatie dat zelfs met deze nieuwe behandeling, slechts iets meer dan de helft van de patiënten 4 jaar na diagnose nog leven, is echter tekenend voor de prangende nood aan verdere optimalisatie van therapieën.

FLT3 is een transmembraan eiwit bestaande uit een extracellulair ligandbindend domein (ECD), een enkele transmembranaire helix (TM) en een intracellulair tweedelig tyrosine-kinasedomein (TKD). Op basis van deze opbouw, wordt FLT3 ingedeeld in de 3^{de} klasse van de tyrosine-kinase receptoren (RTK-III), samen met CSF-1R, KIT receptor, PDGFR α en PDGFR β . In inactieve toestand bevindt elk van deze receptoren zich aan het celmembraan als een monomeer. De kinase-activiteit wordt hierbij onderdrukt door een interactie van de juxtamembraanregio met beide lobben van het kinase. Activatie van de receptor wordt geïnitieerd door binding van het ligand met het ECD van 2 receptoren. Hoewel dergelijke interactie voor elk lid van de RTK-III leidt tot een transactivatie van TKDs, manifesteert FLT3 zich als de enige uitzondering door de manier waarop: structurele en biofysische studies tonen aan dat FLT3 de enige receptor is waarvoor er geen ligand-geïnduceerde interacties waargenomen konden worden tussen membraan-proximale domeinen van 2 ligand-geassocieerde receptoren. Met een paradigma voor een receptoractivatie waarin expliciet geen rol is weggelegd voor extracellulaire reciproke receptorinteracties, is FLT3 inderdaad de vreemde eend in de bijt.

Terzelfdertijd hebben we kennis van 2 oncogene puntmutaties in het ECD waarvan is aangetoond dat ze leiden tot een constitutieve activatie van de receptor. Ondanks het atomaire model van het ECD, kon tot op heden de transformerende eigenschappen van deze mutaties niet gekaderd worden binnen het huidige paradigma van receptoractivatie. Naar analogie met de andere receptoren, is er wel een vermoeden dat ze leidden tot een ligand-onafhankelijke dimerisatie van receptoren,

gemedieerd door de membraan-proximale domeinen - zij het dus via exact datzelfde mechanisme dat opvallend afwezig is bij wild-type FLT3 activatie.

In **Hoofdstuk A** wordt een korte inleiding gegeven tot de hematopoëse en de rol van FLT3 hierin. Vervolgens wordt het huidige paradigma van receptoractivatie besproken, en toegelicht hoe ligandbinding aan de extracellulaire domeinen leidt tot een activatie van de intracellulaire kinase-activiteit. Deze kennis laat toe om het moleculair mechanisme te bespreken achter de 2 types FLT3-mutaties die het vaakst voorkomen bij AML-patiënten, tezamen met hoe de farmaceutische industrie tracht deze gemuteerde receptoren te inhiberen. Er wordt dieper in gegaan op voorlopige klinische resultaten van de zogenaamde tyrosine-kinase-inhibitoren, aangezien de problematiek die met dergelijke doelgerichte therapieën gepaard gaat, de aanleiding geeft tot het onderzoek besproken in **Hoofdstuk C**.

De dichotomie in de rol van de membraan-proximale regio's tussen enerzijds opmerkelijk afwezig in wild-type condities, en prominent aanwezig in een gemuteerde context anderzijds, vormt de rationale voor het onderzoek gepresenteerd in **Hoofdstuk B**. Het probleem wordt benaderd door 2 nieuwe liganden te ontwikkelen die het mogelijk maken om m.b.v. isothermale titratiecalorimetrie (ITC) eventuele coöperatieve mechanismen in de ligand-receptorbinding bloot te leggen.

Vermits de resultaten van elk experiment, uitgevoerd met de nieuw ontwikkelde liganden, zullen gespiegeld worden aan de resultaten met het wild-type ligand, dienden we er ons eerst van te vergewissen dat deze laatste van goede kwaliteit was. Hiervoor werden 3 experimenten uitgevoerd, die samen aantonen dat het in-huis geproduceerde ligand inderdaad *in vitro*, *ex vivo* en *in vivo* het fysiologisch effect van het endogene ligand op potente wijze imiteert.

Vervolgens wordt voor elk van de twee nieuwe liganden, het monomere FL_{L27D} en heterodimere FL_{WT/KO}, toegelicht welke strategie gevolgd werd om deze te genereren. We tonen aan dat beide liganden na productie de fysicochemische eigenschappen vertoonden die we verwachtten, en bewijzen dat ze elk in staat zijn om slechts één receptor te binden – in tegenstelling tot het wild-type ligand. De hoge expressie-opbrengst van FL_{L27D} liet bovendien toe om de eiwitkarakteristatie een niveau hoger te tillen m.b.v. X-stralen eiwitkristallografische experimenten. Hiermee konden we overtuigend aantonen dat de puntmutatie inderdaad enkel een structurele adaptatie veroorzaakt ter hoogte van de dimerisatie-site, zonder de bindings-site van de receptor te beïnvloeden. Naast de validatie van FL_{L27D} voor het gebruik in een coöperativiteitsanalyse met behulp van ITC, geven deze X-stralen diffractie-experimenten ons voor het eerst een uniek beeld van de receptorconformatie in een inactieve toestand. We namen hierbij een opmerkelijke compacte toestand van de receptor waar, waarin het eerste membraan-distale domein een interactie aangaat met het meest membraan-proximale domein. Deze nieuwe kijk op een mogelijks auto-inhiberend mechanisme ter hoogte van de extracellulaire regio krijgt dan ook een prominente plaats in het later voorgestelde activatiemechanisme.

Alvorens over te gaan op de bespreking van de ITC experimenten, wordt toegelicht welke maatregelen er zijn genomen om te verzekeren dat conclusies en vergelijkingen van thermodynamische parameters gestoeld konden worden op een solide statistische basis – voor zover

wij weten, een unicum in het veld van thermodynamische analyses. De ITC experimenten zelf tonen finaal op een ondubbelzinnige wijze aan dat ligandbinding door FLT3 een meerstapsreactie is met 2 coöperatieve gebeurtenissen. De eerste gebeurtenis gaat gepaard met een intra-moleculaire heroriëntatie van het ligand. De tweede en grootste coöperatieve gebeurtenis, is te wijten aan ligand-geïnduceerde receptor-receptor-interacties.

In het tweede luik van **Hoofdstuk B** wordt getracht het oncogene karakter van 2 klinisch geïdentificeerde oncogene puntmutaties in het ECD te plaatsen in een structureel-mechanistisch kader. De eerste van de twee puntmutanten, een threonine naar isoleucine puntmutatie, vertoonde onverwacht geen effect in onze biofysische karakterisatie. Verrassend genoeg resulteerde het wel in een hogere-resolutiestructuur van de receptor, waardoor we voor het eerst een atomair model van het 5^{de} domein konden modelleren. Deze liet op zijn beurt toe om de positie te bepalen van de 2^{de} puntmutatie, een substitutie van serine-451 naar een fenylalanine. De analogie met oncogene mutaties in een gelijkaardige regio van de KIT receptor, versterkte ons vermoeden dat deze mutatie de wederzijdse receptoraffiniteit zou kunnen verhogen, en wel tot een niveau die ligand-onafhankelijke receptor-interacties mogelijk maakt.

Vervolgens wordt het effect van de fenylalanine-substitutie op de thermodynamica van ligandbinding volledig ontleed, waarbij we de gevolgen van deze mutatie voor zowel de entropische kost als voor de enthalpische component, rationaliseren. De observatie dat de substitutie een negatieve invloed uitoefent op de enthalpische component, geeft immers aan dat de mutatie eerder de aard van een bestaande interactie-site beïnvloedt, dan dat het een nieuwe site creëert.

Hoofdstuk B wordt afgesloten met een discussie waarin de impact van de resultaten uitvoerig wordt besproken en finaal een nieuw FLT3-activatiemechanisme wordt voorgesteld. Naast de aanwezigheid van een autoinhiberende extracellulaire conformatie, voorziet dit mechanisme een meer prominente rol voor de membraan-proximale interacties die FLT3 mechanistisch terug verenigt met zijn RTK-III familieleden.

Na de structureel-biofysische dissectie van ligandbinding aan de extracellulaire regio van FLT3, wordt in **Hoofdstuk C** volledig van koers veranderd en focussen we ons op het gedrag van FLT3 als membraanewit. De start van het voorgestelde onderzoek werd gegeven door twee observaties in de literatuur: de invloed van oncogene mutaties in AML op de subcellulaire localisatie van de receptor enerzijds, en de observatie van een ligand-gemedieerde resistentie van tyrosine-kinase-inhibitoren (TKIs) anderzijds. Hoewel deze laatste duidelijk gedocumenteerd is voor alle huidige veelbelovende TKIs, en reeds is gecorreleerd met het falen van twee TKIs in klinische studies, lijken zowel de academische wereld als de farmaceutische industrie tot nog toe weinig belang te hechten aan dit onverklaarde fenomeen.

Onze preliminaire resultaten van flow cytometrie-experimenten bevestigen dat membraan-expressie van een oncogene FLT3 variant, FLT3_{D835Y}, enkel dat van het wild-type niveau bereikt in aanwezigheid van een TKI. Verrassend genoeg blijkt inhibitie met deze inhibitor slechts weinig effect te hebben op het ligand-gemedieerde internalisatiegedrag van de receptor. Er wordt geargumenteed dat als internalisatie van de receptor een oorzakelijk gevolg is van zijn activatie, een constitutief

geactiveerde receptor een internalisatiesignaal uitzendt nog voor deze het plasmamembraan heeft bereikt. Bijgevolg zal inhibitie van de autofosforylatie de normale cellulaire translocatiemechanismen herstellen, waardoor membraanexpressie van deze receptor wordt verhoogd. Aan het celmembraan wordt deze receptor echter blootgesteld aan stimulatie door het ligand, die de TKI wegconcurrereert ten voordele van een activatie van de receptor.

Dat de voorgestelde hypothese mogelijks vergaande gevolgen kan hebben voor de wijze waarop FLT3 gericht geïnhibeerd wordt in een klinische context, wordt uitvoerig besproken in de discussie van **Hoofdstuk C**. Tot slot sluiten we dit doctoraatsonderzoek af met mogelijke strategieën die toelaten de huidige generatie TKIs toch te blijven gebruiken als supplement in een chemotherapeutische behandeling.

Summary

Stichting tegen Kanker (<https://www.kanker.be>) estimates that by the end of this year, approximately 18 million individuals worldwide will be confronted with a cancer diagnosis. The American Cancer Society expects more than 21.000 of those novel patients will be diagnosed with acute myeloid leukemia (AML), the most common type of leukemia in adults. Although advances in therapy have resulted in significant improvements in outcomes for younger patients, the prognosis of the population with the highest incidence rate remains dramatic: almost 50% of all new patients will be over 65 years old, and as much as 85% of them will die of their disease within 2 years of diagnosis.

Studies show that in 20-30% of all patients, intracellular mutations in FLT3 are at the root of the constitutive proliferation signal of the AML blasts. Such mutations are associated with an unfavorable prognosis in which a fast relapse rate after initial remission, is translated into an increased risk of death. Given that activating mutations in FLT3 are among the most common genetic lesions found in AML, considerable efforts have been made to specifically target this receptor in a clinical setting. Although administration of most of these tyrosine kinase inhibitors (TKIs) as monotherapies often results in remission, all patients eventually relapse within a few weeks. Last year's approval of midostaurin, the first TKI treatment of newly-diagnosed FLT3-mutated AML, added to a classical chemotherapy regimen, promised to mark a new era of targeted agents for the treatment of AML. The modest increase of the 4-year survival rate from 44% to 51%, illustrates the road ahead in decreasing AML related deaths.

FLT3 is a transmembrane protein featuring an extracellular ligand-binding domain (ECD), a single-pass transmembrane domain (TM) and an intracellular split kinase domain (TKD). This particular modular organization is characteristic for the Class-3 of receptor tyrosine kinases (RTK-III), a family harboring CSF-1R, KIT receptor, PDGFR α and PDGFR β . Dormant RTK-III members reside at the cell membrane as monomers, in which the juxtamembrane region maintains the inactive state of the kinase domain. Activation of the receptor is initiated by binding of the ligand to the membrane-distal domains of 2 receptors. Although all RTK-III will eventually transition into an activated state by this event, its divergent molecular mechanism in doing so, profiles FLT3 as a notable exception. Indeed, structural and biophysical studies have shown that FLT3 is the only receptor for which no ligand-induced receptor-receptor contacts between the membrane-proximal domains could be detected. Consequently, ligand-induced homotypic contacts are devoid from the FLT3 activation paradigm, which proclaims this ligand-receptor assembly as the odd man out.

Simultaneously, the molecular mechanism behind two oncogenic mutations in the ECD remains difficult to marry with this FLT3 activation paradigm, even with the crystallographic model of the ECD to our disposal. In analogy with activating point mutations in the ECD of KIT receptor, it was hypothesized that these mutations result in a ligand-independent receptor dimerization, nucleated by an increased reciprocal affinity of membrane-proximal domains – even though such interactions were conspicuously absent for wild-type receptor activation.

This doctoral dissertation is centered around FLT3 and oncogenic variants thereof. It starts with a brief introduction into hematopoiesis in **Chapter A**, detailing the role of FLT3 in healthy individuals. This is

continued by a more detailed discussion of the FLT3 activation paradigm, explaining how ligand-binding at the extracellular regions is translated into an activation of the intracellular kinase activity. This knowledge allows elucidation of the molecular principles behind transforming mutations in the TKD, and how such oncogenic mutations are addressed in a clinical context. As the observed issues accompanying the main strategy in the therapeutic targeting of FLT3 provide the rationale behind presented experiments in Chapter C, we close the introduction with an overview of clinical results of FLT3-targeting drugs.

In **Chapter B**, we sought to clarify the apparent dichotomy in homotypic receptor contacts in the wild-type versus oncogenic context of FLT3. We approached this problem by rationally engineering two novel FLT3 ligands, which we envisioned to unmask elements of cooperativity in the assembly of the extracellular FL-FLT3 complex.

Since results of ITC experiments featuring these two engineered ligands would be measured up against the thermodynamic parameters of wild-type ligand binding, we acknowledged the need for a full confidence that in-house produced FL_{WT} reflects the effect of endogenous FL stimulation. We therefore assayed the bioactivity of recombinant FL in three orthogonal assays, showing that FL indeed potently mimics the effect of endogenous FL stimulation *in vitro*, *ex vivo* and *in vivo*.

We continue by explaining the applied strategy to engineer two novel FLT3 ligands, monomeric FL_{L27D} and heterodimeric FL_{WT/KO}. We show that both ligands after production and purification feature expected physicochemical properties, and confirm that they only recruit 1 receptor into complex formation. Crystallization experiments featuring FL_{L27D}, alone and in complex with the extracellular domain of FLT3, confirm that the structural adaptation in FL_{L27D} is limited to the dimeric interface and does not introduce conformational changes in the receptor-binding epitope. Aside from validating FL_{L27D} as ideally suited for the envisioned analysis of cooperativity, these experiments provided us for the first time with a view on the receptor's conformation in absence of an activating ligand. Arguably the most remarkable feature of this observed compact conformation is the interaction between the most membrane-distal domain and most membrane-proximal domain. Considering this interaction as an extracellular autoinhibitory mechanism that prevents illegitimate receptor activation at the cell membrane, we endowed this tethered conformation with a prominent role in the proposed revision of the activation mechanism.

Prior to the ITC experiments, we detail the efforts that have been put into the generation of a statistical framework that allows analysis and statistical comparison of all derived thermodynamic parameters. Finally, the subsequent set of ITC analysis show, for the first time, that assembly of ternary ligand-receptor complex is a multi-step reaction featuring two levels of cooperativity. The first level is provided by an intramolecular reorientation of the ligand, whilst ligand-induced receptor interactions provide the second and largest cooperative increase in affinity.

The second section of **Chapter B** attempts to rationalize the oncogenic character of two clinically identified oncogenic FLT3 mutations in a structural-mechanistic framework. Unexpectedly, the threonine-343 to isoleucine point mutation does not seem to affect ligand-binding in the context of a construct comprising only the extracellular domain of FLT3. It did however result in a higher-resolution

X-ray crystallographic model of FLT3_{D1-D5}, in which domain 5 could for the first time confidently be modeled into an electron density map. This model furthermore allowed mapping of the location of the second oncogenic point mutation, a substitution of serine-451 to a phenylalanine. Comparison with structural models of KIT receptor and oncogenic variants thereof, fortified our hypothesis that such point mutation could indeed increase the reciprocal affinity of two FLT3 oncovariants.

Having both wild-type and monomeric FL at our disposal, we were finally able to perform a full thermodynamic dissection of ligand binding onto this oncogenic receptor variant. We can show that the presence of this mutation alters all thermodynamic parameters of the interaction with FL_{WT}, but does not seem to affect binding of the monomeric FL_{L27D}. The latter observation, in combination with the observed reduction in entropic penalty upon binding of FL_{WT}, confirms that Phe451 is buried in a reciprocal receptor interaction upon ligand binding. The detrimental effect on the enthalpic component of the FL_{WT}:FLT3_{S451F} interaction, implies that this mutation alters an existing interaction site rather than creating a new one.

The impact of all these observations are the subject of the discussion section at the end of **Chapter B**, and are crystalized into a proposal for a novel FLT3 activation paradigm, including the autoinhibitory extracellular conformation and with a higher emphasis on the ligand-induced receptor interactions that reunite FLT3 mechanistically with the RTK-III family.

After this structural and biophysical dissection of extracellular FLT3 ligand binding, we switched gears in **Chapter C** and focused on the ligand-modulated membrane behavior of FLT3 in a cellular context. Motivation for the presented experiments were given by two observations made elsewhere: the effect of TKIs on the sub-cellular localization of oncogenic FLT3 variants on the one hand, and the observation of a ligand-dependent TKI-resistance on the other.

Our preliminary flow cytometry results seem to confirm that membrane presentation of an oncogenic FLT3 variant, FLT3_{D835Y}, only reaches wild-type levels in presence of a TKI. The inhibited state notwithstanding, stimulation with the activating ligand surprisingly elicits a strong internalization of both the wild-type and oncogenic receptor. Providing arguments that internalization is a direct consequence of receptor activation, allows to infer that a constitutively activated receptor broadcasts a constitutive internalization signal that prevents translocation to the cell membrane. Consequently, inhibiting the oncogenic autophosphorylation using TKIs, re-establishes normal cellular trafficking and restores membrane expression. Given that FL seems to outcompete TKIs for inhibition of the receptor, such increased membrane expression allows this oncogenic receptor to be activated by the presence of its extracellular ligand.

As debated in the discussion section of **Chapter C**, if correct, the impact of this hypothesis can arguably have far-reaching consequences for the current strategies in clinical targeting of FLT3 via TKIs. Fortunately, we can simultaneously provide possible solutions, and make suggestions for strategies that allow addition of TKIs into chemotherapy regimen.

CHAPTER A

Introduction

1. FLT3 plays a guiding role in hematopoiesis

1.1. Hematopoiesis: the source of cellular diversity in the blood compartment

Hematopoiesis, the process responsible for the cellular repertoire of blood components, is initiated during embryonic development and continued throughout life to replenish the different subtypes of blood cells. In vertebrates, blood development involves two waves of hematopoiesis (Galloway and Zon 2003; Jagannathan-Bogdan and Zon 2013; Orkin and Zon 2008). During the primary wave, a primitive erythroid progenitor population operates from the extra-embryonic yolk sac to seed the early embryonic megakaryocytes and macrophages. The main purpose of this primitive wave is the generation of red blood cells that facilitate tissue oxygenation during the rapid growth of the embryo (Orkin and Zon 2008). As these erythroid progenitors are not pluripotent, this primitive wave is only transitory and followed by the so-called definitive wave. Similar to the primary wave in hematopoiesis, definitive hematopoiesis starts in the yolk sac, but will temporarily transition into the liver and finally establishes the definitive hematopoietic compartment in the bone marrow and thymus. These pluripotent hematopoietic stem cells (HSC) do not only have the ability to replenish their own compartment, but can differentiate into progenitor cells of all hematopoietic lineages (Figure 1) (Jagannathan-Bogdan and Zon 2013; Taviani et al. 2010). Interestingly, even in adults, most of the tissue-resident macrophages still originate from these yolk-sac derived erythroid-myeloid progenitors (Guilliams et al. 2014; Hoeffel et al. 2015). Only for the intestine it has been shown that self-maintaining embryonic gut-macrophages are supplemented by a continuously refreshing population of bone marrow-derived monocytes (Bain et al. 2014; De Schepper et al. 2018).

HSC continuously give rise to the variety of differentiated blood cells in a process that is controlled by lineage-determining transcription factors. These factors, of which expression is induced by binding of cytokines onto cell-surface expressed receptors (Metcalf 2008), have the ability to promote their own lineage differentiation and simultaneously act against factors favoring other differentiation options. Some of these transcription factors are not restricted to a given lineage and can become dispensable once cells have reached their differentiated state, while expression of others is continuously required to maintain a given cellular identity (Sichien et al. 2016; Orkin 2000). Therefore, the action of key transcriptional regulators is context-dependent and often the result of (in)direct antagonism (Orkin 2000; Orkin and Zon 2008).

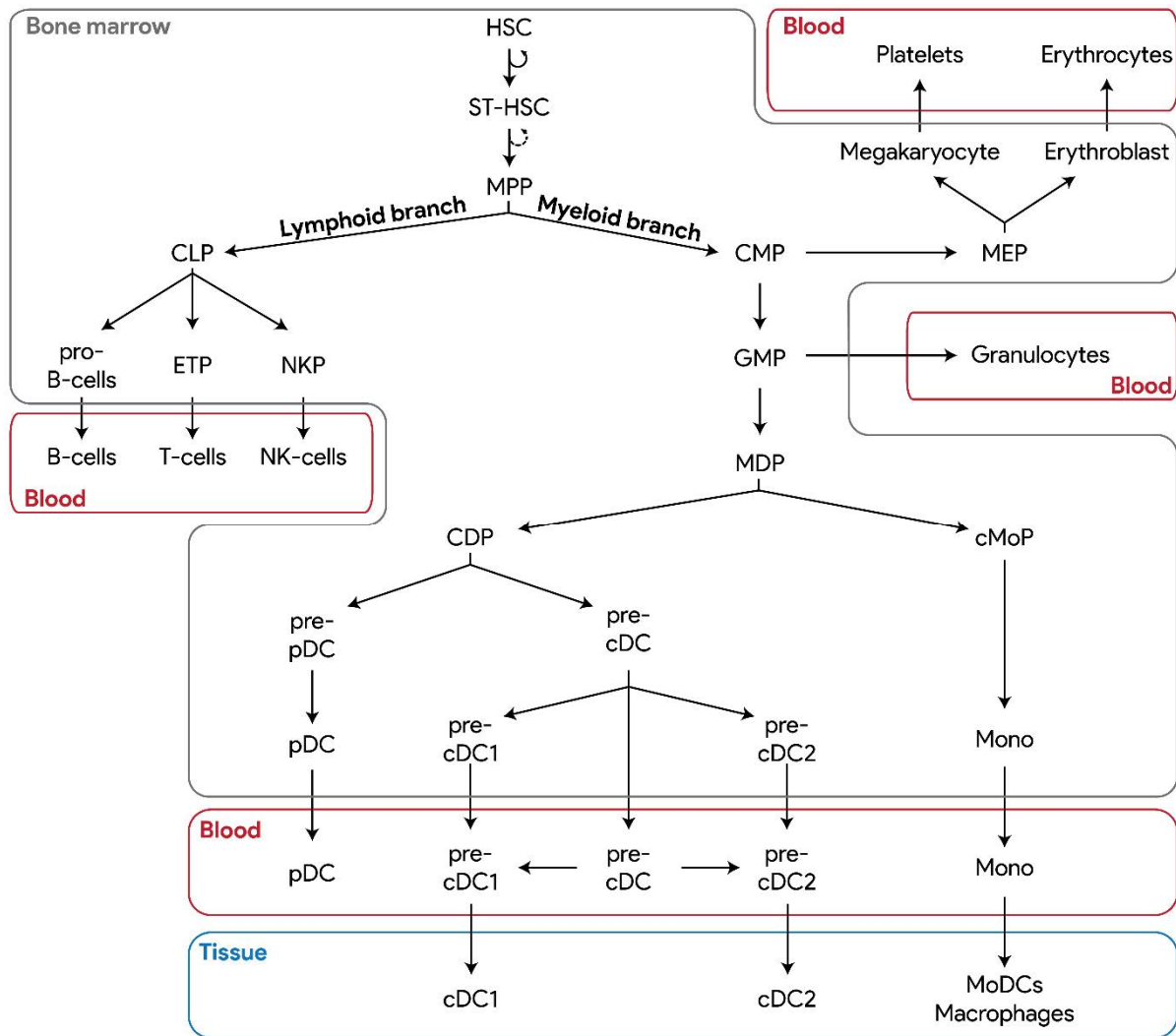


Figure 1. All cellular elements of the blood arise from pluripotent hematopoietic stem cells in the bone marrow. HSC: hematopoietic stem cell; ST-HSC: short-term HSC; MPP: multipotent progenitor; CLP: common lymphoid progenitor; ETP: early T-cell progenitor; NKP: nature killer NK progenitor; CMP: common myeloid progenitor; MEP: megakaryocyte-erythrocyte progenitor; GMP: granulocyte-macrophage progenitor; MDP: macrophage-dendritic cell (DC) progenitor; cMoP: common monocyte progenitor; Mono: monocyte; MoDC: monocyte-derived DC; CDP: common DC progenitor; pDC: plasmacytoid DC; cDC: classical DC.

1.2. FLT3 exerts its function throughout the lifetime of a dendritic cell

Aside from hematopoietic cells, the bone marrow also contains stromal cells that support hematopoiesis by the production of cytokines such as Fms-like tyrosine kinase receptor 3 (FLT3) ligand (FL), stem cell factor (SCF), thrombopoietin and erythropoietin. These cytokines bind to cognate receptors expressed at the surface of HSCs and their progeny, thereby influencing proliferation rates, differentiation paths, progenitor functions and cell survival (Orkin 2000).

One such notable receptor is FLT3, which is expressed at the surface of multi-potent progenitors (MPPs) in the hematopoietic compartment, and is responsible for the development of dendritic cell (DC) subsets (Figure 2). Upregulation of FLT3 is indeed synchronized with the loss of self-

renewal potential of FLT3-negative HSCs in the bone marrow (Boyer et al. 2011). HSCs first transition into a short-term HSC (ST-HSC) population with limited self-renewal capacity, marked by an intermediate FLT3 expression. Subsequent increase in FLT3 expression levels further mark the differentiation into the MPPs (Beaudin, Boyer, and Forsberg 2014a). Interestingly, it has been shown that although every hematopoietic cell line passing the MPP stadium is at some point dependent on FLT3 signaling, MPPs still proliferate in an *FLT3*^{-/-} background, albeit at a lower rate and with the occurrence of a 70% reduction in common lymphoid progenitors (CLPs) and a 20% reduction in common monocyte progenitors (CMPs) (Figure 1) (Beaudin, Boyer, and Forsberg 2014a; Guilliams et al. 2014).

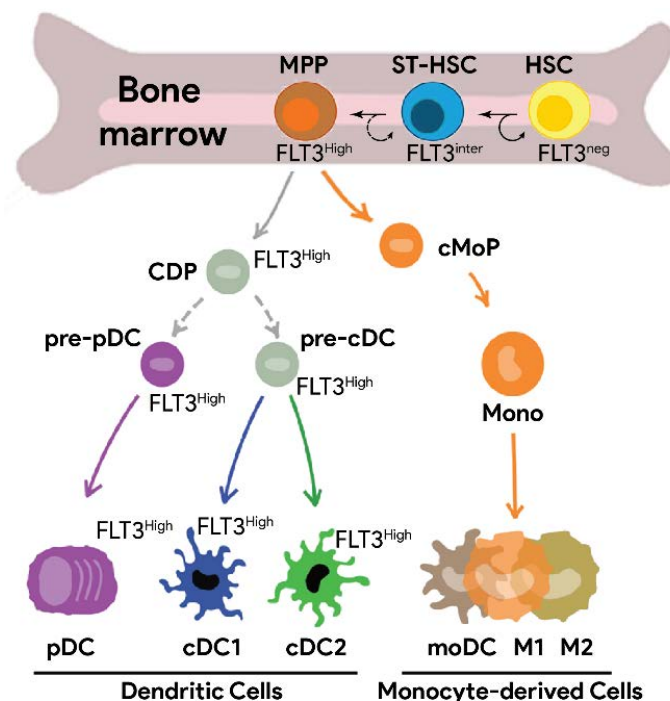


Figure 2. FLT3 expression during hematopoiesis. FLT3-negative hematopoietic stem cells (HSC) generate short-term HSC (ST-HSC) with an intermediate FLT3 expression. ST-HSC differentiate into multi-potent progenitors (MPP) with high FLT3 expression levels. MPPs generate common dendritic cell (DC) progenitors (CDP) and common monocyte progenitors (cMoP). The latter that give rise exclusively to monocytes and do not express FLT3 at their surface. In contrast, FLT3 expression on CDPs remains high throughout the generation of plasmacytoid DCs (pDCs), classical type 1 DCs (cDC1s) and type 2 DCs (cDC2s). Figure adapted from Martin Guilliams and van de Laar 2015 and Sichié et al. 2016. A more complete view on hematopoiesis can be found in, for example, Martin Guilliams, Mildner, and Yona 2018.

Expression of FLT3 remains high on MPP-derived macrophage-DC progenitors (MDP), common DC precursors (CDPs) and differentiated DCs. Although MDPs do not require FLT3 for their maintenance, their compartment is significantly enlarged in response to FLT3 Ligand (FL). In contrast, differentiated peripheral DCs do depend on FLT3 signaling, both for homeostasis and for expansion (Waskow et al. 2008). Given the ability of DCs to continuously monitor the environment they reside in, present antigens to naïve T-cells in lymph nodes and activate those if necessary, DCs are widely regarded as

the professional antigen presenting cells (APCs). The role of FLT3 signaling is therefore crucial in maintaining the link between the innate and adaptive immune systems.

FLT3-dependent DCs can be divided into 3 subsets: plasmacytoid DCs (pDCs), classical DCs type 1 (cDC1s) and classical DCs type 2 (cDC2s) (Figure 1) (Merad et al. 2013; Scott and Lambrecht 2016; Sichié et al. 2017). All DCs express the major histocompatibility complex type 2 (MHCII), a key signature of APCs, although pDCs express this to a lower amount (H. Nakano, Yanagita, and Gunn 2001). pDCs furthermore differentiate themselves from cDCs by a morphology that resembles those of plasma cells, by a more restricted expression of pattern recognition receptors (PRRs) and by their ability to secrete large amounts of type-1 interferon (IFN- α) in response to viral infections (Colonna, Trinchieri, and Liu 2004; Scott and Lambrecht 2016; Sichié et al. 2017). In contrast to the cDCs, their ability to activate naïve T-cells is controversial (Colonna, Trinchieri, and Liu 2004).

cDCs are the classical dendritic cells, as initially described in 1973 by Steinman and Cohn (Steinman and Cohn 1973), a discovery rewarded by the Nobel prize for Physiology or Medicine in 2011. cDCs reside in peripheral tissues and continuously sample their environment by macropinocytosis and phagocytosis. Processed antigens are always presented at their surface in complex with MHCII, but under steady-state conditions, the turnover of those complexes is rather fast (Scott and Lambrecht 2016). This however changes in response to activation of their PRRs, for example during a pathogenic infection. These so-called mature cDCs show a lower turnover of the peptide-MHCII complexes at their surface and an increased expression of CD86 and CD80, ligands for CD28 receptor expressed by T-cells (Larsen et al. 1992; Sallusto 1995). As a consequence of an increased expression of chemokine receptor 7 and an increased locomotive activity (Dieu et al. 1998), they enter the lymphatics and migrate into the paracortex of the nearest draining lymph node. That enables them to present the peptide-MHCII complex to naïve CD4⁺ T-cells which, by additional signaling of several ligand:receptor pairs, become activated effector T-cells. In general, cDC1s polarize T-cells towards Th1 cells, whilst cDC2s preferentially lead to the generation of Th2 and Th17 cells (De Becker et al. 1998; Oppmann et al. 2000; Scott and Lambrecht 2016). Importantly, expression of non-cDC-derived peptides on MHC class I molecules, allows cDC1s to activate CD8⁺ T-cells, thereby generating so-called cytotoxic T-lymphocytes in a process called cross-presentation (Edelson et al. 2010).

1.2.1. FLT3 is a member of the class-3 receptor tyrosine kinases

The ability of hematopoietic cells to respond to the presence of extracellular FL, is mediated by expression of the transmembrane receptor FLT3 at their cell surface. From a structural point of view, FLT3 is classified under the class-3 receptor tyrosine kinases (RTK-III) (M. a Lemmon and Schlessinger 2010). This family of RTKs harbors a total of 5 members, including KIT receptor, colony-stimulating factor 1 receptor (CSF-1R), platelet-derived growth factor receptor alpha (PDGFR α) and PDGFR-beta (PDGFR β). Although RTK-III activating ligands can be classified into two structural folds (short-chain α -helical bundles for FLT3, KIT and CSF-1R versus an all- β -strand cysteine knot fold for the PDGFRs; Figure 3A), all receptors are characterized by an identical modular architecture and are activated by similar principles (Figure 3B) (Verstraete and Savvides 2012). Herein, binding of a dimeric ligand onto an RTK-

III induces dimerization of the latter, resulting in transactivation of the tyrosine kinase domains and activation of downstream signaling pathways.

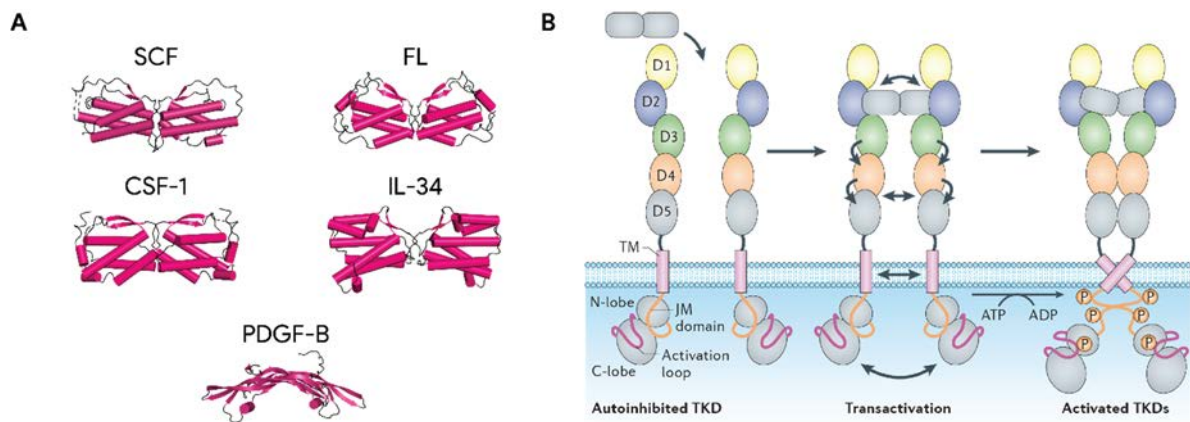


Figure 3. General principles in ligand-dependent activation of RTK-III. **A.** Cognate cytokine ligands for RTK-III show two distinct structural folds. SCF, CSF1, IL-34 and FL are four-helical bundle cytokines. PDGF cytokines all feature a cysteine-knot growth factor fold. Cytokines are shown in cartoon representation with secondary elements colored in red and loop regions colored in black. **B.** Despite the two distinct structural folds, all cytokines activate their receptors via similar principles. Ligands simultaneously bind to the membrane-distal domains (D1, D2 and/or D3) of two receptors, facilitating homotypic interactions between membrane-proximal domains (D4 and/or D5) and possibly between transmembrane domains (TMs). Generation of such ternary complex induces transphosphorylation of the inhibitory juxtamembrane (JM) domain, eventually resulting in a full activation of the kinase activity. Figure from Verstraete & Savvides 2012.

1.2.2. The FL:FLT3 complex: the odd man out

With the notable exception of CSF-1R, for which pre-formed dimers have been described, most dormant RTK-IIIs reside as auto-inhibited monomers at the membrane and are only activated in presence of their cognate ligand(s) (W. Li and Stanley 1991; Elegheert et al. 2011). Ligand-binding is always mediated by at least one of the 3 membrane-distal immunoglobulin (Ig)-like domains of the extracellular region (ECD, D1 to D5) (Figure 3B). As a consequence of their bivalent nature, each ligand is capable of recruiting two receptors, thereby establishing a ternary ligand:receptor complex. Being brought in close proximity facilitates the engagement into homotypic receptor-receptor contacts, mediated by the membrane-proximal Ig-like domains.

Although such ligand-induced extracellular homotypic receptor interactions have shown to be present for all other RTK-III, they are conspicuously absent for FLT3 - as was predicted by the absence of the conserved dimerization motive in the EF-loop of FLT3 domain 4 (Figure 4A) (Felix et al. 2015; Luo et al. 2015; Verstraete et al. 2011; Yuzawa et al. 2007). The absence of homotypic interactions was first shown by performing ITC experiments with FLT3 constructs for which the membrane-proximal domains were step-wise removed (Figure 4C). Similar experiments involving truncated CSF-1R species were previously able to show that presence of CSF-1R_{D4-D5} increased the affinity for CSF-1 by a factor of 16 (K_D of 14 nM using CSF-1R_{D1-D5} versus a K_D of 213 nM using CSF-1R_{D1-D3}). In contrast, removal of FLT3_{D5} and FLT3_{D4-D5} resulted in only a moderate change in affinity for the ligand, suggesting that the

membrane-proximal domains do not contribute significantly to the overall affinity of FLT3 for its ligand. It should however be noted that the stability of FLT3_{D1-D3} was reported to be sub-par compared to FLT3_{D1-D5} and FLT3_{D1-D4}. Reasons for this instability are unknown, but the phenomenon is reflected by the ITC-determined stoichiometry and by the observation that size-exclusion chromatography on the FL:FLT3_{D1-D3} mixture at the end of an ITC experiment, showed a large amount of FLT3_{D1-D3} in the unbound form – despite the superstoichiometric amounts of the ligand.

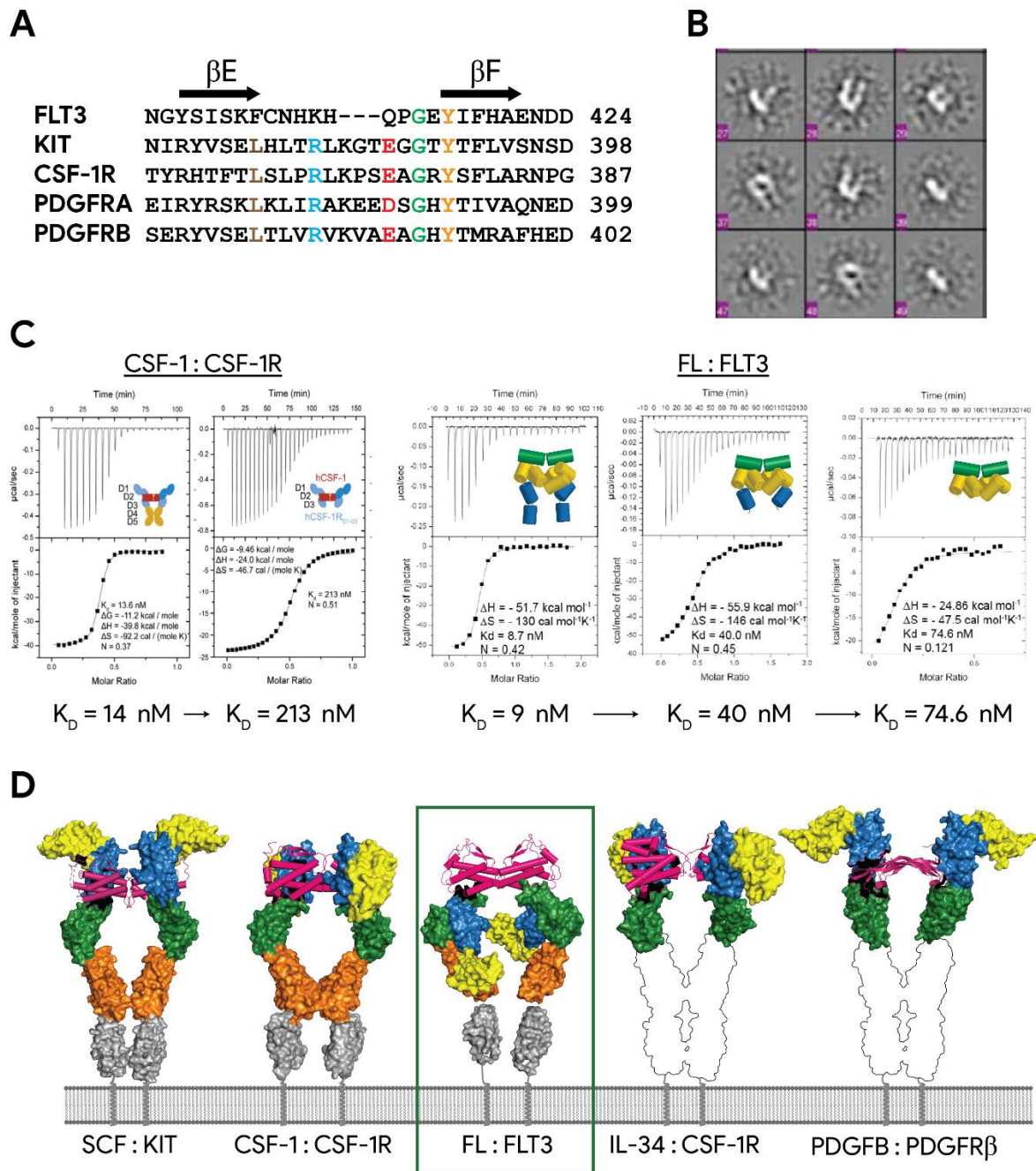


Figure 4. Current state-of-the-art defines FLT3 as the odd man out. A. FLT3 displays an atypical domain 4 (D4) $\beta E\beta F$ -loop that lacks the conserved D4-interaction motif. D4-mediated homotypic interactions feature a salt bridge between an arginine residue (blue) of one receptor and a glutamate or aspartate residue (red) from the other receptor. For KIT, it has been shown that the rotamer conformation allowing this conserved glutamate to engage in reciprocal interactions, is

further stabilized by an electrostatic interaction with a conserved tyrosine residue (orange). Figure from Verstraete et al. 2011 **B**. Selected class averages from preliminary negative-stain electron microscopy data illustrate that most FL:FLT3 complexes adopt an “open” conformation. Figure adapted from Verstraete et al. 2011. **C**. Isothermal titration calorimetry (ITC) experiments show that stepwise removal of the membrane-proximal domains only have limited effect on the affinity of FLT3 for the ligand, in contrast to similar experiments with CSF-1R variants. From left to right: CSF-1R_{D1-D5}, CSF-1R_{D1-D3}, FLT3_{D1-D5}, FLT3_{D1-D4} and FLT3_{D1-D3}. Figure from Elegheert et al. 2011 and adapted from Verstraete et al. 2011. **D**. Current available structures of RTK-III highlighting the absence of homotypic receptor contacts in the FL:FLT3_{D1-D5} complex. Receptors are shown in surface representation, cytokines as cartoons. From left to right: SCF:KIT_{D1-D5}, CSF-1:CSF-1R_{D1-D5}, FL:FLT3_{D1-D5}, IL-34:CSF-1R_{D1-D3} and PDGFB:PDGFR_{D1-D3}. Figure from Verstraete & Savvides 2012.

The open “horseshoe” ring structure lacking homotypic receptor contacts, together with negative-stain electron microscopy data, furthermore supported the conclusion that FLT3 is the only RTK-III that does not appear to engage into homotypic interactions upon ligand binding (Figure 4B and Figure 4D). Interestingly, some EM micrographs did reveal an interaction between FLT3_{D4} (Figure 4B), raising the possibility that homotypic interactions could be enhanced within the spatial confinement of the cell membrane.

Analysis of the Catalogue Of Somatic Mutation In Cancer (COSMIC) reveals that oncogenic mutations in FLT3 have been detected in every domain of the receptor, including the ECD and TM domain (Forbes et al. 2008). One such point mutation, a substitution of serine-451 to phenylalanine, has been shown to activate the receptor in absence of the ligand, providing a constitutive proliferation signal of transformed BaF3 cells (Fröhling et al. 2007). Interestingly, this mutation conferred partial resistance to midostaurin (formerly known as PKC412), the first tyrosine-kinase inhibitor (TKI) approved for the treatment of FLT3-mutated AML (Stone et al. 2017). To date, this oncogenic S451F point mutation has been found in a total of 11 AML patients, but its underlying transforming principles remain poorly understood, as is the puzzling observation that a mutation in the ECD domain can confer resistance to a kinase-binding TKI. Given its location in FLT3_{D5}, it is hypothesized that Phe451 might drive ligand-independent FLT3 dimerization by increasing the mutual affinity of the membrane-proximal domains (Figure 5A) (Verstraete and Savvides 2012; Verstraete et al. 2011). Likewise, a substitution of threonine-343 to isoleucine, an oncogenic mutation discovered in a patient with acute lymphoid leukemia, has been hypothesized to stabilize a receptor conformation prone to engage in ligand-independent receptor-receptor contacts (Figure 5B) (Jiang et al. 2005; Verstraete and Savvides 2012).

Given the postulation that FLT3 is the only RTK-III for which homotypic receptor contacts are no part of the activation mechanism, such hypothesis inevitably raises questions regarding the completeness of this model, even in a non-oncogenic context.

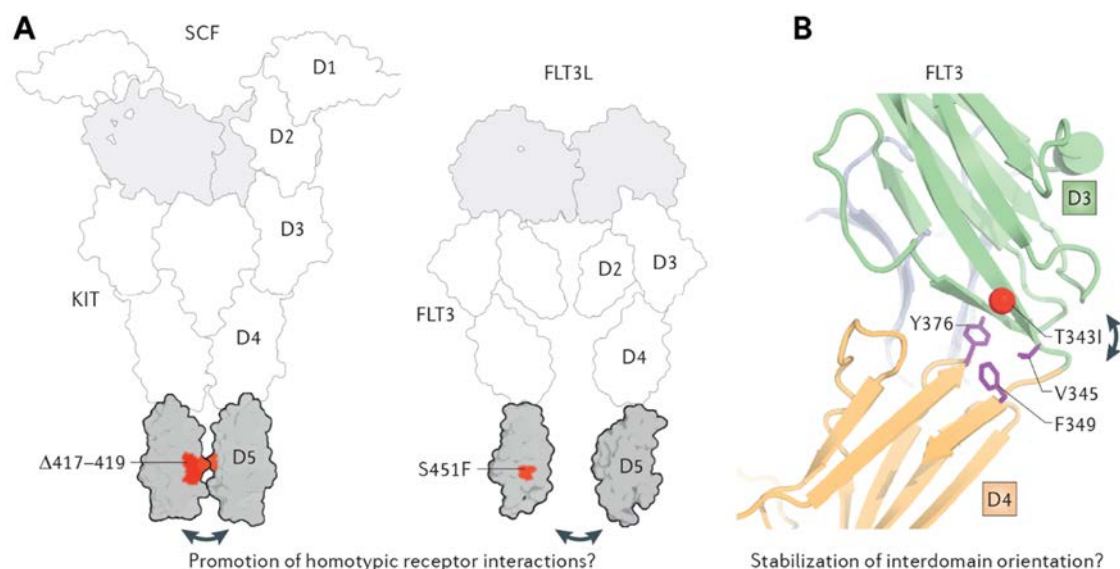


Figure 5. Possible structural consequences of oncogenic FLT3 mutations. **A.** Although its location cannot be confidently mapped on the structure of domain 5, the position of Ser451 roughly coincides with the mutational hot-spot region (residues 417-419) of KIT receptor. The later have shown to increase ligand-induced receptor interactions to such an extent that they promote ligand-independent receptor dimerization. **B.** Thr343 maps at the conserved D3-D4 elbow region, a structural feature allowing rotation of the membrane-proximal domains to engage in ligand-induced homotypic receptor contacts. Mutation of Thr343 to isoleucine might stabilize a dimerization-prone conformation of the membrane-proximal domains. Figure from Verstraete and Savvides 2012.

1.2.3. The juxta-membrane region coordinates autoinhibition of the kinase activity.

The 63-85% sequence identity between RTK-III kinase domains and the observed level of their structural similarity, indicate that the mechanistic principles mediating transition from an inactive autoinhibited conformation to an active kinase domain is conserved among all RTK-III (Griffith et al. 2004; Mol et al. 2003, 2004; Liang et al. 2016; Klug, Kent, and Heinrich 2018). Indeed, regardless of the engagement into homotypic receptor interactions, assembly of a ternary activated extracellular complex, possibly in synergy with lateral interactions of the transmembrane (TM) domains, juxtaposes the intracellular tyrosine kinase domains (TKD) allowing transphosphorylation of the juxtamembrane (JM) region, thereby alleviating the autoinhibitory state (Opatowsky et al. 2014a).

The crystal structure of the cytoplasmic region of FLT3 has been solved already in 2004, and provides a structural basis for the autoinhibitory properties of the juxtamembrane (JM) region (Griffith et al. 2004). In the absence of ligand, the JM region adopts an autoinhibitory conformation by inserting itself into the catalytic pocket between the N- and C-lobe of the TKD, physically impeding ATP binding by sterically occluding entrance to the catalytic site. Mediated by residues Tyr572 and Ser574, the N-terminal JM region furthermore electrostatically sequesters Asp829, a conserved residue essential in coordinating the magnesium ion at the active site (Figure 6A). This conformation, in which Phe830 is pointing away from the ATP binding site, is referred to as the “Asp829-Phe830-Gly831 (DFG)-out” conformation. The dynamic transition from “DFG-out” to “DFG-in”, whereby the phenylalanine orients itself towards the ATP binding site, is considered a strictly conserved mechanism among a wide

range of kinases (Treiber and Shah 2013). Finally, the inactive conformation of the kinase domain is further stabilized by an interaction between the activation loop (mediated by Tyr842 and Arg834) and the catalytic loop (mediated by Asp811) (Figure 6B).

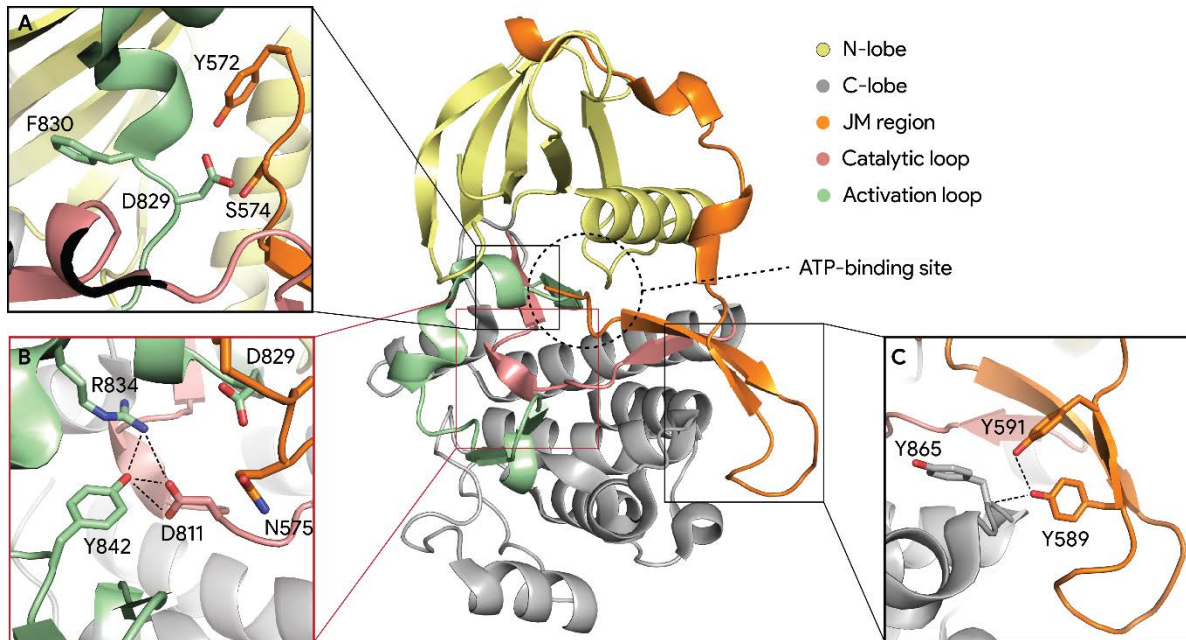


Figure 6. The juxtamembrane region stabilizes an inactive “DFG-out” conformation of the kinase. Central. The intracellular region of FLT3 shown in cartoon representation. **A.** Close-up of the JM domain interactions with Asp829, thereby stabilizing the DFG-out position. **B.** Residues from the activation loop (Arg834 and Tyr842) further stabilize the nucleotide-binding Asp811 of the catalytic loop. **C.** Phosphorylation of Tyr589 and Tyr591 will disrupt the interaction with the backbone C α of Tyr865, and causes the JM domain to swing out of its autoinhibitory conformation. Figure generated from PDB 1RJB.

In the presence of ligand, FL-mediated activation starts with juxtaposition of two TKDs that induces a low level of kinase activity allowing transphosphorylation of Tyr589 and/or Tyr591 (Figure 6C). As a result of the charged and bulky phosphate moieties, phosphorylation prevents the JM domain from positioning next to the C-lobe (Griffith et al. 2004). Consequently, the JM region undergoes a conformational change that opens the entrance to the catalytic site. Finally, binding of ATP causes the activation loop to swing outwards into the DFG-in orientation, a conformation that allows substrates to enter the catalytic site and therefore potentiates the TKD to its full functional role (Griffith et al. 2004; Klug, Kent, and Heinrich 2018). Transphosphorylated residues at multiple sites of the dimeric partner serve as a docking site for phospho-tyrosine-binding proteins initiating the signaling cascade. Specifically for FLT3, binding of FL marks the activation of several signaling pathways, such as PI3K/Akt/mTOR and RAS/MEK/ERK, which are both involved in cell survival and proliferation (S. D. Lyman et al. 1993; Dosil, Wang, and Lemischka 1993; Lavagna-Sévenier et al. 1998).

2. Leukemia: hematopoiesis in overdrive

Current models suggest that a HSC undergoes 2 - 20 divisions a year, theoretically acquiring between 0.07 to 0.86 exonic mutations each year (J. S. Welch et al. 2012). Although most of these mutations are synonymous, some of them will confer an advantage to the cell in terms of survival or proliferation rate – being the first step in leukemogenesis (J. S. Welch et al. 2012; Ding et al. 2012; Bolouri et al. 2018). It is however suggested that only after occurrence of a second, so-called progression mutation, the undifferentiated cells start proliferating at a high rate (Welch, Ley, Link, & Miller, 2012). The result is leukemia: an uncontrolled proliferation of immature hematopoietic cells (Döhner, Weisdorf, and Bloomfield 2015). These immature proliferating cells are denominated “blasts” and can be recognized by their large, oval nucleus (Figure 7). As shown by the bone marrow aspirates, those blasts essentially overgrow the entire bone marrow cellular population and eventually leak into the circulatory system.

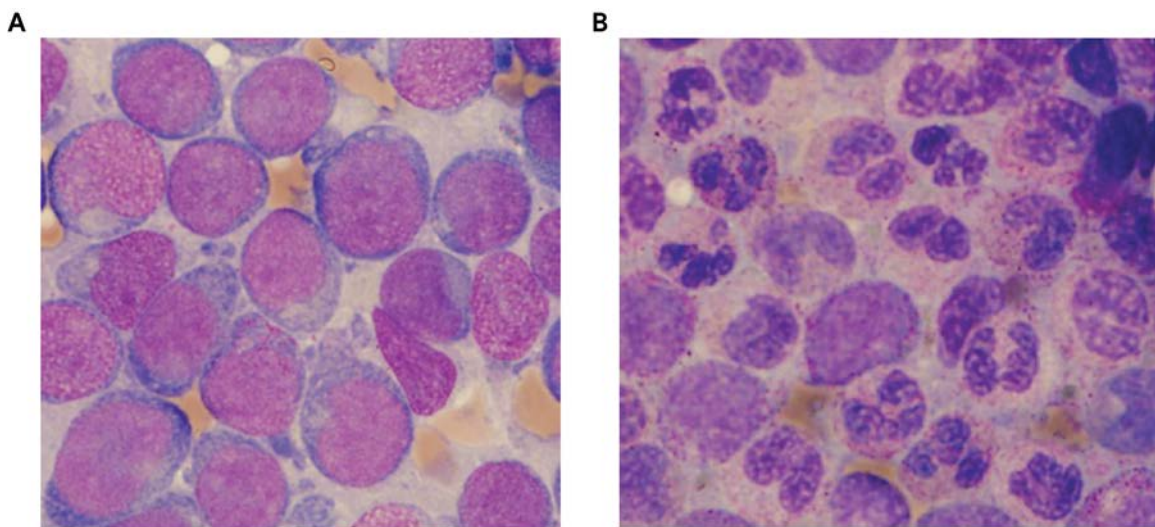


Figure 7. Bone marrow aspirates of **A.** an AML patient and **B.** an AML patient with normal BM morphology after treatment. Figure from Sexauer et al. 2012.

The hostile takeover of the bone marrow by leukemic blasts comes in expense of development of all downstream differentiated hematopoietic cells (Figure 1). As a consequence, most patients seek medical attention for symptoms as dyspnea, weakness and night sweats, or for only experiencing prolonged fatigueness or the notion of bruising easily (Pratz and Levis 2017). Notably, impediment of erythrocyte development reduces the amount of redness in the blood, which lies at the root of the diseases name: originally referred to by Virchow as ‘*weisses blut*’, later became *leukemia*, coming from the Greek ‘*leukos*’ (*white*) and ‘*haima*’ (*blood*).

The NIH National Cancer Institute estimates that in the United States alone, more than 60.000 new patients, on average 66 years old, will be diagnosed with a form of leukemia by the end of 2019 – constituting 3.5% of all new cancer cases and placing leukemia at the 10th position of common types of cancer (NIH n.d.). However, the prediction that almost 4% of all cancer-related deaths in 2019 will be due to leukemia, promotes this cancer to the 7th position of all cancer-related deaths. In general, the 5-year survival rate of leukemia is 61.4%, but disease progression and prognostics dramatically depend on the specific type of leukemia.

Based on markers presented by the blasts, leukemias can be classified as myeloid leukemias, lymphocytic leukemias and mixed phenotype acute leukemia (MPAL). Chronic and acute myeloid leukemia (CML and AML respectively) are the result of immature proliferating cells from the myeloid branch (Figure 1). With 35% of all leukemias, AML is the most common type of leukemia in adults. Lymphocytic leukemias, either chronic (CLL) or acute (ALL), are characterized by blasts showing markers of cells from the lymphoid branch (Figure 1). Those lymphoblasts can be further immunophenotyped into B-cell ALL, T-cell ALL and early T-cell (ETP-) ALL. Although ALL only constitutes 10% of all leukemias in adults, about 75% percent of all childhood leukemias are immunophenotyped as ALL. Finally, two to five percent of all acute leukemia patients display markers from both the myeloid and lymphoid branch, constituting a third type of leukemia - MPAL (Weinberg and Arber 2010; Ye and Wang 2014). Those markers can be present on a single blast population (biphenotypic) or displayed by distinct blast populations (bilineal) (Mi et al. 2018).

Based on molecular-cytogenetics, all three types of leukemia can be further segregated into subgroups. As those subgroups are known to respond differently towards specific drugs, such molecular characterization has become increasingly important in choosing the correct treatment strategy (for example: Arber et al. 2016; Litzow and Ferrando 2015; Pratz and Levis 2017; Wolach and Stone 2015).

Although the underlying mutations are often characteristic for a given subtype of leukemia, activating mutations in FLT3 have been reported in 11-35% of MPAL patients, in 35% of ETP-ALL patients and in 25-35% of AML patients (Alexander et al. 2018; Neumann et al. 2013; Takahashi et al. 2018). Although FLT3-mutated patients only constitute a minority of all leukemia patients, presence of these mutations confers a poor prognosis for each one of those subtypes. The presence of activation mutations in FLT3 on prognosis and response to (FLT3-targeted) therapy are best characterized for AML, where they present the largest subgroup. AML will therefore be discussed in greater depth during this introduction.

2.1. Acute myeloid leukemia

2.1.1. AML develops according to a two-hit model of leukemogenesis

Whole-genome sequencing profiling to map the genomic landscape in pediatric and adult AML, together with results of animal models, have provided evidence that development of AML requires a series of interacting mutations (Ding et al. 2012; J. Welch et al. 2012; Bolouri et al. 2018; Papaemmanuil et al. 2016; Lau et al. 2016; Sallmyr et al. 2008; Kelly et al. 2002; L. Li et al. 2008; Ley et al. 2013). A so-called "2-hit model" postulates that a first class of mutations, conferring an enhanced survival and/or proliferation advantage, have to occur in conjunction with class II mutations that result in an impairment of normal differentiation (J. Welch et al. 2012; De Kouchkovsky and Abdul-Hay 2016; Gilliland and Griffin 2002). Class II mutations have shown to arise early during leukemogenesis and do not overt to AML, although these mutations can manifest themselves in, for example, cytopenia (Heuser, Thol, and Ganser 2016; J. Welch et al. 2012). Chromosomal translocations resulting in

chimeric proteins such as PML-RARA, AML1-ETO and CBF β -SMMHC are for example dominant-negative inhibitors of core binding factor, which is required for a normal hematopoietic development (Okuda et al. 1998; Westendorf et al. 1998; Yergeau et al. 1997; Castilla et al. 1996). Other notable class II mutations are those in the genes coding for nucleophosmine (NPM1) and CCAAT/enhancer-binding protein alpha (CEBPA) (reviewed by, for example, Stirewalt and Radich 2003; Bacher, Schnittger, and Haferlach 2010). Common class I mutations on the other hand, are activating mutations of tumor protein 53 (TP53), neuroblastoma proto-oncogene protein p21 (NRAS), KIT and FLT3, and often result in a constitutive phosphorylation of signal transducer and activator of transcription 3 (STAT3) (Cook et al. 2014; Ghoshal (Gupta), Baumann, and Wetzler 2008; Yamada and Kawauchi 2013). However, likewise to class I mutations, they cannot induce AML themselves - although FLT3 mutations are able to induce a prominent myeloproliferation in mice (Lau et al. 2016; B. H. Lee et al. 2007). Recently, a third class of mutations emerged, harboring mutations in DNA-methylation related genes that affect both cellular differentiation as well as proliferation by alternation of normal epigenetics. Frequently mutated class III genes include those of DNA methyltransferase 3 alpha (*DNMT3A*), Ten-eleven translocation methylcytosine dioxygenase 2 (*TET2*), isocitrate dehydrogenase 1 (*IDH1*) and *IDH2* (J. Welch et al. 2012; Patel et al. 2012; Ley et al. 2013; Mardis et al. 2009; Ley et al. 2010; Yamashita et al. 2010). Interestingly, recent data seems to indicate that mutations in *DNMT3A* can already be present in a premalignant LT-HSC (Shlush et al. 2014). Although unable to cause neoplasms on themselves, mutations such as those in *DNMT3A* that are associated with an increased risk of hematologic neoplasms have led to the definition of “clonal hematopoiesis of indeterminate potential” (CHIP) as a new disease entity (Heuser, Thol, and Ganser 2016).

2.1.2. AML groups an impressive panoply of interacting genetic alternations

Although already considered heterogeneous for three decades, the enormous cytogenetic heterogeneity of AML has only become apparent in the past 15 years (Döhner, Weisdorf, and Bloomfield 2015). Indeed, the WHO classifies AML into a total of 9 subtypes and a staggering 63 sub-subtypes (Arber et al. 2016). Several of those genetic lesions have been identified as prognostic markers with clinical significance and are used to guide the therapeutic approach. In general, mutations in *NPM1* are detected in 25-35% of patients with AML and confer, if associated with a normal karyotype, a favorable prognosis. Likewise, biallelic mutations in *CEBPA*, found in 6-10% of all patients, are associated with favorable outcomes. In contrast, so-called internal tandem duplications (ITD) in FLT3, found in approximately 20-25% of AML patients, are in general associated with unfavorable outcome, both in terms of overall survival as well as disease-free survival, and both when treated with chemotherapy alone as well as having undergone allo-HSCT (Hu et al. 2014; Brunet et al. 2012; Yanada et al. 2005).

However, an immediate consequence of the “2-hit model” is that both pathogenesis and behavior of AML heavily depends on the interplay between different genetic alternations. Inclusion of genetic abnormalities in addition to FLT3 is now used for risk stratification by both the European LeukemiaNet (ELN) and the National Comprehensive Cancer Network (NCCN) (Döhner et al. 2017; O’Donnell et al. 2017). Although both institutes classify presence of *FLT3*^{ITD} mutations with a high allelic ratio and in

absence of other (known) cytogenetic alternations or molecular abnormalities, as an adverse risk factor, the ELN continues stratification and classifies a high-allelic ratio of *FLT3*^{ITD} in presence of *NPM1* mutations as an intermediate risk factor. Co-occurrence of *NPM1* mutations and a low-allelic *FLT3*^{ITD} ratio is on the other hand considered as a favorable risk factor.

As it has been shown that the number of exonic mutations in hematopoietic stem cells are positively correlated with age, it comes as no surprise that the landscape of somatic variants in pediatric AML is remarkably different from that in adults (J. Welch et al. 2012; Bolouri et al. 2018). Whereas mutations in *DNMT3A*, *IDH1*, *IDH2* and *NPM1* have shown to be more frequently present in adult AML patients, pediatric subjects showed a higher mutational status of Wilms' tumor 1 (*WT1*) and *NRAS*, and tended to have more structural alternations, fusions and focal copy number alternations than adult patients. Interestingly, some interactions of *FLT3*^{ITD} with other genomic alternations appear to be age specific: in contrast to adults, co-occurrence of *FLT3*^{ITD} and *NPM1* mutations confers a superior outcome in pediatric patients (Bolouri et al. 2018). This observation might have its origin in the finding that co-occurring *FLT3* and *NPM1* mutations are frequently accompanied with *DNMT3A* mutations in adults, but not in children (Bolouri et al. 2018; Papaemmanuil et al. 2016).

The importance of the age-correlated mutational burden in AML genomes and the interplay between founding and progression mutations, could explain why pediatric AML patients show a 5-year survival rate of 70%, compared to 5-year survival rate of 27% of adult AML patients (NIH n.d.; Alexander et al. 2017). Importantly, these studies forewarn extrapolation of findings in adult AML to pediatric AML, and should motivate to test emerging therapies in both adult and childhood populations separately. It furthermore confronts us with a notion that using knowledge regarding somatic mutations as a guide for risk stratification and treatment might be inadequate, as not only the interplay between different mutations could be largely unexplored ground, but also the possible molecular consequences of a genetic alternation could remain uncharacterized. For example, it has only recently been shown that mutations in polycomb repressive complex 2 Subunit (*SUZ12*), embryonic ectoderm development (*EED*) or enhancer of zeste 2 polycomb repressive complex 2 subunit (*EZH2*) promote transcription of *FLT3* with a constitutive activation of the receptor and T-ALL or EPT-ALL as a consequence (J. Zhang et al. 2018). These patients have been shown to benefit from *FLT3*-targeting therapies, but would require an off-label administration of midostaurin, which is only FDA-approved for newly diagnosed *FLT3*-mutated AML.

2.1.3. Until 2017, standard treatment of AML remained unchanged for 15 years

Per 2016 World Health Organization (WHO) update on myeloid disorders, AML is diagnosed by at least 20% myeloblasts in the peripheral blood or bone marrow (Arber et al. 2016). This diagnosis is quickly followed by a conventional so-called 7 + 3 induction chemotherapy regimen, consisting of a 7 days infusion with cytarabine and 3 days of an anthracycline, mostly idarubicin or daunorubicin (Döhner et al. 2017; Grunwald and Levis 2013; Pratz and Levis 2017). Final diagnosis of AML is based on a morphologic assessment of bone marrow specimens and blood smears, analysis of cell-surface or cytoplasmic markers, identification of abnormal cytogenetics and screening for selected molecular genetic lesions (Döhner et al. 2017; Döhner, Weisdorf, and Bloomfield 2015; Pratz and Levis 2017).

After complete remission, patients with a favorable genetic risk profile typically only undergo consolidation chemotherapy, whereas those with intermediate- and unfavorable-risk AML are recommended for allogeneic hematopoietic stem cell transplantation (allo-HSCT) followed by maintenance therapy (Davis, Benjamin, and Jonas 2018; Döhner et al. 2017; Eda et al. 2010; Ho et al. 2015; Stone et al. 2017).

The 7 + 3 chemotherapy regimen has formed the backbone in initial treatment of AML, but is only started after assessment whether a patient is considered sufficiently fit for such invasive induction chemotherapy. Although the importance of age in the assessment of risk of treatment-related mortality is under debate (Kantarjian et al. 2006; Klepin et al. 2013; Klepin 2014; Deschler et al. 2013; Giles et al. 2007), it is still a major determinant in the decision. The only treatment alternatives for patients considered unfit are supportive care, low-intensity treatment or clinical trials with experimental treatments. It therefore comes as no surprise that median 5-year overall survival (OS) for patients younger than 60 years is approximately 40%, compared to about 10% overall survival for patients older than 60 (NIH n.d.; Döhner et al. 2017; De Kouchkovsky and Abdul-Hay 2016). However, even when patients older than 60 years are considered fit for induction therapy, only 40-60% achieve complete remission, versus 60-85% of patients younger than the age of 60. As troublesome as these statistics are, they become even more worrisome upon observing that the median age of AML diagnosis is between 67-70 years of age (NIH n.d.).

Recognition that the cytogenetic heterogeneity has a severe influence on the outcome of drugs with a specific target, has resulted in testing for and approval of novel therapies targeting specific AML subgroups. These include Gemtuzumab ozagamicin (Mylotarg, Pfizer), a humanized drug-conjugated antibody targeting CD33 for treatment of CD33-positive AML patients; CPX-351 (Vyxeos, Jazz Pharmaceuticals), a novel formulation of cytarabine and daunorubicin, for the treatment of newly-diagnosed AML with myelodysplastic-related changes; Enasidenib (Idhifa, Agios Pharmaceuticals and Celgene Corporation), an inhibitor for IDH2 for IDH2-mutant positive AML patients and ivosidenib (Tibsovo, Agios Pharmaceuticals, Inc.), and IDH1 inhibitor for adult patients with relapsed or refractory acute myeloid leukemia (AML) with a susceptible IDH1 mutation. Since mid-2017, midostaurin (Rydapt, Novartis Pharmaceuticals), a multi-targeted kinase inhibitor has been approved for the treatment of newly diagnosed FLT3-mutated AML, whilst gilteritinib (XOSPATA, Astellas Pharma Inc.) gained FDA approval for the treatment of adult patients with refractory or relapsed FLT3-mutated AML. Furthermore, clinical trials are ongoing for drugs targeting BCL2, FLT3, FLT3_{ITD}, TKD-mutated FLT3, IDH1, neural precursor cell expressed, developmentally down-regulated 8 (NEDD8)- activating enzyme (NAE), CD123 and more.

Reviewing all of these novel drugs, their targets and performance in clinical phase would fall beyond the scope of this introduction, and has been done elsewhere (for example: Davis, Benjamin, and Jonas 2018; Luppi et al. 2018; Sheridan 2017a; Wei and Tiong 2017). Given its central role in this doctoral thesis, we will focus on the most promising FLT3-targeting drugs.

2.2. Oncogenic FLT3 mutations abolish autoinhibition of the kinase domain

As discussed previously, mutations in FLT3 are found in approximately 20-30% of AML patients, and their occurrence is associated with a poor outcome. With the few notable exceptions discussed previously, almost all of these oncogenic mutations map to the TKD, and induce a constitutive phosphorylation of the latter (Figure 8) (Kiyoi et al. 1998b; Yamamoto et al. 2001).

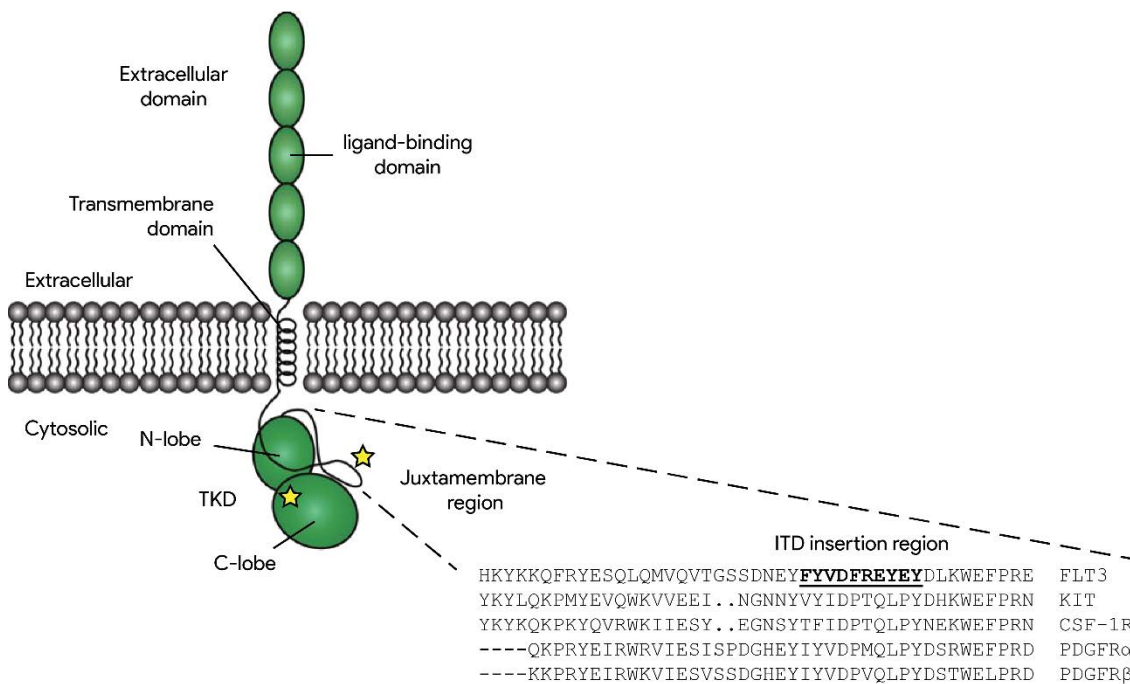


Figure 8. Two main types of oncogenic mutations cause constitutive receptor activation. FLT3 is a transmembrane receptor with an extracellular ligand-binding region, a single-pass transmembrane domain and an intracellular tyrosine kinase domain. In steady-state conditions, the activity of the kinase is suppressed by interactions with the juxtamembrane (JM) region. The two types of oncogenic mutations detected in AML patients, map at a different location in the TKD (indicated by stars). 4 – 68 amino acids long tandem duplications between residues Phe590 and Tyr599 (marked in bold underlined font in the sequence alignment) in the JM region are expected to abolish optimal positioning for maintaining the kinase in its inactive conformation. Likewise, mutations in the C-lobe (lower green oval) are predicted to destabilize the inactive conformation of the kinase domain. Figure adapted from Chan 2011.

The first of two distinct types of mutations in the TKD are internal tandem duplications (ITD) in the JM region, found in approximately 15-20% of all patients with AML and associated with a high relapse rate and, consequently, reduced overall survival (Kiyoi et al. 1999; Kottaridis et al. 2002; Thiede et al. 2002; Fröhling et al. 2002; Badar et al. 2015a). The crystal structure of the TKD of FLT3 revealed that the presence of these 4 to 68 amino acids long duplications in the JM domain, are likely to prevent an optimal positioning of the JM domain into the TKD, and probably disrupt the complementary interaction with the N-lobe and the activation loop (Figure 6) (Griffith et al. 2004). As such, the aberrant JM domain permanently remains in the unattached conformation, allowing ATP to freely enter the catalytic site and resulting in a ligand-independent constitutive activation of the receptor.

Point mutations at position Asp835 within the activation loop of the C-lobe, resulting mostly in a tyrosine, represent a second class of activating TKD mutations and can be found in approximately 7%

of all AML patients (Yamamoto et al. 2001; Forbes et al. 2011). Most reports suggest these mutations confer a negative prognosis, albeit not as damning as the presence of ITD mutations (Thiede et al. 2002; Moreno et al. 2003; Yanada et al. 2005). The structural principle underlying this point mutation is less clear, but it is expected that Asp835 stabilizes the closed DFG-out form of the activation loop (Griffith et al. 2004). Consequently, mutation to a tyrosine, threonine or histidine would favor the conformational swing of the activation loop into the DFG-in position and facilitate the transition to an active kinase conformation.

3. Clinical targeting of FLT3-mutated AML

During the past two decades, the clear correlation between AML and the presence of ITD and other TKD mutations in FLT3 has spurred the development of therapeutic agents specifically targeting FLT3 (Kiyoi et al. 1998a). As a result, several small-molecule tyrosine kinase inhibitors (TKIs) were developed to efficiently inhibit constitutive phosphorylation of oncogenic FLT3 variants *in vitro*. Unexpectedly, clinical outcomes when administering these agents as monotherapies were only modestly successful, which motivated clinical testing of strategies that incorporated these TKIs into existing chemotherapies. Mid-2017, the efforts of one such strategy came to fruition by the FDA and EU approval of midostaurin for the treatment of newly-diagnosed FLT3-mutated AML (Stone et al. 2017), whilst other new-generation FLT3 inhibitors are still in the pipeline. In the following sections, we briefly touch upon the most promising TKIs and their performance in a clinical setting. We furthermore highlight some notable exceptions to this strategy, focusing on FLT3-inhibition in an antibody-based approach.

3.1. FLT3 tyrosine-kinase inhibitors

3.1.1. Classification

Based on their level of specificity for FLT3, TKIs are typically classified as belonging to either the first-generation multi-targeting TKIs, or to the more FLT3-specific second-generation TKIs. The first-generation TKIs, including sunitinib, sorafenib, lestaurtinib and midostaurin, are the result of the initial wave of drugs used in treatment of solid tumors by nonselective inhibition of various kinases – coincidentally including oncogenic FLT3 variants. Due to their promiscuous nature, the use of these agents is often correlated with significant toxicity. Indeed, a Phase II study of midostaurin as a monotherapy at a dose of 75 mg three times daily did not only fail to have sufficient clinical activity in patients with relapsed FLT3-mutated AML, but furthermore lead to the death of 2 patients by treatment-related pulmonary events (Stone et al. 2005). In contrast, second-generation TKIs (i.e. quizartinib, crenolanib and gilteritinib) are expected to show less off-target side effects.

Alternatively, TKIs can be classified according to the specific conformation of the kinase they bind and stabilize. All inhibitors compete with ATP for binding at the catalytic site, but so-called Type-I inhibitors stabilize the TKD with the activation loop in the DFG-in position (i.e. open/active conformation), while Type-II inhibitors require the loop in the DFG-out (i.e. closed/inactive) conformation. Given that mutations in the JM region and TKD activation loop disrupt the autoinhibitory

state of the kinase, such mutations are expected to confer increased resistance to Type II inhibitors. Midostaurin, sunitinib and lestaurtinib are shown to be type-I inhibitors, whilst sorafenib and quizartinib are classified as Type II.

3.1.2. Sunitinib, a first-generation Type I inhibitor

Sunitinib is a Type 1 multi-targeted TKI shown to have activity against all RTK-III, all RTK-V and the glial cell-line-derived neurotrophic factor receptor RET (O'Farrell et al. 2003). It has already gained FDA approval for treatment of renal cell carcinoma and gastro-intestinal stromal tumors, and has shown *in vivo* activity against TKD-mutated FLT3 in a phase I study (O'Farrell et al. 2003). Another phase 1 trial, mainly designed to evaluate toxicity, found that all 4 FLT3-mutated AML patients responded to the treatment, albeit for only a short period of time of 4 to 16 weeks (Fiedler et al. 2005). A third study finally explored the use of sunitinib in combination with traditional induction and consolidation chemotherapy in patients aged over 60 years old. Inhibition of constitutive FLT3 phosphorylation was observed in > 50% of patients receiving 200 mg daily (Fiedler et al. 2015). However, given the severe adverse side effects at already 75 mg a day (Fiedler et al. 2005), it remains to be seen how well this TKI will perform in later clinical trials.

3.1.3. Sorafenib, a first-generation Type II inhibitor

Likewise to sunitinib, sorafenib is a multi-targeted TKI with activity against FLT3, VEGFR, KIT and RAF kinase (Auclair et al. 2007). As a single agent, sorafenib's efficacy seems to be limited by side effects at doses necessary to inhibit FLT3 *in vivo* (Leick and Levis 2017). Sorafenib is a Type II inhibitor stabilizing the inactive conformation of the kinase domain and therefore predicted to be more sensitive to escape mutations. Indeed, it has been shown that upon relapse after complete remission with sorafenib as monotherapy, patients did not respond to further therapy due to an expanded population of leukemic cells harboring Asp835 mutations (Man et al. 2012).

Sorafenib has been more studied in combination with conventional induction chemotherapy, but with uncertain results. In Phase II SORAML trial (Röllig et al. 2015), addition of sorafenib versus placebo added to standard induction and consolidation chemotherapy was tested in patients with previously untreated AML. Outcomes revealed that addition of sorafenib prolonged the median event-free survival compared to placebo (21 months vs 9 months), significantly increasing the 3-year event-free survival (40% vs 22%, p-value 0.013). However, no differences in event-free survival could be detected between patients with FLT3 mutations and those without, nor could the researchers detect an improvement in overall survival. In contrast, a large phase II trial of sorafenib plus standard 7 + 3 induction therapy in patients older than 60 years (Serve et al. 2013), showed a worse outcome for the sorafenib arm, and even when limiting the analysis to the FLT3-ITD subgroup, no benefits of sorafenib addition could be detected. In a relapsed setting, addition of sorafenib has shown to significantly increase complete remission rates in FLT3-mutated patients compared to wild-type FLT3 (14 out of 15 patients and 36 out of 54 patients respectively; p-value 0.03) (Ravandi et al. 2010), however only in combination with idarubicin and cytarabine. Addition of sorafenib to azacytidine showed no significant effect on median survival (Ravandi et al. 2013).

Finally, usage of sorafenib has also been tested in a post-transplant setting. Interestingly, a retrospective review of 65 FLT3-ITD patients with relapsed disease treated with sorafenib monotherapy, followed by allo-HSCT were shown to develop resistance less frequently (38%) and significantly later (197 days) than those who had not undergone allo-HSCT (47% and 136 days) (MetzelDer et al. 2012).

3.1.4. Lestaurtinib, a first-generation Type II inhibitor

Lestaurtinib is a staurosporine analog with a broad spectrum of activity against various kinases, such as FLT3, JAK2, VEGFRs and TrKA. A first notable occurrence of lestaurtinib was in a phase 2 clinical trial as first-line treatment of elderly patients considered unfit for chemotherapy (Knapper et al. 2006). Although only modestly successful in terms of outcome, this study is memorable for developing the plasma inhibitory activity (PIA) assay, which allowed for the first time correlating *in vivo* drug responses to *ex vivo* FLT3 inhibition (Figure 9A). Indeed, *in vitro* studies have suggested that inhibition of FLT3 autophosphorylation to below 15% of baseline activity is necessary to achieve a strong cytotoxic effect on blasts (B. D. Smith et al. 2004). Analysis of patient plasma allowed to distinguish between clinical non-responders and hematological responders, and showed that all clinical responders to the drug achieved an FLT3 inhibition below 15% of baseline. In contrast, no clinical responses were observed in patients for which 85% FLT3 inhibition failed to be sustained. These findings motivated collection of PIA assay data during the randomized phase 3 Caphalon 204 study, testing the effect of addition of lestaurtinib to chemotherapy administered to relapsed patients (Levis et al. 2011). They observed that addition of lestaurtinib only resulted in a 5% higher probability for achieving complete remission, versus patients on chemotherapy alone, and therefore concluded that addition of lestaurtinib to standard salvage chemotherapy in relapsed FLT3-mutated AML did not seem to offer benefits. However, it was also shown that only 58% of patients reached inhibition to less than 15% of baseline, and they were furthermore able to correlate these inhibition levels with remission rates.

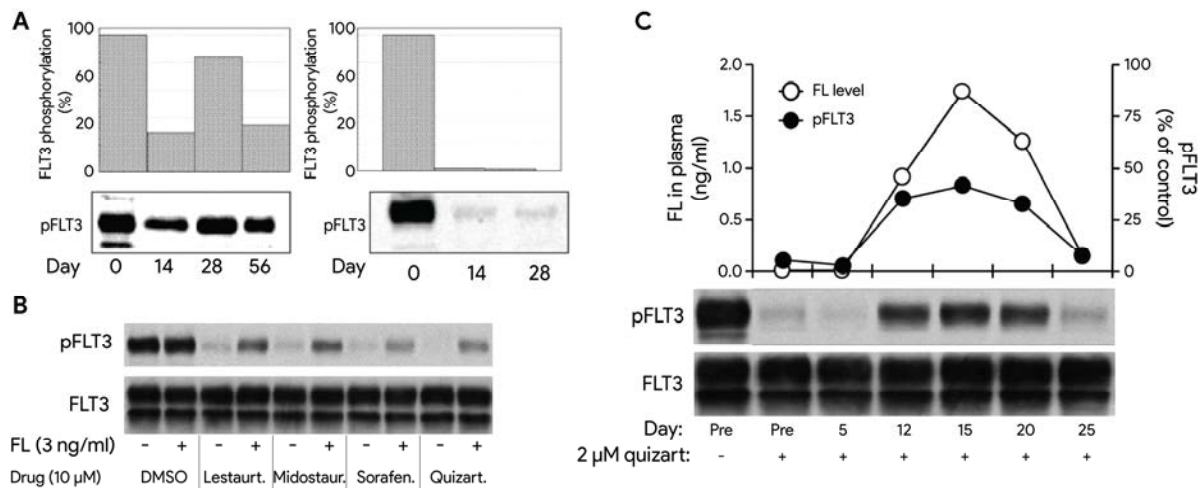


Figure 9. FLT3 ligand impedes inhibition in vivo. **A.** The plasma inhibitory activity (PIA) assay allows correlation between clinical response and FLT3 inhibition. FLT3_{ITD}-transfected cells were exposed to patient plasma samples obtained 12h after lestaurtinib administration and analyzed by immunoblotting. Plasma of a clinical-non responder (left) could not inhibit constitutive FLT3 phosphorylation. In contrast, plasma of a clinical responder showed significant reduction in FLT3_{ITD} phosphorylation after day 14. Figure adapted from Knapper et al. 2006 **B.** FL induces resistance to various TKIs. Stimulation with 3 ng/ml is sufficient to reduce the phosphorylation-suppressing effects of all tested TKIs in vitro. Figure adapted from Sato et al. 2011. **C.** FL impairs inhibition of FLT3 autophosphorylation *in vivo*. Plasma of one patient receiving induction chemotherapy at indicated time points, analyzed by the PIA assay. Upon *in vitro* incubation, quizartinib was added. Chemotherapy-induced increase in serum levels of FL could be correlated with an insufficient quizartinib-mediated inhibition of FLT3_{ITD} autophosphorylation. Figure adapted from Sato et al. 2011.

Together with preliminary blood samples from patients of AML15 and AML17 trials, two clinical studies assessing the addition of lestaurtinib to first-line chemotherapy in FLT3-mutated AML (Knapper et al. 2017), it was shown by Sato and colleagues (Sato et al. 2011b) that increased levels of FL in plasma of non-responders was at the root of the observed TKI resistance. Interestingly, analysis of patient samples revealed that serum concentrations of FL were 100-fold elevated already on day 15 of induction chemotherapy (Figure 9C), and continued to increase with another factor 10 to a 3251 pg/ml after the fourth course of chemotherapy. These findings were especially disturbing considering they could show that 3 ng/ml FL is able to impede TKI-mediated FLT3 inhibition of not only lestaurtinib, but also sorafenib, midostaurine and quizartinib (Figure 9B). The latter is still today considered as one of the most promising second-generation FLT3-targeting TKIs, whilst midostaurin received both FDA and EU approval for treatment of newly-diagnosed FLT3-mutated AML (Stone et al. 2017).

3.1.5. Midostaurin, a first-generation type I inhibitor

Midostaurin is a pan-kinase inhibitor, originally developed to inhibit protein C kinase, and later showed to be effective against both FLT3-ITD and FLT3-TKD mutations (Weisberg et al. 2002; Breitenbuecher et al. 2009). Preclinical and early-phase clinical trials indicated that midostaurin followed a rather complicated pharmacokinetic profile with 2 active metabolites and indicated that the drug as a single agent reduced blast count both at the periphery and the bone marrow, but was unlikely to induce remissions. However, its promising effect on blast reduction together with results showing it could be

safely combined with induction and consolidation therapy, led to a phase III Randomized AML trial in FLT3 in patients less than 60 years old trial (RATIFY, Stone et al. 2017).

The trial was conducted at 225 sites in 17 countries, and enrolled a total of 717 patients between 18 and 59 years of age, who had newly diagnosed AML and had not previously received antineoplastic therapy. Patients were stratified according to the subtype of FLT3 mutation, and randomized to receive midostaurin or a placebo in addition to traditional 7 + 3 regimen and consolidation chemotherapy. On completion of consolidation, patients continued to receive midostaurin as a single agent for 12 months. Results showed that although addition of midostaurin did not significantly increase the rate of complete remission compared to administration of a placebo (58.9% vs 53.5%, p-value of 0.15), they did observe that 4-year overall survival rates in patients receiving midostaurin was increased to 51.4%, compared to 44.3% in the placebo arm. Furthermore, although event-free median survival was on average only prolonged by 5.2 months (8.2 vs 3.0 months for midostaurin versus placebo, p-value 0.002), patients did have a significant 21.6% lower likelihood of having an event (p-value 0.002), which translated into a 7.6% increase in 4-year event-free survival rates in the midostaurin arm. Given these results, it was arguably the 23% reduction in the risk of death compared to those who received chemotherapy alone, that earned the drug its approval (Sheridan 2017). Further review of the data showed that survival rates of the two arms separated quickly, and remained roughly parallel thereafter, suggesting that midostaurin's main benefit appears to be during the initial stages of the treatment, inducing a deeper remission and therefore allowing more patients to undergo allo-HSCT. Unexpectedly the effect of midostaurin did not appear to depend on the type of FLT3 mutation present in patients, despite that the presence of high-allelic ITD mutations was presumed to show a higher impact of treatment with this inhibitor (Sheridan 2017).

3.1.6. Quizartinib, a second-generation Type II inhibitor

Similar to crenolanib and gilteritinib, quizartinib is a second-generation inhibitor developed specifically to inhibit FLT3. Quizartinib shows an IC_{50} of less than 1 nM in culture media, which is an order of magnitude better than previous studied TKIs (Zarrinkar et al. 2009). Quizartinib showed encouraging results for FLT3-mutated AML in a phase I trial as monotherapy, in which 9/17 FLT3-ITD patients responded versus 5/37 FLT3 wild-type patients (J. E. Cortes et al. 2013). Interestingly, instead of observing the typical loss of cellularity in bone marrow as a consequence of cytotoxic chemotherapy, the bone marrow of quizartinib-treated patients was shown to remain hypercellular. Further analysis confirmed that quizartinib induced terminal differentiation rather than apoptosis of bone marrow blast, without changing the FLT3-ITD allelic ratio. Encouraging results of several phase 2 studies with quizartinib as monotherapy in refractory or relapsed settings, resulted in a phase 3 study testing quizartinib as monotherapy versus salvage chemotherapy in relapsed FLT3-ITD mutated AML patients (NCT02039726). As a clinical first for FLT3 inhibitors, it was demonstrated by an abstract on the 23rd Annual Congress of the European Hematology Association that quizartinib can significantly improve overall survival. Indeed, median overall survival was increased to 6.2 months, compared to 4.7 months in the arm receiving chemotherapy alone. A significant 24% reduction in risk of death (p-value 0.0177) translated itself into a median overall survival over 27% versus 20% in the chemotherapy arm (J. Cortes et al. 2018). Although only a modest improvement, the higher specificity of quizartinib marks it as a

more tolerable regimen compared to chemotherapy. Finally, a second phase 3 study has been initiated to compare the effect of quizartinib versus placebo administered with standard induction and consolidation therapy (NCT02668653). However, as resistance to quizartinib by TKD mutations (by point-mutations involving Asp835 or Phe691) has already been detected in patients who relapsed after complete remission from quizartinib, the results of such trial remain to be awaited (Catherine C. Smith et al. 2012).

3.1.7. Crenolanib, a second-generation Type I inhibitor

Crenolanib was originally developed as a potent inhibitor of PDGFRs, but was found to have activity against FLT3-ITD and FLT3-TKD mutations, particularly at position Asp835 (Lewis et al. 2009; Galanis et al. 2014). It furthermore lacked significant activity against KIT, responsible for the myelosuppressive effect of quizartinib when administered at higher doses (J. E. Cortes et al. 2013). Several phase II studies have been performed, one of which tested addition of crenolanib to standard 7 + 3 induction chemotherapy as a first-line treatment in FLT3-mutated AML, resulting in a promising 96% of patients in complete remission. Importantly, only 3 of the 9 patients older than 60 years relapsed in the 6 months follow up (Wang et al. 2016). With these encouraging results, a phase 3 clinical trial was designed to investigate the efficacy of crenolanib versus midostaurin in FLT3-mutated AML patients (NCT03258931).

3.1.8. Gilteritinib, a second generation type I inhibitor

Gilteritinib is a pyrazinecarboxamide derivative shown to be a potent inhibitor of FLT3 and AXL, a member of the Tyro3-Axl-Mer (TAM) receptor tyrosine kinase family implied as modulators of FLT3 activity (L. Y. Lee et al. 2017). The only phase I/II study to date showed that gilteritinib resulted in a complete remission of 83% of FLT3-mutated patients (Perl et al. 2017), resulting two several phase 3 studies that will test gilteritinib versus salvage chemotherapies in relapsed/refractory FLT3-mutated AML: NCT03182244 and NCT02421939. Although the results are still largely unpublished, *ad interim* analysis of the latter motivated the FDA to greenlight gilteritinib for treatment of relapsed/refractory AML with activating FLT3 mutations. Furthermore, a phase 1 study testing safety and tolerability of administered gilteritinib in combination with induction and consolidation therapy, is now recruiting newly diagnosed AML patients (NCT02236013).

3.2. Extracellular FLT3-targeting drugs

The longstanding correlation between AML and intracellular kinase mutations in FLT3, together with the large know-how regarding kinase inhibitors, has concentrated the industries focus on development of TKIs. Given the often observed off-target effects of such inhibitors and the 63-85% sequence identity in the kinase domain between RTK-III alone, development of a specific FLT3-targeting TKI was expected to be a challenging endeavor from the start.

3.2.1. IMC-EB10 and IMC-NC7, neutralizing monoclonal anti-FLT3 antibodies.

Providing an answer to the modest success of initial clinical studies with TKIs, and to provide an alternative for the – mostly – elder patients that were found unfit to receive the aggressive chemotherapy that TKIs are often added to, ImClone developed two neutralizing monoclonal anti-FLT3 antibodies, IMC-EB10 and IMC-NC7 (Y. Li et al. 2004). Antibodies do confer a high specificity, a high binding affinity and are often better tolerated than non-specific kinase inhibitors, as has been demonstrated by the observation that the maximum tolerated dose of some drugs was not always sufficient to achieve an adequate response (Stone et al. 2005; B. D. Smith et al. 2004; Knapper et al. 2006). Both antibodies were able to block FL-mediated FLT3 activation to a different degree, and were shown to partially inhibit mutant FLT3 in Ba/F3 transfected cells – but surprisingly not in primary AML samples (Piloto et al. 2005). Although unable to induce a cytotoxic response by themselves, both effectively resulted in cell lysis of FLT3-expressing cells *in vitro* through the antibody-dependent cell-mediated cytotoxicity pathway – although this effect was mainly observed for IMC-EB10. Inoculation of nude mice with mutant FLT3-transfected Ba/F3 cell lines, could furthermore show that IMC-EB10 treatment significantly prolonged the survival of mice, although by an unknown mechanism (Y. Li et al. 2004). The absence of FLT3 inhibition on primary AML samples and the poorly-understood effect of these antibodies on ITD-mutated FLT3 signaling notwithstanding, a phase 1 clinical study was performed to test the efficacy and safety of IMC-EB10 in patients with relapsed AML. As it has been shown that the oncogenic cell population at relapse is often more addicted to FLT3 signaling than at diagnosis, this choice of patient population is arguably the reason for the observed lack of efficacy in treatment of these patients (Sanford et al. 2015; Kottaridis et al. 2002; Levis 2011b; Y. Nakano et al. 1999; Reiter et al. 2018; L. Shih et al. 2018). Although abandoned shortly after these results, the antibody is now being tested in a pre-clinical AML setting as an Fc-optimized variant by Synimmune (Synimmune n.d.).

3.2.2. Bispecific FLT3- and CD3- targeting antibody

Already in the mid-eighties it has been demonstrated that bispecific antibodies can exert an agonistic effect on T-cell receptors by binding the CD3 complex (Staerz, Kanagawa, and Bevan 1985; Perez et al. 1985; Jung, Ledbetter, and Müller-Eberhard 1987). As such, those antibodies are able to activate T-cells, resulting in the lysis of specifically cells targeted by the second Fab moiety of the antibody (Staerz, Kanagawa, and Bevan 1985; Perez et al. 1985; Jung, Ledbetter, and Müller-Eberhard 1987). Indeed, Durben and colleagues have already described how such engineered antibody variant induced T-cell activation, T-cell proliferation and resulted in a reduction of leukemic cells in 8 out of 9 PBMC preparations of AML patients (Durben et al. 2015).

Interest in such approach appears to be not limited to the academic setting, as both Amgen and Pfizer seem to have developed full-length anti-FLT3xCD3 bispecific antibodies (Djuretic et al. n.d.; Goldstein et al. 2017; patent WO/2017/021362). Interestingly, whereas the poster publication of Pfizer notes that targeting extracellular domain 4 of FLT3 seems to result in a more effective AML cell depletion, Amgen does not disclose the binding epitope of their so-called FLT3 Bite[®] species. However, one Amgen patent does explicitly mention targeting of the pre-domain 1 region of FLT3 to prevent any

competition with ligand binding. However, without the availability of data for any, the choice of strategy in terms of success remains to be seen. Furthermore, as it has been shown that constitutive activated forms of FLT3 reside predominantly intracellular, addition of TKIs might be required to elicit a clinical response in FLT3-mutated AML patients (Schmidt-Arras et al. 2005; Choudhary et al. 2009; Reiter et al. 2018). Indeed, membrane-expression levels of oncogenic FLT3 variants in certain AML patient-derived xenografts and AML cell lines can be restored by addition of quizartinib and crenolanib, and has shown to considerably increase T-cell mediated cytotoxicity in cell lines heterozygous or homozygous for oncogenic FLT3 variants (Jetani et al. 2018; Reiter et al. 2018).

3.2.3. The extracellular small-molecule inhibitor BDT001

In a recent paper, Rivat and colleagues establish FLT3 as a target for the alleviation of peripheral neuropathic pain (PNP) in mice (Rivat et al. 2018). Using the X-ray structure of FLT3 in complex with its activating ligand FL, *in silico* screening of approximately 3 million commercially available compounds resulted in the identification and validation of BDT001 as an inhibitor of FL-induced receptor activation. Interestingly, they showed that BDT001 inhibited FLT3 phosphorylation in an FL-independent fashion, suggesting that BDT001 is an FLT3 negative allosteric modulator. As the focus of this research was in the field of PNP, we can only wonder about the effect of this first-in-class FLT3 modulator in AML.

4. Outlook

Our lab was the first to describe the structural principles underlying the assembly of an extracellular FL:FLT3 complex (Verstraete et al. 2011). Supported by calorimetric titration experiments featuring various truncated variants of FLT3 and comparisons with homologous RTK-III and -V, an activation paradigm was proposed in which ligand-induced receptor contacts were conspicuously absent. However, the notion that the most plausible molecular mechanism underlying two point mutations, discovered in patients and confirmed *in vitro* to be oncogenic, implied receptor contacts similar to its RTK-III siblings, motivated us to revisit the possibility of ligand-induced receptor contacts in Chapter B.

The importance of in-depth insights into the basic principles behind the initial step in FLT3 activation, becomes increasingly clear upon studying the observations of FL-mediated TKI resistance. Although this phenomenon explains why almost all FLT3-targeting TKIs fail to keep patients into sustained complete remission, and is implied to be at the root of the clinical failure of the inhibitor lestaurtinib, it is still poorly understood – if at all. In Chapter C, we present preliminary data connecting several data points in literature that for the first time provide a possible mechanism.

In conclusion, both industry and academia have for more than two decades intensively focused on FLT3 for establishing new drugs, classifying patients, determining prognoses, and as indicator for minimal residual disease. However, until the FDA approval of midostaurin for first-line treatment of FLT3-mutated AML last year, this field of oncology was nevertheless one of the only remaining without any targeted therapies available, which can be considered illustrative of the rather disappointing results all previous clinical phases concluded with. Even though addition of midostaurin to 7 + 3 induction and consolidation regimens resulting in a 23% reduction in risk of death, is an important

achievement for AML patients, a 4-year overall survival of 51.4% shows there is still a long way ahead. The work presented in this doctoral thesis aims to extend our current knowledge regarding FLT3 biology, and will hopefully contribute towards increasing the prospects of AML patients.

5. References

- Alexander, Thomas B., Zhaohui Gu, Ilaria Iacobucci, Kirsten Dickerson, John K. Choi, Beisi Xu, Debbie Payne-Turner, et al. 2018. *The Genetic Basis and Cell of Origin of Mixed Phenotype Acute Leukaemia*. *Nature*. Vol. 562. Springer US. <https://doi.org/10.1038/s41586-018-0436-0>.
- Alexander, Thomas B., Lei Wang, Hiroto Inaba, Brandon M. Triplett, Stanley Pounds, Raul C. Ribeiro, Ching Hon Pui, and Jeffrey E. Rubnitz. 2017. "Decreased Relapsed Rate and Treatment-Related Mortality Contribute to Improved Outcomes for Pediatric Acute Myeloid Leukemia in Successive Clinical Trials." *Cancer*. <https://doi.org/10.1002/cncr.30791>.
- Arber, D.A., A. Orazi, R. Hasserjian, M.J. Borowitz, M.M. Beau Le, C.D. Bloomfield, M. Cazzola, and J.W. Vardiman. 2016. "The 2016 Revision to the World Health Organization Classification of Myeloid Neoplasms and Acute Leukemia." *Blood* 127 (20): 2391–2406. <https://doi.org/10.1182/blood-2016-03-643544>.
- Auclair, D., D. Miller, V. Yatsula, W. Pickett, C. Carter, Y. Chang, X. Zhang, et al. 2007. "Antitumor Activity of Sorafenib in FLT3-Driven Leukemic Cells." *Leukemia*. <https://doi.org/10.1038/sj.leu.2404508>.
- Bacher, Ulrike, Susanne Schnittger, and Torsten Haferlach. 2010. "Molecular Genetics of Acute Myeloid Leukemia." *Current Opinion in Oncology* 22: 646–55. <https://doi.org/10.1017/CBO9780511471001.012>.
- Badar, Talha, Hagop M. Kantarjian, Graciela M. Nogueras-Gonzalez, Gautam Borthakur, Guillermo Garcia Manero, Michael Andreeff, Marina Konopleva, et al. 2015. "Improvement in Clinical Outcome of FLT3 ITD Mutated Acute Myeloid Leukemia Patients over the Last One and a Half Decade." *American Journal of Hematology* 90 (11): 1065–70. <https://doi.org/10.1002/ajh.24140>.
- Bain, Calum C., Alberto Bravo-Blas, Charlotte L. Scott, Elisa Gomez Perdiguero, Frederic Geissmann, Sandrine Henri, Bernard Malissen, Lisa C. Osborne, David Artis, and Allan Mc I. Mowat. 2014. "Constant Replenishment from Circulating Monocytes Maintains the Macrophage Pool in the Intestine of Adult Mice." *Nature Immunology*. <https://doi.org/10.1038/ni.2967>.
- Beaudin, Anna E, Scott W Boyer, and E Camilla Forsberg. 2014. "Flk2/Flt3 Promotes Both Myeloid and Lymphoid Development by Expanding Non-Self-Renewing Multipotent Hematopoietic Progenitor Cells." *Experimental Hematology* 42 (3): 218–229.e4. <https://doi.org/10.1016/j.exphem.2013.11.013>.
- Becker, Geneviève De, Véronique Moulin, Françoise Tielemans, Fabrizio De Mattia, Jacques Urbain, Oberdan Leo, and Muriel Moser. 1998. "Regulation of T Helper Cell Differentiation in Vivo by Soluble and Membrane Proteins Provided by Antigen-Presenting Cells." *European Journal of Immunology*. [https://doi.org/10.1002/\(SICI\)1521-4141\(199810\)28:10<3161::AID-IMMU3161>3.0.CO;2-Q](https://doi.org/10.1002/(SICI)1521-4141(199810)28:10<3161::AID-IMMU3161>3.0.CO;2-Q).
- Bolouri, Hamid, Jason E. Farrar, Timothy Triche, Rhonda E. Ries, Emilia L. Lim, Todd A. Alonzo, Yussanne Ma, et al. 2018. "The Molecular Landscape of Pediatric Acute Myeloid Leukemia Reveals Recurrent Structural Alterations and Age-Specific Mutational Interactions." *Nature Medicine* 24 (1): 103–12. <https://doi.org/10.1038/nm.4439>.
- Boyer, Scott W., Aaron V. Schroeder, Stephanie Smith-Berdan, and E. Camilla Forsberg. 2011. "All Hematopoietic Cells Develop from Hematopoietic Stem Cells through Flk2/Flt3-Positive Progenitor Cells." *Cell Stem Cell* 9 (1): 64–73. <https://doi.org/10.1016/j.stem.2011.04.021>.
- Breitenbuecher, Frank, Susanne Schnittger, Rebekka Grundler, Boyka Markova, Birgit Carius, Alexandra Brecht, Justus Duyster, Torsten Haferlach, Christoph Huber, and Thomas Fischer. 2009. "Identification of a Novel Type of ITD Mutations Located in Nonjuxtamembrane Domains of the FLT3 Tyrosine Kinase Receptor." *Blood*. <https://doi.org/10.1182/blood-2007-11-125476>.

- Brunet, Salut, Myriam Labopin, Jordi Esteve, Jan Cornelissen, Gerard Socié, Anna P. Iori, Leo F. Verdonck, et al. 2012. "Impact of FLT3 Internal Tandem Duplication on the Outcome of Related and Unrelated Hematopoietic Transplantation for Adult Acute Myeloid Leukemia in First Remission: A Retrospective Analysis." *Journal of Clinical Oncology* 30 (7): 735–41. <https://doi.org/10.1200/JCO.2011.36.9868>.
- Castilla, Lucio H., Cisca Wijmenga, Qing Wang, Terryl Stacy, Nancy A. Speck, Michael Eckhaus, Miguel Marín-Padilla, Francis S. Collins, Anthony Wynshaw-Boris, and Pu P. Liu. 1996. "Failure of Embryonic Hematopoiesis and Lethal Hemorrhages in Mouse Embryos Heterozygous for a Knocked-in Leukemia Gene CFBF-MYH11." *Cell*. [https://doi.org/10.1016/S0092-8674\(00\)81388-4](https://doi.org/10.1016/S0092-8674(00)81388-4).
- Choudhary, Chunaram, Jesper V. Olsen, Christian Brandts, Jürgen Cox, Pavankumar N G Reddy, Frank D. Böhmer, Volker Gerke, et al. 2009. "Mislocalized Activation of Oncogenic RTKs Switches Downstream Signaling Outcomes." *Molecular Cell* 36 (2): 326–39. <https://doi.org/10.1016/j.molcel.2009.09.019>.
- Colonna, Marco, Giorgio Trinchieri, and Yong Jun Liu. 2004. "Plasmacytoid Dendritic Cells in Immunity." *Nature Immunology*. <https://doi.org/10.1038/ni1141>.
- Cook, Amy M., Liang Li, Yinwei Ho, Allen Lin, Ling Li, Anthony Stein, Stephen Forman, Danilo Perrotti, Richard Jove, and Ravi Bhatia. 2014. "Role of Altered Growth Factor Receptor-Mediated JAK2 Signaling in Growth and Maintenance of Human Acute Myeloid Leukemia Stem Cells." *Blood*. <https://doi.org/10.1182/blood-2013-05-505735>.
- Cortes, Jorge E., Hagop Kantarjian, James M. Foran, Darejan Ghirdaladze, Mamia Zodelava, Gautam Borthakur, Guy Gammon, et al. 2013. "Phase I Study of Quizartinib Administered Daily to Patients with Relapsed or Refractory Acute Myeloid Leukemia Irrespective of FMS-like Tyrosine Kinase 3-Internal Tandem Duplication Status." *Journal of Clinical Oncology: Official Journal of the American Society of Clinical Oncology* 31 (29): 3681–87. <https://doi.org/10.1200/JCO.2013.48.8783>.
- Cortes, Jorge, Samer Khaled, Giovanni Martinelli, Alexander E. Perl, Siddhartha Ganguly, Nigel Rusell, Alwin Krämer, et al. 2018. "Quizartinib Significantly Prolongs Overall Survival in Patients with FLT3-Internal Tandem Duplication-Mutated (MUT) Relapsed/Refractory AML in the Phase 3, Randomized, Controlled QUANTUM-R Trial." 16 Jun. 2018. https://learningcenter.ehaweb.org/eha/2018/stockholm/218882/jorge.cortes.quizartinib.significantly.prolongs.overall.survival.in.patients.html?f=topic=1574*media=3.
- Davis, Julian R., David J. Benjamin, and Brian A. Jonas. 2018. "New and Emerging Therapies for Acute Myeloid Leukaemia." *Journal of Investigative Medicine*, 1–8. <https://doi.org/10.1136/jim-2018-000807>.
- Deschler, Barbara, Gabriele Ihorst, Uwe Platzbecker, Ulrich Germing, Eva März, Marcelo De Figuerido, Kurt Fritzsche, et al. 2013. "Parameters Detected by Geriatric and Quality of Life Assessment in 195 Older Patients with Myelodysplastic Syndromes and Acute Myeloid Leukemia Are Highly Predictive for Outcome." *Haematologica*. <https://doi.org/10.3324/haematol.2012.067892>.
- Dieu, M C, B Vanbervliet, A Vicari, J M Bridon, E Oldham, S Aït-Yahia, F Brière, A Zlotnik, S Lebecque, and C Caux. 1998. "Selective Recruitment of Immature and Mature Dendritic Cells by Distinct Chemokines Expressed in Different Anatomic Sites." *J. Exp. Med.* <https://doi.org/10.1084/jem.188.2.373>.
- Ding, Li, Timothy J. Ley, David E. Larson, Christopher a. Miller, Daniel C. Koboldt, John S. Welch, Julie K. Ritchey, et al. 2012. "Clonal Evolution in Relapsed Acute Myeloid Leukaemia Revealed by Whole-Genome Sequencing." *Nature* 481 (7382): 506–10. <https://doi.org/10.1038/nature10738>.
- Djuretic, Ivana, Veena Krishnamoorthy, Cesar Sommer, Danielle Dettling, Kris Poulsen, Wei Chen, Hu

- Wenyeu, et al. n.d. "Poster Abstract: A Novel Full Length Anti-FLT3 CD3 Bispecific Antibody for the Treatment of Acute Myeloid Leukemia." *ASH Annual Meeting*, Abstract 1445 Session 616.
- Döhner, Hartmut, Elihu Estey, David Grimwade, Sergio Amadori, Frederick R Appelbaum, Thomas Büchner, Hervé Dombret, et al. 2017. "Review Article Diagnosis and Management of AML in Adults : 2017 ELN Recommendations from an International Expert Panel." *Blood* 129 (4): 424–48. <https://doi.org/10.1182/blood-2016-08-733196.424>.
- Döhner, Hartmut, Daniel J. Weisdorf, and Clara D. Bloomfield. 2015. "Acute Myeloid Leukemia." *The New England Journal of Medicine* 373 (12): 1136–52. <https://doi.org/10.1056/NEJMra1406184>.
- Dosil, Mercedes, Shulin Wang, and Ihor R Lemischka. 1993. "Mitogenic Signalling and Substrate Specificity of the Flk2/Flt3 Receptor Tyrosine Kinase in Fibroblasts and Interleukin 3-Dependent Hematopoietic Cells." *Molecular and Cellular Biology*. <https://doi.org/10.1128/MCB.13.10.6572>. Updated.
- Durben, Michael, Dominik Schmiedel, Martin Hofmann, Fabian Vogt, Tina Nübling, Elwira Pyz, Hans Jörg Bühring, et al. 2015. "Characterization of a Bispecific FLT3 X CD3 Antibody in an Improved, Recombinant Format for the Treatment of Leukemia." *Molecular Therapy* 23 (4): 648–55. <https://doi.org/10.1038/mt.2015.2>.
- Eda, Hiroyuki, Jian Zhang, Robert H Keith, Marshall Michener, David R Beidler, and Joseph B Monahan. 2010. "Macrophage-Colony Stimulating Factor and Interleukin-34 Induce Chemokines in Human Whole Blood." *Cytokine* 52 (3): 215–20. <http://www.ncbi.nlm.nih.gov/pubmed/20829061>.
- Edelson, Brian T., Wumesh KC, Richard Juang, Masako Kohyama, Loralyn A. Benoit, Paul A. Klekotka, Clara Moon, et al. 2010. "Peripheral CD103⁺ Dendritic Cells Form a Unified Subset Developmentally Related to CD8 α ⁺ Conventional Dendritic Cells." *The Journal of Experimental Medicine*. <https://doi.org/10.1084/jem.20091627>.
- Elegheert, Jonathan, Ambroise Desfosses, Alexander V Shkumatov, Xiongwu Wu, Nathalie Bracke, Kenneth Verstraete, Kathleen Van Craenenbroeck, et al. 2011. "Extracellular Complexes of the Hematopoietic Human and Mouse CSF-1 Receptor Are Driven by Common Assembly Principles." *Structure* 19 (12): 1762–72. <https://doi.org/10.1016/j.str.2011.10.012>.
- Fiedler, Walter, Sabine Kayser, Maxim Kebenko, Melanie Janning, Jürgen Krauter, Marcus Schittenhelm, Katharina Götze, et al. 2015. "A Phase I/II Study of Sunitinib and Intensive Chemotherapy in Patients over 60 Years of Age with Acute Myeloid Leukaemia and Activating FLT3 Mutations." *British Journal of Haematology* 169 (5): 694–700. <https://doi.org/10.1111/bjh.13353>.
- Fiedler, Walter, Hubert Serve, Hartmut Döhner, Michael Schwittay, Oliver G. Ottmann, Anne Marie O'Farrell, Carlo L. Bello, et al. 2005. "A Phase 1 Study of SU11248 in the Treatment of Patients with Refractory or Resistant Acute Myeloid Leukemia (AML) or Not Amenable to Conventional Therapy for the Disease." *Blood* 105 (3): 986–93. <https://doi.org/10.1182/blood-2004-05-1846>.
- Forbes, S A, G Bhamra, S Bamford, E Dawson, C Kok, J Clements, A Menzies, J W Teague, P A Futreal, and M R Stratton. 2008. "The Catalogue of Somatic Mutations in Cancer (COSMIC)." Edited by Jonathan L Haines, Bruce R Korf, Cynthia C Morton, Christine E Seidman, J G Seidman, and Douglas R Smith. *Current Protocols in Human Genetics Editorial Board Jonathan L Haines et Al* Chapter 10 (March): Unit 10.11. <http://www.pubmedcentral.nih.gov/articlerender.fcgi?artid=2705836&tool=pmcentrez&render type=abstract>.
- Forbes, S A, Nidhi Bindal, Sally Bamford, Charlotte Cole, Chai Yin Kok, David Beare, Mingming Jia, et al. 2011. "COSMIC: Mining Complete Cancer Genomes in the Catalogue of Somatic Mutations in Cancer." *Nucleic Acids Research* 39 (Database issue): D945-50. <https://doi.org/10.1093/nar/gkq929>.

- Fröhling, Stefan, Richard F. Schlenk, Jochen Breitruck, Axel Benner, Sylvia Kreitmeier, Karen Tobis, Hartmut Döhner, and Konstanze Döhner. 2002. "Prognostic Significance of Activating FLT3 Mutations in Younger Adults (16 to 60 Years) with Acute Myeloid Leukemia and Normal Cytogenetics: A Study of the AML Study Group Ulm." *Blood* 100 (13): 4372–80. <https://doi.org/10.1182/blood-2002-05-1440>.
- Fröhling, Stefan, Claudia Scholl, Ross L. Levine, Marc Loriaux, Titus J. Boggon, Olivier a. Bernard, Roland Berger, et al. 2007. "Identification of Driver and Passenger Mutations of FLT3 by High-Throughput DNA Sequence Analysis and Functional Assessment of Candidate Alleles." *Cancer Cell* 12 (6): 501–13. <https://doi.org/10.1016/j.ccr.2007.11.005>.
- Galanis, Allison, Hayley Ma, Trivikram Rajkhowa, Abhijit Ramachandran, Donald Small, Jorge Cortes, and Mark Levis. 2014. "Crenolanib Is a Potent Inhibitor of Flt3 with Activity against Resistance-Confering Point Mutants." *Blood* 123 (1): 94–100. <https://doi.org/10.1182/blood-2013-10-529313>.
- Galloway, Jenna L, and Leonard I Zon. 2003. "3 Ontogeny of Hematopoiesis: Examining the Emergence of Hematopoietic Cells in the Vertebrate Embryo" 53: 139–58. [https://doi.org/10.1016/S0070-2153\(03\)53004-6](https://doi.org/10.1016/S0070-2153(03)53004-6).
- Ghoshal (Gupta), Sampa, Heinz Baumann, and Meir Wetzler. 2008. "Epigenetic Regulation of Signal Transducer and Activator of Transcription 3 in Acute Myeloid Leukemia." *Leukemia Research*. <https://doi.org/10.1016/j.leukres.2007.11.035>.
- Giles, Francis J., Gautam Borthakur, Farhad Ravandi, Stefan Faderl, Srdan Verstovsek, Deborah Thomas, William Wierda, et al. 2007. "The Haematopoietic Cell Transplantation Comorbidity Index Score Is Predictive of Early Death and Survival in Patients over 60 Years of Age Receiving Induction Therapy for Acute Myeloid Leukaemia." *British Journal of Haematology*. <https://doi.org/10.1111/j.1365-2141.2006.06476.x>.
- Gilliland, D Gary, and James D Griffin. 2002. "The Roles of FLT3 in Hematopoiesis and Leukemia." *Blood* 100: 1532–42.
- Goldstein, Rebecca, Anja Henn, Priya Koppikar, Ivonne Archibeque, Brendon Frank, Mercedesz Balazs, Christoph Dahlhoff, et al. 2017. "Abstract: Evaluation of a FLT3 Bite for Acute Myeloid Leukemia." *Blood* 130 (Suppl 1): 1354.
- Griffith, James, James Black, Carlos Faerman, Lora Swenson, Michael Wynn, Fan Lu, Judith Lippke, and Kumkum Saxena. 2004. "The Structural Basis for Autoinhibition of FLT3 by the Juxtamembrane Domain." *Molecular Cell* 13 (2): 169–78. [https://doi.org/10.1016/S1097-2765\(03\)00505-7](https://doi.org/10.1016/S1097-2765(03)00505-7).
- Grunwald, Michael R., and Mark J. Levis. 2013. "FLT3 Inhibitors for Acute Myeloid Leukemia: A Review of Their Efficacy and Mechanisms of Resistance." *International Journal of Hematology* 97 (6): 683–94. <https://doi.org/10.1007/s12185-013-1334-8>.
- Guilliams, Martin, F Ginhoux, C Jakubzick, S H Naik, N Onai, B U Schraml, E Segura, R Tussiwand, and S Yona. 2014. "Dendritic Cells, Monocytes and Macrophages: A Unified Nomenclature Based on Ontogeny." *Nat Rev Immunol* 14 (8): 571–78. <https://doi.org/10.1038/nri3712>.
- Guilliams, Martin, Alexander Mildner, and Simon Yona. 2018. "Developmental and Functional Heterogeneity of Monocytes." *Immunity* 49 (4): 595–613. <https://doi.org/10.1016/j.immuni.2018.10.005>.
- Heuser, Michael, Felicitas Thol, and Arnold Ganser. 2016. "Clonal Hematopoiesis of Indeterminate Potential." *Deutsches Aerzteblatt Online*, 317–22. <https://doi.org/10.3238/arztebl.2016.0317>.
- Ho, Anthony D., Johannes Schetelig, Tilmann Bochtler, Markus Schaich, Kerstin Schäfer-Eckart, Mathias Hänel, Wolf Rösler, et al. 2015. "Allogeneic Stem Cell Transplantation Improves Survival in Patients with Acute Myeloid Leukemia Characterized by a High Allelic Ratio of Mutant FLT3-

- ITD.” *Biology of Blood and Marrow Transplantation*.
<https://doi.org/10.1016/j.bbmt.2015.10.023>.
- Hoeffel, Guillaume, Jinmiao Chen, Yonit Lavin, Donovan Low, Francisca F. Almeida, Peter See, Anna E. Beaudin, et al. 2015. “C-Myb+Erythro-Myeloid Progenitor-Derived Fetal Monocytes Give Rise to Adult Tissue-Resident Macrophages.” *Immunity* 42 (4): 665–78.
<https://doi.org/10.1016/j.immuni.2015.03.011>.
- Hu, Bei, Praveen Vikas, Mohamad Mohty, and Bipin N. Savani. 2014. “Allogeneic Stem Cell Transplantation and Targeted Therapy for FLT3/ITD+ Acute Myeloid Leukemia: An Update.” *Expert Review of Hematology* 7 (2): 301–15. <https://doi.org/10.1586/17474086.2014.857596>.
- Jagannathan-Bogdan, Madhumita, and Leonard I. Zon. 2013. “Hematopoiesis.” *Development*, no. 140: 2463–67. <https://doi.org/10.1016/B978-0-12-374984-0.00686-0>.
- Jetani, Hardikkumar, Irene Garcia-Cadenas, Thomas Nerreter, Simone Thomas, Julian Rydzek, Javier Briones Meijide, Halvard Bonig, et al. 2018. “CAR T-Cells Targeting FLT3 Have Potent Activity against FLT3-ITD+AML and Act Synergistically with the FLT3-Inhibitor Crenolanib.” *Leukemia* 32 (5): 1168–79. <https://doi.org/10.1038/s41375-018-0009-0>.
- Jiang, Jingrui, J Guillermo Paez, Jeffrey C Lee, Ronghai Bo, Richard M Stone, Daniel J DeAngelo, Ilene Galinsky, et al. 2005. “Identifying and Characterizing a Novel Activating Mutation of the FLT3 Tyrosine Kinase in AML.” In *Cellular and Molecular Biology Abstracts*. Vol. 55. <http://www.ncbi.nlm.nih.gov/pubmed/15178581>.
- Jung, G, JA Ledbetter, and HJ Müller-Eberhard. 1987. “Induction of Cytotoxicity in Resting Human T Lymphocytes Bound to Tumor Cells by Antibody Heteroconjugates.” *Proc. Natl. Acad. Sci. USA* 84 (13): 4611–15.
- Kantarjian, Hagop, Susan O’Brisn, Jorge Cortes, Francis Giles, Stefan Faderl, Elias Jabbour, Guillermo Garcia-Manero, et al. 2006. “Results of Intensive Chemotherapy in 998 Patients Age 65 Years or Older with Acute Myeloid Leukemia or High-Risk Myelodysplastic Syndrome: Predictive Prognostic Models for Outcome.” *Cancer*. <https://doi.org/10.1002/cncr.21723>.
- Kelly, L. M., J. L. Kutok, I. R. Williams, C. L. Boulton, S. M. Amaral, D. P. Curley, T. J. Ley, and D. G. Gilliland. 2002. “PML/RAR and FLT3-ITD Induce an APL-like Disease in a Mouse Model.” *Proceedings of the National Academy of Sciences*. <https://doi.org/10.1073/pnas.122233699>.
- Kiyoi, H., M. Towatari, S. Yokota, M. Hamaguchi, R. Ohno, H. Saito, and T. Naoe. 1998a. “Internal Tandem Duplication of the FLT3 Gene Is a Novel Modality of Elongation Mutation Which Causes Constitutive Activation of the Product.” *Leukemia* 12 (9): 1333–37. <https://doi.org/10.1038/sj.leu.2401130>.
- Kiyoi, H, Tomoki Naoe, Yasuyuki Nakano, Shohei Yokota, Saburo Minami, Shuichi Miyawaki, Norio Asou, et al. 1999. “Prognostic Implication of FLT3 and N-RAS Gene Mutations in Acute Myeloid Leukemia.” *Blood* 93 (9): 3074–80. <https://doi.org/10.1182/blood.v99.12.4326>.
- Kiyoi, H, M Towatari, S Yokota, M Hamaguchi, R Ohno, H Saito, and T Naoe. 1998b. “Internal Tandem Duplication of the FLT3 Gene Is a Novel Modality of Elongation Mutation Which Causes Constitutive Activation of the Product.” *Leukemia : Official Journal of the Leukemia Society of America, Leukemia Research Fund, U.K* 12 (9): 1333–37. <https://doi.org/10.1038/sj.leu.2401130>.
- Klepin, Heidi D. 2014. “Geriatric Perspective: How to Assess Fitness for Chemotherapy in Acute Myeloid Leukemia.” *Hematology*. <https://doi.org/10.1182/asheducation-2014.1.8>.
- Klepin, Heidi D., Ann M. Geiger, Janet A. Tooze, Stephen B. Kritchevsky, Jeff D. Williamson, Timothy S. Pardee, Leslie R. Ellis, and Bayard L. Powell. 2013. “Geriatric Assessment Predicts Survival for Older Adults Receiving Induction Chemotherapy for Acute Myelogenous Leukemia.” *Blood*. <https://doi.org/10.1182/blood-2012-12-471680>.

- Klug, Lillian R., Jason D. Kent, and Michael C. Heinrich. 2018. "Structural and Clinical Consequences of Activation Loop Mutations in Class III Receptor Tyrosine Kinases." *Pharmacology and Therapeutics*. <https://doi.org/10.1016/j.pharmthera.2018.06.016>.
- Knapper, Steven, Alan K. Burnett, Tim Littlewood, W. Jonathan Kell, Sam Agrawal, Raj Chopra, Richard Clark, Mark J. Levis, and Donald Small. 2006. "A Phase 2 Trial of the FLT3 Inhibitor Lestaurtinib (CEP701) as First-Line Treatment for Older Patients with Acute Myeloid Leukemia Not Considered Fit for Intensive Chemotherapy." *Blood* 108 (10): 3262–70. <https://doi.org/10.1182/blood-2006-04-015560>.
- Knapper, Steven, Nigel Russell, Amanda Gilkes, Robert K. Hills, Rosemary E. Gale, James D. Cavenagh, Gail Jones, et al. 2017. "A Randomized Assessment of Adding the Kinase Inhibitor Lestaurtinib to First-Line Chemotherapy for FLT3-Mutated AML." *Blood* 129 (9): 1143–54. <https://doi.org/10.1182/blood-2016-07-730648>.
- Kottaridis, Panagiotis D., Rosemary E. Gale, Stephen E. Langabeer, Marion E. Frew, David T. Bowen, and David C. Linch. 2002. "Studies of FLT3 Mutations in Paired Presentation and Relapse Samples from Patients with Acute Myeloid Leukemia: Implications for the Role of FLT3 Mutations in Leukemogenesis, Minimal Residual Disease Detection, and Possible Therapy with FLT3 Inhibitors." *Blood* 100 (7): 2393–98. <https://doi.org/10.1182/blood-2002-02-0420>.
- Kouchkovsky, I De, and M Abdul-Hay. 2016. "Acute Myeloid Leukemia: A Comprehensive Review and 2016 Update." *Blood Cancer Journal* 6 (7): e441. <https://doi.org/10.1038/bcj.2016.50>.
- Larsen, C P, S C Ritchie, Thomas C Pearson, Peter S Linsley, and Robin P Lowry. 1992. "Functional Expression of the Costimulatory Molecule, B7/BB1, on Murine Dendritic Cell Populations." *The Journal of Experimental Medicine*. <https://doi.org/10.1002/eji.201040913>.
- Lau, Colleen M., Simone A. Nish, Nir Yogev, Ari Waisman, Steven L. Reiner, and Boris Reizis. 2016. "Leukemia-Associated Activating Mutation of Flt3 Expands Dendritic Cells and Alters T Cell Responses." *The Journal of Experimental Medicine* 213 (3): 415–31. <https://doi.org/10.1084/jem.20150642>.
- Lavagna-Sévenier, C., S. Marchetto, D. Birnbaum, and O. Rosnet. 1998. "FLT3 Signaling in Hematopoietic Cells Involves CBL, SHC and an Unknown P115 as Prominent Tyrosine-Phosphorylated Substrates." *Leukemia*. <https://doi.org/10.1038/sj.leu.2400921>.
- Lee, Benjamin H., Zuzana Tothova, Ross L. Levine, Kristina Anderson, Natalija Buza-Vidas, Dana E E. Cullen, Elizabeth P. McDowell, et al. 2007. "FLT3 Mutations Confer Enhanced Proliferation and Survival Properties to Multipotent Progenitors in a Murine Model of Chronic Myelomonocytic Leukemia." *Cancer Cell*. <https://doi.org/10.1016/j.ccr.2007.08.031>.
- Lee, Lauren Y., Daniela Hernandez, Trivikram Rajkhowa, Samuel C. Smith, Jayant Ranganathan Raman, Bao Nguyen, Donald Small, and Mark Levis. 2017. "Preclinical Studies of Gilteritinib, a next-Generation FLT3 Inhibitor." *Blood*. <https://doi.org/10.1109/TMAG.2017.2762351>.
- Leick, Mark B., and Mark J. Levis. 2017. "The Future of Targeting FLT3 Activation in AML." *Current Hematologic Malignancy Reports*, 1–15. <https://doi.org/10.1007/s11899-017-0381-2>.
- Lemmon, Mark a, and Joseph Schlessinger. 2010. "Cell Signaling by Receptor Tyrosine Kinases." *Cell* 141 (7): 1117–34. <https://doi.org/10.1016/j.cell.2010.06.011>.
- Levis, Mark. 2011. "FLT3/ITD AML and the Law of Unintended Consequences." *Blood* 117 (26): 6987–90. <https://doi.org/10.1182/blood-2011-03-340273>.
- Levis, Mark, Farhad Ravandi, Eunice S. Wang, Maria R. Baer, Alexander Perl, Steven Coutre, Harry Erba, et al. 2011. "Results from a Randomized Trial of Salvage Chemotherapy Followed by Lestaurtinib for Patients with FLT3 Mutant AML in First Relapse." *Blood* 117 (12): 3294–3301. <https://doi.org/10.1182/blood-2010-08-301796>.

- Lewis, Nancy L., Lionel D. Lewis, Joseph P. Eder, Nandi J. Reddy, Feng Guo, Kristen J. Pierce, Anthony J. Olszanski, and Roger B. Cohen. 2009. "Phase I Study of the Safety, Tolerability, and Pharmacokinetics of Oral CP-868,596, a Highly Specific Platelet-Derived Growth Factor Receptor Tyrosine Kinase Inhibitor in Patients with Advanced Cancers." *Journal of Clinical Oncology* 27 (31): 5262–69. <https://doi.org/10.1200/JCO.2009.21.8487>.
- Ley, Timothy J., Li Ding, Benjamin J Raphael, Andrew J Mungall, and et al. 2013. "Genomic and Epigenomic Landscapes of Adult De Novo Acute Myeloid Leukemia The Cancer Genome Atlas Research Network." *The New England Journal of Medicine*. <https://doi.org/10.1056/NEJMoa1301689>.
- Ley, Timothy J., Li Ding, Matthew J. Walter, Michael D. McLellan, Tamara Lamprecht, David E. Larson, Cyriac Kandoth, et al. 2010. "DNMT3A Mutations in Acute Myeloid Leukemia." *New England Journal of Medicine*. <https://doi.org/10.1056/NEJMoa1005143>.
- Li, Li, Obdulio Piloto, Ho Bao Nguyen, Kathleen Greenberg, Kogo Takamiya, Frederick Racke, David Huso, and Donald Small. 2008. "Knock-in of an Internal Tandem Duplication Mutation into Murine FLT3 Confers Myeloproliferative Disease in a Mouse Model." *Blood*. <https://doi.org/10.1182/blood-2007-08-109942>.
- Li, W, and E R Stanley. 1991. "Role of Dimerization and Modification of the CSF-1 Receptor in Its Activation and Internalization during the CSF-1 Response." *The EMBO Journal*.
- Li, Yiwen, Hongli Li, Mei Nai Wang, Dan Lu, Rajiv Bassi, Yan Wu, Haifan Zhang, et al. 2004. "Suppression of Leukemia Expressing Wild-Type or ITD-Mutant FLT3 Receptor by a Fully Human Anti-FLT3 Neutralizing Antibody." *Blood* 104 (4): 1137–44. <https://doi.org/10.1182/blood-2003-07-2585>.
- Liang, Ling, Xiao E. Yan, Yuxin Yin, and Cai Hong Yun. 2016. "Structural and Biochemical Studies of the PDGFRA Kinase Domain." *Biochemical and Biophysical Research Communications* 477 (4): 667–72. <https://doi.org/10.1016/j.bbrc.2016.06.117>.
- Litzow, Mark R., and Adolfo A. Ferrando. 2015. "How I Treat T-Cell Acute Lymphoblastic Leukemia in Adults." *Blood*. <https://doi.org/10.1182/blood-2014-10-551895>.
- Luppi, Mario, Francesco Fabbiano, Giuseppe Visani, Giovanni Martinelli, and Adriano Venditti. 2018. "Novel Agents for Acute Myeloid Leukemia." *Cancers* 10 (11): 429. <https://doi.org/10.3390/cancers10110429>.
- Lyman, S D, L James, J Zappone, P R Sleath, M P Beckmann, and T Bird. 1993. "Characterization of the Protein Encoded by the Flt3 (Flk2) Receptor-like Tyrosine Kinase Gene." *Oncogene*.
- Man, Cheuk Him, Tsz Kan Fung, Christa Ho, Heron H C Han, Howard C H Chow, Alvin C H Ma, William W L Choi, et al. 2012. "Sorafenib Treatment of FLT3-ITD + Acute Myeloid Leukemia: Favorable Initial Outcome and Mechanisms of Subsequent Nonresponsiveness Associated with the Emergence of a D835 Mutation." *Blood*. <https://doi.org/10.1182/blood-2011-06-363960>.
- Mardis, Elaine R., Li Ding, David J. Dooling, David E. Larson, Michael D. McLellan, Ken Chen, Daniel C. Koboldt, et al. 2009. "Recurring Mutations Found by Sequencing an Acute Myeloid Leukemia Genome." *New England Journal of Medicine*. <https://doi.org/10.1056/NEJMoa0903840>.
- Merad, Miriam, Priyanka Sathe, Julie Helft, Jennifer Miller, and Arthur Mortha. 2013. "The Dendritic Cell Lineage: Ontogeny and Function of Dendritic Cells and Their Subsets in the Steady State and the Inflamed Setting." *Annual Review of Immunology* 31 (1): 563–604. <https://doi.org/10.1146/annurev-immunol-020711-074950>.
- Metcalfe, Donald. 2008. "Hematopoietic Cytokines." *Blood* 111 (2): 485–91. <https://doi.org/10.1182/blood-2007-03-079681>.
- MetzelDer, S. K., T. SchroeDer, A. Finck, S. Scholl, M. Fey, K. Götze, Y. C. Linn, et al. 2012. "High Activity

- of Sorafenib in FLT3-ITD-Positive Acute Myeloid Leukemia Synergizes with Allo-Immune Effects to Induce Sustained Responses." *Leukemia*. <https://doi.org/10.1038/leu.2012.105>.
- Mi, Xiaoli, Gabriel Griffin, Winston Lee, Sanjay Patel, Robert Ohgami, Chi Young Ok, Sa Wang, et al. 2018. "Genomic and Clinical Characterization of B/T Mixed Phenotype Acute Leukemia Reveals Recurrent Features and T-ALL like Mutations." *American Journal of Hematology* 93 (11): 1358–67. <https://doi.org/10.1002/ajh.25256>.
- Mol, Clifford D., Douglas R. Dougan, Thomas R. Schneider, Robert J. Skene, Michelle L. Kraus, Daniel N. Scheibe, Gyorgy P. Snell, Hua Zou, Bi Ching Sang, and Keith P. Wilson. 2004. "Structural Basis for the Autoinhibition and STI-571 Inhibition of c-Kit Tyrosine Kinase." *Journal of Biological Chemistry* 279 (30): 31655–63. <https://doi.org/10.1074/jbc.M403319200>.
- Mol, Clifford D., Kheng B. Lim, Vandana Sridhar, Hua Zou, Ellen Y.T. Chien, Bi Ching Sang, Jacek Nowakowski, Daniel B. Kassel, Ciarán N. Cronin, and Duncan E. McRee. 2003. "Structure of a C-Kit Product Complex Reveals the Basis for Kinase Transactivation." *Journal of Biological Chemistry* 278 (34): 31461–64. <https://doi.org/10.1074/jbc.C300186200>.
- Moreno, Isabel, Guillermo Martín, Pascual Bolufer, Eva Barragán, Eva Rueda, José Román, Pascual Fernández, et al. 2003. "Incidence and Prognostic Value of FLT3 Internal Tandem Duplication and D835 Mutations in Acute Myeloid Leukemia." *Haematologica* 88 (01): 19–24. <https://doi.org/10.1097/00010694-197802000-00008>.
- Nakano, Hideki, Manabu Yanagita, and Michael Dee Gunn. 2001. "Cd11c⁺ B220⁺ Gr-1⁺ Cells in Mouse Lymph Nodes and Spleen Display Characteristics of Plasmacytoid Dendritic Cells." *The Journal of Experimental Medicine*. <https://doi.org/10.1084/jem.194.8.1171>.
- Nakano, Yasuyuki, Hitoshi Kiyoi, Shuichi Miyawaki, Norio Asou, Ryuzo Ohno, Hidehiko Saito, and Tomoki Naoe. 1999. "Molecular Evolution of Acute Myeloid Leukaemia in Relapse: Unstable N-Ras and FLT3 Genes Compared with P53 Gene." *British Journal of Haematology* 104 (4): 659–64. <https://doi.org/10.1046/j.1365-2141.1999.01256.x>.
- Neumann, Martin, Ebru Coskun, Lars Fransecky, Liliana H. Mochmann, Isabelle Bartram, Nasrin Farhadi Sartangi, Sandra Heesch, et al. 2013. "FLT3 Mutations in Early T-Cell Precursor ALL Characterize a Stem Cell Like Leukemia and Imply the Clinical Use of Tyrosine Kinase Inhibitors." *PLoS ONE* 8 (1). <https://doi.org/10.1371/journal.pone.0053190>.
- NIH, National Cancer Institute. n.d. "Cancer Stat Facts: Leukemia - Acute Myeloid Leukemia (AML)." Accessed November 21, 2018. <https://seer.cancer.gov/statfacts/html/amyl.html>.
- O'Donnell, Margaret R., Martin S. Tallman, Camille N. Abboud, Jessica K. Altman, Frederick R. Appelbaum, Daniel A. Arber, Vijaya Bhatt, et al. 2017. "Acute Myeloid Leukemia, Version 3.2017: Clinical Practice Guidelines in Oncology." *JNCCN Journal of the National Comprehensive Cancer Network*. <https://doi.org/10.6004/jnccn.2017.0116>.
- O'Farrell, Anne Marie, James M. Foran, Walter Fiedler, Hubert Serve, Ron L. Paquette, Maureen A. Cooper, Helene A. Yuen, et al. 2003. "An Innovative Phase I Clinical Study Demonstrates Inhibition of FLT3 Phosphorylation by SU11248 in Acute Myeloid Leukemia Patients." *Clinical Cancer Research* 9 (15): 5465–76.
- Okuda, T, Z Cai, S Yang, N Lenny, C J Lyu, J M van Deursen, H Harada, and J R Downing. 1998. "Expression of a Knocked-in AML1-ETO Leukemia Gene Inhibits the Establishment of Normal Definitive Hematopoiesis and Directly Generates Dysplastic Hematopoietic Progenitors." *Blood*.
- Opatowsky, Yarden, Irit Lax, Francisco Tomé, Franziska Bleichert, Vinzenz M. Unger, and Joseph Schlessinger. 2014. "Structure, Domain Organization, and Different Conformational States of Stem Cell Factor-Induced Intact KIT Dimers." *Proceedings of the National Academy of Sciences* 111 (5): 1772–77. <https://doi.org/10.1073/pnas.1323254111>.

- Oppmann, Birgit, Robin Lesley, Bianca Blom, Jackie C. Timans, Yuming Xu, Brisdell Hunte, Felix Vega, et al. 2000. "Novel P19 Protein Engages IL-12p40 to Form a Cytokine, IL-23, with Biological Activities Similar as Well as Distinct from IL-12." *Immunity*. [https://doi.org/10.1016/S1074-7613\(00\)00070-4](https://doi.org/10.1016/S1074-7613(00)00070-4).
- Orkin, Stuart H. 2000. "Diversification of Haematopoietic Stem Cells to Specific Lineages." *Nature Reviews Genetics* 1 (1): 57–64. <https://doi.org/10.1038/35049577>.
- Orkin, Stuart H., and Leonard I. Zon. 2008. "Hematopoiesis: An Evolving Paradigm for Stem Cell Biology." *Cell* 132 (4): 631–44. <https://doi.org/10.1016/j.cell.2008.01.025>.
- Papaemmanuil, Elli, Moritz Gerstung, Lars Bullinger, Verena I. Gaidzik, Peter Paschka, Nicola D. Roberts, Nicola E. Potter, et al. 2016. "Genomic Classification and Prognosis in Acute Myeloid Leukemia." *New England Journal of Medicine* 374 (23): 2209–21. <https://doi.org/10.1056/NEJMoa1516192>.
- Patel, Jay P., Mithat Gönen, Maria E. Figueroa, Hugo Fernandez, Zhuoxin Sun, Janis Racevskis, Pieter Van Vlierberghe, et al. 2012. "Prognostic Relevance of Integrated Genetic Profiling in Acute Myeloid Leukemia." *New England Journal of Medicine*. <https://doi.org/10.1056/NEJMoa1112304>.
- Perez, P, RW Hoffman, S Shaw, JA Bluestone, and DM. Segal. 1985. "Specific Targeting of Cytotoxic T Cells by Anti-T3 Linked to Anti-Target Cell Antibody." *Nature* 31 (316): 354–356.
- Perl, Alexander E, Jessica K Altman, Jorge Cortes, Catherine Smith, Mark Litzow, Maria R Baer, David Claxton, et al. 2017. "Selective Inhibition of FLT3 by Gilteritinib in Relapsed or Refractory Acute Myeloid Leukaemia: A Multicentre, First-in-Human, Open-Label, Phase 1/2 Study." *The Lancet Oncology*, 1–15. [https://doi.org/10.1016/S1470-2045\(17\)30416-3](https://doi.org/10.1016/S1470-2045(17)30416-3).
- Piloto, Obdulio, Mark Levis, David Huso, Yiwen Li, Hongli Li, Mei Nai Wang, Rajiv Bassi, et al. 2005. "Inhibitory Anti-FLT3 Antibodies Are Capable of Mediating Antibody-Dependent Cell-Mediated Cytotoxicity and Reducing Engraftment of Acute Myelogenous Leukemia Blasts in Nonobese Diabetic/Severe Combined Immunodeficient Mice." *Cancer Research* 65 (4): 1514–22. <https://doi.org/10.1158/0008-5472.CAN-04-3081>.
- Pratz, Keith W, and Mark Levis. 2017. "How I Treat FLT3-Mutated AML." *Blood* 129 (5): 565–72. <https://doi.org/10.1182/blood-2016-09-693648.BLOOD>.
- Ravandi, Farhad, Mona Lisa Alattar, Michael R. Grunwald, Michelle A. Rudek, Trivikram Rajkhowa, Mary Ann Richie, Sherry Pierce, et al. 2013. "Phase 2 Study of Azacytidine plus Sorafenib in Patients with Acute Myeloid Leukemia and FLT-3 Internal Tandem Duplication Mutation." *Blood*. <https://doi.org/10.1182/blood-2013-01-480228>.
- Ravandi, Farhad, Jorge E. Cortes, Daniel Jones, Stefan Faderl, Guillermo Garcia-Manero, Marina Y. Konopleva, Susan O'Brien, et al. 2010. "Phase I/II Study of Combination Therapy with Sorafenib, Idarubicin, and Cytarabine in Younger Patients with Acute Myeloid Leukemia." *Journal of Clinical Oncology*. <https://doi.org/10.1200/JCO.2009.25.4888>.
- Reiter, K., H. Polzer, C. Krupka, A. Maiser, B. Vick, M. Rothenberg-Thurley, K. H. Metzeler, et al. 2018. "Tyrosine Kinase Inhibition Increases the Cell Surface Localization of FLT3-ITD and Enhances FLT3-Directed Immunotherapy of Acute Myeloid Leukemia." *Leukemia* 32 (2): 313–22. <https://doi.org/10.1038/leu.2017.257>.
- Rivat, Cyril, Chamroeun Sar, Ilana Mechaly, Jean-Philippe Leyris, Lucie Diouloufet, Corinne Sonrier, Yann Philipson, et al. 2018. "Inhibition of Neuronal FLT3 Receptor Tyrosine Kinase Alleviates Peripheral Neuropathic Pain in Mice." *Nature Communications* 9 (1): 1042. <https://doi.org/10.1038/s41467-018-03496-2>.
- Röllig, Christoph, Hubert Serve, Andreas Hüttmann, Richard Noppeney, Carsten Müller-Tidow, Utz

- Krug, Claudia D. Baldus, et al. 2015. "Addition of Sorafenib versus Placebo to Standard Therapy in Patients Aged 60 Years or Younger with Newly Diagnosed Acute Myeloid Leukaemia (SORAML): A Multicentre, Phase 2, Randomised Controlled Trial." *The Lancet Oncology*. [https://doi.org/10.1016/S1470-2045\(15\)00362-9](https://doi.org/10.1016/S1470-2045(15)00362-9).
- Sallmyr, Annahita, Jinshui Fan, Kamal Datta, Kyu Tae Kim, Dan Grosu, Paul Shapiro, Donald Small, and Feyruz Rassool. 2008. "Internal Tandem Duplication of FLT3 (FLT3/ITD) Induces Increased ROS Production, DNA Damage, and Misrepair: Implications for Poor Prognosis in AML." *Blood*. <https://doi.org/10.1182/blood-2007-05-092510>.
- Sallusto, F. 1995. "Dendritic Cells Use Macropinocytosis and the Mannose Receptor to Concentrate Macromolecules in the Major Histocompatibility Complex Class II Compartment: Downregulation by Cytokines and Bacterial Products." *Journal of Experimental Medicine*. <https://doi.org/10.1084/jem.182.2.389>.
- Sanford, David, William G. Blum, Farhad Ravandi, Rebecca B Klisovic, Gautam Borthakur, Walker Alison R., Guillermo Garcia-Manero, et al. 2015. "Efficacy and Safety of an Anti-FLT3 Antibody (Ly3012218) in Patients with Relapsed Acute Myeloid Leukemia." *Journal of Clinical Oncology*, abstract 7059.
- Sato, Takashi, Xiaochuan Yang, Steven Knapper, Paul White, B. Douglas Smith, Steven Galkin, Donald Small, Alan Burnett, and Mark Levis. 2011. "FLT3 Ligand Impedes the Efficacy of FLT3 Inhibitors in Vitro and in Vivo." *Blood* 117 (12): 3286–93. <https://doi.org/10.1182/blood-2010-01-266742>.
- Schepper, Sebastiaan De, Simon Verheijden, Javier Aguilera-Lizarraga, Maria Francesca Viola, Werend Boesmans, Nathalie Stakenborg, Iryna Voytyuk, et al. 2018. "Self-Maintaining Gut Macrophages Are Essential for Intestinal Homeostasis." *Cell* 175 (2): 400–415.e13. <https://doi.org/10.1016/j.cell.2018.07.048>.
- Schmidt-Arras, D.E., A. Bohmer, Boyka Markova, Chunaram Choudhary, Hubert Serve, and F.D. Bohmer. 2005. "Tyrosine Phosphorylation Regulates Maturation of Receptor Tyrosine Kinases." *Molecular and Cellular Biology* 25 (9): 3690. <https://doi.org/10.1128/MCB.25.9.3690>.
- Scott, Charlotte L., and Bart N. Lambrecht. 2016. "Conventional Dendritic Cells: Identification, Subsets, Development and Functions." In *Encyclopaedia of Immunobiology, Volume 3*, 374–83.
- Serve, Hubert, Uta Brunnberg, Oliver Ottmann, Christian Brandts, Björn Steffen, Utz Krug, Ruth Wagner, et al. 2013. "Sorafenib in Combination with Intensive Chemotherapy in Elderly Patients with Acute Myeloid Leukemia: Results from a Randomized, Placebo-Controlled Trial." *Journal of Clinical Oncology* 31 (25): 3110–18. <https://doi.org/10.1200/JCO.2012.46.4990>.
- Sexauer, Amy, Alexander Perl, Xiaochuan Yang, Michael Borowitz, Christopher Gocke, Trivikram Rajkhowa, Christian Thiede, et al. 2012. "Terminal Myeloid Differentiation in Vivo Is Induced by FLT3 Inhibition in FLT3/ITDAML." *Blood* 120 (20): 4205–14. <https://doi.org/10.1182/blood-2012-01-402545>.
- Sheridan, Cormac. 2017. "First New Drug Approval for AML in 15 Years." *Nature Biotechnology* 35 (8): 696–98. <https://doi.org/10.1038/nbt0817-696>.
- Shih, Lee-yung, Chein-fuang Huang, Jin-hou Wu, Tung-liang Lin, Po Dunn, Po-nan Wang, and Ming-chung Kuo. 2018. "Internal Tandem Duplication of FLT3 in Relapsed Acute Myeloid Leukemia : A Comparative Analysis of Bone Marrow Samples from 108 Adult Patients at Diagnosis and Relapse" 100 (7): 2387–93. <https://doi.org/10.1182/blood-2002-01-0195>.Supported.
- Shlush, Liran I., Sasan Zandi, Amanda Mitchell, Weihsu Claire Chen, Joseph M. Brandwein, Vikas Gupta, James A. Kennedy, et al. 2014. "Identification of Pre-Leukaemic Haematopoietic Stem Cells in Acute Leukaemia." *Nature*. <https://doi.org/10.1038/nature13038>.
- Sichien, Dorine, Bart N. Lambrecht, Martin Guillems, and Charly L. Scott. 2017. "Development of

- Conventional Dendritic Cells: From Common Bone Marrow Progenitors to Multiple Subsets in Peripheral Tissues." *Mucosal Immunology* 10 (4): 831–44. <https://doi.org/10.1038/mi.2017.8>.
- Sichien, Dorine, Charlotte L. Scott, Liesbet Martens, Matthias Vanderkerken, Sofie Van Gassen, Maud Plantinga, Thorsten Joeris, et al. 2016. "IRF8 Transcription Factor Controls Survival and Function of Terminally Differentiated Conventional and Plasmacytoid Dendritic Cells, Respectively." *Immunity* 45 (3): 626–40. <https://doi.org/10.1016/j.immuni.2016.08.013>.
- Smith, B Douglas, Mark Levis, Miloslav Beran, Francis Giles, Hagop Kantarjian, Karin Berg, Kathleen M Murphy, Tianna Dausess, Jeffrey Allebach, and Donald Small. 2004. "Single Agent CEP 701, a Novel FLT3 Inhibitor, Shows Biologic and Clinical Activity in Patients with Relapsed or Refractory Acute Myeloid Leukaemia." *Blood* 103 (10): 3369–76. <https://doi.org/10.1182/blood-2003-11-3775>.Supported.
- Smith, Catherine C., Qi Wang, Chen-Shan Chin, Sara Salerno, Lauren E. Damon, Mark J. Levis, Alexander E. Perl, et al. 2012. "Validation of ITD Mutations in FLT3 as a Therapeutic Target in Human Acute Myeloid Leukaemia." *Nature* 485 (7397): 260–63. <https://doi.org/10.1038/nature11016>.
- Staerz, Uwe D., Osami Kanagawa, and Michael J. Bevan. 1985. "Hybrid Antibodies Can Target Sites for Attack by T Cells." *Nature*. <https://doi.org/10.1038/314628a0>.
- Steinman, RM, and ZA Cohn. 1973. "Identification of a Novel Cell Type in Peripheral Lymphoid Organs of Mice." *J Exp Med*. <https://doi.org/10.1084/jem.137.5.1142>.
- Stirewalt, Derek L, and Jerald P Radich. 2003. "The Role of FLT3 in Haematopoietic Malignancies." *Nature Reviews Cancer* 3 (9): 650–65. <http://www.ncbi.nlm.nih.gov/pubmed/12951584>.
- Stone, Richard M., Daniel J. DeAngelo, Virginia Klimek, Ilene Galinsky, Eli Estey, Stephen D. Nimer, Wilson Grandin, et al. 2005. "Patients with Acute Myeloid Leukemia and an Activating Mutation in FLT3 Respond to a Small-Molecule FLT3 Tyrosine Kinase Inhibitor, PKC412." *Blood* 105 (1): 54–60. <https://doi.org/10.1182/blood-2004-03-0891>.
- Stone, Richard M., Sumithra J. Mandrekar, Ben L. Sanford, Kristina Laumann, Susan Geyer, Clara D. Bloomfield, Christian Thiede, et al. 2017. "Midostaurin plus Chemotherapy for Acute Myeloid Leukemia with a FLT3 Mutation." *New England Journal of Medicine*, NEJMoa1614359. <https://doi.org/10.1056/NEJMoa1614359>.
- Synimmune. n.d. "Synimmune GmbH: Flysyn." Accessed November 25, 2018. <https://www.synimmune.de/products/flysyn/>.
- Takahashi, Koichi, Feng Wang, Kiyomi Morita, Yuanqing Yan, Peter Hu, Pei Zhao, Abdallah Abou Zhar, et al. 2018. "Integrative Genomic Analysis of Adult Mixed Phenotype Acute Leukemia Delineates Lineage Associated Molecular Subtypes." *Nature Communications* 9 (1). <https://doi.org/10.1038/s41467-018-04924-z>.
- Tavian, Manuela, Katia Biasch, Lidia Sinka, Judith Vallet, and Bruno Péault. 2010. "Embryonic Origin of Human Hematopoiesis." *International Journal of Developmental Biology* 54 (6–7): 1061–65. <https://doi.org/10.1387/ijdb.103097mt>.
- Thiede, C, C Stuedel, B Mohr, M Schaich, U Schaekel, M Bornhaeuser, M Wermke, et al. 2002. "Analysis of FLT3-Activating Mutations in 979 Patients with Acute Myelogenous Leukemia: Association with FAB Subtypes and Identification of Subgroups with Poor Prognosis." *Blood* 99 (12): 4326–35.
- Treiber, Daniel K., and Neil P. Shah. 2013. "Ins and Outs of Kinase DFG Motifs." *Chemistry and Biology* 20 (6): 745–46. <https://doi.org/10.1016/j.chembiol.2013.06.001>.
- Verstraete, Kenneth, and Savvas N Savvides. 2012. "Extracellular Assembly and Activation Principles of Oncogenic Class III Receptor Tyrosine Kinases." *Nature Reviews. Cancer* 12 (11): 753–66. <https://doi.org/10.1038/nrc3371>.

- Verstraete, Kenneth, Gonzalez Vandriessche, Mariska Januar, Jonathan Elegheert, Alexander V. Shkumatov, Ambroise Desfosses, Kathleen Van Craenenbroeck, et al. 2011. "Structural Insights into the Extracellular Assembly of the Hematopoietic Flt3 Signaling Complex." *Blood* 118 (1): 60–68. <https://doi.org/10.1182/blood-2011-01-329532>.
- Wang, Eunice S., Richard M. Stone, Martin S. Tallman, Roland B. Watler, John R. Eckardt, and Robert Collins. 2016. "Crenolanib, a Type I FLT3 TKI, Can Be Safely Combined with Cytarabine and Anthracycline Induction Chemotherapy and Results in High Response Rates in Patients with Newly Diagnosed FLT3 Mutant Acute Myeloid Leukemia (AML)." *Blood* 128: 1071.
- Waskow, Claudia, Kang Liu, Guillaume Darrasse-Jèze, Pierre Guermonprez, Florent Ginhoux, Miriam Merad, Tamara Shengelia, Kaihui Yao, and Michel Nussenzweig. 2008. "The Receptor Tyrosine Kinase Flt3 Is Required for Dendritic Cell Development in Peripheral Lymphoid Tissues." *Nature Immunology* 9 (6): 676–83. <https://doi.org/10.1038/ni.1615>.
- Wei, Andrew H., and Ing S. Tiong. 2017. "Midostaurin, Enasidenib, CPX-351, Gemtuzumab Ozogamicin, and Venetoclax Bring New Hope to AML." *Blood*. <https://doi.org/10.1182/blood-2017-08-784066>.
- Weinberg, O. K., and D. A. Arber. 2010. "Mixed-Phenotype Acute Leukemia: Historical Overview and a New Definition." *Leukemia*. <https://doi.org/10.1038/leu.2010.202>.
- Weisberg, Ellen, Christina Boulton, Louise M. Kelly, Paul Manley, Dorian Fabbro, Thomas Meyer, D. Gary Gilliland, and James D. Griffin. 2002. "Inhibition of Mutant FLT3 Receptors in Leukemia Cells by the Small Molecule Tyrosine Kinase Inhibitor PKC412." *Cancer Cell*. [https://doi.org/10.1016/S1535-6108\(02\)00069-7](https://doi.org/10.1016/S1535-6108(02)00069-7).
- Welch, John S., Timothy J. Ley, Daniel C. Link, Christopher a. Miller, David E. Larson, Daniel C. Koboldt, Lukas D. Wartman, et al. 2012. "The Origin and Evolution of Mutations in Acute Myeloid Leukemia." *Cell* 150 (2): 264–78. <https://doi.org/10.1016/j.cell.2012.06.023>.
- Welch, JS, TJ Ley, DC Link, and CA Miller. 2012. "The Origin and Evolution of Mutations in Acute Myeloid Leukemia." *Cell* 150 (2): 264–78. <https://doi.org/10.1016/j.cell.2012.06.023>.The.
- Westendorf, Jennifer J, Cindy M Yamamoto, Noel Lenny, James R Downing, Michael E Selsted, and Scott W Hiebert. 1998. "The t(8;21) Fusion Product, AML-1-ETO, Associates with C/EBP-Alpha, Inhibits C/EBP-Alpha-Dependent Transcription, and Blocks Granulocytic Differentiation." *Molecular and Cellular Biology*. <https://doi.org/10.1128/mcb.20.6.2075-2086.2000>.
- Wolach, Ofir, and Richard M. Stone. 2015. "How I Treat Mixed-Phenotype Acute Leukemia." *Blood*. <https://doi.org/10.1182/blood-2014-10-551465>.
- Yamada, Osamu, and Kiyotaka Kawauchi. 2013. "The Role of the JAK-STAT Pathway and Related Signal Cascades in Telomerase Activation during the Development of Hematologic Malignancies." *JAK-STAT*. <https://doi.org/10.4161/jkst.25256>.
- Yamamoto, Y., H. Kiyoi, Y. Nakano, R. Suzuki, Y. Koder, S. Miyawaki, N. Asou, et al. 2001. "Activating Mutation of D835 within the Activation Loop of FLT3 in Human Hematologic Malignancies." *Blood* 97 (8): 2434–39. <https://doi.org/10.1182/blood.V97.8.2434>.
- Yamashita, Y., J. Yuan, I. Suetake, H. Suzuki, Y. Ishikawa, Y. L. Choi, T. Ueno, et al. 2010. "Array-Based Genomic Resequencing of Human Leukemia." *Oncogene*. <https://doi.org/10.1038/onc.2010.117>.
- Yanada, M, K Matsuo, T Suzuki, H Kiyoi, and T Naoe. 2005. "Prognostic Significance of FLT3 Internal Tandem Duplication and Tyrosine Kinase Domain Mutations for Acute Myeloid Leukemia: A Meta-Analysis." *Leukemia* 19 (8): 1345–49. <https://doi.org/10.1038/sj.leu.2403838>.
- Ye, Zi Xing, and Shu Jie Wang. 2014. "Mixed Phenotype Acute Leukemia." *Chinese Medical Journal*. <https://doi.org/10.3760/cma.j.issn.0366-6999.20132468>.

- Yergeau, Donald A., Christopher J. Hetherington, Qing Wang, Pu Zhang, Arlene H. Sharpe, Michael Binder, Miguel Marín-Padilla, Daniel G. Tenen, Nancy A. Speck, and Dong Er Zhang. 1997. "Embryonic Lethality and Impairment of Haematopoiesis in Mice Heterozygous for an AML1-ETO Fusion Gene." *Nature Genetics*. <https://doi.org/10.1038/ng0397-303>.
- Zarrinkar, Patrick P., Ruwanthi N. Gunawardane, Merryl D. Cramer, Michael F. Gardner, Daniel Brigham, Barbara Belli, Mazen W. Karaman, et al. 2009. "AC220 Is a Uniquely Potent and Selective Inhibitor of FLT3 for the Treatment of Acute Myeloid Leukemia (AML)." *Blood*. <https://doi.org/10.1182/blood-2009-05-222034>.
- Zhang, Jingliao, Yingchi Zhang, Man Zhang, Chao Liu, Xiaoming Liu, Jie Yin, Peng Wu, Xiaojuan Chen, and Wenyu Yang. 2018. "FLT3 Pathway Is a Potential Therapeutic Target for PRC2-Mutated T-Cell Acute Lymphoblastic Leukemia." *Blood* 132 (23): 2520–24.

Problem definition and research aims

Ligand-induced extracellular receptor-receptor interactions are considered a general feature for almost all RTK-III. For instance, such homotypic contacts have been shown to be essential in coupling ligand-binding to kinase activation in the KIT receptor. It has come as a surprise that extensive structural and biophysical characterization of the extracellular FL-FLT3 complex using X-ray crystallography, negative-stain electron microscopy and isothermal titration calorimetry, showed that this complex is conspicuously devoid of homotypic receptor contacts. However, providing a structural framework for the transforming mechanism underlying two oncogenic mutations that map in the extracellular domain is only possible by assuming that receptor-receptor contacts are a possibility. In contrast to what has been postulated, it therefore seems that receptor activation can be driven by homotypic receptor interactions either in a canonical RTK-III fashion or in a novel fashion, if the circumstances would allow.

Whether the point mutations have only awoken the dormant ability of the receptor to engage in such interactions, or whether they enhance otherwise weak homotypic receptor interactions that previous studies have missed, are the outstanding questions for which **Chapter B** attempts to provide an answer.

Chapter B is centered on the extensive structural and biophysical characterization of wild-type and oncogenic FLT3 variants by studying interactions involving the extracellular region. **Chapter C**, on the other hand, focusses on the cell membrane expression of wild-type and intracellularly-mutated FLT3 oncovariants. The longstanding correlation between AML and activating mutations in FLT3, have spurred the development of tyrosine kinase inhibitors (TKIs) targeting FLT3. The unsatisfactory results when tested as monotherapy, motivated the pharmaceutical industry to include these TKIs into existing chemotherapy regimens, despite the risk of evoking TKI-resistance by doing so. Indeed, the alarming observations that serum levels of FL are exponentially increased after chemotherapy and that such concentrations confer resistance against TKI, should forewarn to include these inhibitors into chemotherapy regimens. The lack of mechanistic insights explaining this phenomenon, is arguably the reason why this issue is too often ignored and why combination of TKIs and chemotherapy is still the mainstay of current FLT3-targeting clinical studies.

The research presented in **Chapter C** attempts to provide insights into why oncogenic FLT3 variants reside predominantly in the endoplasmic reticulum, how TKIs can influence their glycan maturation and membrane translocation and, finally, whether these observations can be linked to ligand-mediated TKI resistance.

CHAPTER B

Biophysical and structural characterization of wild-type and oncogenic FLT3

Clinical development of novel drugs for the treatment of AML predominantly focuses on inhibition of the intracellular kinase domain of FLT3, but all strategies employed suffer from FLT3 Ligand-mediated resistance. Meanwhile, the molecular mechanism underlying a driver mutation in the extracellular domain of FLT3 and its negative effects on the only FDA approved drug for FLT3-mediated AML, midostaurin, remains an open question. Receptor dimerization in a ligand-independent manner is the most intuitive hypothesis for the molecular mechanism underlying this S451F driver mutation. Such hypothesis further suggest that receptor-receptor contacts, also known as homotypic receptor interactions, in a ligand-dependent manner must be relevant for the activation of the wild-type receptor. Using two novel engineered FLT3 ligands, we performed a full thermodynamic and kinetic dissection of the transition from a binary encounter cytokine-receptor complex to a ternary activated cytokine-receptor complex. Our studies have revealed cooperativity at two stages within this transition. Integrating similar experiments using a receptor construct endorsed with an AML driver mutation, together with a crystallographic model describing a novel conformation of the inactive state of the receptor, we propose an updated receptor-activation paradigm with a higher emphasis on ligand-induced receptor contacts. Given the clinical importance of FLT3 as a target in the treatment of AML and the apparent FL-driven TKI resistance, this work offers not only novel ways to prevent the emerging resistance, but opens new avenues to aid future rational drug design.

1. Ligand-binding of FLT3 is a cooperative event

1.1. Benchmarking of recombinant FL bioactivity *in vitro*, in primary cells and *in vivo*.

Fms-like tyrosine kinase receptor 3 (FLT3) is a type-1 transmembrane receptor tyrosine kinase, expressed at the cell surface of early hematopoietic progenitors and all dendritic cell (DC) populations, plasmacytoid DCs, classical type 1 DCs (cDC1s) and type 2 DCs (cDC2s) (Beaudin, Boyer, and Forsberg 2014a; Waskow et al. 2008). Signalling through FLT3 is crucial for establishing the cellular repertoire of the blood and is initiated by binding of its cognate ligand FLT3 Ligand (FL) to the receptor's extracellular domain (ECD) (Verstraete et al. 2011). In contrast to other RTK-III family members such as CSF-1R, KIT and PDGFR β , this first key step in the signalling cascade of FLT3 is hallmarked by the apparent absence of ligand-induced receptor contacts (Elegheert et al. 2011; Felix et al. 2013, 2015; Yuzawa et al. 2007; P. H. Chen, Unger, and He 2015; Verstraete et al. 2011). Such dissonance contrasts with the bivalent nature of the ligand, which does bring the two extracellular receptor domains in close proximity to each other. The discovery of constitutively activating point mutations in the ECD of FLT3 prompted us to further explore the possibility of ligand-induced receptor contacts (Fröhling et al. 2007; Jiang et al. 2005).

Already in 2009, our research group established protocols for efficient *in vitro* refolding and purification of *E. coli*-expressed recombinant human FL (Verstraete et al. 2009). Although slightly optimized, these protocols allowed production of recombinant FL throughout this doctoral study. However, a thorough analysis of how FLT3 becomes activated, how a point mutation in the ECD influences the kinetics of this interaction, and how this effect is modulated by different ligands, requires full confidence that in-house produced FL indeed reflects the effect of endogenous FL stimulation. Thus, by exploiting the species cross-reactivity of FL we investigated the bioactivity of recombinant FL via three orthogonal approaches at physiologically relevant concentrations (Figure 1).

First, we analyzed whether in-house produced FL was able to differentiate the bone marrow-resident common dendritic cell precursor (CDP) into a heterogeneous DC population consisting of conventional DCs (cDC1 and cDC2) and plasmacytoid DCs (pDCs) (Waskow et al. 2008; Beaudin, Boyer, and Forsberg 2014b). To this end, bone marrow (BM) cells from multiple C57BL/6 mice were isolated and stimulated with different concentrations of FL, purified with inclusion of an extra endotoxin-removal step in the protocol. After a 7-day treatment, the BM derived cell culture was harvested and analyzed by flow cytometry for their viability and the presence of pDCs, cDC1s and cDC2s (Figure 1A). The data was fitted to a hierarchical generalized linear model using Genstat, allowing prediction of cell viability, DC population sizes and standard errors.

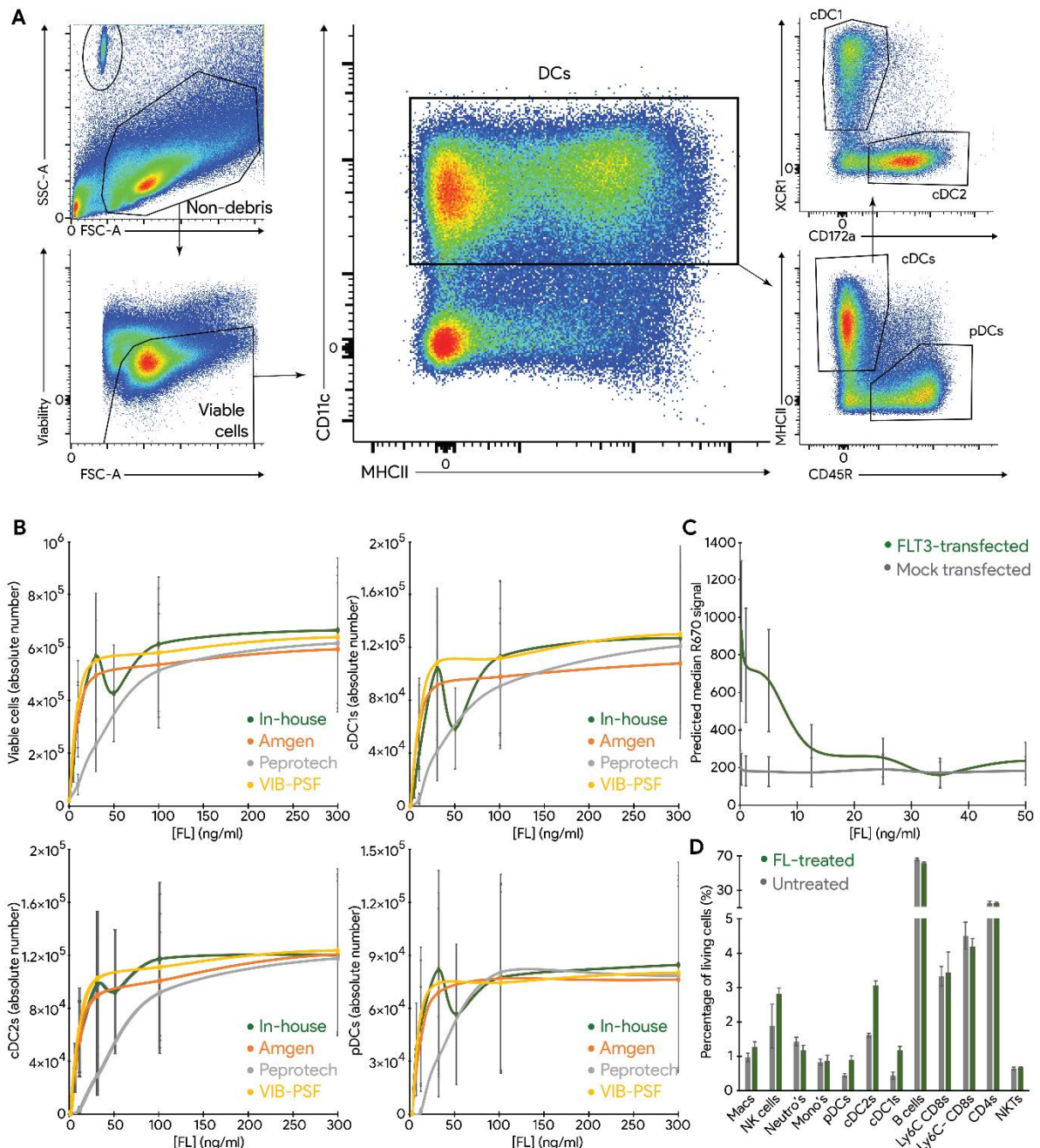


Figure 1. In-house produced recombinant FLT3 ligand is potentially differentiating cells in vitro and in vivo. Production of recombinant FL in *E. coli* as reported previously (Verstraete et al. 2009) results in a highly bioactive protein species. **A. Global gating strategy for flow cytometry analysis of stimulated bone marrow cells.** After a 7-day treatment with FL, all 3 different DC populations were quantified according to the indicated gates. Data is representative for a BM cell population stimulated with 300 ng/ml FL. **B. In-house produced FL is equipotent to commercially available FL.** BM cells were stimulated for 7 days with FL from indicated sources, after which flow cytometry was used to determine viability (upper left) and the absolute number of cDC1s (upper right), cDC2s (lower left) and pDCs (lower right). A comparison was made between in-house produced recombinant FL (dark green) and FL purchased from Amgen (orange), Peprotech (gray) and the VIB Protein Service Facility (yellow). **C. In-house produced FL is capable of internalizing membrane-expressed FLT3 at low concentrations.** FLT3- (green) and mock-transfected (gray) suspension-adapted HEK293S cells were stimulated with indicated concentrations of recombinant FL and stained with an APC-linked anti-FLT3 antibody prior to flow cytometry analysis. **D. In-house produced FL can expand all 3 DC subsets in vivo.** Mice were injected daily with 100 µg/ml FL. After 10 days, the spleens were analyzed for indicated cell populations (green) and compared to the populations of untreated mice (gray).

As is evident from the comparison in **Figure 1B**, in-house produced FL serves as a potent survival factor for BM cells and differentiation factor for all 3 DC subsets. Regression analysis of the cell viability showed that in-house produced FL was potent in generating a large cell population by promoting cell survival and/or proliferation. The $EC_{50} = 12.48 \pm 4.77$ ng/ml for viability is similar to the IC_{50} of most other tested commercial sources of FL, except from Peprotech. FL acquired from the latter was less potent at low concentrations ($EC_{50} = 45.22 \pm 6.8$ ng/ml), despite being the only source tested of which the ligand was of murine species.

Secondly, a flow cytometry protocol was developed that allowed to quantitatively analyze FLT3 expression at the cell surface of suspension-adapted HEK293S cells using an APC-linked anti-FLT3 antibody. Two days post-transfection, cells were stimulated with indicated concentrations of FL for 15 minutes, stained for FLT3 membrane expression and subsequently analysed by flow cytometry (**Figure 1C**).

The flow cytometry data querying FLT3 membrane expression shows that in-house produced FL significantly lowers FLT3 membrane presentation from concentrations of 1 ng/ml onwards (p-value of 0.032). We furthermore observe that 12.5 ng/ml is the last concentration for which FLT3 membrane levels are still significantly higher than those of the mock-transfected background at the 5% confidence level (p-value of 0.023). Although several orders of magnitude higher than endogenous serum levels of human FL, such concentrations of recombinant human FL levels are comparable to those used in literature for *ex vivo* or *in vitro* stimulation of membrane-expressed FLT3.

As it has been shown that administration of FL can dramatically increase the levels of all DC subsets in humans and mice (Pulendran et al. 1999, 2000), we finally analyzed if the in-house produced FL was able to increase distinct DC subsets *in vivo*. Mice were treated with daily injections of 10 µg FL and after 7 days, the spleen was analyzed for the indicated cell populations and compared to untreated mice (**Figure 1D**). As expected from *ex vivo* PBMC differentiation, daily administration of in-house produced FL was indeed able to increase all three subpopulations of DCs.

As shown elsewhere, our in-house produced FL was shown to potently activate its receptor in FLT3-expressing cancer cell lines. Our data further shows that the produced ligand is capable of internalizing the receptor at low concentrations, and is a potent DC differentiation and proliferation factor *ex vivo* and *in vivo*.

1.2. Engineering of a monomeric FLT3 Ligand

1.2.1. Rationale

In the current paradigm of FL-mediated FLT3 activation, each subunit of the dimeric ligand binds one receptor, resulting in the formation of a ligand:receptor complex obeying a 1:2 stoichiometry (1 ligand dimer bound to 2 receptor molecules). A key feature of the FLT3 ligand:receptor-complex is that in contrast to all other members of the RTK-III family, binding of the ligand does not appear to elicit homotypic receptor interactions (Chapter A – Section 1.2.2).

Nevertheless, the discovery and validation of two point mutations in the extracellular region of the receptor as a driver mutation in acute myeloid and lymphoid leukemia (Fröhling et al. 2007; Jiang et al. 2005), has lead us to hypothesize that receptor activation can be driven by homotypic receptor interactions, if the circumstances allow for it. If such a point mutation has awoken the dormant ability of the receptor to engage in such interactions, or whether it enhances otherwise very weak homotypic interactions, or even if the wild-type receptor does display ligand-induced receptor:receptor-interactions *in vivo*, is still an outstanding question.

Homotypic receptor interactions mediated by ligand binding are the structural hallmark of many RTK (M. a Lemmon and Schlessinger 2010). The mechanistic implications of this observation have been far reaching because the assembly of a number of such ligand-RTK complexes appears be cooperative – either positive or negative. This is based on the experimental observation that the affinity of binary ligand-receptor encounter complexes is lower than the affinity of the ligand-receptor interaction in the fully assembled ternary state in the case of positive cooperativity, or higher, in the case of negative cooperativity. For instance, studies on CSF-1R have shown that by stepwise removal of the membrane-proximal domains indeed have a detrimental effect on the receptors ability to establish high affinity complexes with its ligands CSF-1 and IL-34 (Elegheert et al. 2011, 2012; Ma et al. 2012b). Likewise, abolishing the conserved dimerization motif in domain 4 of KIT has shown to result in a receptor species with a severely compromised ligand-induced kinase activity, despite that the affinity of stem cell factor for KIT lacking the membrane-proximal domains 4 and 5 is, in contrast to CSF-1R, indistinguishable to full length KIT ectodomain (M. Lemmon et al. 1997; Yuzawa et al. 2007). Consistently, mutations that increase the reciprocal affinity of the membrane-proximal domains, have been identified as the underlying cause behind activating mutations in patients with gastrointestinal stromal tumors (Ashman and Griffith 2013; Forbes et al. 2011). Finally, the assembly principles underlying the PDGF-PDGFR interaction has been proposed to be based in part on negative cooperativity principles (Shim et al. 2010).

In contrast to such clear examples of ligand-receptor assemblies employing cooperativity principles, the situation with FLT3 has been much less clear. This is because previous experiments with an FLT3 construct lacking the two membrane-proximal domains, did not lead to a clear thermodynamic fingerprint that would allow assigning any significant role of these domains on the receptors affinity for its ligand. Furthermore, crystal structures of FLT3 extracellular domains in complex with FL have shown that homotypic receptor interactions are absent – a result validated by preliminary negative-stain electron microscopy (Verstraete et al. 2011). It was noted however, that the stability of the

construct bearing only the first 3 FLT3 domains was questionable, resulting in a suboptimal ITC experiment. Inspired by the clever use of a monomeric CSF-1 molecule that confirmed the importance of ligand-induced receptor interactions to constitute a high-affinity ligand:receptor complex (Elegheert et al. 2012), we set out to engineer a monomeric FLT3 ligand to supplement previous ITC studies on FLT3.

1.2.2. Strategy

The availability of several crystallographic models of FL, both unbound (PDB 1ETE) and in complex with its receptor (PDB 3QS7, 3QS9 and unpublished data), provided the structural basis for developing a strategy to disrupt the dimeric interface of FL without introducing significant changes in the receptor-binding epitope. Following the strategy to monomerize CSF-1 (Elegheert et al. 2012), several constructs were generated with a tandem duplication of region 18-30, of which some had one or multiple point mutations at sites playing a key

role at the dimeric interface. However, despite extensive optimization of the purification protocols, we did not succeed in purifying a monomeric species that was stable in solution. Therefore, we resorted to a more targeted approach by introducing a single point mutation targeting leucine-27 (Leu27) at the heart of the dimeric interface (Figure 2). In each protomer, Leu27 is located at the tip of a loop formed by residues Leu26 to Gln29, protruding into the hydrophobic inner of the four-helical bundle of the accompanying protomer. By mutating Leu27 to an aspartate, we hypothesized that the entropic penalty for burying a charged residue in the hydrophobic inners of the second protomer would be detrimental for any dimerization event to happen. Interestingly, earlier work by Graddis et al. (Graddis et al. 1998) had identified a Leu27 to proline mutation in FL, based on a random mutagenesis, that was deficient in dimerization at low protein concentrations.

1.2.3. FL_{L27D} is monomeric and engages in a 1:1 stoichiometric complex with FLT3.

Expression of FL_{L27D} from mammalian HEK cells (Aricescu, Lu, and Jones 2006) and in *E. coli* followed by *in vitro* refolding of FL_{L27D} (Verstraete et al. 2009), led to a stable and monodisperse protein that eluted in a size-exclusion chromatography (SEC) experiment as a protein with a significantly lower hydrodynamic radius (R_{hyd}) compared to wild-type FL (FL_{WT}) (Figure 3A, green and gray curves). Multi-angle laser light scattering (SEC-MALLS) analysis of these proteins during elution from SEC led to a

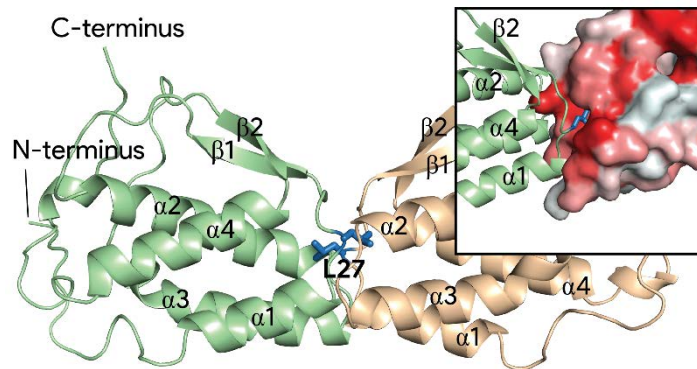


Figure 2. The dimeric interface of FL is centered around Leu27. Cartoon representation of FL (PDB 1ETE) with the constituting protomers colored green and sand. Coloring according the Eisenberg hydrophobicity scale (inset, surface representation, red is more hydrophobic) illustrates how Leu27 of each protomer (blue) is inserted into the hydrophobic inner of the other.

molecular weight (MW) determination of 35 and 17 kDa for FL_{WT} and FL_{L27D} respectively (Figure 3B). Importantly, even at concentrations as high as 1.7 mg/ml, no concentration-dependent dimerization could be detected.

We conclude that these experimentally determined values are in excellent agreement with their theoretical MWs and confirm that FL_{L27D} is indeed a monomeric species in solution.

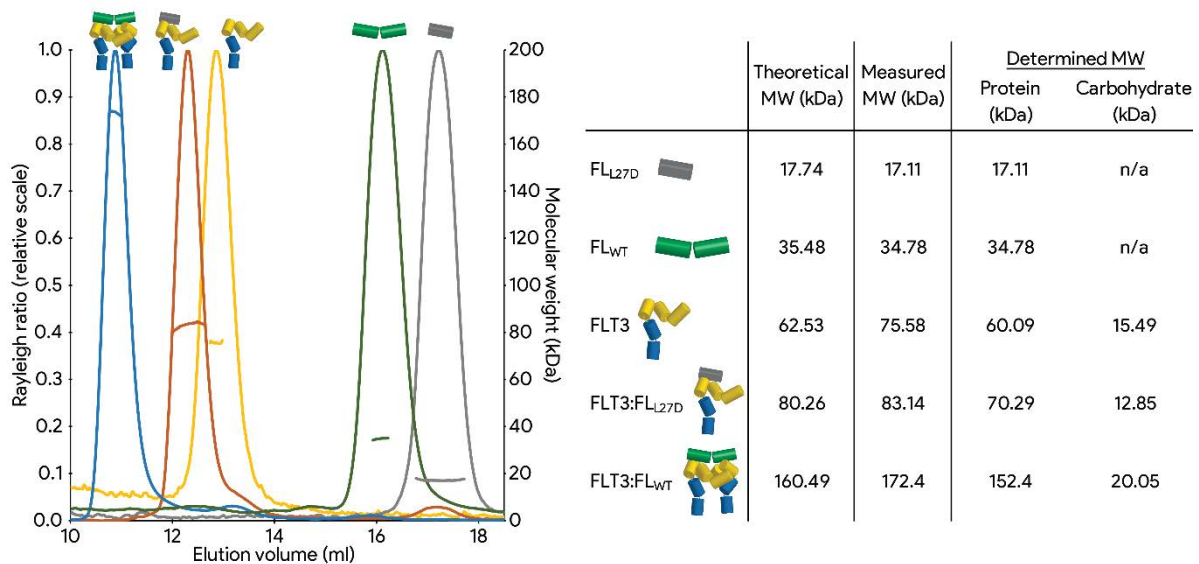


Figure 3. FL_{L27D} is a stable monomer capable of binding only one FLT3 molecule. **A. SEC-MALLS characterization of FL_{WT}, FL_{L27D} and receptor-complexes thereof.** Elution profile monitored by the forward and right-angle laser detector (left axis) plotted against the SEC retention volume, and overlaid with the measured molecular weight (right axis). FL_{WT} (green) is able to recruit 2 FLT3 molecules (yellow) into complex formation (blue), whereas FL_{L27D} (gray) binds FLT3 in an equimolar fashion (red). **B. Summary of the predicted molecular weights**, based on the amino acid sequence, and the MALLS-measured molecular weights, measured by light scattering. Further glycoprotein conjugate analysis of the latter allowed to attribute part of the mass to the glycan content.

Titration of a molar excess of FL_{L27D} to FLT3_{D1-D5} and subsequent SEC-MALLS analysis resulted in a predominantly monodisperse species with a R_{hyd} exceeding that of both molecules alone (Figure 3A, red curve). With only an excess of FL_{L27D} detected, this shift indicates that despite its monomeric nature, FL_{L27D} was still able to recruit all available receptor molecules into complex formation. The molecular species corresponding to 70 kDa as determined by SEC-MALLS is well below that of a FL-mediated receptor complex (152 kDa) (Figure 3B), and therefore allowed us to infer that the apparent FL_{L27D}:FLT3 complex consists of one molecule of FL_{L27D} and one molecule of FLT3.

1.2.4. FL_{L27D} is unable to activate and internalize membrane-expressed FLT3

According to the paradigms of RTK-III activation, a ligand that fails to bring two receptors in close proximity to each other should be unable to activate its receptor. Given the 1:1 stoichiometry of FL_{L27D}:FLT3 complex, we wondered whether monomeric FL_{L27D} would be bioactive. To this end, we performed a bone marrow (BM) cell differentiation assay (Section 1.1) to validate the monomeric nature of FL_{L27D} *ex vivo* (Figure 4). In contrast to the strong potency of FL_{WT} (Figure 4, green curves), stimulation with FL_{L27D} (Figure 4, gray curves) did not result in predicted means that were at the 5%

confidence level (CL) significantly different from the mock-stimulated cells. None of the tested concentrations for FL_{L27D} lead to predicted means that were at the 5% confidence level different from the mock-stimulated condition, nor were they significantly different from each other. These results leave no doubt that even at concentrations of 1 $\mu\text{g/ml}$, FL_{L27D} fails to provide an adequate survival signal to isolated BM cells, let alone stimulate them to differentiate into DCs. Consistent with these observations, preliminary results on receptor internalization (Section 1.1) indicate that FL_{L27D} is unable to internalize the receptor (data not shown).

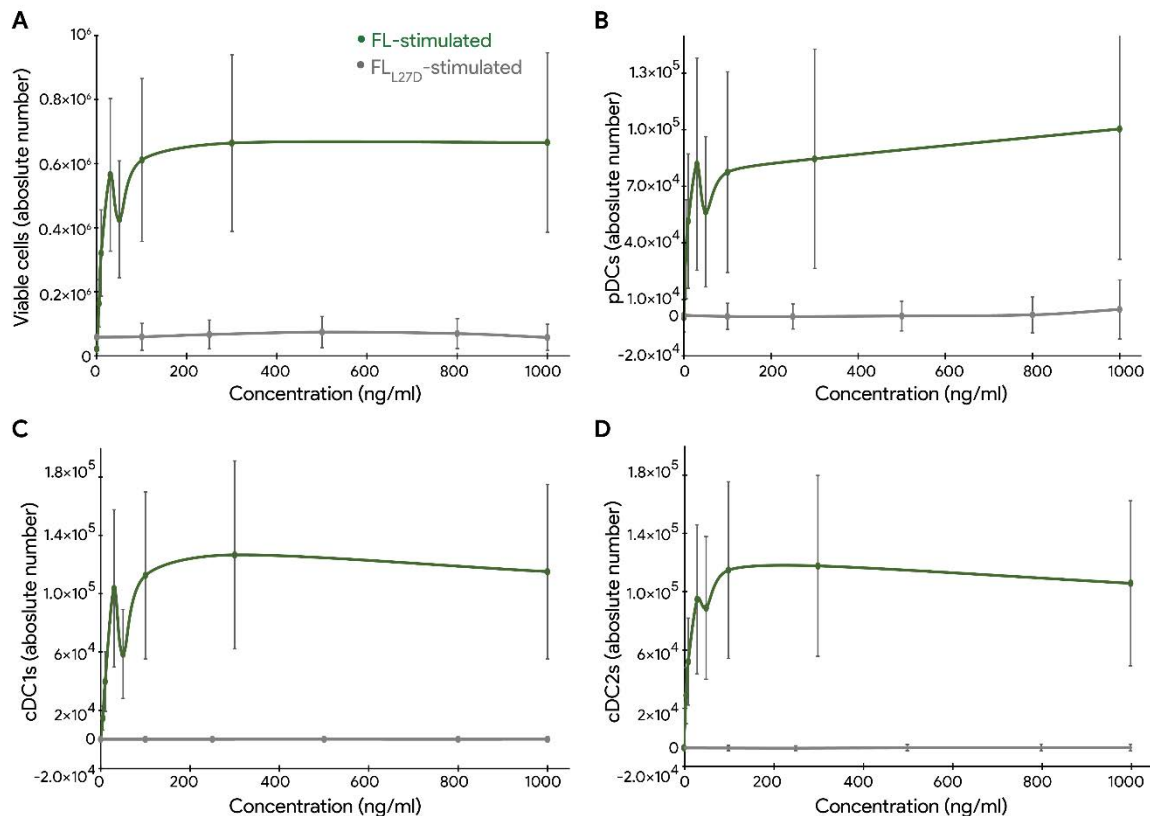


Figure 4. Even at high concentrations, FL_{L27D} fails to differentiate isolated BM cells. In contrast to previous findings that in-house produced FL_{WT} (green curves) was **A.** a highly potent viability factor for isolated BM cells and able to differentiate CDPs into **B.** pDCs, **C.** cDC1s and **D.** cDC2s at low concentrations, stimulation with the monomeric variant FL_{L27D} (gray curves) results in populations that are not statistically different from the unstimulated condition, even at stimulation with concentration as high as 1 $\mu\text{g/ml}$.

1.2.5. Structural differences between FL_{L27D} and FL_{WT} are limited to the dimerization interface region

To further validate that the mutation of leucine-27 to aspartate does not compromise the overall fold of the molecule, we pursued structural characterization of FL_{L27D} by X-ray crystallography. Initial crystallization trials resulted in the identification of multiple crystallization conditions across a wide pH range, all characterized by a high concentration (> 1.8 M) of ammonium sulfate. Subsequent optimization of these initial hits and consecutive crystallographic experiments showed that optimized crystals diffracted synchrotron X-rays to high resolution, although all diffraction patterns showed signs of multiple lattices reflecting the presence of crystal twinning. Nevertheless, we were able to index at

least one crystal to a single crystalline lattice and used the obtained data for determining the crystal structure to 1.65 Å resolution (Table 1, Figure 5).

| <u>Crystallization</u> | | <u>Refinement</u> ^{c,d} | |
|--|--|------------------------------------|-----------------------------|
| Protein | FL _{L27D} | Resolution range (Å) | 18.42 - 1.65 (1.709 - 1.65) |
| Crystallization condition | 2.0 M ammonium sulfate 0.1M HEPES pH 7.5 | Reflections in refinement | 24918 (2403) |
| | | Reflections used for R-free | 1246 (120) |
| | | R-work | 0.1780 (0.2654) |
| Cryoprotectant | none | R-free | 0.2150 (0.2849) |
| <u>Data Collection</u> ^b | | non-hydrogen atoms | 2445 |
| Beamline | PROXIMA 1 (SOLEIL, France) | Macromolecular atoms | 2218 |
| Wavelength (Å) | 0.98 | Ligand atoms | 25 |
| Detector | Pilatus 6M | Solvent atoms | 202 |
| Space group | P1 | Protein residues | 276 |
| a, b, c (Å) | 28.3, 43.49, 46.36 | RMS _{bounds} (Å) | 0.013 |
| α, β, γ (Å) | 82.82, 85.41, 85.1 | RMS _{angles} (°) | 1.59 |
| Resolution (Å) | 18.42 - 1.65 (1.709 - 1.65) | Ramachandran favored (%) | 97.79 |
| Total reflections | 70278 (4053) | Ramachandran allowed (%) | 2.21 |
| Unique reflections | 24918 (2403) | Ramachandran outliers (%) | 0.00 |
| Multiplicity | 2.81 (1.69) | Rotamer outliers (%) | 1.58 |
| Completeness (%) | 95.01 (92.57) | Clashscore | 0.68 |
| Mean I/σ(I) | 10.6 (2.33) | Average B-factor (Å ²) | 22.92 |
| Wilson B-factor (Å ²) ^b | 16.95 | macromolecules | 21.79 |
| R-meas (%) | 7.7 (56.7) | ligands | 64.72 |
| CC1/2 (%) | 99.6 (72.8) | solvent | 30.12 |
| | | TLS groups | 2 |

^a Values in parentheses correspond to the highest-resolution shell. ^b Values reported by XDS. ^c Values reported by Phenix. ^d Final refinement was performed using BUSTER 2.10.3.

Observing its crystallographic model, it is instantly clear that the overall structure of FL_{L27D} superimposes very well with a single protomer of FL_{WT} (Figure 5A). Indeed, not taking the αB-βA loop (residues 25-30) into account, the average Cα root-mean-square deviation (R.M.S.D.) with FL_{WT} (PDB 1ETE) is only 0.851 Å for 120 aligned atoms – indicating no large structural changes in the overall conformation of FL_{L27D}. Given the observation that FL_{L27D} still binds FLT3, it comes as no surprise that the absence of structural deviation from FL_{WT} remains valid for residues 6-13, key players in the largest interaction site of the FL:FLT3 epitope (Verstraete et al. 2011). Importantly, despite the unit cell of the diffracting crystal containing 2 copies of FL_{L27D} (Figure 5B), the 2-fold symmetry axis found within FL_{WT} (Figure 5A, inset) is shifted away from an orientation perpendicular to the longest dimension of each protomer, and now follows the plane of the twisted beta-sheet. Likewise, no combination of symmetry relations can reconstitute the head-to-head dimer resembling F_{WT}, despite that the loop containing Asp27 is located near tightly-packed crystal-lattice contacts.

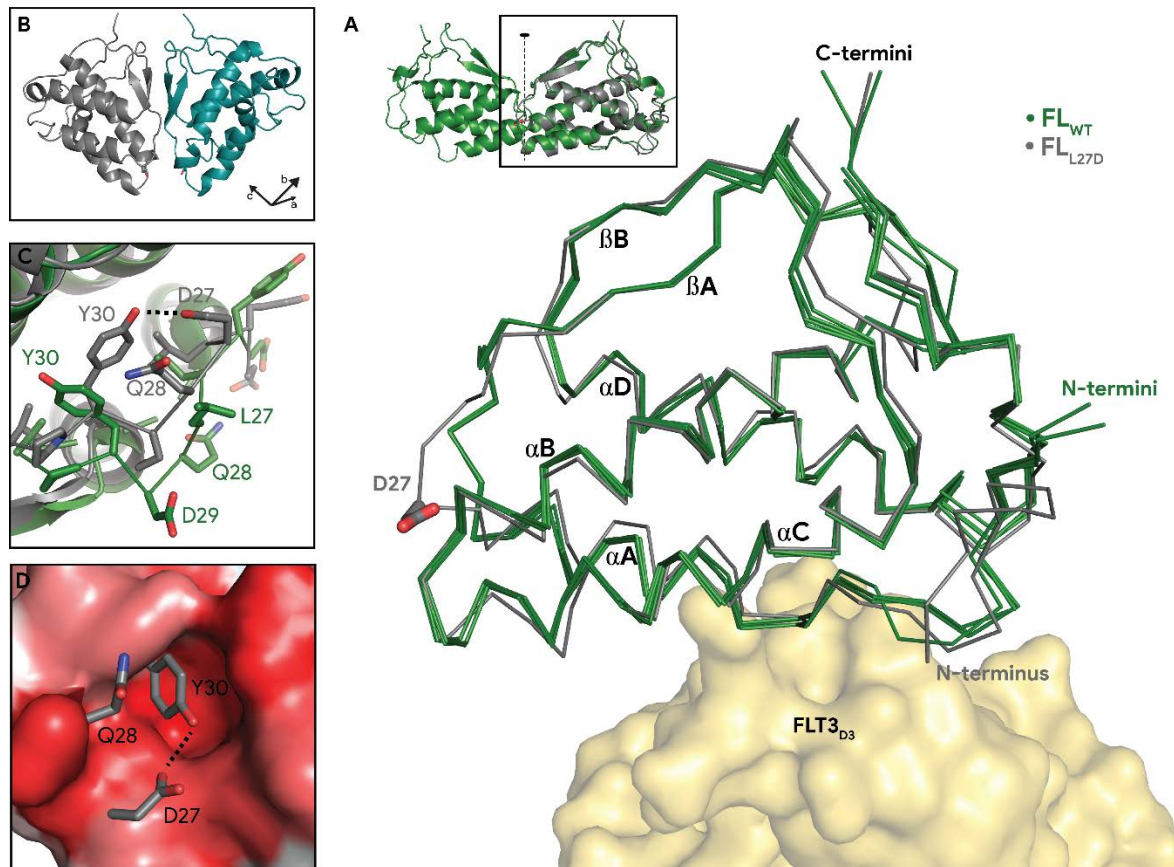


Figure 5. Structural differences between FL_{L27D} and FL_{WT} are limited to the dimerization interface region.

A. Superimposition of FL_{L27D} (gray) and FL_{WT} (green). Crystallographic models of the ligands are shown in cartoon representation with indication of the 2-fold symmetry axis (inset) or in ribbon diagrams (main panel), the sidechain of FL_{L27D-Asp27} is shown as sticks and FLT3 is shown in surface representation. With the exception of the α B- β A loop, the main chain of both FL_{L27D} molecules superimposes very well (average R.M.S.D. of 0.85 Å) with the main chain of all four FL_{WT} copies (PDB 1ETE). **B. The asymmetric unit of FL_{L27D} crystals features a top-to-top packing of molecules.** This topology is distinct from the 2-fold symmetry axis within one FL_{WT} molecule, and supports that the Leu27 to aspartate mutation prevents dimerization even in the context of crystal packing. **C. Detail of the superimposed α B- β A loop of FL_{L27D} (gray) and FL_{WT} (green).** Loop residues are shown as sticks. Hydrogen bonds are indicated with a dashed line. **D. Detail of the superimposed α B- β A loop of FL_{L27D} and FL_{WT}, as viewed from the second FL_{WT} protomer.** FL_{WT} is colored according the Eisenberg hydrophobicity scale (red is more hydrophobic), key residues of FL_{L27D} are shown as sticks. Hydrogen bonds are indicated with a dashed line.

Given that the hydrophobic cavity that sheltered Leu27 of the accompanying FL_{WT} protomer would remain solvent-exposed after the L27D monomerization event, we wondered how FL_{L27D} would structurally compensate for this. When analyzing the conformational changes at the α B- β A loop (Figure 5C), we surprisingly noticed that Asp27 is able to recruit Tyr30 in an intra-molecular hydrogen bond, thus stabilizing the rotamer conformation of the latter in such a way that it effectively closes the hydrophobic cavity that this residue otherwise helps delineating in the model of FL_{WT} (Figure 5D). That Asp27 therefore not only disrupts the hydrophobic dimer interface of FLT3 Ligand, but simultaneously stabilizes the resulting monomer by intra-molecular interactions sealing the otherwise solvent-exposed hydrophobic cavity, is an astonishing example of serendipity and a remarkable showcase of protein plasticity.

Collectively, this crystal structure of FL_{L27D} shows that a single point mutation indeed alters the conformation of the dimeric interface, rendering it incapable of dimerization. However, this structural accommodation remains contained within the region of what was previously the dimeric interface, whilst the receptor-interacting regions remain unaffected. Thus, this model provides a rationale for how a point mutation is able to monomerize the ligand without altering its receptor-binding capacity.

Despite the current knowledge that the ligand adopts a preformed conformation when binding to its receptor, it cannot be excluded that the effects of the monomerizing L27D point mutation extend beyond the region involved in the dimer interface of the wild-type ligand in the presence of its receptor. We therefore sought to examine the FL_{L27D}:FLT3 binding interface via X-ray crystallography of the complex.

1.2.6. The crystal structure of the FL_{L27D}:FLT3 complex confirms an intact receptor-binding interface.

Although the absence of any structural changes in the receptor-binding epitope of FL_{L27D} rationalizes the argument that the monomerizing point mutation does not alter the protein's receptor-binding characteristics, it cannot be excluded that presence of a binding partner could have unanticipated effects on the conformation of residues involved in the interaction site.

We pursued structural evidence for this argument by performing crystallization experiments involving FL_{L27D} and FLT3_{D1-D5}, for which a tetracycline-inducible HEK293S MGAT1^{-/-} TR⁺ cell line was generated (Reeves et al. 2002). This cell line produces proteins with a limited N-linked carbohydrate structures that are more amenable for crystallization experiments (Chang et al. 2007). After biochemical reconstitution and purification of the binary FL_{L27D}:FLT3_{D1-D5} complex, purification tags were enzymatically removed and Man₅GlcNAc₂ glycan trees were trimmed to the first GlcNAc using thrombin and EndoH_f, respectively. The complex was concentrated to 3.5 mg/ml and reproducibly crystallized in conditions containing only sodium phosphate as precipitant. Despite extensive optimization, the rod-like crystals remained smaller than 30 x 30 x 10-30 µm, were cumbersome to cryoprotect, and only diffracted to 6.5 Å with very poor merging statistics.

To increase chances of generating crystals with a higher diffracting quality we reasoned that a single-domain VHH camelid antibody 3FF6, which our group had previously developed against FLT3, could be used as a crystallization adjuvant. The heterotrimeric complex was treated similarly to the dimeric one and concentrated to 3.5 mg/ml. One crystallization condition was discovered and after extensive optimization, multiple datasets were collected of crystals that grew in 0.9 M ammonium sulfate, 10% PEG 8000, MES buffer pH 8.3 set up with a protein:mother liquor drop ratio of 1:4. The crystal yielding the best dataset was cryoprotected with 25% ethylene glycol in a 1.5 M ammonium sulfate, HEPES pH 7.9 stabilization buffer.

Initially, the space group was determined to be P4₃2₁ with favorable values for all indexing statistics, indicating data to 4.2 Å. The resulting dataset was analyzed by *Xtriage* (Adams et al. 2010) to identify idiosyncrasies with the measured X-ray intensities, which revealed that the observed centric reflections were significantly different than is expected from good data. As the L-test and H-test did not imply twinning and the Patterson function p-value did not indicate pseudo-translational symmetry,

we continued working with this dataset. Maximum-likelihood molecular replacement by Phaser from the CCP4 package (Winn et al. 2011; McCoy et al. 2007) was carried out using FLT3_{D2-D3} (PDBID 3QS7) and resulted in placement of the molecule with TFZ and LLG scores of 20.8 and 239 respectively. Importantly, after only one initial cycle of simulated annealing followed by rigid-body refinement, unbiased density for a four-helical bundle could be seen in the F_O-F_C difference density map, confirming the presence of FL_{L27D}. Using the initial solution, one copy of FLT3_{D4} and FL_{L27D} could be automatically placed into the density. After refinement, positive difference density allowed manual placing of FLT3_{D5}, derived from crystallographic model of FLT3_{T343I} in complex with FL (Section 2.1.3).

Despite this initial success, the R-factors stalled alarmingly at R_{free} 0.34. Furthermore, as subsequent cycles of model building in Coot and model refinement with BUSTER (Bricogne et al. 2011) only led to worsening of the crystallographic R-factors, the possibility of operating in the wrong crystallographic space group was raised. Indeed, refinement of the model in P1 readily returned better refinement statistics, whilst refinement in P₄₃, which would appear as P₄₃22 in case of merohedral twinning, did not yield an immediate positive effect on the quality of the electron density map or the statistics. Given this initial diagnosis, we started extensive exploration of different data processing approaches for two different datasets, being the 4.2 Å dataset and one diffracting to 4.6 Å. To guarantee a robust statistical power in the reporting of R_{free}, the percentage of test reflections was increased where needed to contain at least 1000 reflections. Correction for anisotropy was performed using the UCLA Diffraction Anisotropy Server (Strong et al. 2006), and pdb-tools from the Phenix package were used to transfer the R_{free} reflection set from to initial dataset to its anisotropy-corrected sibling. Phasing was performed using Phaser of the CCP4 package and the FL_{L27D}:FLT3_{D2-D5} model from the initial rounds of refinement, and the programs reported in Table 2 were run sequentially without any manual intervention of the model.

Table 2 | Overview of different datasets and corresponding results from consecutively run refinement programs.

| Dataset | Resolution | anisotropy corrected | Space group | BUSTER R _{work} /R _{free} | pdb-redo R _{work} /R _{free} | Phenix R _{work} /R _{free} | BUSTER R _{work} /R _{free} |
|---------|------------|----------------------|--------------------------------|--|--|--|--|
| A | 4.6 Å | no | P1 | 0.2428/0.2498 | 0.322/0.328 | 0.3117/0.3551 | 0.2501/0.2571 |
| A | 4.6 Å | no | P ₄ ₃ 22 | 0.2609/0.3364 | 0.339/0.381 | 0.3247/0.3928 | - |
| B | 4.6 Å | no | P1 | 0.2493/0.2786 | 0.323/0.330 | 0.2997/0.3227 | 0.2608/0.2835 |
| B | 4.6 Å | no | P ₄ ₃ 22 | 0.2750/0.3095 | 0.340/0.369 | 0.3281/0.3750 | - |
| B | 4.3 Å | no | P1 | 0.2555/0.2800 | 0.328/0.340 | 0.3086/0.3377 | 0.2592/0.2852 |
| B | 4.2 Å | no | P ₄ ₃ 22 | 0.2751/0.3063 | 0.350/0.372 | 0.335/0.3777 | - |
| A | 4.6 Å | yes | P1 | 0.2370/0.2579 | 0.298/0.304 | 0.2782/0.3079 | 0.2427/0.2635 |
| A | 4.6 Å | yes | P ₄ ₃ 22 | 0.2580/0.3183 | 0.312/0.391 | - | - |
| B | 4.6 Å | yes | P1 | 0.2447/0.2794 | 0.278/0.300 | 0.2781/0.3071 | 0.2554/0.2858 |
| B | 4.6 Å | yes | P ₄ ₃ 22 | 0.2740/0.2997 | 0.336/0.389 | - | - |
| B | 4.8 Å | yes | P1 | 0.2465/0.2785 | 0.281/0.306 | 0.2807/0.3056 | 0.2566/0.2866 |
| B | 4.8 Å | yes | P ₄ ₃ 22 | 0.2714/0.3043 | 0.328/0.364 | - | - |

The results in Table 2 show that all three refinement programs agree that P1 is the preferred space group, confirming our initial diagnosis of having indexed in the wrong space group. Interestingly, the 2nd BUSTER refinement consistently features higher R_{work} and R_{free} values than the first, indicating that

the sequential refinement of pdb-redo (Joosten et al. 2012) and Phenix worsen the model after the initial refinement using BUSTER. Therefore, modeling was continued using the output model of BUSTER, based on the 4.3 Å resolution dataset in P1 and corrected for anisotropy with a high-resolution cutoff of 4.8 Å, as determined by the UCLA Diffraction Anisotropy Server.

Table 3 | Comparison of refinement statistics after anisotropy correction by different servers.

| Space group | Resolution | anisotropy corrected | Rwork | Rfree |
|-------------|------------|----------------------|--------|--------|
| P1 | 4.3 Å | no | 0.2617 | 0.3094 |
| P1 | 4.8 Å | UCLA server | 0.2666 | 0.3143 |
| P1 | 4.4 Å | STARANISO | 0.2462 | 0.2883 |

Given this rather conservative cutoff, the 4.2 Å resolution dataset was corrected for anisotropy using the STARANISO anisotropy & Bayesian estimation server (Tickle et al. 2018) using $I/\sigma_I=1$ as a high-resolution cutoff. The 4.8 Å resolution model, already

improved by manual model building in coot and further refinement in BUSTER, was used to assess which dataset should be preferred. As evident from Table 3, including higher-resolution data below the 4.8 Å improves the quality of the model despite the presence of mild anisotropy corrected for by the UCLA Diffraction Anisotropy Server. In contrast, anisotropy correction by STARANISO significantly lowered the R_{free} at the expense of 0.1 Å in resolution compared to the untreated dataset.

Table 4 | X-ray data and refinement statistics of FL_{L27D} in complex with FLT3_{D1-D5}

| Crystallization | | Refinement ^{d,e} | |
|--|---|------------------------------------|-------------------------------|
| Protein complex | FL _{L27D} :FLT3 _{D1-D5} :3FF6 | Resolution range (Å) | 47.15 - 4.416 (4.573 - 4.416) |
| Crystallization condition | 0.9 M ammonium sulfate 10% PEG 8000 MES buffer pH 8.3 | Reflections in refinement | 37026 (98) |
| | | Reflections used for R-free | 1836 (4) |
| | | R-work | 0.2320 (0.4075) |
| Cryoprotectant | 25% ethylene glycol | R-free | 0.2840 (0.3046) |
| Structural model | FL _{L27D} :FLT3 _{D1-D5} complex | non-hydrogen atoms | 26692 |
| | | Macromolecular atoms | 26468 |
| | | Ligand atoms | 224 |
| | | Solvent atoms | 0 |
| Data Collection^{b,c} | | Protein residues | 4466 |
| Beamline ^b | PXIII (SLS, Switzerland) | RMS _{bounds} (Å) | 0.014 |
| Wavelength (Å) ^b | 1.00 | RMS _{angles} (°) | 1.88 |
| Detector ^b | Pilatus 2M-F | Ramachandran favored (%) | 77.99 |
| Space group ^b | P1 | Ramachandran allowed (%) | 16.35 |
| a, b, c (Å) ^b | 139.457, 139.5, 143.96 | Ramachandran outliers (%) | 5.66 |
| α, β, γ (Å) ^b | 90, 90.013, 90.005 | Rotamer outliers (%) | 17.66 |
| Resolution (Å) ^c | 49.31 - 4.30 (4.54 - 4.3) | Clashscore | 3.80 |
| Total reflections ^c | 114487 (16898) | Average B-factor (Å ²) | 242.84 |
| Unique reflections ^c | 68043 (10063) | macromolecules | 242.40 |
| Multiplicity ^c | 1.68 (1.68) | ligands | 294.51 |
| Completeness (%) ^c | 92.3 (93.0) | solvent | n/a |
| Mean $I/\sigma(I)$ ^c | 4.2 (0.30) | TLS groups | 16 |
| Wilson B-factor (Å ²) ^b | 205.47 | | |
| R-meas (%) ^c | 11.8 (225.0) | | |
| CC1/2 (%) ^b | 99.8 (22.2) | | |

^a Values in parentheses correspond to the highest-resolution shell. ^b Values reported by XDS. ^c Values reported by STARANISO anisotropy & Bayesian estimation server. ^d Values reported by Phenix. ^e Final refinement was performed in BUSTER 2.10.3

The model discussed below is therefore the result of further model editing in coot followed by refinement with BUSTER using the 4.4 Å STARANISO anisotropy-corrected dataset, indexed in P1. As is apparent from the statistics regarding the data collection and refinement (Table 4), the model discussed below still needs improvement. Nonetheless, it allows to draw some preliminary conclusions.

The crystal structure of the FL_{L27D}:FLT3_{D1-D5} provides direct structural evidence that FL_{L27D} is able to establish a complex with FLT3_{D1-D5}, and delivers key insights into the binding mode of FL_{L27D} to FLT3_{D3} (Figure 6). For all 8 copies in the asymmetric unit, the rigid FLT3_{D2-D4} modules are clearly visible in the electron density map. In contrast, the level to which the two domains at the extremities of the receptor are defined in the electron density map, varies per copy but is overall poor. A crystallographic model of FLT3_{T343I} in complex with FL (Section 2.1.3) was essential for modeling FLT3_{D5}, but despite the availability of a reliable model regarding FLT3_{D1} (PDB 3QS7), this domain remained recalcitrant to modeling, suggesting a high degree of flexibility. Surprisingly, no evidence for the presence of the 3FF6 VHH fragment could be detected in the positive difference density of the $F_{\text{obs}}-F_{\text{calc}}$ calculated map. It therefore seems that despite its presence in the protein mixture as a crystallization adjuvant, 3FF6 was expelled from the FL_{L27D}:FLT3_{D1-D5}:3FF6 complex in favor of crystal packing.

The ambiguity in electron density at domain 1 and domain 5 notwithstanding, the electron density map at the FL_{L27D}-FLT3_{D3} module was detailed enough to confidently trace the main chain of both proteins (Figure 6B). Superimposition of this model with the complex between FL_{WT} and FLT3_{D1-D4} (PDBID 3QS7) shows good structural overlap for the FL:FLT3_{D2-D4} module, reflected by the average root-mean-square deviation (R.M.S.D.) of 1.42 Å at the C_α level (381 aligned atoms). This level of conformational similarity remains valid down to the level of the interaction epitope (Figure 6C). This result is in line with expectations based on the conformational robustness of each FL subunit in terms of structural rearrangements upon binding the receptor (Verstraete et al. 2011), and the high structural similarity between FL and FL_{L27D} at the receptor binding epitope of FL_{L27D} in absence of the receptor (Figure 5A). Importantly, even in the presence of the receptor, no symmetry relationship can be found that would result in a head-to-head interaction of two FL_{L27D} molecules, thereby reconstituting the relative topology of FL_{WT} protomers.

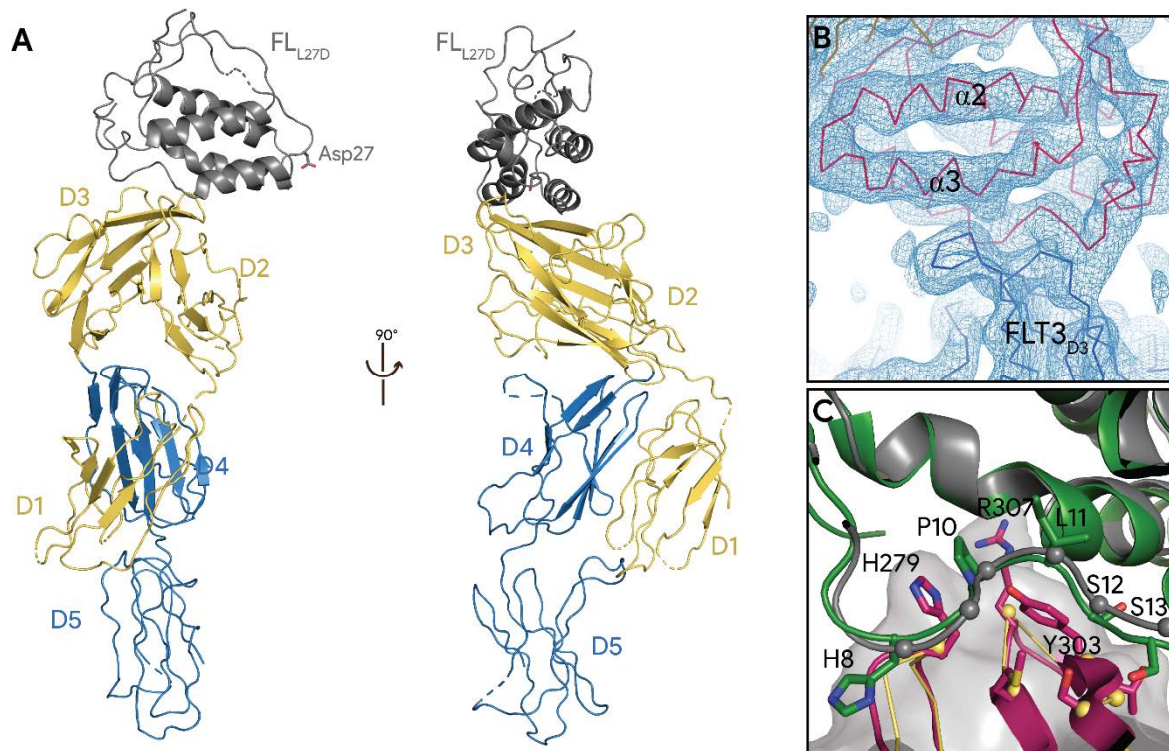


Figure 6. Despite its monomeric nature, the interaction epitope of FL_{L27D} on FLT3 is identical to the binding epitope of its dimeric counterpart. **A. Architecture of the FL_{L27D}:FLT3_{D1-D5} complex.** “Front” and “side” view of the determined X-ray crystallography structure of the complex. FL_{L27D} (gray) is shown in cartoon representation, the sidechain of Asp27 is shown as sticks. The extracellular region of FLT3 is shown in cartoon representation with its individual domains labeled D1 to D5. The first 3 IgG-like domains are colored yelloworange, the 2 membrane-proximal domains are colored blue. **B. Electron density allowed confident main-chain tracing at the interaction interface.** Electron-density map, contoured at 1 σ , is shown as a mesh. FL_{L27D} (red) and FLT3_{D3} (blue) are shown in ribbon representation. **C. Detailed view of FL_{WT}:FLT3_{D1-D5} and FL_{L27D}:FLT3_{D1-D5} superimposed interaction epitopes.** Key residues of the interaction epitope between FL_{WT} (green; cartoon representation) and FLT3_{D1-D5} (fuchsia; cartoon representation overlaid onto a transparent surface representation) are labeled, and their sidechains are shown as sticks. C α atoms of equivalent residues in the complex between FL_{L27D} (gray, cartoon representation) and FLT3_{D1-D5} (yelloworange, ribbon diagram) are shown as spheres.

1.2.7. FLT3_{D1} possibly tethers the inactive form of the receptor.

Already upon reporting the crystallographic model of FLT3 in complex with FL, it was suggested that FLT3_{D1}, atypical in both sequence and positioning relative to the rest of the molecule, could serve as a module that stabilizes the inactive receptor. Given that previous models were always assemblies of FLT3 in presence of the canonical ligand, complexation with FL_{L27D} enabled us for the first time to capture FLT3 in a conformation without an activating ligand.

When the complexes of FL-bound and FL_{L27D}-bound FLT3 are superimposed based on the alignment of the FLT3_{D2-D4} module, several surprising features become apparent (Figure 7). Firstly, by a movement of 108° relative to FLT3_{D2}, domain 1 in the FL_{L27D}-bound form seems to fold back onto domain 4, allowing residues of the BC- and GH-loop of FLT3_{D1} to interact with the extended DE loop (residues 486 to 496) of FLT3_{D5} (Figure 7D). However, this interaction is only made possible by a simultaneous 30.9° reorientation of the latter relative to FLT3_{D4} (Figure 7E). Interestingly, where domain 5 in FL_{WT}-mediated complexes (PDB 3QS9 and Section 2.1.3) adopts different orientations relative to FLT3_{D4}, when superimposing all copies in the asymmetric unit we now observe that all 8

copies in the FL_{L27D}-mediated crystallographic structure structurally superimpose almost perfectly down to the level of FLT3_{D5} (Figure 7C). Thus it appears that the interaction with FLT3_{D1} effectively locks domain 5 in its most extreme position observed so far, effectively pulling this most membrane proximal domain away from the central plane of the FL_{WT}:FLT3_{D1-D5} ternary complex.

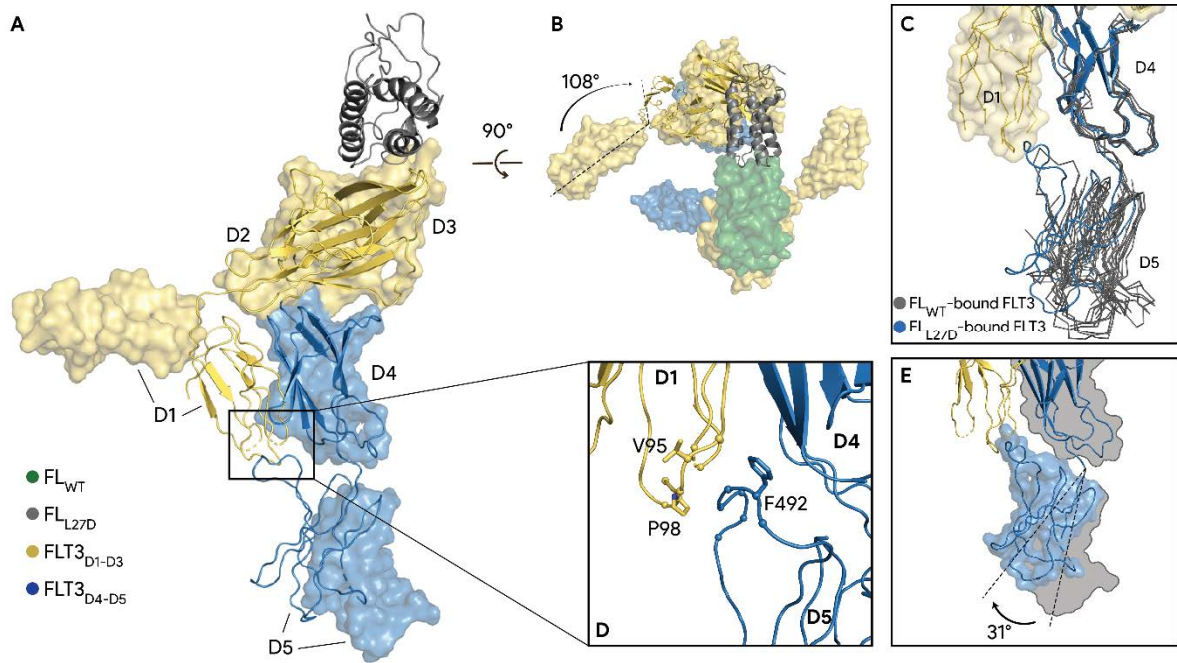


Figure 7. FLT3_{D1} possibly tethers an inactive form of the receptor. Complexation with FL_{L27D} allowed for the first time to capture the extracellular domain of FLT3 without the presence of its activating ligand. **A. “Side” view and B. “top” view of the superimposition between FLT3_{D1-D5} in complex with its two ligands.** The crystallographic complex of FL_{L27D} (gray) and FLT3_{D1-D5} (yellow and blue) are shown in cartoon representation. The (partial) complex between FL_{WT} (green) and FLT3_{D1-D5} (PDB 3QS9) are shown in surface representation. The IgG-like domains of FLT3 are annotated on both structures. **C. The interaction with FLT3_{D1} locks domain 5 in its most extreme observed orientation.** Copies of FLT3 (PDB 3QS9) and FLT3_{T343} (Section 2.1.3) are colored gray, shown in ribbon diagram and superimposed to FLT3 from the FL_{L27D}:FLT3_{D1-D5} crystallographic model (yellow and blue) using FLT3_{D4} as reference. **D. Detailed view on FLT3_{D1}:FLT3_{D5} interaction epitope.** Residues for which the electron density allowed modeling of the sidechains, are shown as sticks. C α atoms of the residues predicted to be part in the interaction, are shown as spheres. **E. Surface representation highlighting the 31° reorientation of FLT3_{D5} relative to FLT3_{D4}.** The contour of FL_{WT}-bound FLT3 is colored gray, FL_{L27D}-bound FLT3_{D1} (yellow orange) and FLT3_{D4} (blue) are shown in cartoon representation. FL_{L27D}-bound FLT3_{D5} (blue) is shown in cartoon onto transparent surface representation.

In conclusion, based on available crystal structures of FLT3 Ligand (FL) and the observation that substitution of leucine-27 to proline results in concentration-dependent dimerization of FL, we engineered an FL variant with a leucine-27 to aspartate substitution (FL_{L27D}). SEC-MALLS analysis showed that FL_{L27D} had the molecular weight of an FL protomer, and was still capable of recruiting all available receptor molecules into a 1:1 stoichiometric complex. *Ex vivo* analysis confirmed that FL_{L27D} could not activate FLT3-receptor mediated signalling pathways, presumably due to the lack of receptor-dimerization capabilities. Finally, crystal structures of FL_{L27D} and its complex with FLT3_{D1-D5} validated the presumption that the L27D mutation only disrupts the dimeric interface without altering

the FLT3 binding epitope. We can therefore conclude that FL_{L27D} is a *bona fide* monomeric equivalent of an FL protomer.

1.3. Engineering a heterodimeric FLT3 Ligand

1.3.1. Rationale and strategy

Inevitably, receptor contacts exclusively mediated by ligand binding impose a level of cooperativity in the assembly of extracellular complex formation. By developing a monomeric ligand variant that employs an identical binding epitope on the receptor as its dimeric sibling, we engineered a tool allowing detection of possible cooperative mechanisms during the assembly of a ternary FL:FLT3 complex. However, as has been demonstrated for the CSF-1:CSF-1R complex (Elegheert et al. 2011, 2012; Felix et al. 2015), such cooperativity can possibly be deconvoluted into two different stages. During the assembly of an activated CSF-1R complex, a first level of cooperativity is detected right after formation of the binary encounter complex, in which an inter-subunit reorientation increases the affinity of the ligand for a second receptor molecule from 3 μ M to 213 nM. Following the formation of a ternary complex, additional receptor:receptor-contacts further lower the overall Gibbs free energy of this complex. As such, these receptor contacts effectively increase affinity for the ligand by a factor of 15 ($K_D = 14$ nM), which represents a second step of positive cooperativity. For the CSF-1:CSF-1R complex, it has been postulated that the sampling of the conformational space by the ligand is a prerequisite to allow homotypic receptor interactions taking place (Felix et al. 2015).

Such inter-unit plasticity has been described for FL, where one can observe a 5-6° increase in the tilt angle along the 2-fold axis when comparing the structure of unbound and bound FL (Verstraete et al. 2011). However, as no evidence could be found for subsequent homotypic receptor contacts, the relevance of this conformational change and its contribution to the overall affinity of the receptor for its ligand, remained an open question.

By generating a monomeric variant of FL, we effectively overcome the experimental limitations imposed by the instability of FLT3_{D1-D3} and can now probe for possible cooperativity during assembly of an activated FLT3 receptor complex. However, in such an experimental setup, one would not be able to further distinguish between cooperativity at the level of the ligand, cooperativity at the level of the receptor or an interplay of cooperativity at both levels. Additional experiments with a ligand featuring a dimeric interface but yet unable to bind 2 receptors simultaneously, would therefore greatly complement the experiments done with FL and FL_{L27D}. We envisioned such ligand as a heterodimeric FL species (FL_{WT/KO}), consisting of one wild-type protomer in complex with a second protomer, of which the receptor-binding was abolished (Figure 8A).

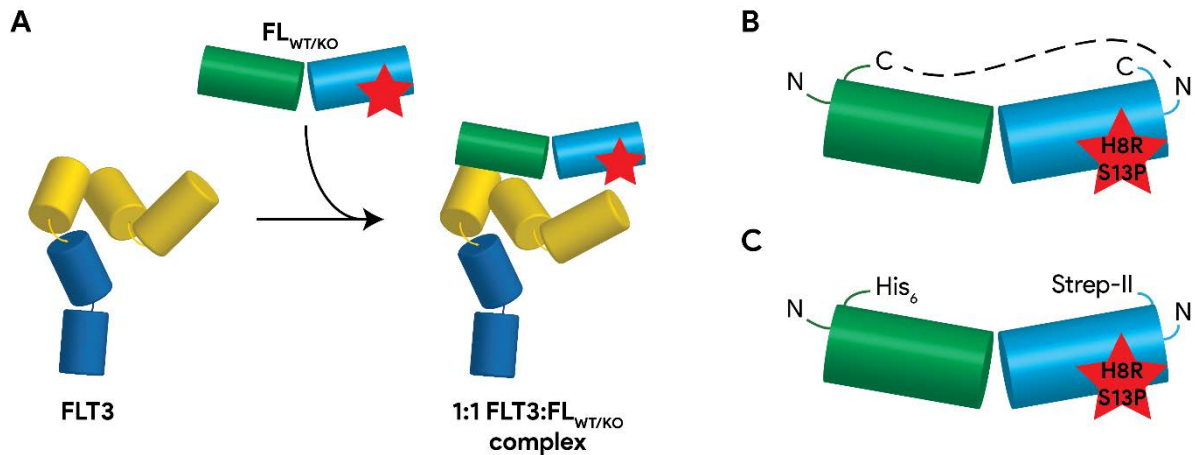


Figure 8. A heterodimeric FL_{WT/KO} variant capable of recruiting only 1 receptor. **A.** Principle of complex formation. An FL variant in which a wild-type protomer (green) heterodimerizes with a protomer with an abolished FLT3 binding epitope (blue, star indicates mutations) can only engage one receptor into complex formation. **B.** Principle of a translationally linked heterodimeric FL_{WT/KO} variant. N- and C-termini are indicated, dashed line represents the linker. **C.** Principle of a heterodimer in a co-expression setup. The presence of two different tags allows tandem purification of the heterodimer.

The observation that SCF, ligand for KIT, exists as a monomer in solution and dimerizes in a highly dynamical event, forewarned that a heterodimeric FL_{WT/KO} species might swap protomers, generating 3 FL variants in equilibrium (FL_{WT/WT}, FL_{WT/KO} and FL_{KO/KO}) (Hsu et al. 1997; Z. Zhang et al. 2000). As a covalently linked dimer would probably show a lower tendency to swap protomers, we initially followed the approach of Lu *et al.* to generate a translationally-linked FL molecule (Lu et al. 2002) (Figure 8B). However, instead of linking two wild-type FL protomers, knock-out point mutations would be introduced to abolish receptor binding in one of the protomers. Such engineered FLT3 ligand would thus consist of two translationally linked FL protomers of which only one would be able to bind the receptor, and at the same time allowing for inter-subunit reorientations.

Inspiration for such knock-out mutations was found in a study by Graddis *et al.* (Graddis et al. 1998) describing different amino acid substitutions within FL that effectively alter the ligand's activity. By mapping their findings on the model of FL in complex with FLT3 (Verstraete et al. 2011), we generated a construct in which histidine-8 and serine-13 were exchanged for an arginine and a proline respectively (FL_{H8R-S13P}).

In a first stage, attempts were made to reproduce the data from Lu *et al.* (Lu et al. 2002) and generate an FLT3 ligand of which the protomers were fused using a (GGGS)₃ linker. We were however not able to express and purify this construct as a stable and well-behaving protein, although we applied several small changes to the linker and eventually generated a construct with (GGS)₂₀ linker to counteract the possibility of a suboptimal linker length. Expression was tried using both HEK293T cells and *E. coli* as expression host. Driven by these disappointing results, we finally cloned FL_{H8R-S13P} with a Strep-II tag, which by co-expressing with hexahistidine-tagged FL_{WT} would allow us to purify a heterodimeric construct using 2-step tandem affinity chromatography, exploiting first the presence of the hexahistidine tag, followed by a purification based on the presence of the Strep-II tag (Figure 8C).

Expression and purification of this heterodimeric species were first performed in HEK293T cell line, transfected with a 1:1 DNA-ratio of both constructs. A first attempt for large-scale expression and purification resulted in not more than 500 µg protein, but subsequent expression campaigns were not able to repeat this result. Meanwhile, bacterial expression and *in vitro* refolding following protocols established for FL_{WT} (Verstraete et al. 2009) failed, even after several optimizations. Notably, attempts to purify and refold *E. coli*-expressed FL_{H8R-S13P} in the absence of FL_{WT}, resulted in severe precipitation upon dialysis. Guided by a growing suspicion that the problem of a low yield might be reflecting an inherent biochemical problem during protein folding, we expressed FL_{H8R-S13P} by transient transfection of HEK293T on a small scale and evaluated expression levels by Western blotting (Figure 9). Considering optimal amounts for transfection determined by Aricescu and colleagues (Aricescu, Lu, and Jones 2006), HEK293T cells were transfected with different ratios of DNA coding for each construct. The different tags on each protomer allowed for discrete analysis of their expression.

Figure 9 demonstrates that the titration of plasmid DNA coding for FL_{WT} to plasmid DNA coding for FL_{H8R-S13P} seems to quench the expression levels of the latter. This effect can be seen both when the total amount of transfected DNA does not exceed optimal amounts (Figure 9A; optimal DNA amounts are considered 100%) as well as when increasing only the absolute amounts of DNA coding for FL_{WT} to a total above the optimal (Figure 9B; optimal DNA amounts are considered as 100%). Together, these two experiments indicate that upon transfecting increasing amounts of its coding DNA, FL_{WT} seems to be able to take over the translational machinery at the expense of the expression of FL_{H8R-S13P}. It is not known if this is due to the two point mutations, to the Strep-II tag, or a combination of both.

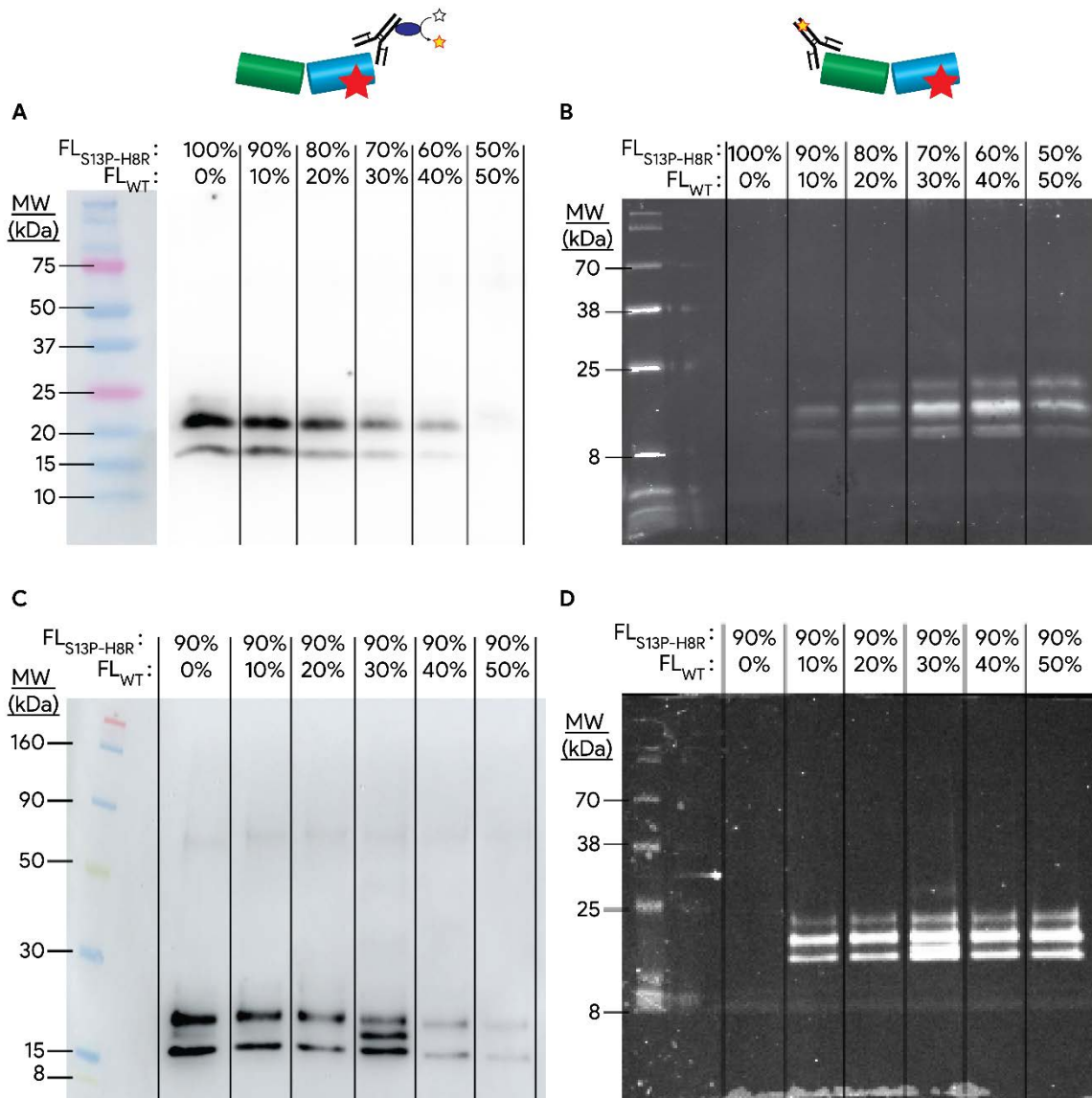


Figure 9. Titration of DNA coding for FL_{WT} quenches expression of FL_{H8R-S13P}. Based on protocols of Aricescu and colleagues, the optimal amounts of transfected DNA was considered as 100%. FL_{H8R-S13P} was detected using an HRP-conjugated anti-Strep-II antibody (left panels), FL_{WT} was detected using a Dylight™800-conjugated anti-c-terminal-6xHis antibody (right panels). **A, B.** Gradual replacement of plasmid DNA coding for FL_{H8R-S13P} by DNA coding for FL_{WT} quickly diminishes expression of the first. Moving from a transfection using exclusively DNA for FL_{H8R-S13P} (100% + 0%) to an equal concentration of both constructs (50%+50%) has a detrimental effect on expression of FL_{H8R-S13P}. **C, D.** Gradually adding more plasmid DNA coding for FL_{WT} reveals a hostile take-over of the translation machinery. Step-wise addition of plasmid DNA coding for FL_{WT} (0% to 50%) to DNA coding for FL_{H8R-S13P} (90% throughout) shows that even 10% of the first (second lane) decreases expression of the latter.

Based on the results of the expression tests, a 9:1 ratio of plasmid DNA coding for FL_{H8R-S13P} and FL_{WT} respectively, was used for large-scale expressions in both HEK293T and suspension-adapted HEK293S cells. Although balancing of the transfected DNA ratios allowed purification of this heterodimeric species, the total yield from several batches was 0.6 mg, which met sample requirements for initial characterization of the sample by SEC-MALLS.

1.3.2. MALLS analysis confirms that FL_{WT/KO} only binds one receptor molecule

Prior studies on the related hematopoietic cytokine stem cell factor (SCF) had suggested that SCF dimerization is concentration dependent and dynamic, implying the ability of SCF protomers to swap (Z. Zhang et al. 2000; Hsu et al. 1997). Being aware that this possibility could apply in the case of FL, we initiated biophysical characterization of the heterodimeric FL_{WT/KO} with an experiment allowing to detect such protomer swapping. To this end, we kept FL_{WT/KO} for 4 days at 4°C, followed by overnight incubation at room temperature, and subsequently analyzed both the unbound protein and its complex with FLT3_{D1-D5} on SEC-MALLS (Figure 10).

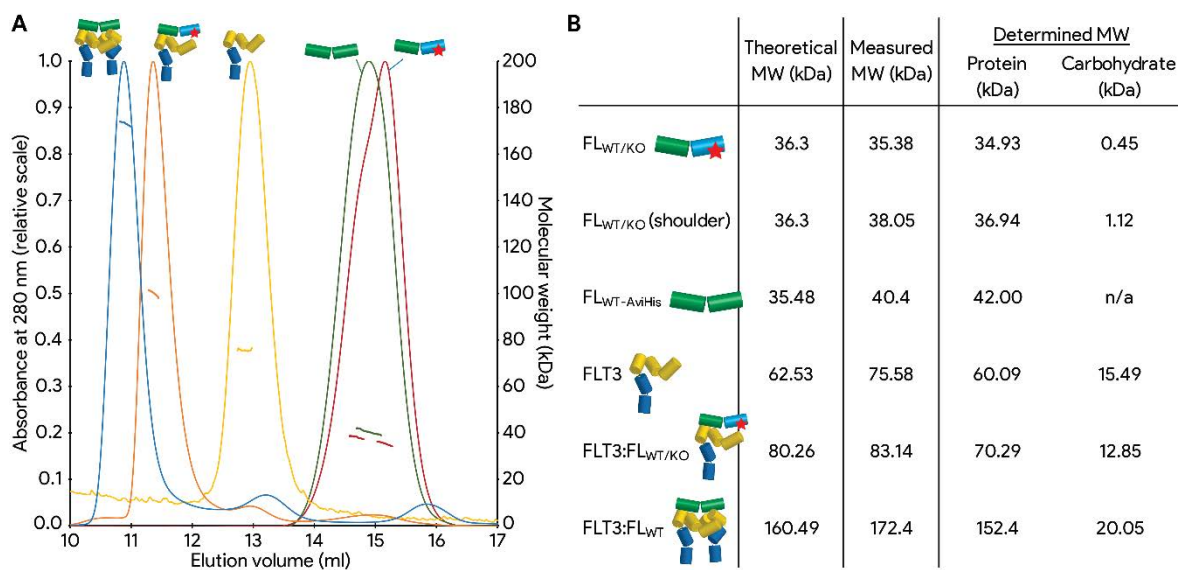


Figure 10. FL_{WT/KO} forms a binary complex with FLT3_{D1-D5}. **A.** SEC-MALLS analysis of FL_{WT}, FL_{WT/KO} and receptor-complexes thereof. Elution profile monitored by the absorbance at 280 nm (left axis) plotted against the SEC retention volume, and overlaid with the measured molecular weight (right axis). FL_{WT} (green) is able to recruit 2 FLT3_{D1-D5} molecules (yellow) into complex formation (blue). Despite prolonged incubation to allow for protomer swapping, titration of FL_{WT/KO} (red) to FLT3_{D1-D5} (orange) only results a complex significantly lighter than FL_{WT}:FLT3. **B. Summary of the MALLS-derived molecular weights.** Theoretical masses were estimated by their amino acid sequence, the MALLS-measured molecular weights were determined by light scattering. Further glycoprotein conjugate analysis of the latter allowed to attribute part of the mass to the glycan content.

Heterodimeric FL_{WT/KO} eluted on SEC-MALLS as a protein species with a large shoulder, indicative for a heterogeneous protein sample (Figure 10A, red curve). However, the shoulder and main peak have a MALLS-determined MW of 37 kDa and 35 kDa respectively, being both in good agreement with the theoretical determined MW of 36 kDa (Figure 10B). As both the retention volume and MW correspond well to those of mammalian-expressed FL_{WT} (Figure 10A, green curve) and given that both protein species are recruited to an apparent monodisperse 1:1 complex with FLT3_{D1-D5} (Figure 10A, orange curve) with a MALLS-determined MW of 70 kDa, it can be inferred that both protein species are variants of FL_{WT/KO}, and possibly differ from each other by their glycosylation pattern. Importantly, no protein species could be detected with an R_{hyd} or MW comparable to those of the ternary FL_{WT}:FLT3_{D1-D5} complex (Figure 10A, blue curve), not even after a prolonged period of time. These

results indicate that no significant protomer swapping occurs in solution within the tested time frame of 5 days.

Thus, to complement our dissection of cooperativity in the assembly of a ternary FL_{WT}:FLT3 complex, we engineered a heterodimeric ligand, FL_{WT/KO}, comprising a wild-type FL protomer on the one hand, and a protomer with an abolished receptor binding epitope on the other. As our initial attempts to generate such ligand as a fused heterodimeric species remained unsuccessful, we endowed both protomers with different tags to enable isolation of the non-covalent heterodimeric protein. This approach allowed for tandem purification of such a non-covalent heterodimer, albeit with low yields. SEC-MALLS analysis showed that this protein species could recruit only one receptor into a complex, confirming that the double knock-out mutation indeed abolishes the FLT3 binding epitope of that protomer. Importantly, prolonged incubation did not give any indications for protomer swapping, confirming the stability of this heterodimer in solution.

1.4. ITC analysis suggests binding cooperativity in the assembly of the FL:FLT3 complex

1.4.1. Development of a pipeline to allow statistically robust analysis and comparison of ITC data

During this doctoral study, novel tools were developed and validated to allow detection, quantification, and deconvolution of possible cooperative events upon assembly of a ternary FL:FLT3_{D1-D5} complex by isothermal titration calorimetry (ITC). However, without prior knowledge about their magnitude, analyzing differences – or the absence thereof - in thermodynamic parameters of various interactions should be supported by a statistical framework that allows for evaluating significance. Although such approach of analyzing experimental data is far from new, it does require a few considerations when applied to ITC measurements.

Firstly, it is often overlooked that ITC experiments performed with the same batch of protein are only technical replicates, and thus do not provide an independent estimation of the thermodynamic parameters. As such, they at best only allow to infer statistical conclusions regarding the protein from that particular batch. Suppose, for example, a receptor that can bind 2 ligands, L₁ and L₂. Whilst the receptor and L₁ were expressed and purified correctly, L₂ is only partially folded due to experimental conditions. In this situation, multiple ITC experiments using the same batches would repeatedly yet erroneously show that ligand L₁ is a higher-affinity binder than ligand L₂, without reflecting the true underlying thermodynamics. To eliminate such sources of spurious variation in the determination of the thermodynamic parameters, multiple biological distinct samples – in itself subject to capturing random variation from protein expression, purification, and storage – should be measured. For FLT3 expressed from a stable cell line, best practice would imply generation of multiple stable cell lines for which independent purifications could be considered as the best approximation of biologically distinct. Unfortunately, we had only one monoclonal stable cell line available, and therefore considered all independent expression and purification campaigns as biological replicates. In contrast, all three ligands – FL_{WT}, FL_{L27D} and FL_{WT/KO} – are purified from either a transformed bacterial host, either a

transiently transfected mammalian cell culture. Therefore, each of their expression campaigns – if performed independently - is the closest approximation of a biological replicate.

Secondly, thermodynamic parameters derived from an ITC experiment can be affected by small changes in buffer composition depending on the nature of the interacting amino acids. Therefore, buffer-to-buffer variation might contribute to the variation in the determined parameters. We therefore aliquoted a 6-liter buffer batch that was stored at -20°C and only thawed upon buffer-exchanging the proteins of interest. Unless stated differently, all ITC experiments presented in this study have been performed in that exact same buffer.

Furthermore, as differences between the determined thermodynamic parameters of different interactions might be small, we preferred an objective analysis of the ITC data without the necessity to intervene in baseline determination, thereby influencing peak shape determination and integration. Brought to our attention by Brautigam and colleagues, we made use of a series of tools allowing an automated ITC peak shape analysis (Keller et al. 2012; Brautigam et al. 2016) followed by a statistical modeling of binding isotherm and estimation of the thermodynamic values via Sedphat (Zhao, Piszczek, and Schuck 2015).

Stepping away from the traditional yet biologically irrelevant estimation of the stoichiometry using ITC, Sedphat was used to determine the fraction of (in)competent molecules in the cell. The choice of model was based on previously shown MALLS experiments. For FL_{L27D}:FLT3_{D1-D5} and FL_{WT/KO}:FLT3_{D1-D5} interaction a model was selected that assumes a 1:1 ligand:receptor interaction, whilst the model for the canonical FL_{WT}:FLT3_{D1-D5} interaction assumed a 1:2 stoichiometry. Confidence for the correctness of this approach was given by comparing the derived thermodynamic values with the ones determined using Origin, PEAQ-ITC Analysis and NanoAnalyze software. Representing the data in a traditional Final Figure is, to our knowledge, only possible by showing data of one or multiple experiments in one plot. As such a plot becomes readily very complex to read, we have chosen one representative experiment for the thermogram and isotherm, whilst thermodynamic parameters are displayed as derived from the complete data analysis.

Finally, the Sedphat-estimated thermodynamic parameters of all ITC experiments, including the experiments with FLT3_{t-WT}, FLT3_{T343I} and FLT3_{t-S451F} (Sections xx), were assembled into a single dataset to estimating the effect of receptor and ligand identity on the different thermodynamic parameters. The classic approach to predict the relationship between 2 variables relies on linear models that describe the effect of the explanatory variable (e.g. ligand identity) on the response variable (e.g. the enthalpy). In its most simple form, such linear regression model is represented as:

$$y = \beta_0 + \beta_1 x + \varepsilon$$

where

- y = response variable (e.g. enthalpy of interactions involving FLT3_{WT})
- x = explanatory variable (e.g. ligand identity)
- β_0 = the y-intercept of the regression line
- β_1 = the slope of the curve
- ε = the error term, used to account for the variability in y that cannot be explained by the linear relationship between x and y.

Our dataset however comprises multiple of such explanatory variables, each one possibly contributing to observed variability of a given thermodynamic parameter. For example, when going through the list with thermodynamic parameters of all performed ITC interactions, the differences in ΔH will not only be in function of the ligand identity (FL_{WT}, FL_{L27D} and FL_{WT/KO}), but also in function of the used receptor (FLT3_{WT}, FLT3_{T343I}, FLT3_{L-WT} and FLT3_{S451F}). When the relation between a single response variable and multiple explanatory variables is investigated, a multiple linear regression model of the following form is required:

$$y = \beta_0 + \beta_1 x_1 + \beta_2 x_2 + \dots + \beta_n x_n + \varepsilon$$

where

- y = response variable
- x_n = is the nth explanatory variable
- β_0 = the y-intercept of the regression line
- β_n = The regression coefficient of nth explanatory variable, representing the independent contribution of x_n to the prediction of y

The purpose of our experiment is to assess the importance of the ligand and the receptor as individual explanatory variates and their interaction on the thermodynamic parameter of interest. Hence, the multiple linear regression model can be written as:

$$y = \beta_0 + \beta_1 x_1 + \beta_2 x_2 + \beta_3 x_3 + \varepsilon$$

where

- y = the thermodynamic parameter of interest
- x_1 = the ligand variable
- x_2 = the receptor variable
- x_3 = the interaction between the ligand and the receptor variable
- β_0 = the y-intercept of the regression line
- $\beta_1, \beta_2, \beta_3$ = the corresponding regression coefficients.

For ease of understanding, the multiple linear model for our experiment so far constructed can be written symbolically as follows:

$$\text{response} = \text{ligand} + \text{receptor} + \text{ligand.receptor} + \text{error}$$

with ligand and receptor as main qualitative variables, also called factors, having three (FL_{WT}, FL_{L27D} and FL_{WT/KO}) and four (FLT3_{WT}, FLT3_{T343I}, FLT3_{t-WT} and FLT3_{S451F}) levels, respectively, and ligand.receptor as the interaction term having 12 levels corresponding with all possible combinations between the four receptor and three ligand levels.

However, a strict prerequisite for the validity of the predicted model, is the assumption that all explanatory variables and their determined regression coefficients, are independent from each other. This prerequisite is however invalidated by the inclusion of technical replicates.

Consider, for example, 6 batches of a receptor (R_{b1} to R_{b6}), 3 batches of a ligand L1 (L1_{b1} to L1_{b3}) and 3 batches of a second ligand L2 (L2_{b1} to L2_{b3}) (Figure 11). Each of these batches have been used in an ITC experiment to determine the enthalpy of the interaction, resulting in 6 groups with 3 measurements each.

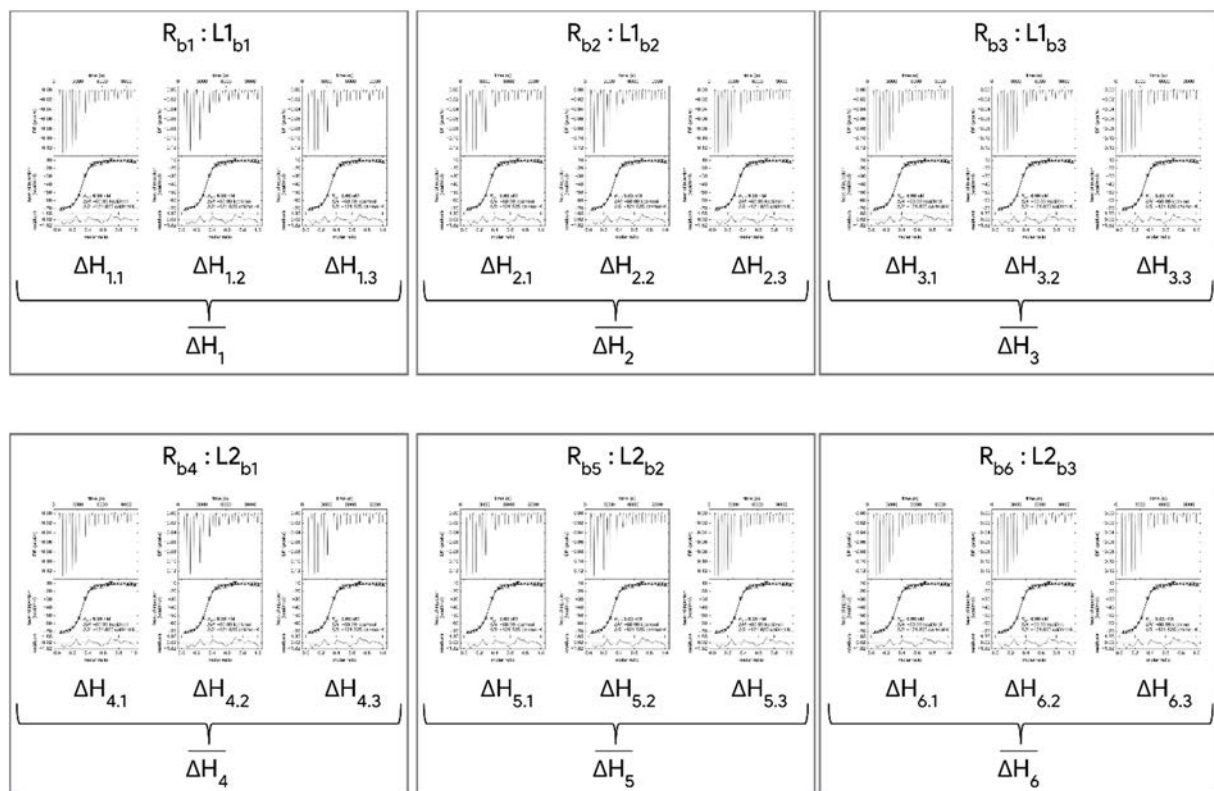


Figure 11. Hypothetical ITC dataset comprising experiments between a receptor and 2 ligands to determine the enthalpy of the interactions. Experiments grouped within one box, are considered technical replicates, whilst each group is considered to be a biological replicate.

When only considering the group of $R_{b_1}:L_{1b_1}$ interactions, $\Delta H_{1.1}$, $\Delta H_{1.2}$ and $\Delta H_{1.3}$ can be regarded as statistically independent. At the level of the whole dataset however, determined enthalpies within a given group of ligand:receptor-interactions are potentially more similar to each other, and can therefore not be considered independent.

A first approach to this problem, is to aggregate the data within one group by averaging its measurements. This would result in 6 independent values for ΔH ($\bar{\Delta H}_1$ to $\bar{\Delta H}_6$) suited for regression analysis. However, this approach does not take full advantage of the data, as only 6 instead of 18 datapoints are used for the regression analysis. A second approach is to analyze the data from one group separately from the others. In the example above, we would therefore perform 6 regression analyses rendering 6 models – of which none has taken advantage of information in the other groups. The third and preferred approach to analyze such hierarchical data, is by a linear mixed model that takes both the technical replicates as well as the true replicates into account. These so-called structural components are inherent to the designed experiment, and possibly contribute to the variation of the response variable without being truly part of the dependency of y on x .

The ITC data presented in this dissertation involves repeated measurements on the same ligand-receptor combination, what we call technical replicates or subsamples, while the batches are the true replications. To accommodate for the possible variation of the thermodynamic parameters due to differences between the different batched measurements, a structural component needs to be included in the model:

$$\text{response} = \text{ligand} + \text{receptor} + \text{ligand.receptor} + \underline{\text{batch}} + \underline{\text{subsample}} + \text{error}$$

with batch and subsample as random terms (underlined) accounting for the structure of the experiment, and the factors ligand, receptor and the interaction term ligand.receptor being the fixed terms that used to model the explanatory components of the study.

Linear models containing fixed and random terms are called linear mixed models (LMMs). Inferences from these models rely on assumptions about the distribution of the response variable. Two of the most important assumptions are that the residuals, and hence the observed responses, have a common variance and follow a Normal distribution. These properties are required to make the F- and t-distributions valid for statistical inference such as hypothesis testing. For all thermodynamic parameters but K_D , these properties were fulfilled and a linear mixed model was fitted to the data. However, some types of response, such as counts, are known to have a Poisson distribution instead of a Normal one – which was the situation for the K_D . This response could nevertheless be analyzed using a so-called generalized linear model (GLM). This class of models allow the response to arise from one of several different probability distributions, extending the analysis methods to situations other than the Normal distribution. Generalized linear mixed models (GLMMs) further extend the GLMs framework by allowing to include additional random terms in the linear model in a way similar to LMMs catering for structural variation. Hierarchical generalized linear mixed models (HGLMMs), finally,

provide another way of modelling non-Normal data when there are several sources of error variation. Like GLMMs, they extend the GLMs to include additional random terms in the linear predictor. However, they do not constrain these additional terms to follow a Normal distribution. They thus provide a much richer set of models.

This so-called Hierarchical Generalized Linear Mixed Model (HGLMM) predicts each of the thermodynamic parameters by the following linear predictor vector:

$$\eta = \mathbf{X}\boldsymbol{\beta} + \mathbf{Z}\mathbf{v}$$

with

$\eta =$ the link function of the outcome variable (i.e. one of the four thermodynamic parameters). This is an $N \times 1$ column vector with

$N =$ The total amount of observations for this thermodynamic parameter (In our example, $N = 18$).

$\mathbf{X} =$ An $N \times p$ design matrix with:

$p =$ the predictor variables (In the example above, the dataset contains ITC experiments for 2 ligands and 1 receptor, therefore $p = 7$)

$\boldsymbol{\beta} =$ A $p \times 1$ vector containing the regression parameters (β_1, β_2, \dots) of the multiple regression models performed within each group of technical replicates.

$\mathbf{Z} =$ The $N \times q$ design matrix with:

$q =$ the random effects (ϵ) of the multiple regression models performed within each group of technical replicates (for our dataset, $q = 8$).

$\mathbf{v} =$ the $q \times 1$ vector containing the random replicate effects.

This vector model is able to predict each thermodynamic parameter of each ligand-receptor interaction by combining data from the individual multiple regression analyses, performed within each group of replicates. The non-dependency of technical replicates is thus being taken into account, however without losing information of the individual experiments, as would be the situation when aggregating the data. Furthermore, a random term is fitted to correct to account for possible random variation between the different biological replicates.

Thus, to take into account the non-dependency of technical replicates, the possible random variation between the different biological replicates and the apparent Poisson distribution of the K_D , a HGLMM model was fitted to the thermodynamic data. For all thermodynamic parameters but the K_D , this model considered a Normal distribution of both the fixed and random effects. Only upon modeling the K_D , a Poisson distribution of the fixed effects and a Gamma distribution of the random effects was assumed.

The ITC dataset used in this doctoral thesis contains all four thermodynamic parameters of 3 ligands and 4 receptors, with $N=38$, $p=7$ and $q=8$. Inspection of residual plots revealed no departures from normality or homogeneity of variance for ΔH (p-value 0.042), $-T\Delta S$ (p-value 0.876) and ΔG (p-value 0.017) at the 1% confidence level. After log-transformation of the data, the residuals for the K_D followed a Normal distribution as well (p-value 0.060). The means and standard errors of the thermodynamic parameters were predicted and displayed on the thermogram to generate the familiar Final Figure. Interestingly, for each of the thermodynamic parameters, the HGLMM could attribute a non-zero amount of the observed variance to differences between biological or technical replicates. This finding shows that there is indeed batch-to-batch variation between different biological samples and their technical replicates, and highlights the importance of including replicate as random term in the HGLMM model in order to capture part of the observed random variance and, hence, to gain more power to assess the significance of the ligand and receptor identity.

In conclusion, to statistically compare ITC-derived thermodynamic parameters of all distinct ligand-receptor interactions, we made sure to 1. distinguish between biological and technical replicates, 2. perform all experiments in the same buffer batch, 3. objectively analyze our data using NITPIC and Sedphat, 4. predict all thermodynamic parameters using a statistical model and, finally, 5. make a statistical comparison to determine the significance of their difference (Figure 12).

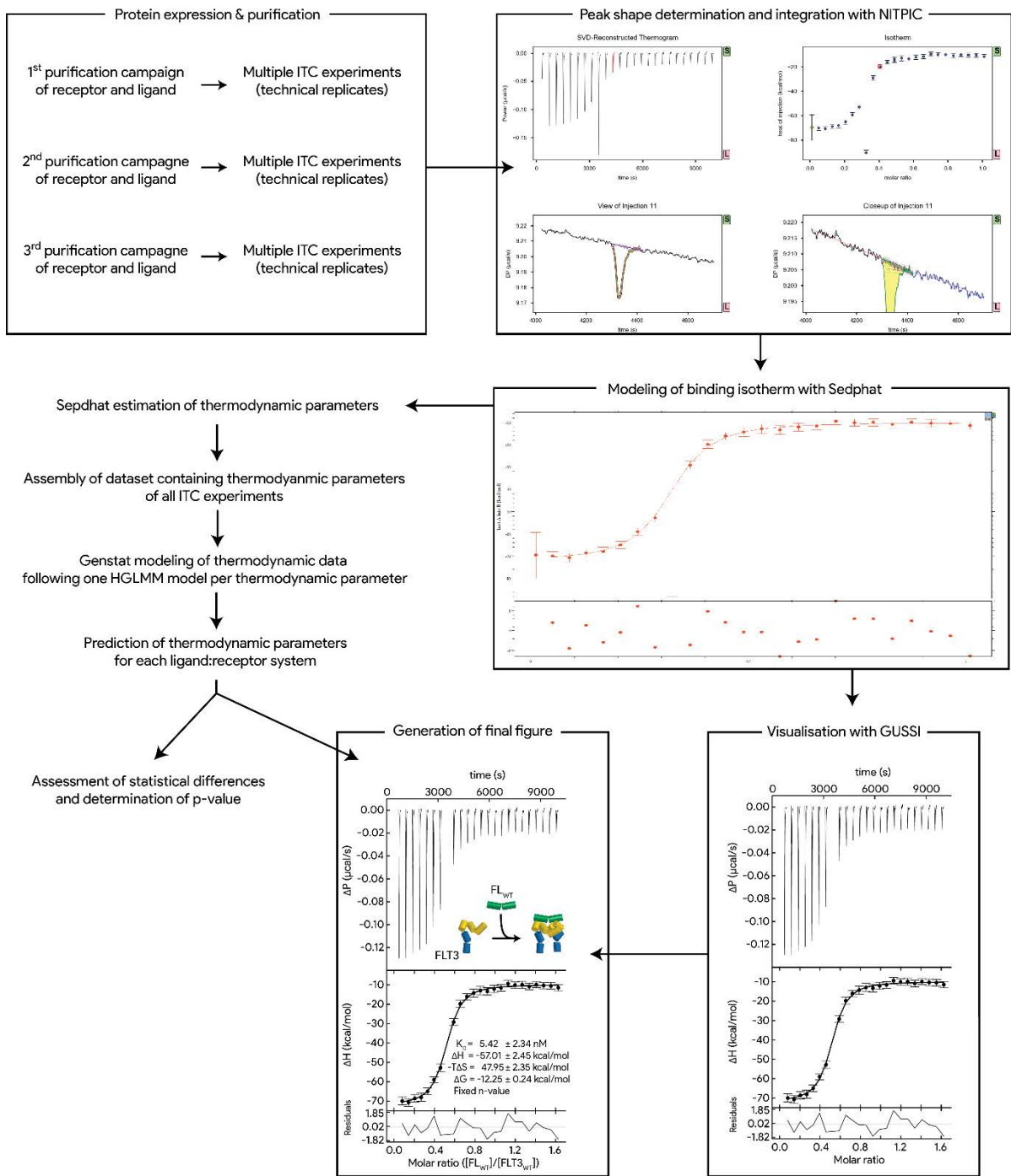


Figure 12. Overview of the pipeline for automated ITC data analysis, statistical modeling of all thermodynamic parameters and assessment of the significance of their differences.

1.4.2. Monomerizing FL severely impacts the thermodynamics and kinetics of receptor binding

If assembly of a ternary FL:FLT3 receptor complex would truly be devoid of any ligand-induced interactions, the ligand binding interface would consequently be the only defining factor in the receptors affinity for its ligand. In such a scenario, the determined affinity of the receptor for a given ligand should be independent from the oligomeric state of that ligand, as all ligands employ an identical interaction interface (Section 1.2.6) (Figure 13A). On the other hand, if ligand-induced receptor-receptor interactions are an integral part of the assembly mechanism, titrations with FL_{L27D} will result in removal of the cooperative character of the ligand-receptor complex. Indeed, this would be reflected in a drastic reduction to the overall affinity of the FLT3:FL_{L27D} complex and would accordingly impact all relevant thermodynamic and kinetic parameters (Figure 13B).

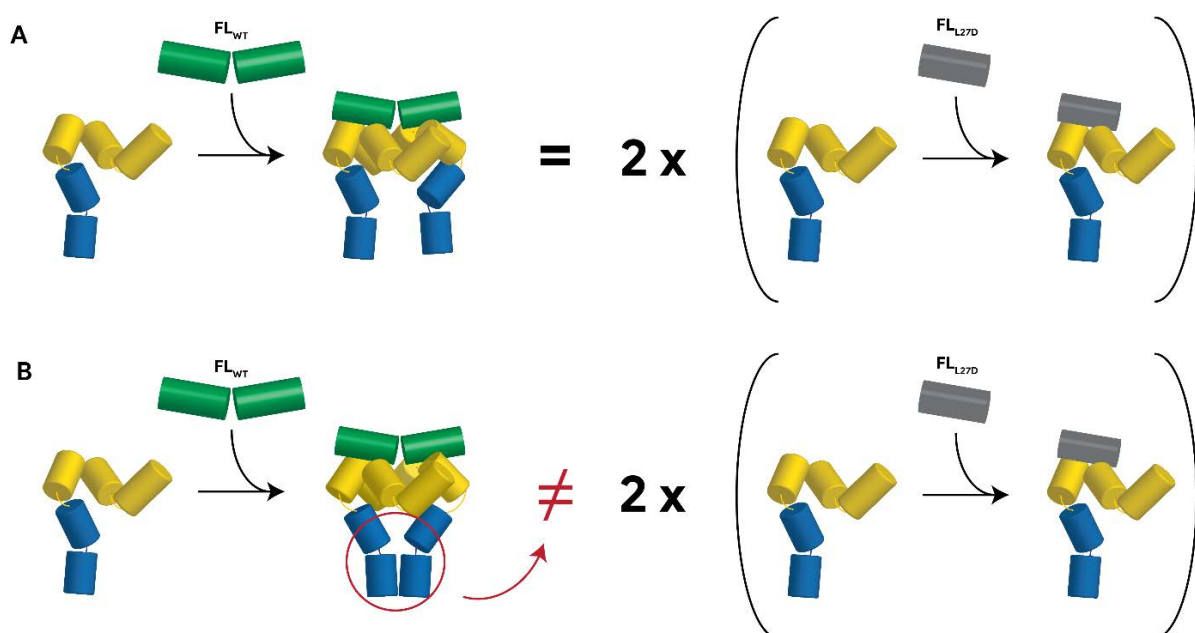
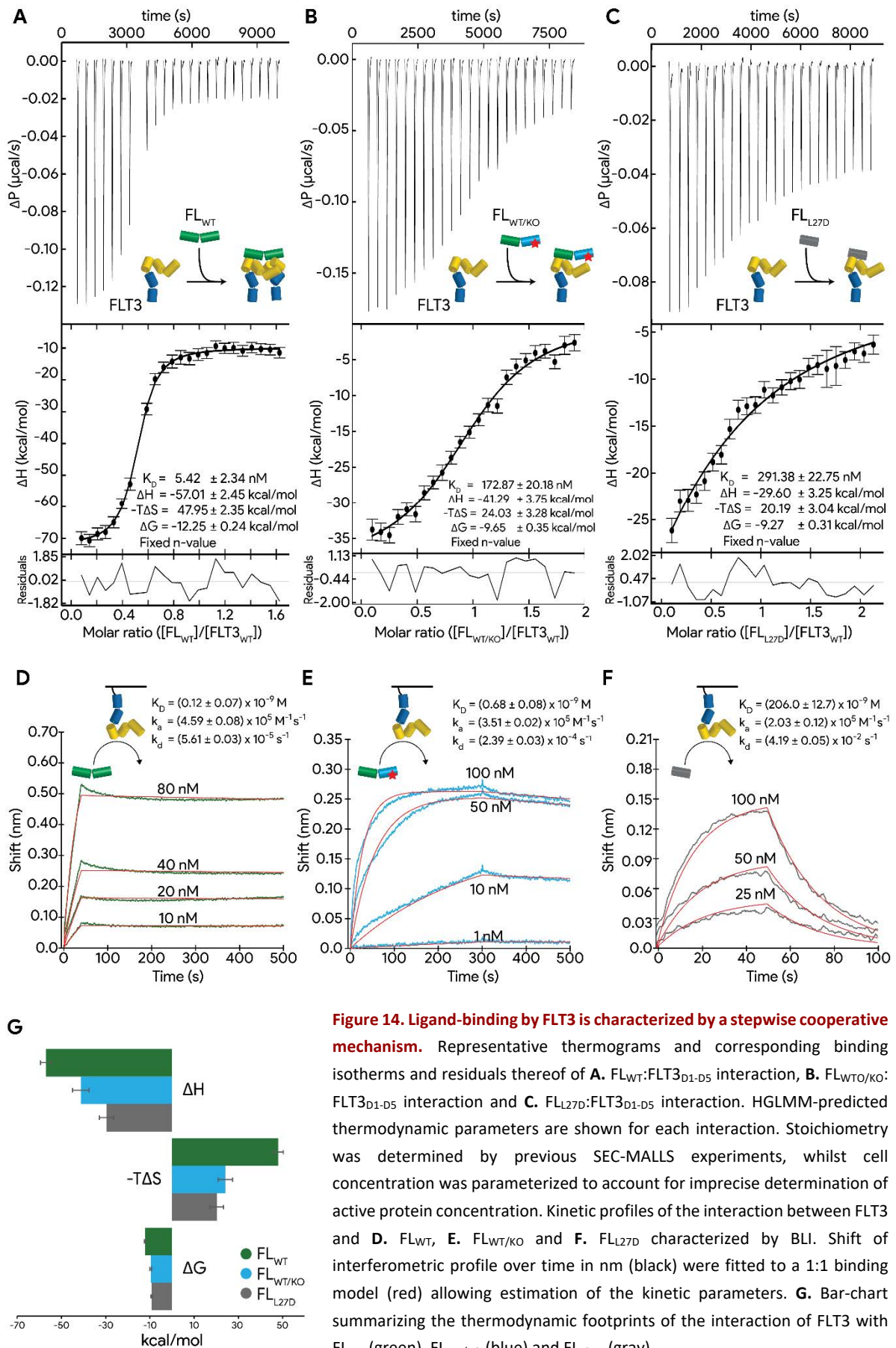


Figure 13. Detection of ligand-induced receptor interactions using engineered ligands. **A.** Scenario in which FL_{WT} (green)-binding does not result in homotypic receptor interactions. As the affinity of FLT3 for a protomer is only determined by the FL_{protomer}:FLT3 binding epitope, this affinity is not expected to be altered when the ligand is not able to recruit a second receptor. **B.** Ligand-induced homotypic receptor contacts, for example mediated by the membrane-proximal domains (blue), would increase the affinity of FLT3 for FL_{WT} in a cooperative fashion. Consequently, the affinity of FLT3 for ligands that fail to recruit a second receptor, will be lowered as a consequence of the receptor's ability to establish further receptor-mediated interactions. These scenarios are illustrated by binding events featuring FL_{WT} and FL_{L27D}, but a similar reasoning applies for binding events involving FL_{WT} and FL_{WT/KO}.

We therefore performed a full thermodynamic dissection of the interaction of FLT3 with all three ligands by ITC (Figure 14A-C), followed by a kinetic characterization using biolayer interferometry (BLI) (Figure 14D-F). For BLI, *in vitro* biotinylated FLT3 was immobilized on the surface of streptavidin-coated sensors. Subsequent to the dissociation step in custom-made kinetics buffer, each sensor was incubated with a given concentration of the ligand.

Our results show that a stoichiometric 1:1 complex of FL_{L27D} with FLT3_{D1-D5} indeed is characterized by an enthalpic component that is almost half of the enthalpic release using FL_{WT} (-30 ± 3 kcal/mol and -57 ± 2 kcal/mol resp., p-value < 0.001) (Figure 14A, 14C and 14G). Unexpectedly, the lowered entropic penalty (20.19 kcal/mol and 47.95 kcal/mol resp., p-value = 0.012) by nearly 58% appears to be insufficient to compensate for the loss in enthalpy, thus resulting in a K_D of 291 nM, which is about 54-fold lower than the affinity of FLT3_{D1-D5} for its canonical ligand FL (5.42 nM, p-value < 0.001). Supporting this unambiguous evidence for cooperativity, ITC experiments featuring FL_{WT/KO} enabled us to distil out two levels of contributions from this (Figure 14B). With a K_D of 173 nM, the affinity of FLT3_{D1-D5} for FL_{WT/KO} is situated between those of FL_{WT} and FL_{L27D} (p-values < 0.01 for both differences), and implies that intra-molecular reorientation of the subunits is able to increase the affinity of FL for its receptor. Interestingly, this effect appears to be caused solely by a favorable increase in polar interactions, as only the increase of the enthalpic component (p-value 0.025) by 43 %, but not the difference in entropic penalty (p-value 0.397) is significant at the 5% confidence level.



Preliminary BLI experiments also suggest the 2-staged cooperativity, and shed light onto the kinetics underlying this difference (Figure 14D-F). Although determined affinities for the ligands differ more than a 1700-fold, there is strikingly little difference in their association rate (k_a) for binding the receptor. Interestingly, the difference in affinity is reflected by a dissociation rate (k_d) that appears to be a factor of ~ 750 faster for the $FL_{L27D}:FLT3_{D1-D5}$ complex compared to the $FL_{WT}:FLT_{D1-D5}$ complex. A mechanism by which FLT3 binds its monomeric ligand at the same rate as its dimeric counterpart, but fails to further lock the interaction by subsequent homotypic receptor contacts would indeed elegantly unite the ITC and BLI data. However, the lack of replicates of BLI-experiments and statistics on the kinetic data should caution about making such conclusions. In addition, immobilization of the receptor rather than the cytokine may introduce additional complications in the assembly process. Nevertheless, this set of experiments dissecting the thermodynamics of binding for three different ligands - FL_{WT} , $FL_{WT/KO}$ and FL_{L27D} – to FLT3, supplemented with preliminary kinetic data, show for the first time that transition of a binary cytokine-receptor encounter complex to a ternary $FL_{WT}:FLT3$ complex features a 2-staged mechanism endowed by cooperativity.

2. Unraveling mechanistic principles underlying oncogenic driver mutations in the extracellular domain of FLT3

2.1. Introduction

The NIH National Cancer Institute estimates that this year almost 20,000 new patients will be diagnosed with acute myeloid leukemia in the United States alone, accounting for more than 30% of all new leukemia cases (NIH n.d.). The 5-year survival rate of only 27.4% furthermore implies that more than 10,000 patients in the United States will have died by the end of this year. Unfortunately, approximately 30% of newly-diagnosed patients will be confronted with even poorer statistics, as they harbor mutations in the FLT3 receptor (Thiede et al. 2002; Whitman et al. 2001; Fröhling et al. 2002). Especially patients with internal tandem duplications (ITD) in the receptors juxtamembrane domain (FLT3_{ITD}) have an increased rate of relapse and shorter overall survival compared to similarly-aged patients lacking those mutations (Kiyoi et al. 1998b; Badar et al. 2015b; Fröhling et al. 2002; Schnittger et al. 2002; Kayser et al. 2009). FLT3 is a transmembrane receptor expressed at the surface of early hematopoietic progenitor cells and dendritic cells. The receptor is a member of the class III of tyrosine kinase receptors (RTK-III), including CSF-1R, KIT, PDGFR α and PDGFR β , all characterized by a similar modular build featuring an extracellular domain (ECD), a single membrane-spanning helix (TM) followed by a juxtamembrane (JM) region and finally a intracellular tyrosine kinase domain (TKD) (M. a Lemmon and Schlessinger 2010; Verstraete and Savvides 2012). Under steady-state conditions, inactive FLT3 resides as a monomer at the cell membrane, and is activated upon binding of its cognate ligand FLT3 Ligand (FL). Given its bivalent nature of the latter, binding of FL to domain 3 of two FLT3 receptors brings those in close proximity to each other, and marks the start of receptor-mediated signaling pathways (Verstraete et al. 2011). Activating mutations in the intracellular region account for the lion's share of all FLT3-mutated AML cases, although large-scale sequencing efforts have identified somatic mutations in the ECD and TM domains of cancer patients as well (Forbes et al. 2008), although their effect on prognosis is often unknown.

ITD-mutated FLT3 can be detected in approximately 25% of all AML patients. Given its longstanding correlation with adverse prognosis for AML, the mechanistic principles underlying this tandem duplication have been established early on and are nowadays considered as common knowledge (Chapter A - Section 2.2). However, clinical identification and validation of two novel oncogenic mutations in the extracellular domain of FLT3, a threonine-343 to isoleucine (T343I) and serine-451 to phenylalanine (S451F) substitution, illustrated that our understanding of oncogenic mutations should be extended to go beyond those that map in the cytoplasmic regions (Fröhling et al. 2007; Jiang et al. 2005). Given the absence of any structural information regarding the assembly mechanisms underlying FLT3 activation, the molecular principles behind these transforming mutations were at that time only poorly understood, if at all. Interestingly, FLT3_{S451F} was noted to be the only variant analyzed showing a 16-fold increased IC₅₀ in inducing a cytotoxic effect with midostaurin, the only small molecule tyrosine kinase inhibitor (TKI) approved for treatment of newly-diagnosed FLT3-mutated AML (Stone et al. 2017).

In 2011, Verstraete and colleagues (Verstraete et al. 2011) were the first to provide structural insights into the extracellular assembly of the activated FLT3 signalling complex. Supported by strong experimental arguments, an FLT3 activation mechanism was proposed in which ligand-induced extracellular homotypic receptor contacts were conspicuously absent. As has been acknowledged at that moment and confirmed later, FLT3 was the only RTK-III/V family member to do so (Leppänen and Tvorogov 2013; Markovic-Mueller et al. 2017; Ruch et al. 2007; Yan Yang et al. 2010; Yan Yang, Yuzawa, and Schlessinger 2008; P. Chen, Unger, and He 2015; Yuzawa et al. 2007; Felix et al. 2015; Elegheert et al. 2011). The transforming character of a S451F point mutation in the most membrane-proximal domain could however not be readily explained within this proposed model: the electron density map for domain five of FLT3 (FLT3_{D5}) was of too poor quality to allow detailed modeling of this domain, let alone map the location of Ser451. However, it was hypothesized that the location of this transforming mutation might superimpose with a mutational gain-of-function (GOF) hot-spot region in domain 5 of KIT, known for promoting ligand-independent receptor dimerization and activation (Figure 15A) (Verstraete and Savvides 2012; Yuzawa et al. 2007; Reshetnyak et al. 2013, 2015). Likewise, the only hypothesis explaining the oncogenic behavior of the T343I mutation assumed a stabilization of a dimerization-prone receptor conformation (Figure 15B). It was therefore suggested that both mutations promoted the interaction of two receptor molecules in absence of the ligand - even though such homotypic receptor interactions might, in contrast to the other 4 RTK-III, not be part of the canonical activation mechanism (Verstraete and Savvides 2012).

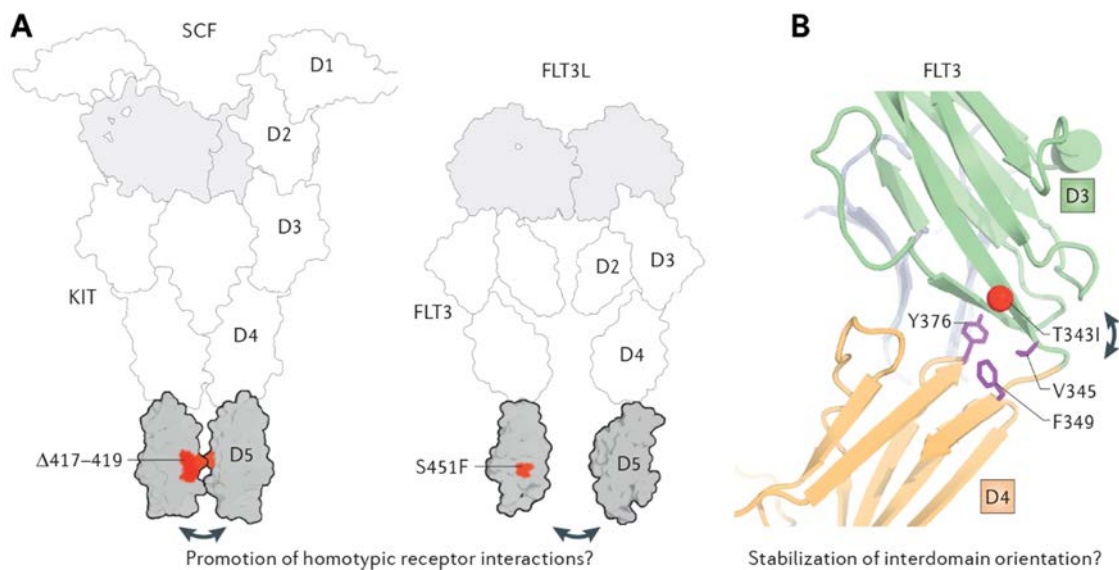


Figure 15. Possible structural consequences of oncogenic FLT3 mutations. **A.** Although its location cannot be confidently mapped on the structure of domain 5, the position of Ser451 roughly coincides with the mutational hot-spot region (residues 417-419) of KIT receptor. The latter have shown to increase ligand-induced receptor interactions to such an extent that they promote ligand-independent receptor dimerization. **B.** Thr343 maps at the conserved D3-D4 elbow region, a structural feature allowing rotation of the membrane-proximal domains to engage in homotypic ligand-induced receptor contacts. Mutation of Thr343 to isoleucine might stabilize a dimerization-prone conformation of the membrane-proximal domains. Figure from Verstraete and Savvides 2012.

In the previous chapter, we showed for the first time that transition of a binary encounter complex to a ternary FL:FLT3 complex, is a multi-step reaction with at least two distinct levels of positive cooperativity (Section 0). A first level of cooperativity is provided by an increase of electrostatic favorable interactions, driven by an inter-subunit reorientation, following assembly of the binary encounter complex. The second level is arguably provided by additional receptor contacts upon establishing a ternary FL:FLT3 receptor complex. Unfortunately, this is where the analysis ended: the data did not allow identification of the receptor moiety that could be held responsible for this cooperative effect. Although, by taking steric limitations imposed by ligand binding into account, we infer that this role could be played by either the most membrane-distal FLT3_{D1}, or the conventional membrane-proximal domains FLT3_{D4-D5}.

Given the hypothesis that mutations in the extracellular region can drive ligand-independent receptor dimerization, we wondered if such mutations might affect the cooperativity observed for the ligand:receptor interaction. If so, we envisioned that these findings would deliver more insights into the mediators of cooperativity in the context of a wild-type receptor.

2.1 Results

2.1.1. A T343I point mutation in FLT3 does not alter the thermodynamics of ligand binding

To explore the possibility that oncogenic point mutations in the extracellular region of FLT3 might affect the cooperativity of ligand binding, we established a monoclonal HEK293S MGAT1^{-/-} TR⁺ cell line (Reeves et al. 2002) allowing tetracycline-inducible expression of FLT3_{D1-D5} carrying the T343I mutation (FLT3_{T343I}). After expression and purification, this receptor construct was subjected to a preliminary ITC analysis with FL_{WT} and FL_{L27D} (Figure 16). ITC thermograms were analyzed objectively as described before (Section 1.4.1) and the Sedphat-determined thermodynamic parameters were an integral part of the dataset that was used for GHLM modeling. Comparing the predicted thermodynamic parameters of the FL_{WT}:FLT3_{T343I} interaction with the FL_{WT}:FLT3_{WT} interaction, no significant difference could be detected at the 5% confidence level (CL) (p-values > 0.75 for differences in K_D , ΔH and $-T\Delta S$; p-value of 0.29 for differences in ΔG). Similarly, none of the predicted thermodynamic parameters for the interaction with FL_{L27D} showed a significant difference from those of the FL_{L27D}:FLT3_{WT} interaction at the 5% CL (p-values for all differences > 0.53). This led to the conclusion that this point mutation does not affect ligand-binding in the context of a construct comprising only the extracellular domain of its receptor.

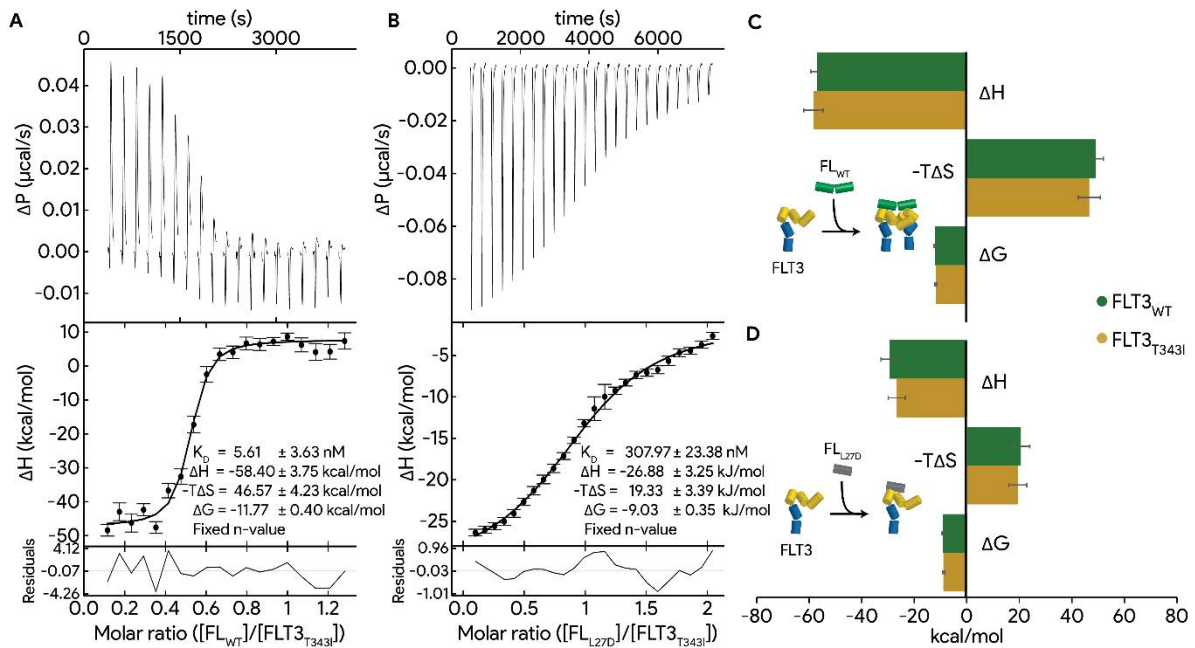


Figure 16. A threonine-343 to isoleucine substitution in the extracellular domain of FLT3 has no effect on the thermodynamics of ligand binding. Representative thermograms and corresponding binding isotherms and residuals of FLT3_{T343I} interaction with **A.** FL_{WT} and **B.** FL_{L27D}. HGLMM-predicted thermodynamic parameters are shown for each interaction. Stoichiometry was determined by SEC-MALLS experiments for FLT3_{WT}, whilst cell concentration was parameterized to account for imprecise determination of active protein concentration. Bar-chart summarizing and comparing thermodynamic footprints of **C.** FL_{WT} and **D.** FL_{L27D} interaction with FLT3_{WT} (green) and FLT3_{T343I} (brown). When comparing the two receptors, none of the thermodynamic parameters differ significantly at the 5% confidence level.

2.1.2. A Thr343Ile mutation does not induce any conformational changes in FLT3 upon binding to FL_{WT}

To obtain structural insights into how FLT3 accommodates the presence of the oncogenic T343I point mutation, we sought to determine the crystal structure of FLT3_{T343I} in complex with its activating ligand. Crystallization trials identified several conditions allowing crystal formation and growth. In general, crystals grew in a wide range of ammonium citrate tribasic solutions buffered around pH 7, using 4-15% PEG 3350 as precipitant. Interestingly, conditions allowing crystallization were initially characterized by a morphologically amorphous precipitate, in which crystals could be detected from 20-25 days incubation onwards. After the initial discovery, crystals grew to larger dimensions at the expense of the precipitate and finally stabilized with several crystals in a clear drop, deprived of its precipitate. In contrast to the multitude of crystals that grew in subsequent optimization screens at 20°C and only diffracted to 10-20 Å, incubation of the screens at 14°C yielded 4 crystals, of which 3 were morphologically not single. The one single crystal, grown at 75 mM ammonium citrate tribasic pH 7.4 and 14% PEG 3350, diffracted to a substantially higher resolution and resulted in a final dataset with diffraction to 3.7 Å. Details regarding the X-ray data collection and refinement statistics are shown in Table 5. While the model at hand is to a large extent correct as evidenced by the refinement R-factors, residual positive difference density in the F_o-F_c map near the only modeled domain 1, showing unmodeled density for what is probably FLT3_{D1} of chain H, prevents us from declaring this structural

analysis as finished. Nevertheless, what is already modeled indicates that no marked conformational differences should be expected.

Table 5 | X-ray data collection and refinement statistics

| <u>Crystallization</u> | | <u>Refinement</u> ^{c,d} | |
|--|--|------------------------------------|-------------------------------|
| Protein complex | FLT3 _{T343I} :FL | Resolution range (Å) | 47.09 - 3.691 (3.822 - 3.691) |
| Crystallization condition | 75 mM ammonium citrate tribasic pH 6.6 4% PEG 3350 | Reflections in refinement | 45944 (4356) |
| | | Reflections used for R-free | 2297 (218) |
| Cryoprotectant | 15 % PEG 335025% 25% ethylene glycol | R-work | 0.2320 (0.4077) |
| | | R-free | 0.2700 (0.4536) |
| | | non-hydrogen atoms | 13260 |
| | | Macromolecular atoms | 13137 |
| | | Ligand atoms | 123 |
| | | Solvent atoms | 0 |
| | | Protein residues | 1958 |
| | | RMS(bounds) (Å) | 0.018 |
| | | RMS(angles) (°) | 1.92 |
| | | Ramachandran favored (%) | 80.03 |
| | | Ramachandran allowed (%) | 14.57 |
| | | Ramachandran outliers (%) | 5.40 |
| | | Rotamer outliers (%) | 15.44 |
| | | Clashscore | 5.61 |
| | | Average B-factor (Å ²) | 238.23 |
| | | macromolecules | 237.83 |
| | | ligands | 280.74 |
| | | solvent | n/a |
| | | TLS groups | 8 |
| <u>Data Collection</u> ^b | | | |
| Beamline | PetraIII-P14 (Germany) | | |
| Wavelength (Å) | 0.98 | | |
| Detector | EIGER 16M | | |
| Space group | P1 | | |
| a, b, c (Å) | 102.428 113.377 123.225 | | |
| α, β, γ (Å) | 105.371 109.47 108.223 | | |
| Resolution (Å) | 47.09 - 3.691 (3.822 - 3.691) | | |
| Total reflections | 84393 (13463) | | |
| Unique reflections | 45955 (7248) | | |
| Multiplicity | 1.84 (1.86) | | |
| Completeness (%) | 94.1 (92.2) | | |
| Mean I/σ(I) | 4.71 (0.46) | | |
| Wilson B-factor (Å ²) ^c | 144.26 | | |
| R-meas (%) | 21.0 (264.1) | | |
| CC1/2 (%) | 99.6 (17.0) | | |

^a Values in parentheses correspond to the highest-resolution shell. ^b Values reported by XDS. ^c Values reported by Phenix. ^d Final refinement was performed in BUSTER 2.10.3

Given the strong similarity in the thermodynamics of the FL_{WT}:FLT3_{T343I} complex, the crystal structure of the ternary FL_{WT}:FLT3_{T343I} complex unsurprisingly unveiled a similar architecture as described for the FL_{WT}:FLT3_{D1-D4} and FL_{WT}:FLT3_{D1-D5} assemblies (PDB 3QS7 and 3QS9) (Figure 17A-B). The crystal structure features 2 copies of a ternary ligand:receptor complex, each one organized in the characteristic open horseshoe ring structure and packed in a head-to-head fashion similar to previous crystal structures, despite the different space group. Structural superimposition of all available copies of FLT3_{WT} on FLT3_{T343I} further confirms the absence of conformational main-chain deviations in the FL:FLT3_{D234} module (average Cα root-mean-square deviation (R.M.S.D.) of 0.90 Å) (Figure 17C). Therefore, it appears that the presence of the oncogenic I343 mutation does not alter the conformation of the ECD, when in complex with its ligand.

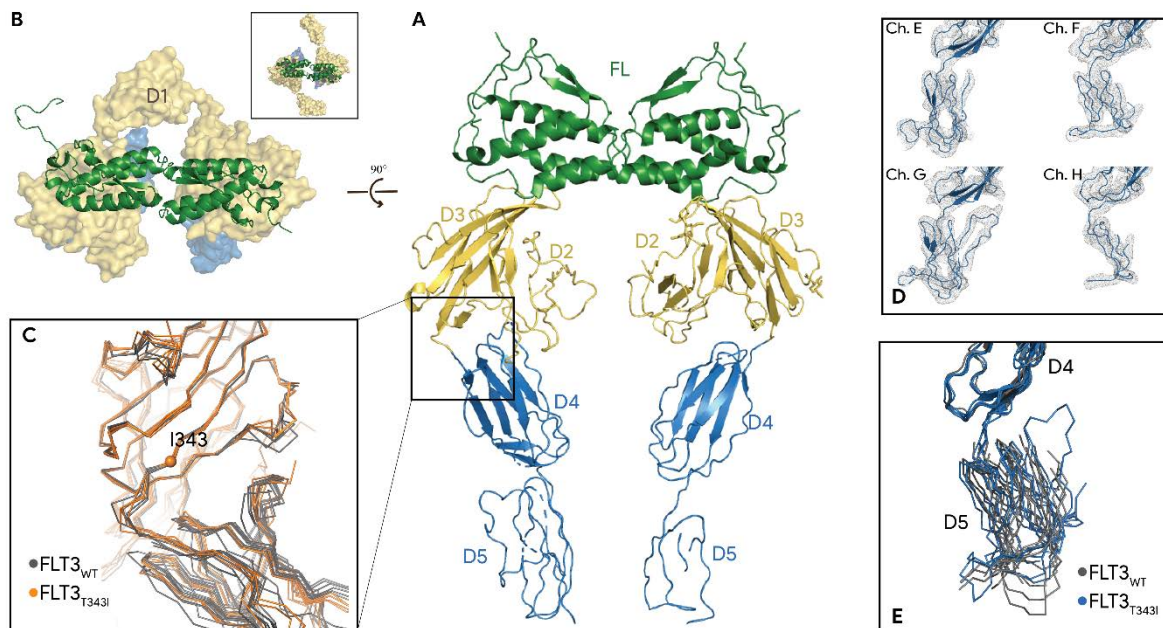


Figure 17. Crystal structure of FL_{WT} in complex with FLT3_{T343I} allows a more accurate model for domain 5. A. Architecture of the FL_{WT}:FLT3_{T343I} ternary complex. “Front” view and B. “top view” of the determined X-ray crystallographic structure of the complex. FL_{WT} (green) is shown in cartoon representation. Domains 2-3 (yellow) and domains 4-5 (blue) of FLT3_{T343I} are labeled and shown either in cartoon representation (“front” view), either in surface representation (“top” view). Inset shows the “top” view of the FL_{WT}:FLT3_{WT} ternary complex (PDB 3QS9). C. I343 does not introduce conformational changes in the D2-D3 module. A total of 8 copies of FLT3_{WT} (PDB 3QS7 and 3QS9, gray ribbon diagrams) superimposed to 4 copies of FLT3_{T343I} (ribbon diagrams, orange) do not reveal I343-induced conformational changes at the C α backbone level. C α atom of I343 is shown as an orange sphere. D. Electron density allowed for the first time to confidently model domain 5. Albeit different for each receptor copy (chain E to G), clear electron density allowed manual model building of FLT3_{D5}. C α backbone for each chain is shown as a cartoon representation, electron density as an isomesh contoured at 1 σ and carved at 3 Å. E. The new crystal structure provides yet another 4 possibilities to the pool of FLT3_{D5} conformations. Superimposition of 4 copies of FLT3_{WT} (PDB 3QS9, gray ribbon diagrams) to domain 4 of copies from FLT3_{T343I} (blue ribbon diagrams) show the pool of conformations that FLT3_{D5} is allowed to sample from.

2.1.3. Crystal structure of the FL_{WT}:FLT3_{T343I} complex allows for a more accurate model for FLT3_{D5}

Arguably the most unanticipated feature of the crystallographic data for the FL_{WT}:FLT3_{T343I} complex, is the clear electron density that appeared for 2 of the 4 copies of FLT3_{D5} (Figure 17D). Unlike previous crystallographic models, entrapment of those two FLT3_{D5} copies in a more ordered crystal packing contact allowed modeling of domain 5 for the first-time at a medium resolution of 3.7 Å. As predicted, FLT3_{D5} is a member of the “C2-set” Ig domains featuring 7 β -strands organized into a ABED/CFG sandwich. We observe that FLT3_{D5} superimposes reasonably well with domain 5 of KIT (C α R.M.S.D. of 4.2 Å; 67 atoms aligned), revealing a preservation of the extended DE-loop (residues 486 to 496) that contributes to the D4-D5 interface in unbound KIT, but is imposed to an altered conformation in the SCF-occupied ectodomain

Similar to the crystallographic structures in 3QS9, the range for which copies of FLT3_{D5} are (un)defined in the electron-density map (Figure 17D), are indicative for the plethora of conformations that FLT3_{D5}

is allowed to sample from, compared to the structurally homogeneous FL:FLT3_{D2-D4} core. Indeed, by adding these novel crystallographic models to the current ensemble of available receptor models (Figure 17E), we observe that the current position of FLT3_{D5} relative to FLT3_{D4} adds yet another array of possible conformations. Recalling that such conformational plasticity was absent in the crystal structure of the receptor bound by an inactive ligand (Section 1.2.6), we are left to wonder about the possible release of conformational restraints on domain 5 upon binding of an activating ligand. Indeed, this could hint a yet unanticipated underlying mechanistic role for FLT3_{D5} in receptor activation.

Thus, thermodynamic characterization of the interaction between FLT3_{T343I} and its two ligands, FL_{WT} and monomeric FL_{L27D}, indicate that the oncogenic T343I mutation does not significantly alter any of the thermodynamic parameters at the 5% CI, compared to the thermodynamic parameters of those interactions featuring FLT3_{WT}. Likewise, the crystal structure of FLT3_{T343I} does not seem to show conformational main-chain deviations from known crystallographic models of FLT3_{WT}, although it delivers for the first time a high-resolution view into the architecture of FLT3_{D5}. Altogether, these experiments show our inability to detect an effect of the T343I point mutation in the context of an extracellular FLT3 construct, despite its implication as a driver mutation for ALL (Jiang et al. 2005).

2.1.4. Serine-451 is poised to initiate oncogenic receptor dimerization via a KIT-like mechanism

Already in 2007, Fröhling and colleagues (Fröhling et al. 2007) described the identification and validation of a serine-451 to phenylalanine (S451F) somatic point mutation in FLT3 in 2 patients diagnosed with AML. The mechanistic principles underlying this transforming mutation in domain 5 were at that time poorly understood. This remained so even with the availability of the crystallographic model featuring FLT3_{WT} in complex with its ligand (Verstraete et al. 2011), as the electron density map did not allow detailed modeling of FLT3_{D5}. Although FLT3 was postulated to be the only RTK-III member for which no ligand-induced receptor contacts were part of the activation paradigm, comparison with the KIT receptor raised the hypothesis that the S451F mutation could drive ligand-independent receptor dimerization. Crystallization experiments of the FL_{WT}:FLT3_{T343I} complex now provided us for the first time with a much more complete and accurate model for FLT3_{D5} (Section 2.1.3). We therefore seized the opportunity to map Ser451 onto this crystallographic model, which surprisingly provided us with several unexpected mechanistic insights concerning the possible mode-of-action of the oncogenic S451F point mutation (Figure 18)

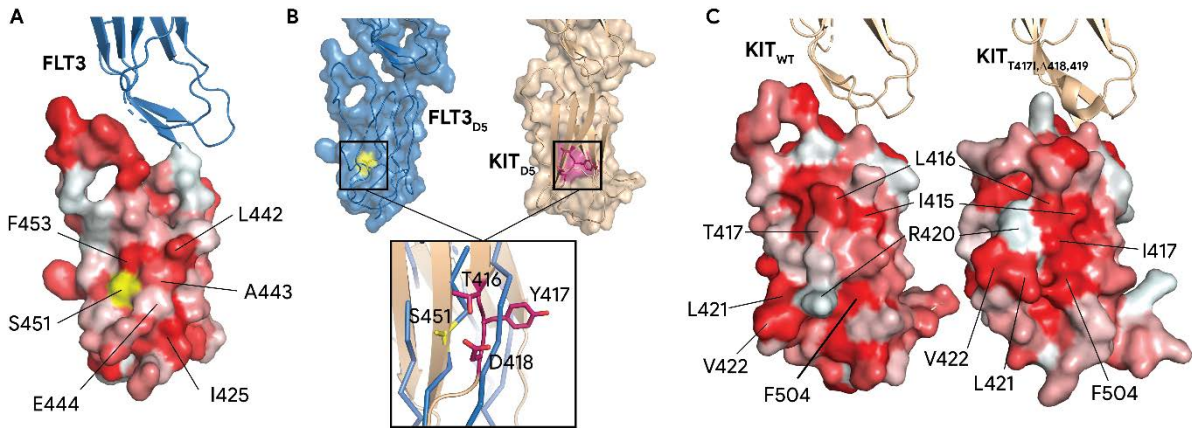


Figure 18. Mapping of S451 on the crystallographic model of FLT3_{D5} and structural comparison with GOF mutations in KIT_{D5}. **A.** S451F has the ability to complete a hydrophobic belt surrounding Glu444. Domain 4 of FLT3 (blue) is shown in cartoon representation. Domain 5 is colored according to the Eisenberg hydrophobicity scale (red is more hydrophobic) and shown in its surface representation. Ser451 is colored yellow. **B.** Superimposition with KIT shows that Ser451 is located close to a well-characterized GOF hot-spot region of KIT. FLT3 (blue) and KIT (PDB 2E9W) (sand) are shown as cartoons overlaid onto transparent surface representations. Ser451 of FLT3 and residues 417-419 of KIT are colored yellow and magenta respectively. Superimposition of KIT onto FLT3_{D4} (inset) shows that Ser451 localizes well with KIT₄₁₇₋₄₁₉. In the inset, FLT3 is shown in ribbon diagram. **C.** Ligand-independent receptor dimerization in KIT_{T417,Δ418,419} is driven by remodeling its surface hydrophobicity. Domain 4 of KIT_{WT} (PDB 2E9W) and KIT_{T417,Δ418,419} (PDB 4PGZ) are colored sand and shown as cartoons. Domain 5 of both models is colored according the Eisenberg hydrophobicity scale and shown in surface representation. Residues involved in oncogenic dimerization are indicated on both models.

Analysis of the surface reveals that Ser451 is located at the edges of a reverse-C shaped hydrophobic region curved around Glu444 (Figure 18A). Replacement of Ser451 by a phenylalanine would arguably transform the reverse-C shaped region to a contiguous hydrophobic belt surrounding Glu444, essentially generating a hydrophobic patch with a negatively charged residue in its center. We envision that a homotypic receptor interaction that effectively buries these residues from the bulk solvent and simultaneously accommodates Glu444 with a charged interaction partner, would cause a considerable increase of bulk-solvent entropy. Given the presence of a bulk-solvent exposed phenylalanine at position 453, such hydrophobic interface could possibly feature an interdigitating stack of four aromatic residues.

Out of all RTK-III, oncogenic mutations in the membrane-proximal domains are arguably best characterized in the SCF:KIT system (Yuzawa et al. 2007; Reshetnyak et al. 2013, 2015). Indeed, several gain-of-function mutations in KIT_{D5} are centered around residues 417-419 and drive cancer development in gastro-intestinal stromal tumors, acute myeloid leukemias, melanoma, and mastocytoma (Ashman and Griffith 2013; Forbes et al. 2011). Those mutations have shown to induce receptor dimerization - and thus receptor activation - in a ligand-independent manner (Yuzawa et al. 2007; Reshetnyak et al. 2015). Superimposition of KIT_{D1-D5} onto FLT3_{T343I} using FLT3_{D4} as a reference, reveals that Ser451 locates remarkably close to the GOF hot-spot region of KIT₄₁₇₋₄₁₉ (Figure 18B). Upon comparing domain 5 of KIT_{WT} with its oncogenic counterpart in KIT_{T417,Δ418-419} (PDB 2E9W and 4PGZ respectively), we note that the exchange of Thr417 for an isoleucine and simultaneous removal of the two downstream residues, essentially concentrates all nearby hydrophobic residues into one patch (Figure 18C). Thus, this oncogenic mutation effectively reshapes the surface of KIT_{D5} to contain a

hydrophobic patch that may help to nucleate the oncogenic dimerization event seen in KIT_{T417I,Δ418,419} (Reshetnyak et al. 2015), and is mechanistically equivalent to the proposed mode-of-action for the oncogenic S451F mutation in FLT3. Interestingly, the energetically unfavorable presence of Arg420 near the hydrophobic patch in KIT_{T417I,Δ418,419} is accommodated by a homotypic interaction with Asn505, which fortifies the expectation of a likewise mechanism for Glu444 in FLT3_{S451F}.

Thus, although the crystal structure of the FL_{WT}:FLT3_{T343I} complex did not reveal a structural adaption to the presence of Ile343, it did provide us with a high-resolution model of FLT3_{D5}. This has allowed mapping of Ser451 onto a structural model and hypothesizing on the mode-of-action behind a transforming S451F mutation. By analyzing the surface hydrophobicity, we observe that mutating Ser451 to a phenylalanine would contribute to establishing a hydrophobic patch. As a similar event is shown to be the driving force behind a constitutive dimerization of oncogenic KIT variants, we envision that by creating a hydrophobic patch, the S451F point mutation is indeed capable of increasing the mutual affinity of membrane proximal domains bearing this substitution.

2.1.5. Large-scale production of FLT3_{S451F} requires addition of thrombin proteolytic site in the FLT3_{D1-D2} linker

The observation that the oncogenic S451F mutation in domain 5 of FLT3 could indeed increase the reciprocal affinity of two FLT3_{S451F} molecules (Section 2.1.4), motivated us to pursue thermodynamic and structural studies of this oncogenic variant of FLT3. To this end, we generated a polyclonal stable HEK293S MGAT1^{-/-} TR⁺ cell line (Reeves et al. 2002) allowing tetracycline-inducible expression and subsequent purification of the extracellular domain of FLT3 bearing the S451F mutation (FLT3_{S451F}). However, in sharp contrast to the 5 mg recombinant protein per liter conditioned medium for FLT3_{WT}, the yield FLT3_{S451F} was limited to 0.3-0.5 mg/l conditioned medium. Although allowing for some experiments, the low sample purity and rapid decrease in expression yield upon propagation of this cell line among other technical problems, motivated us to generate a novel set of monoclonal cell lines using lentiviral transduction (De Groote et al. 2016). Unfortunately, yields of this lentiviral transduced cell lines were even lower and in contrast to what has been described, increasing the puromycin concentration to select for cell lines with a higher copy number inserted into their genome (De Groote et al. 2016), had little or even detrimental effect on the expression level.

Surprisingly, a polyclonal HEK293S MGAT1^{-/-} TR⁺ cell line for stable expression of an FLT3_{S451F} construct featuring a VPRGS thrombin recognition motif between Leu165 and Tyr166 (FLT3_{t-S451F}), developed to improve chances of crystallization by removal of the flexible FLT3_{D1} post-expression, showed an expression yield of 2 - 2.3 mg/l conditioned medium. As such expression yields are well suited for pursuing biophysical studies, we sought confirmation that the thrombin recognition motif did not influence the ligand-binding properties of the receptor. We therefore generated a polyclonal stable HEK293S MGAT1^{-/-} TR⁺ cell line for expression and purification of the wild-type FLT3 construct, endowed with the identical thrombin-recognition site between residues 165 and 166 (FLT3_{t-WT}). The resultant recombinant protein was stable in solution, eluted on a size-exclusion chromatography (SEC) column at the same retention volume as FLT3_{WT} and was capable of binding to its canonical ligand FL_{WT}.

Notably, in contrast to the increased expression yield of FLT3_{t-S451F} compared to FLT3_{S451F}, the yield of 1.5 mg/l of conditioned media for FLT3_{t-WT} was several folds lower than the yield for FLT3_{WT}.

Substantiating the usage of FLT3_{t-S451F} as a valid substitute for the thermodynamic characterization of FLT_{S451F}, was approached by statistically comparing the thermodynamic parameters of FL_{WT} titrations into FLT3_{t-WT} to the parameters of the canonical FL_{WT}:FLT3_{WT} interaction. Two expression campaigns for FLT3_{t-WT} were used to setup an equal amount of ITC experiments with FL_{WT}. The ITC thermograms were analyzed objectively as described before (Section 1.4.1) and the Sedphat-determined thermodynamic parameters were an integral part of the dataset that was used for GHLMM modeling (Figure 19A). Comparing the predicted thermodynamic parameters for the FL_{WT}:FLT3_{t-WT} to the FL_{WT}:FLT3_{WT} interaction, no significant difference could be detected at the 5% CL (p-values > 0.37 for differences in K_D , ΔH and $-\Delta S$, and a p-value of 0.09 for differences in ΔG) (Figure 19B).

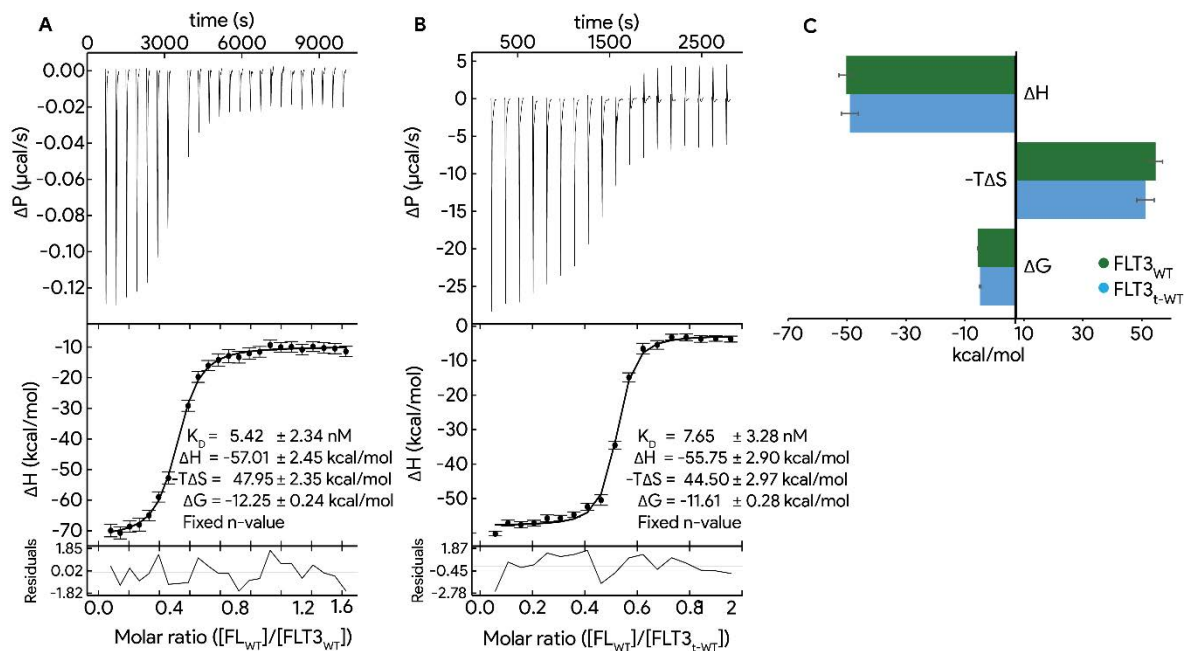


Figure 19. A thrombin-protective site in the FLT3_{D1-D2} linker does not alter thermodynamics of the FL_{WT} interaction.

Representative thermograms and corresponding binding isotherms and residuals of ITC experiments titrating FL_{WT} into **A.** FLT3_{WT} and **B.** FLT3_{t-WT}. HGLMM-predicted thermodynamic parameters are shown for each interaction. Stoichiometry was determined by SEC-MALLS experiments for FLT3_{WT}, whilst cell concentration was parameterized to account for imprecise determination of active protein concentration. **C.** Bar-chart summarizing thermodynamic footprints FL_{WT}:FLT3_{WT} of (green) and FL_{WT}:FLT3_{t-WT} (blue).

Thus, despite having tried both PEI-mediated transfection and lentiviral transduction, only a stable cell line expressing FLT3_{S451F} featuring a thrombin recognition site between domain 1 and 2, FLT3_{t-S451F}, resulted in protein yields amenable for pursuing biophysical and structural studies. The observation that the thermodynamics of ligand-binding does not differ between FLT3_{WT} and FLT3_{t-WT} at the 5% confidence level, suggests that FLT3_{t-S451F} is a valid substitute for FLT3_{S451F} in the determination of thermodynamic parameters of the interaction with its ligands.

2.1.6. S451F mutation in FLT3_{D5} alters the thermodynamics of ligand binding only in presence of a recruited second receptor

The current activation paradigm of FLT3 by its canonical ligand FL strictly posits that no ligand-induced receptor contacts are evoked upon complex formation – rendering FLT3 to be an outlier within the RTK-III and -V families. Thermodynamic analysis of the interaction between FLT3 and two novel engineered FL species, monomeric FL_{L27D} and the heterodimeric FL_{WT/KO}, enabled us for the first time to detect 2 levels of positive cooperativity upon assembling a ternary FL:FLT3 complex (Section 0). Although this analysis suggests that ligand-induced receptor:receptor interactions increase the receptors affinity for FL, it does not allow discrimination between FLT3_{D1}, FLT3_{D4} and/or FLT3_{D5} as the primary contributor to such interface.

Meanwhile, the molecular basis of a clinically discovered oncogenic mutation in FLT3_{D5}, FLT3_{S451F}, remains difficult to explain without acclaiming a role for the membrane-proximal domains in the transition to an activated receptor complex. Mapping of Ser451 onto the structure of domain 5 indeed shows that a substitution by Phe451 could increase the surface hydrophobicity of the membrane-proximal domain in a mechanism analogous to the oncogenic dimerization-inducing mutations in KIT (Section 2.1.4). If this point mutation indeed increases the affinity between the membrane-proximal domains of two receptors, we envisioned that such event would alter the thermodynamics of ligand-binding. We therefore determined the thermodynamic parameters of the interaction between FLT3_{t-S451F} and two ligands, FL_{WT} and monomeric FL_{L27D} (Figure 20). The data is an integral part of the dataset that was fed to the HGLMM model, used to predict the thermodynamic parameters of all interactions and to estimate the statistical significance of their differences at the 5% CL (Section 1.4.1).

Statistical comparison of the thermodynamic parameters of the interactions with titrated FL_{WT} (Figure 20A-18C), shows that the presence of Phe451 alters all thermodynamic parameters but the K_D at the 5% CL. Although titration of FL_{WT} to FLT3_{S451F} results in a K_D that is about 10-fold lower than titrations to FLT3_{WT} ($K_D = 0.54$ nM versus $K_D = 5.4$ nM), affinity is the only thermodynamic parameter that is not significantly different (p-value 0.14). However, given the significant difference in ΔG (p-value < 0.001), we infer that the Phe451 does increase the affinity of the receptor for its ligand. This is further supported by the observation of a 30% decrease in entropic penalty (p-value < 0.001) sufficient to lower the affinity despite of an approximate 16% significant increase in enthalpy (p-value = 0.017). Interestingly, the distinct thermodynamic footprint of FL_{WT}:FLT3_{S451F} interaction disappears entirely upon titrating the monomeric FL_{L27D} into the receptor (Figure 20D-18F). Indeed, analysis of the predicted K_D , ΔG , ΔH and $-\Delta S$ within the HGLMM model could not detect any difference at the 5% CL between FL_{L27D}:FLT3_{WT} and FL_{L27D}:FLT3_{S451F} interactions (p-value of difference in $K_D = 0.101$, p-value of differences in ΔG , ΔH and $-\Delta S$ all > 0.880).

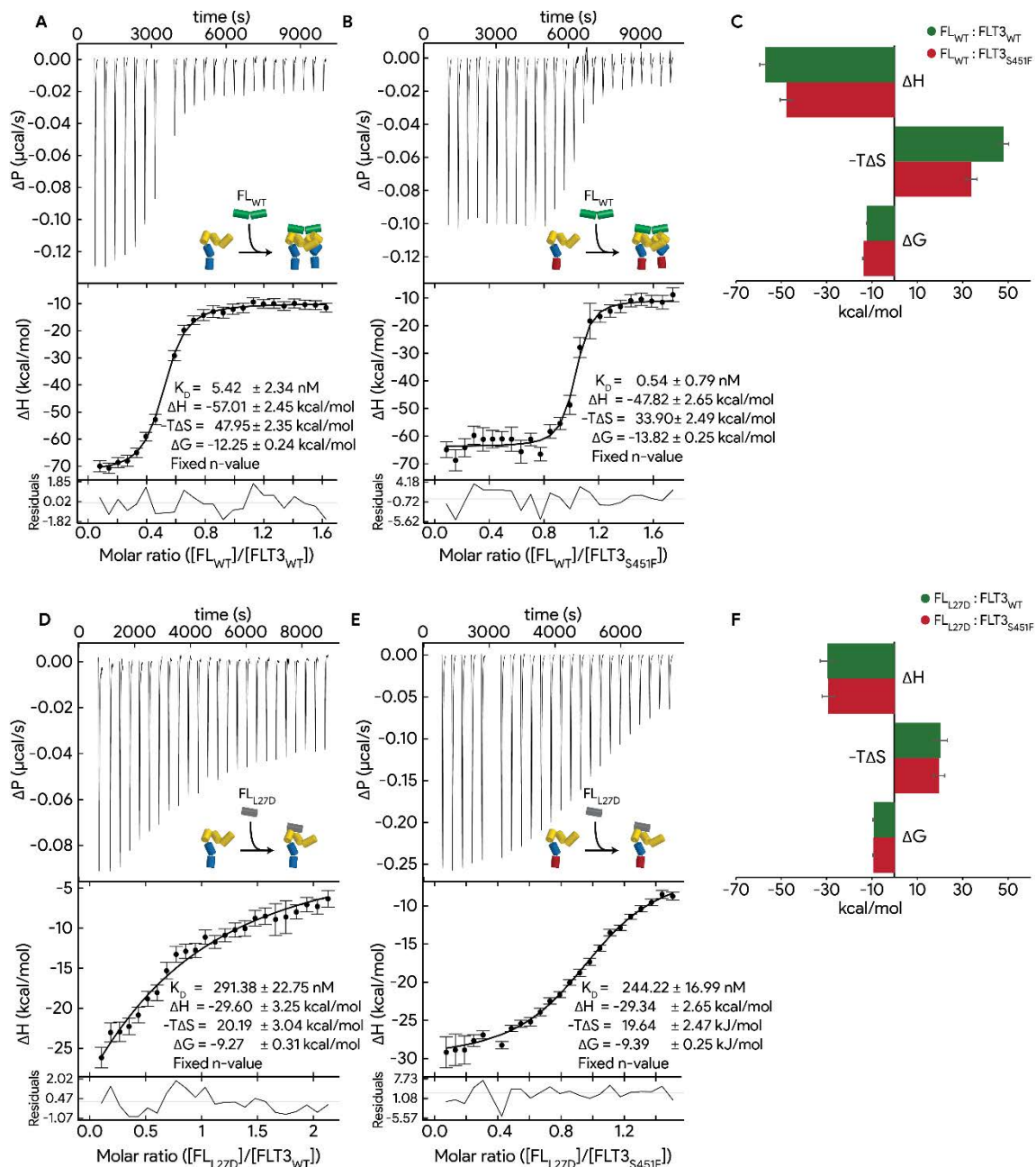


Figure 20. An oncogenic point mutation in domain 5 alters the thermodynamics of ligand binding, but only when cooperativity is at play. Representative thermograms and corresponding binding isotherms and residuals of FL_{WT} titrated to **A.** $FLT3_{WT}$ and **B.** $FLT3_{S451F}$, and FL_{L27D} titrated to **D.** $FLT3_{WT}$ and **E.** $FLT3_{S451F}$. Stoichiometry was determined by previous SEC-MALLS experiments, whilst cell concentration was parameterized to account for imprecise determination of active protein concentration. HGLMM-predicted thermodynamic parameters are shown for each interaction, and summarized in a bar-chart comparing the thermodynamic footprints of the interaction of **C.** FL_{WT} and **F.** FL_{L27D} with $FLT3_{WT}$ (green) and $FLT3_{S451F}$ (red).

In conclusion, although FLT3 is postulated to be the only RTK-III to show no ligand-induced receptor interactions involving the membrane-proximal domains, it was hypothesized that an oncogenic point mutation in domain 5 would drive constitutive receptor dimerization using exactly such a mechanism. Indeed, mapping of Ser451 onto the structure of domain 5 shows that substitution to a phenylalanine

would complement a hydrophobic patch that could increase reciprocal affinity of two receptors in an oncogenic KIT-like mechanism.

Our ITC data now shows that the presence of Phe451 indeed significantly alters the thermodynamic footprint of the interaction between FLT3 and its canonical ligand. Such effect is rather remarkable, considering that this mutation is located 2 domains downstream of the FL:FLT3 binding epitope in a region that is postulated not to be involved in ligand-binding in the wild-type receptor. The observation that this effect on thermodynamics is only apparent when the ligand is able to recruit a second receptor, finally provides sufficient evidence to postulate that presence of Phe451 indeed increases the affinity of FLT3 for its ligand, either by creating a novel interaction site involving the membrane-proximal domains, or by modulating an existing one.

3. Discussion

Almost two decades after establishing that internal tandem duplications (ITD) in the juxtamembrane region of FLT3 result in a constitutively activated oncoprotein, FLT3_{ITD}, US and EU approval of the tyrosine kinase inhibitor (TKI) midostaurin marked what is hopefully the beginning of a new era of targeted therapy against AML (Kiyoi et al. 1998b; Stone et al. 2017). FLT3, which is mutated in approximately 30% of all AML patients, is a single-pass transmembrane receptor and a member of the class-3 of receptor tyrosine kinases (RTK-III)(Deschler and Lübbert 2006; M. a Lemmon and Schlessinger 2010; Verstraete et al. 2011). Although all RTK-III family members are characterized by a similar architecture and activation principles, FLT3 appears to be distinguishing itself by the absence of ligand-induced receptor contacts (M. a Lemmon and Ferguson 2007; Yan Yang, Yuzawa, and Schlessinger 2008; Y. Yang et al. 2010; Verstraete et al. 2011; Elegheert et al. 2011; Verstraete and Savvides 2012; Felix et al. 2015; P. Chen, Unger, and He 2015). In contrast, the molecular mechanism underlying two clinical identified oncogenic point mutations in the extracellular region, T343I and S451F, can only be rationalized in a model allowing for homotypic receptor interactions either via a canonical or a novel mechanism (Fröhling et al. 2007; Jiang et al. 2005; Verstraete and Savvides 2012). Intrigued by this apparent dichotomy in homotypic receptor contacts for a wild-type versus oncogenic context, two new ligands were engineered to further explore possible cooperative events upon assembly of an activated FL:FLT3 complex.

As the results of experiments featuring these two novel ligands would be compared to experiments with the canonical FLT3 Ligand (FL_{WT}), we first sought to validate that in-house produced FL_{WT} reflected the potency of endogenous FL stimulation. The results of three orthogonal approaches show that in-house produced FL_{WT} efficiently transcends species boundaries as a DC differentiation factor both *ex vivo* and *in vivo*, at physiologically relevant concentrations. The development of these assays does therefore not only fortify our confidence in the quality of the in-house produced FL_{WT}, but can furthermore serve as a high-quality benchmark for novel FLT3 ligands to come.

Next, we engineered two novel FL variants, one being the monomeric equivalent of an FL-protomer (FL_{L27D}), the other being a heterodimeric ligand with only one intact receptor binding site (FL_{WT/KO}). Although both were engineered to engage only one FLT3 molecule into complex formation, we

envisioned that their distinct underlying mechanism in doing so, would enable each variant to deliver unique insights into the molecular principles underlying the assembly of a ternary FL:FLT3 receptor complex.

Monomeric FL_{L27D} was generated by exchanging a single amino acid at the heart of the FL-dimerization interface, resulting in a protein species that was stable, well folded and expressible by both bacterial and mammalian cell cultures. Substantial efforts have been made to validate FL_{L27D} as a stable monomeric FL species with an uncompromised FLT3 binding epitope. First, SEC-MALLS analysis confirmed that this protein indeed has the predicted molecular weight of an FL protomer, and is yet still able to recruit an FLT3 molecule into a complex. Secondly, extensive X-ray diffraction experiments featuring the monomeric species alone, and FL_{L27D} in complex with the extracellular domain of FLT3_{D1-5}, left little doubt that the presence of Asp27 in FL_{L27D} only affects the dimer interface without compromising other parts of the fold in general, and the FLT3 binding interface more specifically. Finally, *ex vivo* analysis shows that the monomeric FLT3 ligand is unable to activate FLT3-dependent pathways even at concentrations as high as 1 µg/ml. We can therefore conclude that we were able to modify the dimeric interface of FL with an almost surgical precision, yielding a monomeric FLT3 ligand that employs a binding epitope identical to the canonical FLT3 ligand, but is nevertheless unable to activate the receptor – confirming the spatial prerequisite in the current paradigm of FL-driven FLT3 activation (Felix et al. 2013).

Our co-expression strategy to obtain a heterodimeric FL consisting of one FL_{WT} protomer and one double-mutant FL_{H8R-S13P} protomer resulted in a protein species (FL_{WT/KO}) capable of binding FLT3 in an equimolar fashion, similar to FL_{L27D}. Being well aware of the observation that Stem cell factor (SCF) can swap protomers in solution (Z. Zhang et al. 2000; Hsu et al. 1997), SEC-MALLS analysis of FL_{WT/KO} and the complex thereof with FLT3 was only performed after several days incubation. If dimerization of FL is a dynamic event analogous to SCF, prolonged incubation would have allowed for the emergence of homodimers (i.e. FL_{WT/WT} and FL_{KO/KO} next to FL_{WT/KO}). In such scenario, subsequent addition of FLT3 would generate both 1:1 and 1:2 ligand-receptor complexes. Observing that the largest protein species in solution has a determined molecular weight of approximately 70 kDa, we infer that protomer swapping of FL_{WT/KO} is an event that should not be accounted for within a 5-day timeframe. It has been convincingly demonstrated for FL_{L27D} that the receptor cannot be activated using a ligand that cannot recruit a second receptor. Likewise, we infer that the inability of FL_{WT/KO} to establish a ternary complex, manifest itself by a lack of ligand-induced receptor activation.

Together, our biological and biophysical characterization of all 3 FLT3 ligands (FL_{WT}, FL_{WT/KO} and FL_{L27D}) validate the use of these engineered ligands for exploring cooperativity in ligand binding via isothermal titration calorimetry (ITC). As FL_{L27D} and FL_{WT/KO} only recruit half as many receptors into a complex compared to FL_{WT}, titrations of these ligands into the receptor was expected to show only half as much heat release per injected mol, compared to titrations of FL_{WT} into FLT3. Despite this reduction of enthalpic release by ~50%, the affinity of FLT3 for FL_{L27D} and FL_{WT/KO} was not expected to be significantly altered. Indeed, if ligand-induced receptor interactions are absent upon assembly of a ternary FL:FLT3 complex, then the affinity of a given ligand for FLT3 should not be entangled with its ability to recruit a second receptor into the complex (Section 1.4.2 - Figure 16).

Bolstered by an exhaustive statistical analysis, our comparative ITC experiments employing FL_{WT}, FL_{WT/KO} and FL_{L27D} into FLT3_{D1-D5}, revealed that monomeric FL_{L27D} binds 54-fold less tightly to FLT3 compared to FL_{WT} ($K_D = 291$ nM versus $K_D = 5$ nM). Comparing the thermodynamic signature of both interactions reveals that the lowered affinity can be assigned to an insufficient reduction of the entropic penalty to compensate for the expected halving of enthalpy. The second set of ITC experiments shows that this loss in affinity can be partially attributed to the absence of inter-subunit plasticity. Indeed, experiments featuring FL_{WT/KO} show a 60% increase in affinity for the receptor compared to FL_{L27D}, an effect entirely shouldered by a decrease in the enthalpic component ($K_D = 173$ nM and $\Delta H = -29.60$ kcal/mol versus $K_D = 291$ nM and $\Delta H = -41.29$ kcal/mol). It therefore seems that assembly of the binary encounter complex is quickly followed by electrostatic interactions featuring the second, unoccupied subunit.

This observed first level of cooperativity allows for the first time to assign a possible mechanistic role to the inter-subunit plasticity of FL upon binding of FLT3. Indeed, inter-subunit plasticity upon receptor binding has been observed for all four-helical bundle cytokines that bind an RTK-III (Verstraete et al. 2011; Ma et al. 2012a; Felix et al. 2015; Yuzawa et al. 2007). Locking of such inter-subunit plasticity of CSF-1 into one active conformation has even been proposed as a strict prerequisite for homotypic receptor interactions (Felix et al. 2015). The importance thereof is arguably best demonstrated by the immunomodulating ability of BARG-1 to lock CSF-1 into an inactive conformation, successfully abrogating receptor binding and signaling (Elegheert et al. 2012).

We furthermore observe that the affinity of FLT3 for FL_{WT/KO}, despite being higher than for FL_{L27D}, still is a significant 34-fold lower than its affinity for FL_{WT} ($K_D = 173$ nM versus $K_D = 5$ nM). This second incremental step in affinity therefore reveals the presence of yet another cooperative event upon ligand binding. Having already addressed inter-subunit plasticity, we hereby postulate that ligand-binding induces previously unaddressed receptor contacts or a newly assumed conformational state along the receptor ectodomain that decrease the total free energy of the ternary complex in a cooperative fashion.

To correlate differences in affinity with binding kinetics, we immobilized the receptor onto coated streptavidin tips and performed BLI experiments using all three ligands in solution. These experiments showed that differences in binding kinetics between the different ligands can solely be attributed to increasing dissociation rates. This observation is in line with the notion that all ligands establish identical binary encounter complexes, and subsequent receptor-mediated interactions are responsible for slowing down dissociation.

Although attributing the ability to engage into homotypic interactions between the membrane proximal domains would mechanistically reunite the FLT3 binding principles with all other RTK-III members, our data does not allow identification of FLT3_{D1}, FLT3_{D4} and/or FLT3_{D5} as key players in receptor contacts. Our search for additional insights was approached by the thermodynamic characterization of an FLT3 variant, bearing a clinically identified oncogenic driver mutation in domain 5, S451F, shown to result in a constitutive phosphorylation of the receptors TKD (Fröhling et al. 2007). Expressing the extracellular domain of FLT3 with a S451F mutation at yields allowing structural and

biophysical studies proved to be cumbersome, and eventually required insertion of a thrombin recognition motif in the FLT3_{D1-D2} linker (FLT3_{t-S451F}). The observation that a similar operation in a wild-type context did not significantly alter the thermodynamics of ligand binding, indicates that FLT3_{t-S451F} is indeed a valid substitute for FLT3_{S451F} in determining thermodynamics of ligand binding. The little ITC data available involving FLT3_{S451F} confirms this finding but could not be included into the dataset used for HGLM, as those were performed in a different buffer.

Comparing the thermodynamic footprint of the FL_{WT}:FLT3_{t-S451F} interactions with the one of FL_{WT}:FLT3_{WT}, we observed a significant difference in both enthalpy (ΔH) and entropic penalty ($-\Delta S$), resulting in a significant difference in Gibbs free energy (ΔG). Despite being 10-fold lower, the difference in determined K_D was not significant at the 5% confidence level, possibly as a consequence of comparing very small values on the one hand, and a relatively small dataset on the other.

The reduction of the entropic penalty is arguably a consequence of the imposed restrictions on solvent entropy in the unbound receptor state. Indeed, if a hydrophobic residue is solvent exposed, its side chain will be at the center of a concentric shell of ordered solvent molecules with only limited orientations for inter-molecular hydrogen bonding. When an interaction is able to bury those non-polar residues from the bulk solvent, this cage of restricted solvent molecules is cracked open, resulting into a considerable entropic gain of the buffer component – this hydrophobic effect is nothing else than the main driving force behind protein folding (Serrano et al. 1992; Serrano, Bycroft, and Fersht 1991; Pace et al. 1996; Compiani and Capriotti 2013; Callaway 1994). Specifically for FLT3, we hypothesized that burying of the bulk-solvent exposed Phe451 in a ligand-induced FLT3_{D5}:FLT3_{D5} interaction would mitigate the entropic penalty as a consequence of the favorable effect on the bulk-solvent entropy. We do indeed observe a 58% reduction in the entropic penalty upon comparing titrations of FL_{WT} into FLT3_{WT} versus the mutant FLT3_{S451F}.

Conversely, this hydrophobic effect should not be observed if the ligand is not capable of recruiting a second receptor into the complex. Indeed, the distinct effect of Phe451 on the thermodynamics of FL_{WT} binding completely disappears when comparing thermodynamic parameters between FL_{L27D}:FLT3_{WT} and FL_{L27D}:FLT3_{t-S451F}. Further support for this Phe451-mediated dimerization is given by our ability to, for the first time, map the location of Ser451 onto a model of FLT3_{D5}. This exercise shows that substitution to a Phe451 would complement a hydrophobic patch and as such exert a strong influence on the reciprocal affinity of the whole domain. Such remodeling of the hydrophobic surface distribution has been shown to drive ligand-independent dimerization and oncogenic activation of KIT_{T417I,Δ418-419}, of which the GOF hotspot region co-localizes remarkably well with the location of Ser451 upon superimposition with FLT3. Importantly, presence of Arg420 in the center of the hydrophobic patch of KIT_{T417I,Δ418-419} is compensated by a homotypic interaction with Asn505. Likewise, presence of Glu444 in FLT3_{S451F} should be quenched by a complementary interaction, possibly mediated by Gln447.

Providing a rationale for the negative effect of Phe451 on the enthalpic component of the FL_{WT} binding event, is less straightforward. We envisioned that if this point mutation would create a novel interaction site at the membrane-proximal domains, at least a small gain in enthalpy could be expected, as residues surrounding Phe451 would grasp the opportunity to engage in electrostatic

interactions. Contrarily, we observe a 16 % increase in ΔH , indicating that presence of Phe451 prevents some electrostatic interactions upon ligand binding, compared to the interaction with the wild-type receptor. Such behavior would be expected when the point mutation alters an existing interaction site rather than creating a new one. This so-called enthalpy-entropy compensation upon substituting a polar moiety to an apolar one, is an often observed but much debated phenomenon in the affinity maturation of small molecule binders (Sharp and Sharp 2001; Olsson et al. 2011; Biela et al. 2012; Klebe 2015).

Finally, of the several crystallographic models obtained during this doctoral study, the discovery of a new receptor conformation upon characterizing the FL_{L27D}:FLT3_{WT} complex was arguably the most surprising. Where previous and current crystallographic studies noted a significant domain plasticity of the N-terminal FLT3_{D1} when in complex with FL_{WT}, we now observe a conformation in which FLT3_{D1} is folded back onto domain 2. Furthermore, this conformation appears to stabilize FLT3_{D5} into an orientation away from the imaginary FL_{WT}:FLT3 central axis. Stunned by this compact conformation of the receptor, we are left to wonder about its possible biological role. Given that this conformation restricts the degrees of freedom of the most membrane proximal domains, it could serve as a mechanism to prevent illegitimate membrane-proximal interactions between two FLT3 molecules in absence of the ligand. Such a role for the atypical FLT3_{D1} has been suggested previously (Verstraete et al. 2011; Verstraete and Savvides 2012) and remains an exciting avenue to explore. It could however be argued that an interaction able to successfully restrict the conformational sampling space of FLT3_{D5} and, possibly FLT3_{D4}, is expected to result in a better-defined electron density map for the interacting residues than is observed now. Whilst true, analysis of the atomic displacement parameters (or temperature B-factors) reveals that the B-factors of FLT3_{D1} and FLT3_{D5} are on average 22% and 26% higher than the average ADP value of the FL:FLT3_{D234} core. The lack of clear density for the interacting loops could therefore be equally explained by small movements of the FLT3_{D1-D5} module as a whole. While the observed interaction could be a crystallographic artefact, biologically relevant or somewhere in between, this crystal structure nonetheless highlights the ever-surprising conformational plasticity of the two domains at the receptor's extremities.

In conclusion, we propose a revised activation paradigm of FLT3 that unifies the previous mechanism with our novel findings (Figure 21). We postulate that under steady-state conditions, FLT3 resides at the membrane in a tethered conformation whereby FLT3_{D1} stabilizes FLT3_{D5} in a position away from a possible homotypic interaction site. Although characterized by a high B-value, this tethered conformation indeed imposes unprecedented restrictions onto the domain plasticity at the extremities of the receptor. In the presence of ligand, a binary encounter complex is formed and quickly stabilized by inter-subunit electrostatic interactions. This first cooperative event increases the affinity of the binary encounter complex for recruitment of a second receptor. Being brought into close proximity by ligand binding and fueled by residual inter-subunit plasticity of the ligand, the membrane-proximal domains finally break free from the tethered conformation and subsequently engage into homotypic interactions. We envision that these interactions and possible the simultaneous locking of FL into an active state embody the second and largest layer of cooperativity.

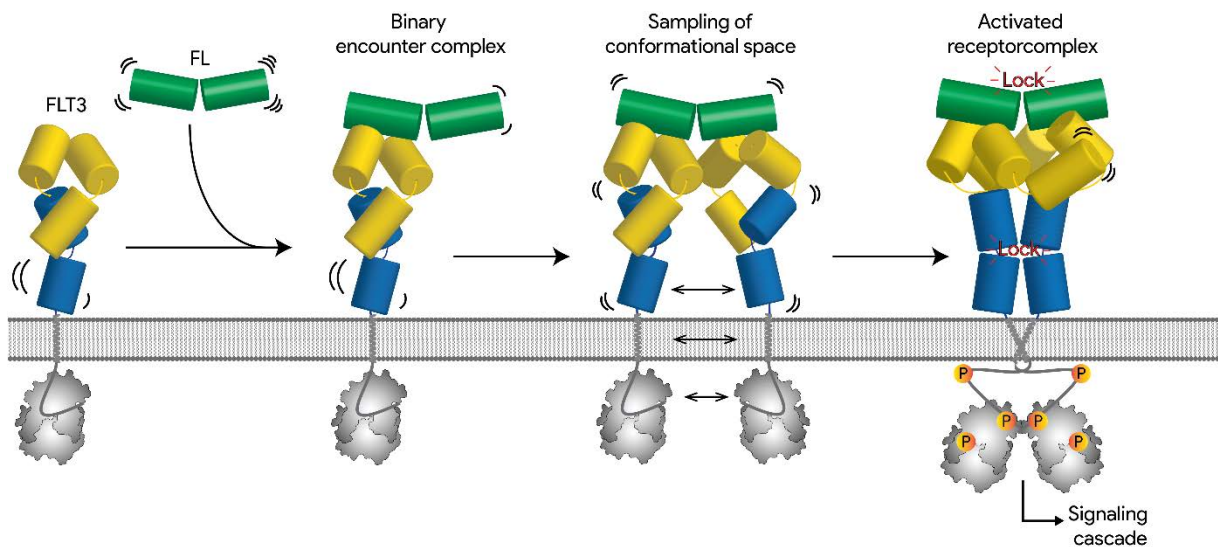


Figure 21. Revised activation paradigm of FL-mediated FLT3 receptor activation. Dormant FLT3 resides as an autoinhibited receptor at the membrane. In presence of the ligand, a binary encounter complex is quickly stabilized by inter-subunit electrostatic interactions. With an increased affinity, a second receptor is recruited to establish a ternary complex. Residual inter-subunit plasticity allows for conformational sampling in FLT3, leading to a receptor dimerization interface between membrane-proximal domains, simultaneously with the release of FLT3_{D1}.

Taking previous ITC experiments featuring a receptor construct lacking domain 5 into account (Verstraete et al. 2011), we envision that the central role for these ligand-induced homotypic interactions in an extracellular context is played by FLT3_{D4}. We suspect that detection of its importance in previous experiments was masked by the instability of the FLT3_{D1-D3} construct (Verstraete et al. 2011). Together with the observation that prototypic SCF-induced homotypic receptor interactions in KIT could not be detected by ITC, these findings show that the importance of FLT3_{D5}-mediated interactions should not be depreciated on the basis of thermodynamic analysis only (M. Lemmon et al. 1997; Yuzawa et al. 2007). In that regard, the large domain plasticity of FLT3_{D5} across different crystallographic complexes, our finding that domain 5 can participate into homotypic contacts in presence the of an oncogenic point mutation and the apparent enthalpy-entropy compensation when it does so, leaves room for the possibility that FLT3_{D5} can play a role in ligand-induced receptor contacts upon assembly of a wild-type complex.

The minor role of FLT3_{D5} in receptor activation, in the context of a soluble ECD construct and possibly at the cell membrane, might explain why bispecific FLT3xCD3 antibodies are more effective in AML cell depletion when FLT3_{D4} is targeted, compared to FLT3_{D5}-targeting antibodies (Djuretic et al., n.d.). In contrast, the FLT3_{D5}-targeting IMC-NC7 antibody has been shown to be resistant to higher ligand concentrations than the FLT3_{D4-D5}-targeting IMC-EB10 antibody (Piloto et al. 2005, patent US8,071,099). Without information of their binding interfaces, it remains difficult to predict which inhibitory effect is consequence of direct competition for binding the epitope involved in homotypic interactions, and which is due to steric hindrance in complex assembly.

In conclusion, this revised activation paradigm incorporates the observed cooperativity of ligand binding, provides a framework for the transforming character of an oncogenic mutation in the extracellular domain and, for the first time, assigns a possible functional role for domains 1 and 5. As such, these results redefine FLT3 from being the odd man out, and reunites the receptor with the RTK-III family.

As functional annotations of FLT3 domains are already used to guide antibody development (e.g. patent WO/2017/021362), we envision that fundamental knowledge on the function of each receptor domain, in both the tethered and activated receptor conformation, will aid the rational targeting of FLT3 in a clinical setting.

4. Outlook

In this doctoral work, the observed cooperative character of ligand binding and mechanistic insights in an oncogenic mutation were distilled into a revised activation paradigm of FLT3, with a more important role for the membrane-proximal domains. The lion's share of arguments presented is based on the determination and statistical comparison of thermodynamic parameters. Consequently, considerable efforts have been made in not only biophysical and structural characterization of the engineered ligands, but also in the development of a robust pipeline allowing statistical analysis.

Of the two engineered ligands, monomeric FL_{L27D} has been characterized best. The combination of *ex vivo* experiments, biophysical SEC-MALLS analysis and structural X-ray crystallography studies of the monomer alone and in complex with the receptor, arguably leave little ground for debating the statement of an unaltered FLT3 binding epitope. Given the observation that CSF-1 monomers can activate CSF-1R at higher concentration in a cellular setup (Zur et al. 2017), the cellular assays developed to characterize FL appeared to be especially useful for ruling out this effect in the context of FL_{L27D}.

The non-trivial expression and purification of FL_{WT/KO} unfortunately didn't allow for an equally exhaustive characterization within the timeframe of this doctoral study. We observed that the protein eluted on SEC-MALLS as a species with a large shoulder. As both peaks are successfully recruited into a complex with FLT3, we inferred that the sample contains a mixture of two FL_{WT/KO} species. Given the prolonged incubation time, partial spontaneous cleavage of the Strep-II® tag could indeed result in two species. Performing SEC-MALLS experiments in a time-scaled setup, supported by Western-blot analysis to detect both tags, would allow us to trace such an event. The low purification yield however tremendously impedes such experiments. Given that FL_{H8R-S13P} cannot be produced in *E. coli*, which decreases the chance of successful crystallization experiments, it would therefore be wise to invest more time in optimization of the construct. In that regard, a matrix of possibilities can be created to determine if either the tag, either the nature of one point mutation, either the coincidence of the two mutations, either a combination of these three are at the root of the observed biochemical instability. The suboptimal expression notwithstanding, the SEC-MALLS observation that this engineered ligand can still bind one – and only one - FLT3_{D1-5} molecule in an equimolar fashion, provides sufficient confidence for its biochemical stability once this protein is purified.

The statistical framework allowing comparison of all thermodynamic parameters across different interactions, is arguably one of the most ground-breaking aspects of this thesis. To our knowledge, we are the first to present our data as predicted values from a statistical model, generated from a dataset comprising a total of 38 ITC experiments, all performed in the same buffer batch and with special care for distinguishing between biological from technical replicates. Although the call for a more statistical approach in analyzing ITC data is not new (e. g. Brautigam et al. 2016; Keller et al. 2012), studies often do not report how many experiments were performed or how many protein batches were used.

Admittedly, one does not require statistics to detect large effects in thermodynamic parameters (e.g. for comparing the interaction of FLT3_{WT} with FL_{WT} and FL_{L27D}). Nor does a statistical significance provide insights into the biological relevance of an observed difference (e.g. the relevance of $K_D = 0.54$ versus $K_D = 5.4$). The true power of the statistical analysis presented in this thesis, comes into play upon trying to detect small differences between interactions or upon analyzing interactions that are not significantly different. This allowed us, for example, to show that presence of a thrombin site in FLT3_{D1-D2} linker does not significantly alter thermodynamics at the 5% confidence level. Likewise, we could show that presence of Phe451 in the receptor's ectodomain alters the thermodynamics of FL_{WT} binding, but not of the FLT3_{WT}:FL_{L27D} interaction. Similarly, the discussion about enthalpy-entropy compensation is often fueled by the notion that different experimenters and equipment might introduce variation that obfuscates differences (Olsson et al. 2011; Klebe 2015). As our experiments are performed by the same experimenter in the same buffer batch, objectively analyzed by the same software and evaluated by a robust statistical modeling, the derived significance of differences and conclusions are built on solid foundations.

Initially, we planned to approach the kinetic characterization of all interactions via similar statistical principles. However, the low purification yields of FLT3_{S451F} and FLT3_{T343I} impeded BLI experiments for a long time. It has been shown that low-expressing proteins can be immobilized on streptavidin-coated BLI tips without prior purification from conditioned media (Felix et al. 2016), but in our hands this approach introduced an unpredictable variation across different experiments. The suitability of a BLI setup for delivering mechanistic insights into ligand-mediated receptor contacts, was furthermore questioned from the beginning. Although the theoretical surface density of streptavidin on the tip is known, predicting whether receptors are immobilized in close enough proximity to allow for receptor:receptor contacts is difficult, if not impossible. Likewise, even if two receptors are in close proximity, we have no knowledge about imposed restrictions on their relative orientation for engaging in such interactions. Our doubts regarding the suitability were further fueled by the large discrepancy in derived kinetic parameters of the FL_{WT}:FLT3_{WT} interaction when the setup was reversed (i.e. upon immobilizing FL_{WT}). Whilst an immobilized receptor showed a determined K_D of 0.12 nM for FL_{WT}, immobilization of the ligand reduced that affinity by a factor 200 ($K_D = 24.10$ nM). Given that ITC does not impose such restrictions on protein orientation and conformational freedom, we concluded that ITC would be the preferable technique for detecting any cooperativity in ligand binding.

The BLI experiments do give an interesting view on the k_d of all interactions and seem to respect the same sequence upon ordering the interactions according to K_D . However, we cannot explain why BLI, in contrast to ITC, identifies the dimeric interface of FL_{WT} rather than ligand-induced

receptor conformational changes and possible ensuing receptor-receptor interactions as the largest contributor of ligand-mediated cooperativity (K_D of FL_{WT} = 0.12 nM; K_D of FL_{WT/KO} = 0.68 nM; K_D of FL_{L27D} = 206 nM).

During this doctoral study, several crystal structures of receptor and cytokine variants were obtained. From a structural point of view, the tethered conformation of FLT3_{WT} when in complex with its inactivating ligand FL_{L27D} was arguably the most surprising element of this study. Although the stereochemistry of the proposed model is currently sub-par, it is expected that inclusion of reference restraints using the high-resolution model of FL_{L27D}. Furthermore, additional analysis shows that although a P1-indexed dataset results in the best refinement statistics of refinement, the difference with datasets indexed in P2₁ and P222₁ is rather small (Table 6). These results seem to hint toward pseudo-merohedral twinning. If present, the crystallographic model will benefit from the higher symmetry when this is corrected for.

Table 6 | Extension of the refinement results from Table 2

| Dataset | Resolution | Anisotropy corrected | Space group | BUSTER R_{work}/R_{free} |
|---------|------------|----------------------|--------------------|----------------------------|
| B | 4.3 Å | no | P1 | 0.2555/0.2800 |
| B | 4.3 Å | no | P12 ₁ | 0.2716/0.2860 |
| B | 4.3 Å | no | P222 ₁ | 0.2645/0.2789 |
| B | 4.2 Å | no | P4 ₃ | 0.2606/0.3035 |
| B | 4.2 Å | no | P4 ₃ 22 | 0.2751/0.3063 |
| B | 4.3 Å | yes | P1 | 0.2282/0.2639 |
| B | 4.3 Å | yes | P12 ₁ | 0.2397/0.2716 |
| B | 4.3 Å | yes | P222 ₁ | 0.2609/0.2726 |
| B | 4.2 Å | yes | P4 ₃ | 0.2484/0.2870 |
| B | 4.2 Å | yes | P4 ₃ 22 | 0.2705/0.2985 |

The suboptimal nature of the model notwithstanding, this observed conformation of FLT3 is clearly distinct from what has been observed previously in crystallographic structures of FL_{WT}:FLT3_{D1-4}, FL_{WT}:FLT3_{D1-5} and FL_{WT}:FLT3_{T343I_D1-5}, and finally provides a functional role for FLT3_{D1} (Verstraete et al. 2011 and unpublished data). These two arguments have motivated us to include the tethered conformation into the activation paradigm, but additional experiments are needed to solidify this inclusion. For example, small-angle X-ray scattering (SAXS) experiments could be used to determine if such tethered conformation of FLT3 exists in solution by rigid body modeling or ensemble refinement. In that regards, good-quality batch-mode SAXS data has been measured for FLT3_{D1-D5} and will be used to examine the existence of an auto-inhibited FLT3 conformation in solution. Additionally, we could disrupt the interaction interface by mutating the DE-loop of FLT3_{D5}, engineer a glycosylation site in that loop or analyze ligand affinity of constructs lacking domain 1. As these interventions would disrupt the auto-inhibited conformation, an increased affinity of the ligand would be expected. In that regard, the

availability of FLT3 variants with a thrombin-cleavable domain 1 positions those experiments well within reach. Alternatively, we can perform crosslinking mass spectrometry or engineer a cysteine bridge to covalently lock the DE-loop of FLT3_{D5} with the BC- or GH-loop of FLT3_{D1} and by doing so, stall the receptor in its tethered conformation.

This tethered conformation could however only be of importance in preventing ligand-independent receptor activation within the spatial confinement of a membrane. Therefore, all of these experiments should be performed in parallel at the cell membrane. Flow cytometry assays developed during this thesis allow quantitative detection of FLT3 at the cell surface and monitoring of FL-mediated internalization. In conjunction with Western blot analysis to detect phosphorylation of the TKDs, these assays should be able to detect alterations in activation patterns by modulation of this auto-inhibited state, if physiologically relevant.

The notion that mechanistic principles involving the extracellular regions might remain undetected when studying those regions as a soluble entities, might explain why the presence of Ile343 in the receptor does not seem to alter ligand binding. Although only described in an abstract, the transforming capacity of this mutation was confirmed by personal communication.

In contrast, the thermodynamic characterization of FLT3_{T-S451F} turned out to be a stunning example of how a single amino acid substitution in the receptor, can significantly alter virtually every thermodynamic parameter of ligand binding. Whereas the difference in ΔH could have been overlooked if the data was analyzed according to traditional methods, the developed statistical pipeline allowed to situate its significance into a biological context. It was however the addition of ITC experiments with FL_{L27D} that provided the strongest evidence for a domain 5-mediated receptor-receptor interaction. In addition, mapping of Ser451 onto the crystallographic model of FLT3_{D5} and the structural comparison to the wild-type and oncogenic KIT, further fortified our hypothesis of a Phe451-mediated increase in affinity between two FLT3_{S451F} molecules.

Structural studies of FLT3_{S451F} in the ligand-bound and ligand-free forms is arguably the most crucial data missing in the biophysical characterization of this point mutant. Despite extensive screening of crystallization conditions, no condition could be identified that allowed crystal formation and growth. Notably, conditions that reproducibly allowed crystallization of FL:FLT3_{T343I}, failed to show crystals for the FLT3_{S451F}-mediated complex – not even after cross seeding. Although a negative result, this finding implies that the FL:FLT3_{S451F} adopts a conformation that is incompatible with the crystal packing observed for the FL:FLT3_{T343I} complex. The interdigitating of domain 5 modules in bottom-to-bottom packed complexes is in that regard indeed predicted to be incompatible with FLT3_{D4-D5}-mediated receptor interactions. Especially considering the weak nature of those interactions, it is plausible that these homotypic interactions are abolished in favor of crystal packing contacts.

The absence of a crystal structure notwithstanding, mapping of Ser451 onto domain 5 of FLT3_{T343I} did give away how a Phe451-mediated homodimerization could be mediated. The presence of the solvent-exposed Phe453 nearby would possibly position a stack of 4 aromatic residues at the center of this interaction. However, whether FLT3_{D5} is truly endowed with a conformation freedom that allows an almost 90° rotation along the D4-D5 linker, still remains to be seen. Mutating Phe453

to, for example, an alanine in the context of a FLT3_{S451F} construct, could provide evidence for this hypothesis.

Truncated receptor constructs with a lower intrinsic flexibility, bearing the S451F mutation, could possibly increase the success of capturing this mutation in a crystallographic model. As constructs lacking domain 1 do not express at yields amenable for crystallization (K. Verstraete, unpublished data), we engineered a receptor construct featuring a thrombin recognition site in the FLT3_{D1-D2} linker. Although this approach allowed us to generate an FL:FLT3_{D2-D5_S451F} species, we did not succeed in crystallizing this complex. As it has been shown that FLT3_{D5} can be expressed and purified in high yields (D. De Pue, unpublished data), crystallization experiments featuring FLT3_{D5-S451F} are one of the few remaining strategies that could still be initiated. Alternatively, the high purity and stability of the complex does allow characterization by electron microscopy. In that regard, exploratory experiments have been initiated in collaboration with the Gutsche Team of the Institute for Structural Biology (Grenoble, France).

Finally, we are left to wonder why FL-mediated receptor contacts have remained under the radar for so long. We hypothesize that although present and relevant, the strength of these ligand-mediated receptor contacts is considerably lower than similar contacts in KIT and CSF-1R. Especially considering that FLT3_{D5} only contributes little to the homotypic receptor interactions in the context of an extracellular construct, explains the minor effect on K_D upon titrating FL_{WT} into FLT3_{D1-D4} (Verstraete et al. 2011). Further analysis of the ITC data for titrations of FL_{WT} into FLT3_{D1-D3}, indicates that this interaction is characterized by a ΔH only half of the FL_{WT}:FLT3_{D1-D5} interaction, regardless of the minor (albeit not absent) effect on K_D . We therefore hypothesize that the observed instability of this construct has masked detection of cooperativity (Verstraete et al. 2011). Indeed, negative-stain EM data does seem to show a tendency of FLT3_{D4} to engage in homotypic interactions (Verstraete et al. 2011 and unpublished data).

Exploring the avenue that homotypic interactions in FLT3 might play a minor role in receptor activation compared to CSF-1R and KIT, combined with the observation of differential dimerization propensity of transmembrane regions (Finger, Escher, and Schneider 2009), we suggest that the dimerization propensity of CSF-1R, KIT and FLT3 is differentially distributed over the protein (Figure 22).

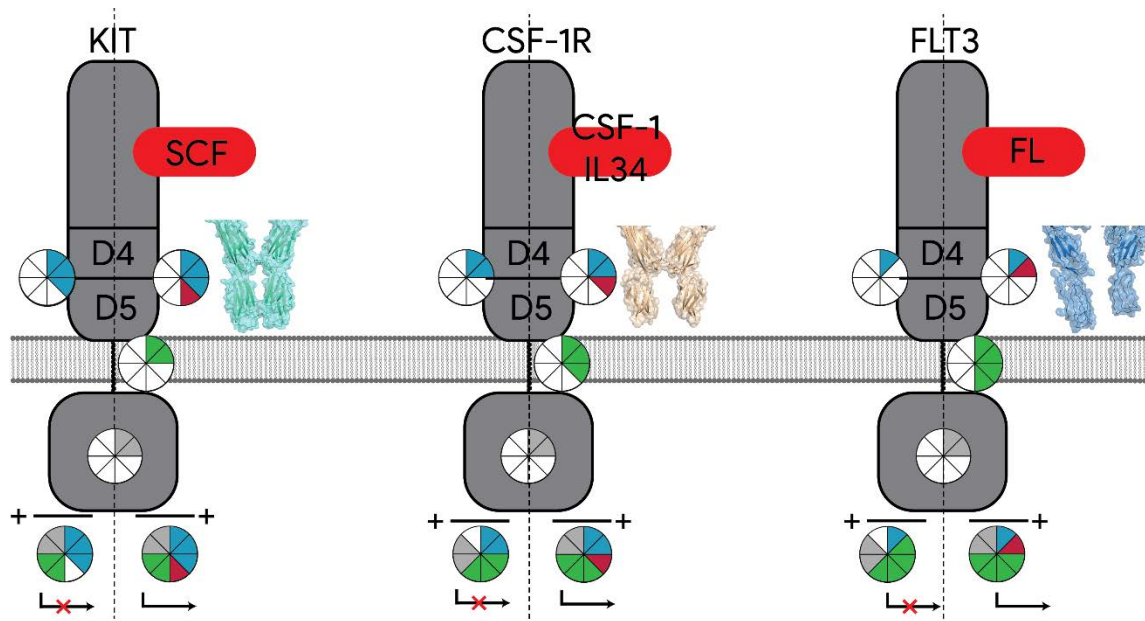


Figure 22. Dimerization propensity is differentially distributed along the ECD and TM regions of RTK-III. Each region of the receptor shows an intrinsic propensity to dimerize, proportional to the number of slices in the pie chart. Only presence of the ligand (right-side of the dashed line) provides sufficient dimerization propensity for the whole molecule to effectively do so. This is indicated by a completed pie chart as a sum of all slices shown above it. The extent of observed homotypic interactions in the ECD is arguably the highest for KIT and the lowest for FLT3, an observation illustrated by the crystal structure of their ligand-mediated complexes. Consequently, the intrinsic dimerization propensity of the TM regions must correlate inversely to this. It has indeed been shown that of displayed receptors, the propensity of the transmembrane domains to self-dimerize is the highest for FLT3 and the lowest for KIT.

We hypothesize that an RTK-III member shows an intrinsic propensity to dimerize. The extent of this intrinsic dimerization propensity should be well balanced: experiments with KIT have shown that abolishing homotypic receptor interactions severely impedes kinase activity even in a ligand-bound complex (Yuzawa et al. 2007). It therefore seems that dimerization of the receptors' extracellular domains is a strict prerequisite for kinase activation. However, their intrinsic propensity to dimerize should not be too high, as this would result in a constitutive dimerization and activation. Indeed, we do observe that a single point mutation is able to tilt the balance towards a ligand-independent receptor dimerization.

Assuming that a 63-85% sequence identity between RTK-III TKDs is an indicator for an equal dimerization propensity across the RTK-III family (Klug, Kent, and Heinrich 2018), we infer that the difference should be localized in the ECD and TM. Well-defined membrane-proximal contacts mediated by both domain 4 and 5 have been observed for KIT, even in the absence of the TM and TKD. Homotypic receptor interactions for CSF-1R in the context of an extracellular construct are limited to domain 4 only. Given the absence of the conserved motif in FLT3, we infer that the dimerization propensity of this receptor is even lower. This would indeed explain why FLT3_{D1-D5} is the only RTK-III showing predominantly an "open" conformation in negative-EM studies. Conversely, it has been shown that the dimerization propensity of the transmembrane domains of FLT3 is the highest among all RTK-III, followed by CSF-1R and only then KIT (Finger, Escher, and Schneider 2009). Therefore, it seems that the dimerization propensity of the ECD is well balanced with that of the TM to provide an intrinsic dimerization proclivity for which the presence of a ligand is both sufficient and necessary.

Experiments shuffling the membrane-proximal domains, TM regions and TKD between all RTK-III, followed by an analysis of receptor activation both in presence and absence of their activating ligands, would arguably provide unique insights into the activation principles underlying all members of the RTK-III family.

5. Experimental procedures

Production of recombinant FLT3 ligands in *E. coli*

Recombinant FL_{WT} and FL_{L27D} was produced according to published methods (Verstraete et al. 2009). Briefly, both proteins were expressed by a Rosetta-gami(DE3) bacterial strain (Novagen) as inclusion bodies. Harvested cell pellets were resuspended in lysis buffer (50 mM Tris pH 8.0, 100 mM NaCl, 1% Triton X-100 and 1 mM EDTA) and lysed by sonication. Inclusion bodies were isolated, washed and solubilized in guanidine buffer (6 M guanidine hydrochloride, 100 mM NaH₂PO₄, 10 mM Tris, 10 mM 2-ME, pH 8.0) by gentle stirring at 40°C, after which the protocol of Verstraete and colleagues was followed to the letter. Endotoxins were removed by washing the nickel-immobilized refolded FLT3 ligands with 5 column volumes 0.1% ampigen (Sigma) phosphate buffer, prior to elution. The produced protein was aliquoted and stored at -80°C until usage.

Expression of recombinant proteins in mammalian cells and purification

cDNA sequences coding for FLT3_{FL} residues Met1 to Ser993, FLT3_{D1-D5} residues Met1 to Asp541 and the pET15b_rhFL plasmid were obtained from Verstraete et al., 2009, 2011. Constructs for transient mammalian expression of secreted proteins carrying a C-terminal thrombin-cleavable AviTag, followed by a hexahistidine sequence, were cloned in the pHLsec vector (Aricescu, Lu, and Jones 2006). For generation of stable cell lines, similar constructs were generated in the pcDNA4/TO vector (Thermo Fisher Scientific). Variants of FLT3 and FL were generated using overlap extension PCR (Heckman and Pease 2007) allowing the PCR for generation of AD fragments to first run 10 cycles without primers. When needed, linker regions were purchased from IDT as GBlocks.

HEK293T cells (ATCC CRL-3216) and HEK293S MGAT1^{-/-} TR⁺ (Reeves et al. 2002) for transient expression experiments and stable cell line generation respectively, were grown to 90% confluence in high glucose DMEM medium supplemented with 10% FCS. Before transfection, medium was exchanged to serum free medium. 25 kDa branched PEI was used as transfection reagent (Aricescu, Lu, and Jones 2006). Stable cell lines were grown to 90% confluence in presence of 50 µg/ml zeocin (Verstraete et al. 2011). To induce expression, the growth medium was replaced by serum-free medium supplemented with 2 µg/ml tetracycline and 3.6 mM valproic acid. After 4-5 days transient or tetracycline-induced expression, the conditioned medium was harvested, cleared of cellular debris by centrifugation and filtered through a 22 µm cut-off bottle top filter. Recombinant hexahistidine-tagged proteins were captured from the conditioned medium by IMAC purification using a cOmplete His-Tag purification column (Roche). After elution with 500 mM imidazole, the eluate was concentrated and further purified by size-exclusion chromatography using HiLoad 16/60 Superdex 75/200 columns (GE Healthcare) with HBS buffer (20 mM HEPES pH 7.4; 150 mM NaCl) as running buffer. Protein purity was evaluated by SDS-PAGE. All produced proteins were aliquoted and stored at -80°C until usage.

Expression of FL_{WT/KO} in mammalian cells and purification

Constructs for transient mammalian expression of FL carrying a C-terminal thrombin-cleavable AviTag, followed by a hexahistidine sequence, were generated in the pHLsec vector (Aricescu, Lu, and Jones 2006). Variants of FL were generated using overlap extension PCR (Heckman and Pease 2007) allowing the AD-generating PCR to first run 10 cycles without primers. To cotranslationally link protomers, linker regions were purchased from IDT as GBlocks. For expression of FL_{H8R-S13P}, a construct for mammalian expression carrying a thrombin-cleavable Strep-II tag was generated in the pHLsec vector.

Expression tests were performed in 6-well plates considering 2.6 µg DNA per well as the optimal amount for transfection (Aricescu, Lu, and Jones 2006). DNA mixtures were prepared prior to addition of PEI. Before transfection, media was replaced with FCS-free DMEM. On day 5 after transfection, the conditioned medium was harvested and filtered prior to SDS-PAGE and Western blotting. Equal volumes of each sample were run on two gels, allowing detection of each construct via different visualization methods. FL_{H8R-S13P} was detected using HRP-conjugated anti-StrepTag II antibodies (Merck) on a Amersham Imager 600 (GE Healthcare). Bands for FL_{WT} were visualized using Dylight™800-conjugated anti-6xHis epitope antibodies (Rockland antibodies & Assays) on an Odyssey Imager (Licor).

For large-scale expression, transfection of HEK293T cells and harvesting of conditioned medium was performed as described earlier. Recombinant proteins were first captured from the conditioned medium by IMAC purification using a cOMplete His-Tag purification column (Roche). Elution was performed with 250 mM imidazole after which the eluate was buffer exchanged to PBS using a HiTrap 5 ml desalting column (GE Healthcare). Strep-tactin affinity chromatography was used to capture the heterodimer based on the presence of the Strep Tag II. The sample was loaded onto a 5 ml prepacked StrepTrap HP column (GE Healthcare). Proteins were eluted using 2.5 µM desthiobiotin (IBA Lifesciences) added to PBS and further purified by size-exclusion chromatography using a HiLoad 16/60 Superdex 75 column (GE Healthcare) with HBS buffer as running buffer.

Generation of stable cell lines using lentiviral transduction

Constructs for transient mammalian expression of secreted FLT3_{D1-D5-WT}, FLT3_{D1-D5-S451F} and FLT3_{D1-D5-T343I} carrying a C-terminal thrombin-cleavable AviTag, followed by a hexahistidine sequence, were generated in the pDG2 vector (De Groote et al. 2016). For each lentivirus production, a 75 cm² tissue culture flask was seeded with 2.8x10⁶ HEK293T cells. Next day, cells were transfected. Twelve micrograms of the lentiviral vector, 3.6 µg pMD2-VSV-G and 7.8 µg pCMV-dR8,91 were added to 1.5 ml final volume of CaCl₂/HEPES buffer (25 mM HEPES pH 7.0, 250 mM NaCl). This solution was dropwise added to 1.5 ml 2xBS/1xHEPES buffer (25 mM HEPES pH 7.0, 274 mM NaCl, 10 mM KCl, 1.24 mM Na₂HPO₄ and 11 mM dextrose), incubated for 10 minutes and added dropwise to the cells. Six hours post-transfection, the medium was replaced by growth medium. Next day, the virus-producing cells were transferred to 32° C and lentivirus production was allowed for another 48h. Virus-containing supernatant was harvested, filtered through a low-protein binding 0.45µm PVDF filter and aliquoted for storage at -70°C.

For transduction, 3 ml of the viral stock was added with 16 µg/ml polybrene before adding to the target cells. HEK293S MGAT1^{-/-} TR⁺ (Reeves et al. 2002) were transduced by 2 consecutive infections of 8h each. Forty-eight hours post transduction, cells were selected by 0.6 µg/ml puromycin,

previously determined to kill 90% of HEK293S MGAT1^{-/-} TR⁺ in 72h. Tetracycline-inducible expression levels were tested via Western blotting 14 days after initial selection. Expression tests were performed in 6-well plates. Before induction, media was replaced with FCS-free DMEM. On day 5 after transfection, the conditioned medium was harvested and filtered prior to SDS-PAGE and Western blotting. Recombinant proteins were detected using Dylight™800-conjugated anti-6xHis epitope antibodies (Rockland antibodies & Assays) on an Odyssey Imager (Licor).

FL-mediated differentiation of primary mice bone marrow cells

Femurs and tibias of C57BL/6J mice, bred and maintained at the Vlaams Instituut voor Biotechnologie (Ghent University) under specific pathogen-free conditions by members of the research groups of Sophie Janssens and Bart Lambrecht, were collected. Bones were crushed with mortar and pestle in RPMI-1640 medium (Invitrogen) supplemented with GlutaMAX (Invitrogen), 10% FCS, 50 μ M 2-ME (Sigma-Aldrich) and 50 μ g/ml gentamycin (Invitrogen), and filtered through a 70- μ M cell sieve. Cells suspensions were cleared for red cells by osmotic lysis. Bone marrow (BM) cells were seeded at 2×10^6 BM cells per well (final concentration), supplemented with indicated final concentrations of FLT3 Ligand (FL) from various sources, or of monomeric FL_{L27D}. At day 7 of culture, cells were collected, washed and stained for 20 min at 4°C in the dark with antibodies. To be able to remove dead cells from our analysis, we used fixable viability dye eFluor506 (eBioscience; used 1/200). Next, cells were resuspended in FACS buffer added with a fixed amount of counting beads (BD Calibrite™ 2-color kit, BD Biosciences) and appropriate single stains were prepared using compensation beads (UltraComp eBeads, ThermoFisher Scientific). The stained samples were acquired on a LSR Fortessa cytometer (BD Biosciences), analysis and graphical output were performed using FlowJo software (Tree Star, Inc.). DCs were gated as alive CD11c⁺ cells from the non-debris. CD45R⁺ MHCII⁻ cells within that pool were identified as pDCs, whereas CD45R⁻ MHCII⁺ cells could be further segregated into CD172a⁻ XCR1⁺ cDC1s and CD172⁺ XCR1⁻ cDC2s. Cell counting beads were used to determine the absolute count of cells in the culture. Count data from all experiments were collected into one dataset and included:

- 11 biological replicates measured over 4 experiments for in-house produced FL_{WT}
- 3 biological replicates measured in 1 experiment for FL_{WT} obtained from Amgen, Peprotech and the VIB Protein Service Facility
- 3 biological replicates measured in 1 experiment for FL_{L27D}
- 5 biological replicates measured over 2 experiments for co-stimulation with FL_{WT} and a potential inhibitory FLT3 ligand, being a fusion protein of FL_{L27D} and 3FF6 nanobody (not discussed in this thesis).

A Hierarchical Generalized Linear Mixed Model (HGLMM) as implemented in Genstat v19 (Baird, Murray, Payne, & Soutar, 2017) was fitted to the data. The linear predictor vector of each of the population counts can be written as follows: $\eta = \mathbf{X}\beta + \mathbf{Z}\mathbf{v}$, where η represents the link function, the matrix \mathbf{X} is the design matrix for the fixed terms SOURCE and CONCENTRATION and their interaction, β is their vector of regression coefficients, \mathbf{Z} is the design matrix for the random replicate terms with technical replicates nested into the biological replicates, and \mathbf{v} is the corresponding vector of random replicate effects. A Poisson distribution with log link was considered for the fixed terms, and a gamma

distribution with log link for the random effects. Inspection of residual plots revealed no departures from normality or homogeneity of variance. T statistics were used to assess the significance of the fixed main and interaction effects estimated as differences to the reference level. Estimated mean values were obtained as predictions from the HGLMM, formed on the scale of the response variable and under the assumption of Normal distribution of residuals at the 1% confidence level. Source of FL and the treatment concentration were chosen as explanatory factors for the population numbers. For convenience of analysis, FL_{L27D} and the cocktail of FL_{WT} and FL_{L27D_3FF6} were considered as different sources of FL. Technical replicates were considered nested into the biological ones, and together added to the model as random terms. Added random terms assumed to be following a Normal distribution. The means and standard errors of the populations sizes were predicted for each concentration and the t-value for each estimated parameter in the mean HGLMM model was converted to a probability, allowing to estimate the significance of the effect on the response variate upon changing explanatory factors, for a given reference condition.

Following antibodies were used: mPDCA1 (120g8; in-house manufactured; used 1/400), XCR1 (ZET; BioLegend; used 1/500), CD11c (N418; eBioscience; used 1/500), CD172a (P84; eBioscience; used 1/100), MHCII (M5/114.15.2; eBioscience; used 1/1000), CD45R (RA3-6B2; BD Pharmingen; used 1/400). Recombinant human FL was obtained from Amgen, VIB Protein Service Facility or made in-house. Recombinant mouse FL was obtained from Peprotech. Recombinant FL_{L27D} and FL_{L27D_3FF6} were made in-house.

FL-mediated FLT3 internalization assay.

Suspension-adapted HEK293S cells were grown and transfected according to proprietary protocols (Nico Callewaert Lab, VIB-UGent Center for Medical Biotechnology). Forty-eight hours post transfection, 24 well plates (24-well suspension plate TC, Sarstedt) were seeded with 500 µl of each cell culture. Plates were overnight incubated in orbital shaker at 37 °C, 8% CO₂. Next day, cells were stimulated with indicated FL concentrations. After 15 minutes incubation, cells were harvested, washed and stained for 20 min at 4°C in the dark with APC rat anti-mouse CD135 (A2F10.1; BD Pharmingen; used 1/100). To be able to remove dead cells from our analysis, we used Fixable Viability Dye eFluor506 (eBioscience; used 1/200). The stained samples were acquired on an LSR Fortessa cytometer (BD Biosciences), analysis and graphical output were performed using FlowJo software (Tree Star, Inc.). Living cells were selected from the non-debris as eFluor506-negative cells, and 10k events in this gate was used as a stopping gate. Median APC signal from living cells was used to quantify FLT3 membrane detection. The data was part of a larger dataset that was fitted to a Hierarchical Generalized Linear Mixed Model (HGLMM) as implemented in Genstat v19 (Baird, Murray, Payne, & Soutar, 2017) (Chapter C – Section 5).

In vivo augmentation of DC populations

C57BL/6 mice (n = 3), bred and maintained at the Vlaams Instituut voor Biotechnologie (Ghent University) under specific pathogen-free conditions, were injected intraperitoneally with 10 µg FL daily, for 7 days. Spleens of treated and untreated (n=3) mice were digested at 37 °C for 30-45 min in RPMI

1640 (61870036; Gibco) containing Liberase TM (0.02 mg/ml; Roche) and DNase I (0.01 U/ml; Roche) after mincing. The obtained cell suspension was cleared of red cells by osmotic lysis.

Following antibodies were used for staining: CD11b (M1/70; BD Pharmingen; used 1/800), Ly6C (HK1.4; eBioscience; used 1/500), NK-1 (PK136; eBioscience; used 1/200), CCR7 (4B12; BD Pharmingen; used 1/100), CD62L (MEL-14; BioLegend; used 1/800), CD8a (SK1; BioLegend; used 1/500), XCR1 (ZET; BioLegend; used 1/500), Ly6G (1A8; BD Pharmingen; used 1/500), CD11c (N418; eBioscience; used 1/500), CD3 (145-2C11; Tonbo; used 1/300), CD19 (1D3; Tonbo; used 1/500), CD86 (PO3; BioLegend; used 1/100), mPDCA1 (120g8; in-house manufactured; used 1/200), CD44 (IM7; BioLegend; used 1/200), MHCII (M5/114.15.2; eBioscience; used 1/500).

Size-exclusion chromatography coupled to multi-angle laser light scattering (SEC-MALLS)

Recombinant proteins and complexes thereof were concentrated to 1 mg/ml and injected onto a Superdex 200 Increase column (GE Healthcare), online with an ultraviolet detector (Shimadzu), a multi-angle laser light scattering miniDAWN TREOS (Wyatt) and an Optilab T-REX refractometer (Wyatt) at 25°C. HBS was used as running buffer at a flow speed of 0.5 ml/min. Data were analyzed using ASTRA6 software (Wyatt). For the analysis of glycosylated protein species, conjugate analysis was performed using theoretical protein extinction coefficients and a dn/dc value 0.16 for the glycan modifier (Bloch 2018).

Protein crystallization and X-ray diffraction experiments

Recombinant proteins were treated with EndoH (New England Biolabs) and 1 U/ μ g protein thrombin (New England Biolabs) to respectively trim N-linked glycosylation (Chang et al. 2007) and to remove purification tags. EndoH and thrombin were removed by size-exclusion chromatography. Vapor-diffusion crystallization experiments were set up using a Mosquito crystallization robot (TTP Labtech) in nano-liter scale SwissSci 96-well triple drop plates. Protein plates were incubated at 293 K or at 287 K. Commercially available sitting drop crystallization screens (Molecular Dimensions, Hampton Research) were used to screen for conditions allowing crystal nucleation and growth. Where indicated, crystals were stepwise cryoprotected before cry-cooling by direct plunging into liquid nitrogen. Seeding of crystallization conditions was performed using the Seed Bead Kit (Hampton Research) following the contemporary protocol. X-ray diffraction experiments were performed at 100 K at the following synchrotron facilities: P13 and P14 beam lines at PETRA III (Hamburg, Germany); Proxima 1 and Proxima 2A beam line at SOLEIL (Gif-sur-Yvette, France); ID23-1 and ID23-2 beam lines at ESRF (Grenoble, France) and PXII beam line at SLS (Villigen, Switzerland).

Crystal structure determination and refinement

Diffraction data was indexed, integrated and scaled using the XDS suite (ref Kabsch 2010). Where indicated, the resulting datasets were truncated and rescaled using UCLA Diffraction Anisotropy Server (Strong et al. 2006) or STARANISO anisotropy & Bayesian estimation server (Tickle et al. 2018). Initial phases were obtained using maximum-likelihood molecular replacement by Phaser from the CCP4 package (Winn et al. 2011; McCoy et al. 2007). Search models were generated from X-ray structures of FL (PDB 1ETE) and FLT3 (PDB 3QS7 and 3QS9). Structure building and refinement was performed

iteratively using COOT (Emsley et al. 2010), PHENIX (Adams et al. 2010) and BUSTER (Bricogne et al. 2011). Notably, the use of Phenix.phase_and_build in refinement of the FL_{WT}:FLT_{3T343I} structure was crucial for maximizing the quality of the electron-density maps for FLT_{3D5}, which was built from scratch into the density of chain G and chain F.

Isothermal titration calorimetry (ITC)

One 6-liter batch HBS buffer (20 mM HEPES pH 7.4; 150 mM NaCl) was prepared, aliquoted and stored at -20°C. Before use, the buffer was filtered through a 20 µm bottle top filter and used to buffer exchange all protein samples using a HiTrap 5 ml desalting column (GE Healthcare). Protein concentrations were estimated spectrophotometrically using the theoretical calculated extinction coefficients. All ITCs were performed at 310 K. The sample cell was stirred at a speed of 400 rpm throughout the ITC experiments performed on a VP-ITC MicroCalorimeter (MicroCal, MA). Titrations on this machine were preceded by an initial injection of 3 µl, and were carried out using 10 µl injections with varying spacing time. ITC experiments on an Affinity ITC (TA Instruments) and PEAQ-ITC (Malvern Panalytical) were carried out using 200 sec spaced injections of 2 µl, preceded by an initial injection of 1 µl. A stirring speed of 75 rpm and 750 rpm throughout was used for experiments on the Affinity ITC and PEAQ-ITC respectively.

All ITC data were analyzed using NITPIC version 1.2.7 (Keller et al. 2012) with default parameters. Calculated heats and error estimates of all injections were spawned to Sedphat (Zhao, Piszczek, and Schuck 2015). Interactions with FL_{WT} were modeled using the “A + B + B <-> {AB} + B <-> ABB with 2 symmetric sites, macroscopic K” model with the following global parameters: incfA = incfB = 0, not refined; Log(Ka1)= 6, refined; dHAB = -25, refined; Log10(Ka2/Ka1) macroscopic= -0.6, not refined; dH(AB)B-dHAB = 0, not refined. Under experiment parameters, it was allowed to fit a baseline and estimate a local correction factor for the cell concentration. Buffer, pH and temperature were filled and, given our setup, we selected to titrate A into B. After a global fit, the estimated thermodynamic parameters of the ABB reaction were calculated from those of the AB estimates.

ITC experiments with FL_{L27D} and FL_{WT/KO} were modeled using the “A + B <-> AB Hetero association” model with the following global parameters: incfA = incfB = 0, not refined; Log(Ka)= 6, refined; dHAB = -10, refined. Under experiment parameters, it was allowed to fit a baseline and estimate a local correction factor for the cell concentration. Buffer, pH and temperature were added to the parameters, and a global fit was performed to estimate the thermodynamic values. For all ITCs, GUSI was used to generate a figure containing the thermogram and isotherms (Brautigam et al. 2016).

The estimated thermodynamic parameters of all ITC experiments were ensembled into a single dataset. The final dataset contained all thermodynamic parameters derived from a total of 38 ITC experiments:

- 3 biological replicates with 2 to 3 technical replicates each for the FL_{WT}:FLT_{3WT} interaction
- 2 biological replicates with 1 and 2 technical replicates each for the FL_{WT/KO}:FLT_{3WT} interaction
- 2 biological replicates with 1 and 4 technical replicates each for FL_{L27D}:FLT_{3WT} interaction
- 1 biological replicate with 4 technical ones for the interaction with FL_{WT}:FLT_{3T343I} interaction
- 2 biological replicates with 2 technical replicates each for the FL_{L27D}:FLT_{3T343I} interaction

- 2 biological replicates with 1 and 4 technical replicates each for the FL_{WT}:FLT3_{t-WT} interaction
- 3 biological replicates with 2 to 3 technical replicates each for the FL_{WT}:FLT3_{t-S451F} interaction
- 3 biological replicates with 1 to 3 technical replicates each for the FL_{L27D}:FLT3_{t-S451F} interaction

A Hierarchical Generalized Linear Mixed Model (HGLMM) as implemented in Genstat v19 (Baird et al. 2017) was fitted to the data. The linear predictor vector of the thermodynamic parameters can be written as follows: $\eta = \mathbf{X}\beta + \mathbf{Z}\nu$, where η represents the link function, the matrix \mathbf{X} is the design matrix for the fixed terms LIGAND and RECEPTOR and their interaction, β is their vector of regression coefficients, \mathbf{Z} is the design matrix for the random replicate terms with technical replicates nested into the biological replicates, and ν is the corresponding vector of random replicate effects. For all thermodynamic parameters but K_D , a normal distribution with identity link was considered for fixed and random effects. For the parameter K_D , a Poisson distribution with log link was considered for the fixed terms, and a gamma distribution with log link for the random effects. T statistics were used to assess the significance of the fixed main and interaction effects estimated as differences to the reference level. Estimated mean values were obtained as predictions from the HGLMM, formed on the scale of the response variable and under the assumption of Normal distribution of residuals at the 1% confidence level. An apparent Poisson distribution of the values for K_D required log-transformation of the data. For all models, ligand and receptor identity were chosen as explanatory factors for the thermodynamic parameter in question. Technical replicates were considered nested into the biological ones, and together added to the model as random terms, possibly contributing to the variation within the response variable. Added random terms assumed to be following a Normal distribution. The means and standard errors of the thermodynamic parameters were predicted and the t-value for each estimated parameter in the mean HGLMM model was converted to a probability, allowing to estimate the significance of the effect on the response variate upon changing one or both explanatory factors, for a given reference ITC interaction.

Biolayer interferometry

Purified recombinant FLT3_{D1-D5} was *in vitro* biotinylated using in-house produced BirA. Excess biotin was removed using a HiTrap 5 ml desalting column (GE Healthcare). BLI experiments were performed at 37°C in kinetics buffer (10 mM HEPES pH 7.4; 150 mM NaCl; 0.3 mM EDTA; 0.05% Tween-20) using an Octet RED96 machine (FortéBio). Streptavidin-coated biosensors were functionalized with biotinylated FLT3 until a response shift of 1 nm, and dipped into solution containing indicated concentrations of the ligand. Non-functionalized biosensors were used during the assay to verify that no non-specific binding was present. Sensor traces of zero concentration conditions and a column of non-functionalized sensors was used to enable double reference subtraction. A 1:1 ligand model was fitted to all data using the FortéBio Data Analysis 9.0.0.4 software.

6. Author contributions

In vivo injections of FL and subsequent analysis of cell populations was performed by Simon Tavernier. For BM differentiation experiments, Simon Tavernier and Kim Deswarte sacrificed mice. Other shown

experiments were performed by Erwin Pannecoucke with experimental and intellectual input of Savvas Savvides, Yehudi Bloch, Steven De Munck, Tajana Devos, and Laurens Raes for the biophysical studies, from Simon Tavernier and Kim Deswarte for the flow cytometry studies and from Marnik Vuylsteke for the statistical analysis.

7. References

- Adams, Paul D. et al. 2010. "PHENIX: A Comprehensive Python-Based System for Macromolecular Structure Solution." *Acta Crystallographica Section D: Biological Crystallography* 66(2): 213–21.
- Aricescu, A Radu, Weixian Lu, and E Yvonne Jones. 2006. "A Time- and Cost-Efficient System for High-Level Protein Production in Mammalian Cells." *Acta crystallographica. Section D, Biological crystallography* 62(Pt 10): 1243–50. <http://www.ncbi.nlm.nih.gov/pubmed/17001101> (July 18, 2012).
- Ashman, Leonie K, and Renate Griffith. 2013. "Therapeutic Targeting of C-KIT in Cancer." *Expert Opinion on Investigational Drugs* 22(1): 103–15. <http://www.tandfonline.com/doi/full/10.1517/13543784.2013.740010>.
- Badar, Talha et al. 2015. "Improvement in Clinical Outcome of FLT3 ITD Mutated Acute Myeloid Leukemia Patients over the Last One and a Half Decade." *American Journal of Hematology* 90(11): 1065–70.
- Baird, D., D. Murray, R. Payne, and D. Soutar. 2017. "Introduction to GenStat for Windows (19th Edition)."
- Beaudin, Anna E, Scott W Boyer, and E Camilla Forsberg. 2014a. "Flk2/Flt3 Promotes Both Myeloid and Lymphoid Development by Expanding Non-Self-Renewing Multipotent Hematopoietic Progenitor Cells." *Experimental hematology* 42(3): 218–229.e4. <http://www.ncbi.nlm.nih.gov/pubmed/24333663>.
- . 2014b. "Flk2/Flt3 Promotes Both Myeloid and Lymphoid Development by Expanding Non-Self-Renewing Multipotent Hematopoietic Progenitor Cells." *Experimental hematology* 42(3): 218–229.e4. <http://www.ncbi.nlm.nih.gov/pubmed/24333663>.
- Biela, Adam et al. 2012. "Ligand Binding Stepwise Disrupts Water Network in Thrombin: Enthalpic and Entropic Changes Reveal Classical Hydrophobic Effect." *Journal of Medicinal Chemistry* 55(13): 6094–6110.
- Brautigam, Chad A et al. 2016. "Integration and Global Analysis of Isothermal Titration Calorimetry Data for Studying Macromolecular Interactions." *Nature protocols* 11(5): 882–94. <http://www.nature.com/gaelnomade.ujf-grenoble.fr/nprot/journal/v11/n5/abs/nprot.2016.044.html>.
- Bricogne, G. et al. 2011. "BUSTER Version 2.10.3." *Cambridge, United Kingdom: Global Phasing Ltd.*
- Callaway, David J.E. 1994. "Solvent-induced Organization: A Physical Model of Folding Myoglobin." *Proteins: Structure, Function, and Bioinformatics*.
- Chang, Veronica T et al. 2007. "Glycoprotein Structural Genomics: Solving the Glycosylation Problem." *Structure (London, England : 1993)* 15(3): 267–73. <http://www.pubmedcentral.nih.gov/articlerender.fcgi?artid=1885966&tool=pmcentrez&render>

- type=abstract (August 11, 2011).
- Chen, Po-han, Vinzenz Unger, and Xiaolin He. 2015. "Structure of Full-Length Human PDGFR β Bound to Its Activating Ligand PDGF-B as Determined by Negative-Stain Electron Microscopy." *Journal of Molecular Biology*. <http://dx.doi.org/10.1016/j.jmb.2015.10.003>.
- Chen, Po Han, Vinzenz Unger, and Xiaolin He. 2015. "Structure of Full-Length Human PDGFR β Bound to Its Activating Ligand PDGF-B as Determined by Negative-Stain Electron Microscopy." *Journal of Molecular Biology* 427(24): 3921–34. <http://dx.doi.org/10.1016/j.jmb.2015.10.003>.
- Compiani, Mario, and Emidio Capriotti. 2013. "Computational and Theoretical Methods for Protein Folding." *Biochemistry*.
- Deschler, Barbara, and Michael Lübbert. 2006. "Acute Myeloid Leukemia: Epidemiology and Etiology." *Cancer* 107(9): 2099–2107.
- Djuretic, Ivana et al. "Poster Abstract: A Novel Full Length Anti-FLT3 CD3 Bispecific Antibody for the Treatment of Acute Myeloid Leukemia." *ASH Annual Meeting*: Abstract 1445 Session 616.
- Elegheert, Jonathan et al. 2011. "Extracellular Complexes of the Hematopoietic Human and Mouse CSF-1 Receptor Are Driven by Common Assembly Principles." *Structure* 19(12): 1762–72. <http://dx.doi.org/10.1016/j.str.2011.10.012>.
- . 2012. "Allosteric Competitive Inactivation of Hematopoietic CSF-1 Signaling by the Viral Decoy Receptor BARF1." *Nature Structural & Molecular Biology* 19(9): 938–47.
- Emsley, P., B. Lohkamp, W. G. Scott, and K. Cowtan. 2010. "Features and Development of Coot." *Acta Crystallographica Section D: Biological Crystallography* 66(4): 486–501.
- Felix, Jan et al. 2013. "Human IL-34 and CSF-1 Establish Structurally Similar Extracellular Assemblies with Their Common Hematopoietic Receptor." *Structure* 9: 1–12. <http://linkinghub.elsevier.com/retrieve/pii/S0969212613000403> (March 8, 2013).
- . 2015. "Structure and Assembly Mechanism of the Signaling Complex Mediated by Human CSF-1." *Structure* 23(9): 1621–31. <http://linkinghub.elsevier.com/retrieve/pii/S0969212615002725>.
- . 2016. "Structural Basis of GM-CSF and IL-2 Sequestration by the Viral Decoy Receptor GIF." *Nature Communications* 7: 13228. <http://www.nature.com/doi/10.1038/ncomms13228>.
- Finger, Carmen, Claudia Escher, and Dirk Schneider. 2009. "The Single Transmembrane Domains of Human Receptor Tyrosine Kinases Encode Self-Interactions." *Science signaling* 2(89): ra56. <http://www.ncbi.nlm.nih.gov/pubmed/19797273> (March 15, 2013).
- Forbes, S A et al. 2008. "The Catalogue of Somatic Mutations in Cancer (COSMIC)." eds. Jonathan L Haines et al. *Current protocols in human genetics editorial board Jonathan L Haines et al* Chapter 10(March): Unit 10.11. <http://www.pubmedcentral.nih.gov/articlerender.fcgi?artid=2705836&tool=pmcentrez&render type=abstract>.
- . 2011. "COSMIC: Mining Complete Cancer Genomes in the Catalogue of Somatic Mutations in Cancer." *Nucleic acids research* 39(Database issue): D945-50. <http://www.pubmedcentral.nih.gov/articlerender.fcgi?artid=3013785&tool=pmcentrez&render type=abstract> (August 12, 2013).
- Fröhling, Stefan et al. 2002. "Prognostic Significance of Activating FLT3 Mutations in Younger Adults (16 to 60 Years) with Acute Myeloid Leukemia and Normal Cytogenetics: A Study of the AML

- Study Group Ulm." *Blood* 100(13): 4372–80.
- . 2007. "Identification of Driver and Passenger Mutations of FLT3 by High-Throughput DNA Sequence Analysis and Functional Assessment of Candidate Alleles." *Cancer Cell* 12(6): 501–13.
- Graddis, T J et al. 1998. "Structure-Function Analysis of FLT3 Ligand-FLT3 Receptor Interactions Using a Rapid Functional Screen." *The Journal of biological chemistry* 273(28): 17626–33. <http://www.ncbi.nlm.nih.gov/pubmed/9651358>.
- De Groote, Philippe et al. 2016. "Generation of a New Gateway-Compatible Inducible Lentiviral Vector Platform Allowing Easy Derivation of Co-Transduced Cells." *BioTechniques* 60(5): 252–59.
- Heckman, Karin L, and Larry R Pease. 2007. "Gene Splicing and Mutagenesis by PCR-Driven Overlap Extension." *Nature protocols* 2(4): 924–32. <http://www.ncbi.nlm.nih.gov/pubmed/17446874> (August 20, 2013).
- Hsu, Y et al. 1997. "The Majority of Stem Cell Factor Exists as Monomer under Physiological Conditions. Implications for Dimerization Mediating Biological Activity." *Journal of Biological Chemistry* 272(10): 6406–15.
- Jiang, Jingrui et al. 2005. "Identifying and Characterizing a Novel Activating Mutation of the FLT3 Tyrosine Kinase in AML." In *Cellular and Molecular Biology Abstracts*, <http://www.ncbi.nlm.nih.gov/pubmed/15178581>.
- Joosten, Robbie P., Krista Joosten, Garib N. Murshudov, and Anastassis Perrakis. 2012. "PDB-REDO: Constructive Validation, More than Just Looking for Errors." *Acta Crystallographica Section D: Biological Crystallography* 68(4): 484–96.
- Kayser, Sabine et al. 2009. "Insertion of FLT3 Internal Tandem Duplication in the Tyrosine Kinase Domain-1 Is Associated with Resistance to Chemotherapy and Inferior Outcome." *Blood*.
- Keller, Sandro et al. 2012. "High-Precision Isothermal Titration Calorimetry with Automated Peak-Shape Analysis." *Analytical chemistry* 84(11): 5066–73.
- Kiyoi, H et al. 1998. "Internal Tandem Duplication of the FLT3 Gene Is a Novel Modality of Elongation Mutation Which Causes Constitutive Activation of the Product." *Leukemia : official journal of the Leukemia Society of America, Leukemia Research Fund, U.K* 12(9): 1333–37.
- Klebe, Gerhard. 2015. "Applying Thermodynamic Profiling in Lead Finding and Optimization." *Nature Reviews Drug Discovery* 14(2): 95–110. <http://dx.doi.org/10.1038/nrd4486>.
- Klug, Lillian R., Jason D. Kent, and Michael C. Heinrich. 2018. "Structural and Clinical Consequences of Activation Loop Mutations in Class III Receptor Tyrosine Kinases." *Pharmacology and Therapeutics*. <https://doi.org/10.1016/j.pharmthera.2018.06.016>.
- Lemmon, Mark et al. 1997. "Kit Receptor Dimerization Is Driven by Bivalent Binding of Stem Cell Factor." *Journal of Biological Chemistry* 272(10): 6311–17.
- Lemmon, Mark a, and Kathryn M Ferguson. 2007. "A New Twist in the Transmembrane Signaling Tool-Kit." *Cell* 130(2): 213–15. <http://www.ncbi.nlm.nih.gov/pubmed/17662934> (January 7, 2012).
- Lemmon, Mark a, and Joseph Schlessinger. 2010. "Cell Signaling by Receptor Tyrosine Kinases." *Cell* 141(7): 1117–34. <http://www.pubmedcentral.nih.gov/articlerender.fcgi?artid=2914105&tool=pmcentrez&render type=abstract> (February 27, 2013).
- Leppänen, Vm, and Denis Tvorogov. 2013. "Structural and Mechanistic Insights into VEGF Receptor 3

- Ligand Binding and Activation." *Proceedings of the ...*: 1–6.
<http://www.pnas.org/content/110/32/12960.short>.
- Lu, Chang-Ming et al. 2002. "Increasing Bioactivity of Flt3 Ligand by Fusing Two Identical Soluble Domains." *Sheng wu hua xue yu sheng wu wu li xue bao Acta biochimica et biophysica Sinica* 34(6): 697–702. <http://www.ncbi.nlm.nih.gov/pubmed/12417909>.
- Ma, Xiaolei et al. 2012a. "Structural Basis for the Dual Recognition of Helical Cytokines IL-34 and CSF-1 by CSF-1R." *Structure (London, England : 1993)* 20(4): 676–87. <http://www.ncbi.nlm.nih.gov/pubmed/22483114> (March 9, 2013).
- . 2012b. "Structural Basis for the Dual Recognition of Helical Cytokines IL-34 and CSF-1 by CSF-1R." *Structure* 20(4): 676–87. <http://linkinghub.elsevier.com/retrieve/pii/S0969212612000664> (April 6, 2012).
- Markovic-Mueller, Sandra et al. 2017. "Structure of the Full-Length VEGFR-1 Extracellular Domain in Complex with VEGF-A." *Structure* 25(2): 341–52. <http://linkinghub.elsevier.com/retrieve/pii/S0969212616304026>.
- McCoy, Airlie J. et al. 2007. "Phaser Crystallographic Software." *Journal of Applied Crystallography* 40(4): 658–74.
- NIH, National Cancer Institute. "Cancer Stat Facts: Leukemia - Acute Myeloid Leukemia (AML)." <https://seer.cancer.gov/statfacts/html/amyl.html> (November 21, 2018).
- Olsson, Tjelvar S G, John E. Ladbury, Will R. Pitt, and Mark A. Williams. 2011. "Extent of Enthalpy-Entropy Compensation in Protein-Ligand Interactions." *Protein Science* 20(9): 1607–18.
- Pace, C N, B A Shirley, M McNutt, and K Gajiwala. 1996. "Forces Contributing to the Conformational Stability of Proteins." *The FASEB Journal*.
- Piloto, Obdulio et al. 2005. "Inhibitory Anti-FLT3 Antibodies Are Capable of Mediating Antibody-Dependent Cell-Mediated Cytotoxicity and Reducing Engraftment of Acute Myelogenous Leukemia Blasts in Nonobese Diabetic/Severe Combined Immunodeficient Mice." *Cancer Research* 65(4): 1514–22.
- Pulendran, B. et al. 2000. "Flt3-Ligand and Granulocyte Colony-Stimulating Factor Mobilize Distinct Human Dendritic Cell Subsets In Vivo." *The Journal of Immunology* 165(1): 566–72. <http://www.jimmunol.org/cgi/doi/10.4049/jimmunol.165.1.566>.
- Pulendran, B et al. 1999. "Distinct Dendritic Cell Subsets Differentially Regulate the Class of Immune Response in Vivo." *Proceedings of the National Academy of Sciences* 96(February): 1036–41.
- Reeves, Philip J, Nico Callewaert, Contreras Roland, and H Gobind Khorana. 2002. "Structure and Function in Rhodopsin: High-Level Expression of Rhodopsin with Restricted and Homogeneous N-Glycosylation by a Tetracycline-Inducible N-Glycosylation by a Tetracycline- HEK293S Stable Mammalian Cell Line." *Proceedings of the National Academy of Sciences of the United States of America* 99(21): 13419–24. <http://www.pnas.org/content/99/21/13419.short> (April 15, 2012).
- Reshetnyak, Andrey V et al. 2013. "Structural Basis for KIT Receptor Tyrosine Kinase Inhibition by Antibodies Targeting the D4 Membrane-Proximal Region." *Proceedings of the National Academy of Sciences of the United States of America* 110(44): 17832–37. http://www.pubmedcentral.nih.gov/articlerender.fcgi?artid=3816449&tool=pmcentrez&render_type=abstract.

- . 2015. “The Strength and Cooperativity of KIT Ectodomain Contacts Determine Normal Ligand-Dependent Stimulation or Oncogenic Activation in Cancer.” *Molecular Cell* 57(1): 191–201. <http://linkinghub.elsevier.com/retrieve/pii/S1097276514009162>.
- Ruch, Claudia et al. 2007. “Structure of a VEGF-VEGF Receptor Complex Determined by Electron Microscopy.” *Nature Structural and Molecular Biology* 14(3): 249–50.
- Schnittger, Susanne et al. 2002. “Analysis of FLT3 Length Mutations in 1003 Patients with Acute Myeloid Leukemia: Correlation to Cytogenetics, FAB Subtype, and Prognosis in the AMLCG Study and Usefulness as a Marker for the Detection of Minimal Residual Disease.” *Blood*.
- Serrano, Luis et al. 1992. “The Folding of an Enzyme. II. Substructure of Barnase and the Contribution of Different Interactions to Protein Stability.” *Journal of Molecular Biology*.
- Serrano, Luis, Mark Bycroft, and Alan R. Fersht. 1991. “Aromatic-Aromatic Interactions and Protein Stability. Investigation by Double-Mutant Cycles.” *Journal of Molecular Biology*.
- Sharp, Kim, and K I M Sharp. 2001. “Entropy — Enthalpy Compensation : Fact or Artifact ? Entropy – Enthalpy Compensation : Fact or Artifact ?” *Protein Science*: 661–67.
- Shim, Ann Hye-Ryong et al. 2010. “Structures of a Platelet-Derived Growth Factor/Propeptide Complex and a Platelet-Derived Growth Factor/Receptor Complex.” *Proceedings of the National Academy of Sciences of the United States of America* 107(25): 11307–12. <http://www.pubmedcentral.nih.gov/articlerender.fcgi?artid=2895058&tool=pmcentrez&render type=abstract> (April 29, 2012).
- Stone, Richard M. et al. 2017. “Midostaurin plus Chemotherapy for Acute Myeloid Leukemia with a *FLT3* Mutation.” *New England Journal of Medicine*: NEJMoa1614359. <http://www.nejm.org/doi/10.1056/NEJMoa1614359>.
- Strong, Michael et al. 2006. “Towards the Structural Genomics of Complexes: Crystal Structure of a PE/PPE Portein Complex from Mycobacterium Tuberculosis.” *Proceedings of the National Academy of Sciences of the United States of America* 103(21): 8060–65.
- Thiede, C et al. 2002. “Analysis of FLT3-Activating Mutations in 979 Patients with Acute Myelogenous Leukemia: Association with FAB Subtypes and Identification of Subgroups with Poor Prognosis.” *Blood* 99(12): 4326–35.
- Tickle, I.J. et al. 2018. “STARANISO.”
- Verstraete, Kenneth et al. 2009. “Efficient Production of Bioactive Recombinant Human Flt3 Ligand in *E. Coli*.” *Protein Journal* 28(2): 57–65. <http://www.ncbi.nlm.nih.gov/pubmed/19184382> (August 30, 2012).
- . 2011. “Structural Insights into the Extracellular Assembly of the Hematopoietic Flt3 Signaling Complex.” *Blood* 118(1): 60–68.
- Verstraete, Kenneth, and Savvas N Savvides. 2012. “Extracellular Assembly and Activation Principles of Oncogenic Class III Receptor Tyrosine Kinases.” *Nature reviews. Cancer* 12(11): 753–66. <http://www.ncbi.nlm.nih.gov/pubmed/23076159> (March 6, 2013).
- Waskow, Claudia et al. 2008. “The Receptor Tyrosine Kinase Flt3 Is Required for Dendritic Cell Development in Peripheral Lymphoid Tissues.” *Nature immunology* 9(6): 676–83. <http://www.pubmedcentral.nih.gov/articlerender.fcgi?artid=2746085&tool=pmcentrez&render type=abstract>.

- Whitman, S. P. et al. 2001. "Absence of the Wild-Type Allele Predicts Poor Prognosis in Adult de Novo Acute Myeloid Leukemia with Normal Cytogenetics and the Internal Tandem Duplication of FLT3: A Cancer and Leukemia Group B Study." *Cancer Research*.
- Winn, Martyn D. et al. 2011. "Overview of the CCP4 Suite and Current Developments." *Acta Crystallographica Section D: Biological Crystallography* 67(4): 235–42.
- Yang, Y., P. Xie, Y. Opatowsky, and J. Schlessinger. 2010. "Direct Contacts between Extracellular Membrane-Proximal Domains Are Required for VEGF Receptor Activation and Cell Signaling." *Proceedings of the National Academy of Sciences* 107(5): 1906–11. <http://www.pnas.org/cgi/doi/10.1073/pnas.0914052107>.
- Yang, Yan, Peng Xie, Yarden Opatowsky, and Joseph Schlessinger. 2010. "Direct Contacts between Extracellular Membrane-Proximal Domains Are Required for VEGF Receptor Activation and Cell Signaling." *Proceedings of the National Academy of Sciences of the United States of America* 107(5): 1906–11. <http://www.pubmedcentral.nih.gov/articlerender.fcgi?artid=2836632&tool=pmcentrez&render type=abstract> (March 8, 2012).
- Yang, Yan, Satoru Yuzawa, and Joseph Schlessinger. 2008. "Contacts between Membrane Proximal Regions of the PDGF Receptor Ectodomain Are Required for Receptor Activation but Not for Receptor Dimerization." *Proceedings of the National Academy of Sciences of the United States of America* 105(22): 7681–86. <http://www.pubmedcentral.nih.gov/articlerender.fcgi?artid=2409387&tool=pmcentrez&render type=abstract>.
- Yuzawa, Satoru et al. 2007. "Structural Basis for Activation of the Receptor Tyrosine Kinase KIT by Stem Cell Factor." *Cell* 130(2): 323–34. <http://www.ncbi.nlm.nih.gov/pubmed/17662946> (March 24, 2012).
- Zhang, Zhongtao et al. 2000. "Crystal Structure of Human Stem Cell Factor: Implication for Stem Cell Factor Receptor Dimerization and Activation." *Proceedings of the National Academy of Sciences of the United States of America* 97(14): 7732–37. <http://www.pubmedcentral.nih.gov/articlerender.fcgi?artid=16613&tool=pmcentrez&renderty pe=abstract>.
- Zhao, Huaying, Grzegorz Piszczek, and Peter Schuck. 2015. "SEDPHAT - A Platform for Global ITC Analysis and Global Multi-Method Analysis of Molecular Interactions." *Methods* 76: 137–48. <http://dx.doi.org/10.1016/j.ymeth.2014.11.012>.
- Zur, Yuval et al. 2017. "Engineering a Monomeric Variant of Macrophage Colony-Stimulating Factor (M-CSF) That Antagonizes the c-FMS Receptor." *Biochemical Journal* 474(15): 2601–17. <http://biochemj.org/lookup/doi/10.1042/BCJ20170276>.

CHAPTER C

Towards unraveling the mechanism of ligand-mediated TKI resistance in AML

Despite disappointing results upon targeting FLT3-driven AML using tyrosine kinase inhibitors (TKI) as monotherapies and in the absence of any alternative approaches, the current generation of TKI remain central to existing chemotherapy regimens against AML. Considering that FLT3 Ligand (FL) mediates TKI resistance even at steady-state serum concentrations, the observation that chemotherapy increases serum levels of FL several folds is all too often ignored. Poor understanding of the mechanism behind this resistance arguably impedes anticipation and prevents formulation of alternative targeting strategies. We developed a flow cytometry assay of which preliminary data indicate that a constitutive-activated FLT3 oncovariant only reaches the cell surface in the presence of midostaurin, the first TKI approved for treatment of AML. Surface expression consequently exposes this receptor to its activating ligand, which remains potent in internalizing the receptor even in the presence of this TKI. Combining these preliminary results with published observations, allows us to formulate a hypothesis whereby TKIs sensitize AML blasts for FL-stimulation by increasing FLT3 membrane expression levels – providing for the first time a mechanism for the clinically observed ligand-induced TKI resistance. Given the plethora of FLT3-specific TKIs in various (pre)clinical stages and recent development of drugs targeting extracellular FLT3, such insights could be crucial in (re)designing effective therapies.

1. Introduction

Acute myeloid leukemia (AML) is a myeloproliferative disease accounting for approximately 25% of all leukemia's worldwide and predominantly affecting elderly people, aged over 60 (NIH n.d.; Deschler and Lübbert 2006). Approximately one-third of those patients show activating mutations in Fms-like tyrosine kinase receptor 3 (FLT3) at diagnosis, and represent a difficult to treat subgroup (Brunet et al. 2012; Hu et al. 2014; Thiede et al. 2002; Fröhling et al. 2002; Whitman et al. 2001; Yanada et al. 2005; Yamamoto et al. 2001; Deschler and Lübbert 2006; Stone et al. 2017). FLT3 is a single-pass transmembrane receptor belonging to class 3 of receptor tyrosine kinases (RTK-III), together with CSF-1R, KIT, PDGFR α and β (M. A. Lemmon and Schlessinger 2010; Verstraete and Savvides 2012). RTK-III are characterized by the same modular build featuring an extracellular region (ECD) with 5 Ig-like domains, a transmembrane (TM) region, a small juxtamembrane (JM) domain and finally an intracellular split tyrosine kinase domain (TKD). In healthy individuals, FLT3 resides as a monomer at the cell membrane and is maintained in an autoinhibited state by an interaction between the JM region and the activation loop of the TKD (Griffith et al. 2004). Due to its bivalent nature, binding of the activating FLT3 Ligand (FL) on the extracellular region of two receptors, induces receptor-receptor contacts interactions followed by concomitant juxtapositioning of the TKDs (Chapter A – Section 1.2). Subsequent transphosphorylation of residues Tyr589 and Tyr591 induces a repositioning of the JM region, finally allowing the TKD to adopt an active conformation.

Internal tandem duplications (ITD) in the JM region of FLT3 can be found in 20-25% of all AML patients and are associated with a poor prognosis and low overall survival (OS), especially if manifested with a high allelic ratio (Hu et al. 2014; Thiede et al. 2002; Fröhling et al. 2002; Whitman et al. 2001; Stone et al. 2017). An additional 7-10% of all patients harbor point mutations in the TKD, most frequently at position Asp835 (Thiede et al. 2002; Yamamoto et al. 2001; Fröhling et al. 2002; Stone et al. 2017). Mutations at this position are always missense substitutions, mostly a tyrosine (D835Y), although substitutions to valine, histidine, glutamate and asparagine has also been identified (Yamamoto et al. 2001; Forbes et al. 2008). Similar to ITD mutations, these Asp835 mutations result in constitutive phosphorylation of the receptor and are correlated with a poor prognosis, although to a lesser degree than FLT3_{ITD} (Fröhling et al. 2002; Yamamoto et al. 2001; Deschler et al. 2013; Yanada et al. 2005).

Despite the longstanding correlation with FLT3 mutations, AML remained until recently one of the few fields in oncology for which no targeted therapy was available, and the mainstay of treatment has been classic chemotherapy followed by allogeneic hematopoietic stem cell transplantation (allo-HSCT) (Mazzarella 2016; Sheridan 2017). Although allo-HSCT in first remission has been recommended for patients with FLT3_{ITD}-positive AML, a higher relapse rate has been observed compared to FLT3_{ITD}-negative AML patients (Brunet et al. 2012; Hu et al. 2014). The approval of midostaurin (previously referred to as PKC412) as the first tyrosine kinase inhibitor (TKI) for the treatment of FLT3-positive AML, promised to be the tipping point, but the actual benefit appeared to be rather modest. Even though midostaurin reduced the risk of death by 23% compared to classical chemotherapy treatment, patients only experienced an 8.2 months of event-free survival compared to 3.0 months of the control group (Stone et al. 2017). The clinical data seems to imply that Midostaurin

administration is mainly beneficial in sustaining remission, allowing more patients to undergo HSCT (Stone et al. 2017; Sheridan 2017; Levis 2017).

In the previous section, we have shown that the assembly of a ternary complex comprising the extracellular domain of FLT3 and its activating ligand FL, is a multi-step mechanism featuring at least two levels of cooperativity. Extrapolating from these new insights we wondered whether these novel mechanistic insights could affect our understanding of the receptor's behavior at the cell membrane. More specifically, our interest was triggered by two studies that demonstrated a gap in understanding of FLT3 biology and that contradict each other when compared. First, it has been shown that stimulation of FLT3_{ITD}-expressing cells with physiological steady-state concentrations of FL impairs inhibition by various TKIs, and that this effect is worsened by chemotherapy induced increase of serum FL concentrations (Sato et al. 2011b). TKIs arguably cannot prevent ligand-induced dimerization of a membrane-expressed receptor but given our current knowledge, TKI-binding and assembly of a ternary ligand:receptor complex are not expected to be mutual exclusive. The observation that concentrations as low as 3 ng/ml impede TKI-mediated inhibition of FLT3 seems to be indicating differently. If and for how long an inhibited ternary ligand:receptor complex would reside at the membrane is a question that confronts us with the realization that we do not know what triggers FLT3_{WT} receptor internalization in the first place. This is further emphasized by the second unexplained observation that FLT3_{ITD} primarily localizes as an immature glycosylated protein species in the endoplasmic reticulum (ER) of transfected cells, and can be detected in endosomes even in absence of FL (Choudhary et al. 2009; Schmidt-Arras et al. 2005; Reiter et al. 2018). Also mice models have shown that FLT3 surface expression is downregulated in both FLT3^{ITD/+} and FLT3^{ITD/ITD} bone marrow-derived cells which, consequently, renders those cells insensitive to exogenous FL stimulation (Lau et al. 2016). Aside from the question what triggers internalization, combining all of these observations unmasks the following conundrum: **how can the presence of an extracellular activating ligand mediate inhibitor resistance of a predominantly intracellular oncoprotein?**

2. Results

We have previously demonstrated our ability to quantitatively detect FLT3 expression at the membrane of transiently transfected suspension HEK293S cells (Chapter B – Section 1.1), We furthermore showed that concentrations as low as 1 ng/ml FL significantly lowered membrane presentation of the receptor at the 5% confidence level (p-value of 0.032). Building onto these results, we grabbed to opportunity to statistically analyze the effect of the TKI midostaurin on the internalization behavior of FLT3_{D835Y} (Figure 1). Although FLT_{ITD} was originally part of the constructs to be analyzed, it was discarded from the set of constructs to reduce sample handling during optimization of the protocol.

At the outset, it should be emphasized that the following results are preliminary, necessitating that all conclusions should be drawn with this cautionary note in mind. The preliminary nature of these experiments notwithstanding, the statistical analysis does provide grounds to infer some surprising

conclusions at a sufficiently high confidence level to allow inclusion of these findings in this doctoral dissertation.

2.1. FLT3_{D835Y} cannot be detected at the cell surface of transiently transfected cells.

Although occurring with a lower frequency, point mutations at position Asp835 have been associated with a different prognosis compared to FLT3_{ITD}, and have been implied to confer a resistance to type II TKI such as sorafenib and quizartinib (C C Smith et al. 2015; Nguyen et al. 2017) (Chapter A – Section 3.1). The most prevalent substitution at this position is Tyr835, which has been shown to result in a ligand-independent constitutively phosphorylated FLT3 variant (Yamamoto et al. 2001). Given that FLT3_{ITD} has been reported to reside predominantly in the ER as an immaturely glycosylated autophosphorylated protein, we wondered if we could detect impaired membrane expression of FLT3_{D835Y} as well (Figure 1C) (Schmidt-Arras et al. 2005; Choudhary et al. 2009; Reiter et al. 2018). Notably, to allow comparison of FL stimulation and midostaurin treatment within the same population of transfected cells, each population was 2 days post-transfection transferred to 12-well plates allowing differential stimulation and treatment of one population.

As shown previously, the signal for FLT3_{WT} differs at the 5% confidence level (CL) from the mock-transfected background just until stimulation with 12.5 ng/ml FL (12.5 ng/ml FL: p-value of 0.023, 25 ng/ml FL: p-value of 0.089). In contrast, we observe that the signal for membrane detection of FLT3_{D835Y} is throughout the whole range of tested FL concentrations not significantly different from the mock background at the 5% CL (unstimulated: p-value of 0.066). Importantly, this difference compared to the mock background only became insignificant at the 5% CL upon extending the amount of experiments. It might therefore be possible that the observed trend in membrane detection of FLT3_{D835Y} is masked by an increased variance in the mock-transfected background from consecutive experiments. Regardless, membrane expression levels of FLT3_{D835Y} are significantly lower than those of FLT3_{WT} (unstimulated: p-value < 0.001). These data therefore validate the observed retention of FLT3 oncovariants in the ER, and seem to indicate a general principle underlying a lowered membrane expression of constitutively activated FLT3 oncoproteins.

2.2. Midostaurin cannot prevent FL-mediated internalization of FLT3

Upon analyzing if overnight incubation with midostaurin affects FLT3 internalization of transfected HEK cells, we surprisingly observed that the effect of Midostaurin on FL-mediated FLT3_{WT} internalization is rather low (Figure 1D). Among all tested concentrations of FL, 12.5 ng/ml was the only one for which midostaurin appeared to significantly affect ligand-induced FLT3_{WT} internalization at the 5% CL (p-value of 0.0047). Similarly to stimulation in the absence of midostaurin, stimulation with FL at concentrations of 25 ng/ml and higher results in a signal that does not differ from the mock background at the 5% CL (p-value of 0.51). Furthermore, we note that incubation with Midostaurin has no significant effect on the signal from the mock-transfected background at the 5% CL. Notably, it has been shown that the used concentration of 50 nM midostaurin is sufficient to inhibit constitutive phosphorylation of FLT3 oncovariants (Nguyen et al. 2017; Reiter et al. 2018). Although we could test for higher concentrations

of midostaurin, these results indicate that this inhibitor only has a modest effect on ligand-induced receptor internalization.

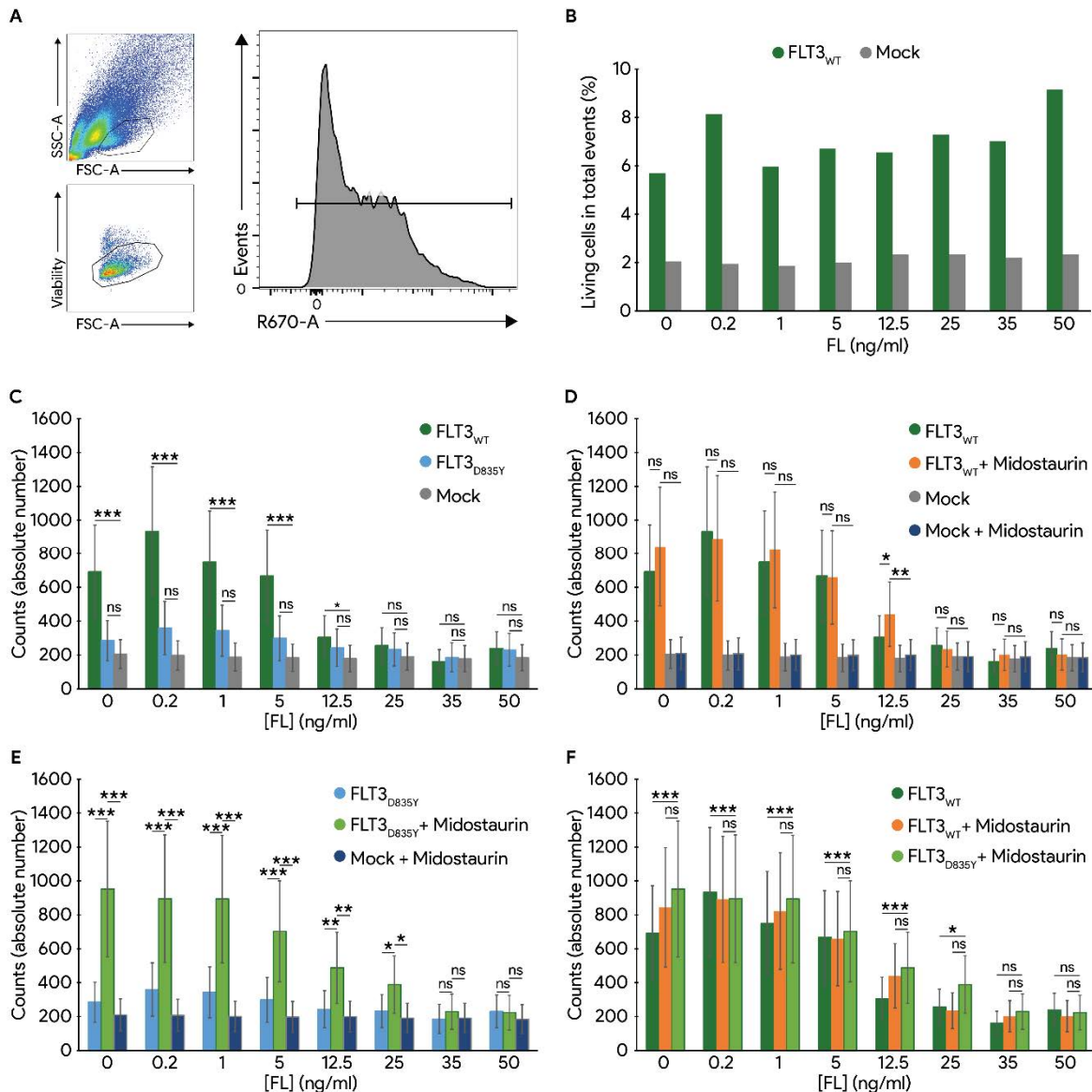


Figure 1. FLT3_{D835Y} presents itself at the membrane only when inhibited, but is nevertheless subject to ligand-induced internalization. **A.** Global gating strategy for flow cytometry analysis of transfected HEK293S cells. Three days post-transfection, cells – either pretreated with midostaurin or not - were stimulated with indicated concentrations of FL and analyzed according to the indicated gates. **B.** Representative experiment indicating that stimulation with FL does not result in a significantly higher cell death, as such selecting for untransfected cells. **C, D, E** and **F** show comparisons of signal for FLT3 at the membrane with or without prior incubation with midostaurin of FLT3_{WT} (resp. dark green and orange), FLT3_{D835Y} (resp. light blue and light green) and mock (resp. gray and dark blue) transfected cells, in function of FL concentration. All data points are HGLMM predicted means. Error bars indicate mean ± SEM. Two-sided t-test: * P < 0.05; ** P < 0.01; *** P < 0.001; ns, not significant.

2.3. Inhibition of FLT3_{D835Y} restores its membrane expression levels equal to FLT3_{WT}

The absence of a clear effect of midostaurin on membrane expression levels and ligand-induced internalization of FLT3 are in clear contrast to the effect of midostaurin on FLT3_{D835Y} (Figure 1E). Where

membrane expression levels of FLT3_{D835Y} did not differ from the mock-transfected background at the 5% CL, we now observe that treatment with midostaurin elevates membrane expression of this oncoprotein to a level well above that of both the background and the untreated condition (p-values < 0.001). Despite presumably inhibited, FLT3_{D835Y} does remain responsive to FL stimulation. Indeed, we observe that the FLT3 membrane expression levels remain significantly higher than the mock background until 35 ng/ml FL (25 ng/ml: p-value of 0.014, 35 ng/ml: p-value of 0.56). Thus it seems that FLT3_{D835Y} is more resistant to FL-mediated internalization than FLT3_{WT} (Figure 1D), although their respective expression levels do not significantly differ at that given FL concentration (p-value 0.67) (Figure 1F).

Together, these preliminary data show that treatment with midostaurin restores membrane expression of FLT3_{D835Y} to a level that is not statistically different at the 5% CL compared to its wild-type counterpart. Its inhibited state notwithstanding, we surprisingly observe that FLT3_{D835Y} is responsive to stimulation with its activating ligand in presence of midostaurin, adopting an internalization behavior similar to FLT3_{WT} transfected cells, regardless pretreatment of the latter.

3. Discussion

Given its longstanding correlation with development and prognosis of AML (Kiyoi et al. 1998b), FLT3 has been the subject of targeted therapies for almost two decades. With the notable exception of IMC-EB10, an anti-FLT3 monoclonal antibody that failed to demonstrate efficacy in a phase 1 clinical study (Yousoufian et al. 2010), FLT3 targeting in a clinical setting has exclusively focused on testing of tyrosine kinase inhibitors. The only transient effect of these agents when used as monotherapy has motivated the incorporation of TKIs into existing chemotherapy regimens, despite the risk of evoking FL-mediated resistance by doing so (Sato et al. 2011b). Indeed, it has been well established that aplasia-inducing radiation and chemotherapy significantly increase FL levels (Wodnar-Filipowicz et al. 1996; Bojko et al. 2002; B. S. D. Lyman et al. 1995), which is exemplified by a 1000-fold increase to more than 3 ng/ml in FL serum levels observed in patients receiving successive courses of chemotherapy (Sato et al. 2011b). The observation that even 1 ng/ml serum concentrations of FL impair the phosphorylation-suppressing effect of the most promising TKIs (Sato et al. 2011b), including midostaurin, should therefore forewarn to include such inhibitors in existing chemotherapy regimens. The apparent inertia of the pharma industry to redefine clinical studies (e.g. recruiting clinical studies NCT02668653, NCT02298166) and the observation that hardly any of the publications in past years describing the development and characterization of novel FLT3 inhibitors address this issue, highlight the field's inadvertence of this poorly-understood phenomenon. Consequently, the presence of chemotherapy-induced TKI resistance has been suggested to be at the root of failure of clinical studies with two TKIs, sorafenib and lestaurtinib (Levis et al. 2011; Knapper et al. 2017; Serve et al. 2013).

With these experiments, we decided to tackle the puzzling FL-mediated TKI resistance and the poorly-understood observation that constitutively activated FLT3 oncovariants predominantly reside intracellularly. We realized that both observations can be unified into a single hypothesis based on two assumptions.

The first consideration is that assembly of a ternary FL:FLT3 complex at the membrane induces a strong tendency for transphosphorylation of the kinase domains. Ligand-induced dimerization of TKDs have indeed been observed for KIT and implied for FLT3, and arguably juxtaposition the kinase domains ideally for initial transphosphorylation (Opatowsky et al. 2014b). Given that the ligand-induced receptor interactions lead to transphosphorylation of the intracellular kinase domains, it is indeed unlikely that a small molecule inhibitor can interfere with this highly cooperative dimerization cascade when it has already reached the level of the cell membrane. Although there is no experimental evidence showing that assembly of a ternary complex is mutually exclusive to binding of TKIs, such assumption does provide a feasible explanation for the observed FL-mediated TKI resistance.

Secondly, we infer that receptor internalization is a natural consequence of receptor phosphorylation. The canonical internalization model of RTKs indeed starts with ligand-induced phosphorylation, providing docking sites for ubiquitinating adaptor molecules (reviewed by (Goh and Sorkin 2013)). It has been shown for KIT and CSF-1R that ligand binding quickly results in phosphorylation of c-Cbl, followed by the ubiquitination and degradation of these receptors (Zeng et al. 2004; P. S. W. Lee et al. 1999). Ubiquitination is generally considered to mark the start of an internalization event, which has shown to be true for CSF-1R (P. S. W. Lee et al. 1999). To our knowledge, no direct data on the internalization biology of FLT3 is available. However, c-Cbl has been shown to physically interact with FLT3, to be phosphorylated in the presence of FLT3 Ligand, and to modulate FLT3 ubiquitination and internalization (Sargin et al. 2007). The DDxpY recognition site for the phosphotyrosine-binding domain of c-Cbl is furthermore present in the juxtamembrane region of FLT3 (residues 587 to 590) (Lupher et al. 1997). It therefore seems likely that ligand-binding of FLT3 induces transphosphorylation of the TKDs, followed by recruitment and phosphorylation of c-Cbl and finally resulting in ubiquitination, endocytosis and degradation of the ligand:receptor complex.

In this chapter, we described our initial results based on flow cytometry experiments that now collectively suggest the following:

1. Presence of a TKI only has a mediocre effect on ligand-induced receptor internalization.
 2. A constitutively active FLT3 variant, FLT3_{D835Y}, only presents itself at the membrane when inhibited and
 3. FLT3_{D835Y} responds to ligand-induced internalization, the inhibited state notwithstanding.
- Building upon the two presumptions that ligand-mediated receptor dimerization outcompetes inhibition by TKIs on the one hand, and that receptor internalization is a consequence of receptor activation, we propose a hypothesis on how the presence of extracellular FL can mediate TKI resistance when the inhibited oncoprotein resides predominantly intracellular ([Figure 2](#)).

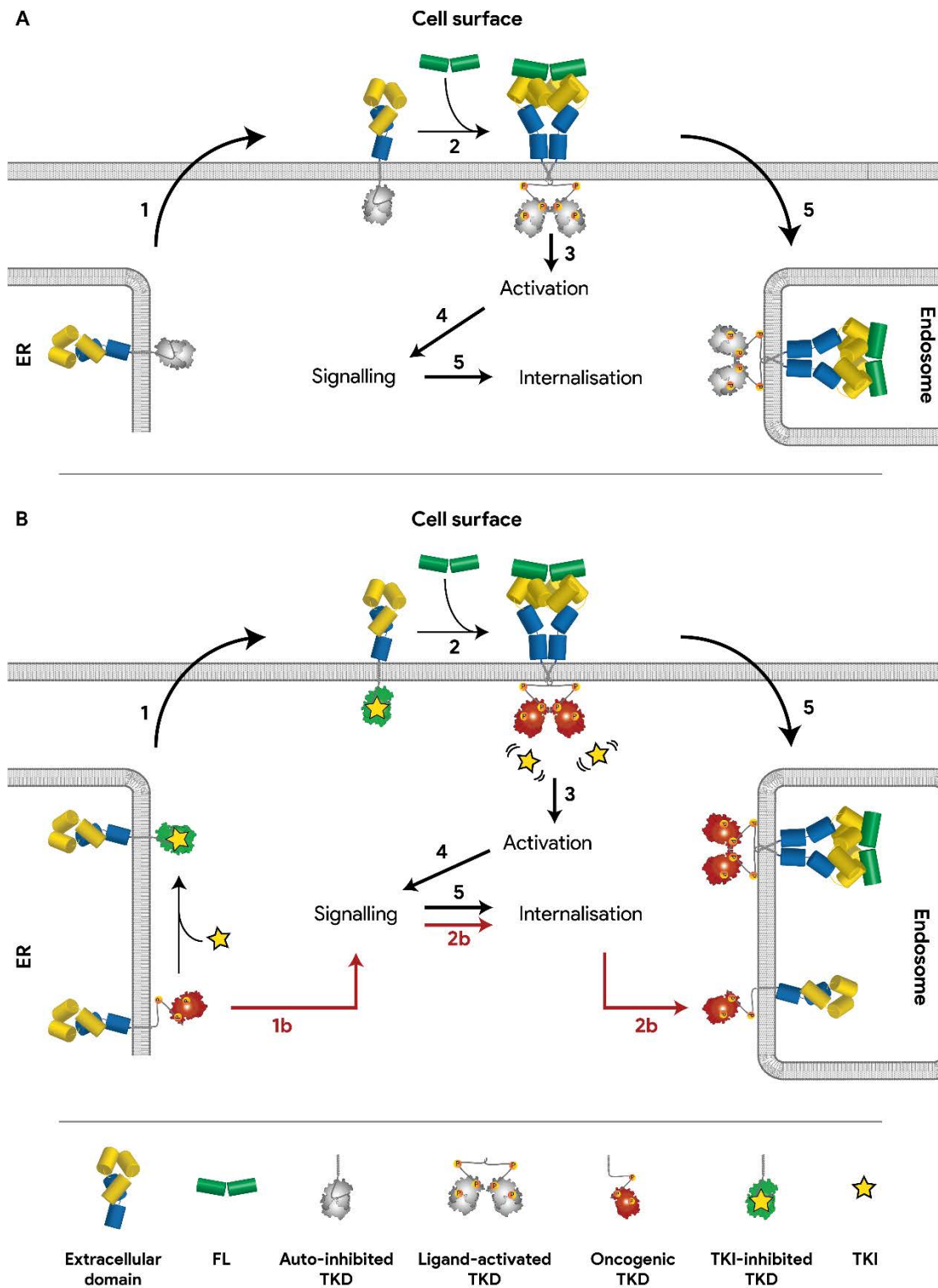


Figure 2. Postulated paradigm explaining FL-induced TKI resistance. **A.** After co-translational translocation, wild-type FLT3 is translocated over the Golgi apparatus to the cell membrane (Step 1). In presence of extracellular FL, a ternary complex is assembled (step 2) resulting in the transphosphorylation of the kinase domains (step 3). This event marks the start of the signalling cascade (step 4) and initiates the internalization process (step 5), followed by degradation. **B.** An oncogenic receptor shortcuts the membrane translocation (red arrows). Constitutive signalling as a consequence of a constitutive activation (Step 1b) results in internalization (step 2b) before the receptor has reached the membrane. Presence of a TKI inhibits constitutive activation and restores normal cellular trafficking of the receptor (black arrows), allowing for ligand-dependent activation.

We postulate that a constitutive activation of the TKD not only results in a constitutive signalling, but also broadcasts a constitutive internalization signal. As such, these oncogenic receptor variants are collected into endosomes before having ever reached the cell membrane. Consequently, inhibition of the autophosphorylation by TKIs will gag the internalization signal and allow translocation of the receptor to the membrane, exposing them to ligand-mediated activation.

This hypothesis is supported by our preliminary data, and provides rationale for observations made elsewhere (Schmidt-Arras et al. 2005; Choudhary et al. 2009; Sato et al. 2011a; Reiter et al. 2018; Jetani et al. 2018). Indeed, the initial evidence that constitutively activated FLT3_{ITD} remained primarily entrapped in the ER as an immature glycosylated protein, has during the course of these experiments been extended to various oncogenic FLT3 variants (Choudhary et al. 2009; Reiter et al. 2018). Most notably, Reiter and colleagues showed that incubation with quizartinib, midostaurin or sorafenib steadily increased FLT3 surface expression of transfected Ba/F3 and U2OS cells in a 24h time frame. Importantly, they were able to confirm this quizartinib-mediated effect on FLT3 membrane expression levels in FLT3-mutated AML cell lines, as well as in patient-derived xenograft cells.

The results of Reiter and colleagues therefore further solidify our proposed paradigm of ligand-induced TKI resistance. First, they confirm that ER retention is indeed a general principle shared by all constitutively activated FLT3 oncovariants. Secondly, the observation that TKI treatment restores glycan maturation simultaneously to membrane expression, implies that mutant receptors are only allowed to follow a wild-type intracellular trajectory if their kinase activity is inhibited. Thirdly, they do not observe an effect of TKI treatment on FLT3 membrane expression levels if the cell line confers two wild-type *FLT3* alleles, a finding that directly confirms our observation. Finally, treatment with TKIs of cell lines heterogeneous for FLT3 mutations only show a moderate effect on FLT3 membrane expression, compared to cells lines with two mutant *FLT3* alleles. This observation implies that FLT3_{WT} translocation is unaffected by the ER retention of an FLT3-mutated variant. In such situation, baseline levels of FLT3 membrane expression are indeed expected to be higher in a FLT3^{WT/ITD} context compared to an FLT3^{ITD/ITD} cytogenetic context. Consequently, the effect of TKI-induced membrane expression can only affect the ER-retained copy, thus resulting in a lower effect of this treatment on total FLT3-membrane expression levels compared to an FLT3^{ITD/ITD} cytogenetic context. As the authors did not compare baseline levels of heterogeneous FLT3-mutated cells to those with a homogeneous FLT3-mutated cytogenetics, this issue remained unaddressed.

Unfortunately, the authors overlooked the observation of FL-mediated TKI-resistance, observed by Sato and colleagues (Sato et al. 2011b). Consequently, they did not evaluate whether this TKI-mediated increase in FLT3 membrane expression rendered cells more responsive to stimulation with FL in terms of phosphorylation signal, internalization signal or proliferation rate. We hypothesize that similarly to its wild-type counterpart, membrane-translocated FLT3 will still be able to bind its ligand despite its inhibited state (Figure 2B). Considering that the cooperative character of ligand-mediated activation successfully outcompetes inhibition by TKIs, this event is followed by receptor activation, signalling, and internalization. Consistent with this notion, our data show that incubation with midostaurin only has a mediocre effect on FL-mediated receptor internalization, and FL-mediated TKI resistance is indeed a well described phenomenon (Sato et al. 2011b).

Despite the excellent quality in documenting the ER-retention and TKI-mediated membrane translocation of FLT3 oncovariants, none of the studies provide a possible mechanism explaining these observations. Likewise, the mechanism underlying FL-mediated TKI resistance still remains poorly understood to date. Our proposed mechanism attempts to unify all of these observations into one paradigm, yet it is only supported by preliminary data and therefore requires additional experiments (Section 4). Nevertheless, if our hypothesis can be experimentally validated, we envision that its implication for the field will be large. If treatment with TKI indeed increases membrane presentation of inhibited oncogenic FLT3 variants without preventing ligand-dependent receptor activation, it dramatically renders AML blasts more responsive to an FL-mediated survival and proliferation signal. Given that chemotherapy is known to increase serum levels of FL, incorporation of these TKI to such regimen would result in an overstimulation of precisely the pathogenic cell type that is being targeted. This would explain what has been noted elsewhere, namely, that the allelic ratio for FLT3_{ITD} over FLT3_{WT} is almost inevitably increased upon relapse, indicating that between treatment and relapse, an oncogenic cell population is being selected for that is more addicted to FLT3 signaling than at diagnosis (L. Y. Shih et al. 2002; Kottaridis et al. 2002; Y. Nakano et al. 1999; Levis 2011a; Reiter et al. 2018). Keeping in mind the observation that successive courses of chemotherapy almost exponentially increase FL serum levels, our proposed mechanism finally provides the rationale for the general notion that TKIs seem to perform better in newly-diagnosed patients compared to patients in relapse.

Besides providing an alarming view on current FLT3-targeting treatment strategies, our hypothesis simultaneously delivers novel opportunities to exploit inhibitor-mediated membrane translocation of oncogenic FLT3. As almost all promising FLT3-targeting TKIs succeed in clearance of peripheral blasts and, in combination with chemotherapy, can result in a complete remission, the effect of TKI could arguably be extended if ligand-induced receptor activation would be prevented. This can be accomplished using a recently developed small molecule targeting the FL:FLT3 binding epitope (Rivat et al. 2018), or by administration of the monoclonal antibody IMC-EB10, for which preclinical testing has already been completed. Conversely, drugs targeting the extracellular region of FLT3 would arguably benefit from co-administration with TKIs, an effect demonstrated by Reiter and colleagues (Reiter et al. 2018). If the mediator of constitutive proliferation in FLT3-dependent blasts indeed resides predominantly intracellular due to a constitutive internalization signal, the presence of TKIs would indeed unearth the receptor and expose the blasts to these drugs. This is especially relevant given the Fc-optimized variant of IMC-EB10 that is under development by Synimmune and the recent efforts by both Amgen and Pfizer to generate a bispecific FLT3-CD3 antibody, highlighting the interest from the industry to explore such path (Synimmune n.d.; Djuretic et al., n.d.; Goldstein et al. 2017; Raum et al. 2017).

In conclusion, our preliminary data indicate that a constitutively-activated FLT3 variant operates mainly from inside the cell and is translocated to the cell membrane upon inhibition with midostaurin. As midostaurin seems to be largely ineffective in preventing ligand-induced receptor activation, such translocation primes the cells for stimulation with FL. This scenario is especially alarming in the context of co-administered chemotherapy, known to increase FL serum levels with several orders of magnitude. Upon validation, our hypothesis for multiple TKIs and oncogenic FLT3 variants will provide

a rationale for the clinically observed FL-mediated TKI resistance, and will enable possible solutions to prevent such resistance and augment the effect of antibody-based FLT3-targeting drugs.

4. Outlook

In this section, we presented preliminary data on membrane presentation of wild-type FLT3 and an oncogenic variant thereof, FLT3_{D835Y}. We show that treatment with midostaurin, the first TKI approved for the treatment of FLT3-mutated AML, pushes membrane presentation of FLT3_{D835Y} to wild-type levels, but has a very limited effect on ligand-induced receptor internalization. Integrating these results into existing observations in the field, motivated us to propose a novel mechanism underlying FL-mediated TKI-resistance. Although our hypothesis brings together all observations into a conceptually straightforward mechanism, further work is advised to fortify the proposed paradigm.

The dataset used for this analysis included 8 and 6 biological replicates for membrane detection of FLT3_{WT} and mock-transfected cells respectively, separated over 4 experiments, and 6 biological replicates for FLT3_{D835Y} spread over 3 experiments. The protocol to determine this membrane expression had to be extensively optimized, and minor optimization was continued in between consecutive experiments. These differences between protocols arguably increased variation between the different samples, resulting in a high standard error of predictions. Although HGLMM analysis attributed a significant portion of the observed variance to the random model, and although the provided dataset was sufficiently large to perform a statistical analysis, more replicates should be generated using identical protocols.

Furthermore, as the antibody used for membrane detection of FLT3 has reported to inhibit binding of FL to FLT3, the possibility exists that pre-treatment with FL blocks binding of the antibody, a result erroneously interpreted as the loss of the antibody-binding epitope as a consequence of receptor internalization. Although no data is available on FLT3 internalization, it has been shown that approximately 80% of ¹²⁵I-labeled FL is internalized within 5 minutes, and that internalization reaches its maximum after 15 minutes (Turner et al. 1996). The time scale of this internalization is in line with internalization kinetics of ¹²⁵I-labeled SCF and CSF-1-induced CSF-1R internalization (Chihara et al. 2010; Yee et al. 1994). Given that FLT3-transfected HEK cells were stimulated for at least 15 minutes before centrifugation, it therefore seems likely that in absence of an TKI, no FL-bound FLT3 is present at the membrane. Therefore, the AB would not be hindered by any competition for the ligand. It is however possible that an FL-bound FLT3 complex remains at the cell membrane in presence of a TKI. In such situation, the competition between FL and the AB would become a serious issue.

Therefore, future experiments should be performed with a novel FLT3 construct featuring an N-terminal V5- or Flag-tag, for which appropriate antibody to detect this construct at the cell membrane are available. To be able to perform the same type of experiments on AML cell lines that naturally express FLT3 and mutants thereof, a non-competitive fluorescently labeled nanobody could be used, validated using the above proposed construct. Such nanobody, although not fluorescently labeled, is already available in our lab.

One of the main assumptions underlying our proposed paradigm, is that internalization is a strict consequence of TKD phosphorylation. Although this is a generalized mechanism for all RTK (Goh and Sorkin 2013), no hard evidence exists for FLT3 internalization biology other than the correlation with c-Cbl (Sargin et al. 2007). Knowing the phosphorylation status of each FLT3 variant for each concentration of FL, is therefore a strict prerequisite to gain confidence in the current hypothesis. Especially the inverse relationship between inhibition by midostaurin on the one hand, and FL-mediated internalization on the other, should be validated by analysis of the phosphorylation states. In addition, although the constitutive nature of FLT3_{D835Y} has been established across various papers, it remains important to validate the construct in our hands.

Notably, substantial efforts have been made to detect phosphorylation of FLT3, ERK1/2 and STAT5 using flow cytometry. When combined with membrane detection of FLT3, such approach would deliver all requested parameters for a given concentration of FL +/- pretreatment in a single run. However, despite extensive optimization of the protocols, we failed to detect a ligand-specific phosphorylation signal. As we observed that ERK1/2 and STAT5 phosphorylation status in transfected cells was consistently higher than the mock-transfected background, we suspect that an increased baseline level of receptor activation due to crowding at the membrane, might have compromised the sensitivity of the assay. In that regard, an expression-inducible cell line might allow for determination of an ideal window in which FLT3 expression is balanced to deliver the required sensitivity on the one hand, but refrains from increasing background phosphorylation levels on the other. Simultaneously, we can test for other anti-phosphoprotein antibodies and perform Western blot analysis.

To further validate the supposition of phosphorylation-induced internalization, we planned to generate a kinase-dead variant of FLT3 by mutating the catalytic Lys644 to methionine or alanine (FLT3_{K644M} and FLT3_{K644A} respectively). Such receptor variant would allow differentiation between complexation-driven and phosphorylation-driven FLT3 internalization. Furthermore, if our current hypothesis holds true, inclusion of the kinase-dead mutation into the construct featuring Tyr835 would restore membrane expression levels of oncogenic FLT3 variants in absence of a TKI, an observation already made for FLT3_{ITD} (Schmidt-Arras et al. 2005). One construct of such variant, FLT3_{K644M-D835Y}, has been generated and tested once, but no membrane presentation of FLT3 could be detected.

Finally, we sought to validate the internalization event orthogonally via fluorescence and total inner reflection fluorescence microscopy, allowing us to detect in real time FLT3 internalization and TKI-mediated membrane translocation of FLT3_{D835Y}. Furthermore, Förster resonance energy transfer by fluorescence lifetime imaging (FRET-FLIM) and single-particle tracking analysis would have allowed us to study dimerization at the cell surface. Given that some of these experiments have been in the pipeline for more than 3 years, substantial effort has been put into this using FLT3_{WT}, but we kept being confronted with unpredictable expression levels, suboptimal cellular localization or unexpected (i.e. absence of) internalization behavior. We suspect the presence of co-translationally-fused fluorescent protein is at the root of these issues, either influencing translation and membrane translocation, and/or affecting ligand-binding and internalization. Indeed, recent studies describing time-resolved FRET on FLT3 utilized a specialized antibody for detection, rather than a translationally linked fluorescent protein (Rivat et al. 2018).

Furthermore, to consolidate the data into a general mechanism, it should be tested if similar observations can be made for other constitutively activated FLT3 variants and other additional TKIs. Experiments by Reiter and colleagues could show that ER retention TKI-induced membrane translocation is a shared concept for all constitutively activated FLT3 variants (Reiter et al. 2018). How these variants respond to FL stimulation in a TKI-treated setting, is however yet to be seen. Other than supporting a generalized paradigm, performing experiments with other, more FLT3-specific TKIs would provide confidence that the effect of treatment indeed originates to silencing the constitutive internalization signal, rather than from off-target effects influencing membrane translocation of these mutants. Co-transfection of FLT3_{WT} and mutated FLT3 variants could furthermore deliver insights on the relation between the allelic burden and ligand-mediated TKI resistance.

Bringing agents into these internalization and proliferation experiments that prevent binding of FL to FLT3, would allow us to orthogonally confirm that FL-mediated TKI resistance is indeed dependent on FLT3 signaling. Simultaneously, such findings would readily provide a solution to resistance, which is expected to affect all TKIs due to their intrinsic FLT3-inhibiting activity. In that regard, we have a small-molecule and FLT3-binding nanobody library in our lab, although both have not been tested yet for neutralizing capacity. Alternatively, the CDR regions of IMC-EB10 and IMC-NC7, two neutralizing antibodies shown to prevent FL-mediated FLT3 activation, have already been cloned in suitable Fab expression vectors. IMC-EB10_{Fab} can be purified and binds FLT3, although with a lower affinity than reported ($K_D = 141$ nM versus $K_D = 158$ pM) (Piloto et al. 2005, Youssoufian et al. 2010, patent US8,071,099 and unpublished data). Furthermore, a crystal structure of this Fab is available (unpublished data). A test expression and purification of IMC-NC7_{Fab} has been performed once, however unsuccessfully. In contrast to IMC-EB10, IMC-NC7 has been shown to inhibit FLT3 activation up to a concentration of 80 ng/ml of FL, despite its lower affinity ($K_D = 450$ pM) (Piloto et al. 2005; Youssoufian et al. 2010, patent US8,071,099). It might therefore be worthwhile to test expression of this Fab a second time, both in adherent cells as well as in suspension adapted cell lines. Furthermore, as the FLT3 x CD3 antibody patent of Amgen provides CDR sequences for 6 FLT3_{D3}-binding antibodies, more Fabs can be generated and tested (patents WO/2017/021362). Although untested for any neutralizing capacity, these antibodies have shown to be resistant to 10 µg/ml FL and are, in contrast to IMC-EB10 and –NC7, expected to bind FLT3 with an unaltered affinity in the context of a Fab-fragment.

Finally, the implications of these observations in HEK cells should be broadened by validation in mice and in AML cell lines. Mice models have shown that an impaired FLT3 membrane expression and eminent irresponsiveness for exogenous FL stimulation, prevented *FLT3^{ITD/ITD}* bone-marrow derived cells to be differentiated into cDCs and pDCs (Lau et al. 2016). We could therefore test if FLT3 membrane expression in *FLT3^{ITD/ITD}* bone-marrow derived cells can indeed be restored to wild-type levels when administering a TKI *in vivo*, or by adding it to the growth media *ex vivo*. Additionally, it could be tested if *FLT3^{ITD/ITD}* bone-marrow derived cells would, in presence of a TKI, again respond to exogenous FL stimulation by generating all 3 DC subtypes.

It has previously been shown that quizartinib-induced membrane expression of oncogenic FLT3 variants is inversely correlated to proliferation rates of MOLM-13, the MV4-11 and the MM6 (Reiter et

al. 2018). How addition of FL would affect these proliferation rates in the presence of quizartinib and other TKIs, is now a very intriguing question. If these results confirm our proposed paradigm and hypothesis, final validation should be sought in comparing the effect of TKIs on FLT3 membrane expression levels and proliferation rates of primary FLT3-mutated AML blasts, FLT3_{WT} AML blasts and samples from healthy donors. Although we acknowledge that material from these resources is limited, and provided that our hypothesis can be validated in AML cell lines and primary material, we do envision that the results of this research will have an immediate impact on the treatment of AML patients.

5. Experimental procedures

Production of recombinant FLT3 ligands in *E. coli*

The pET15b_rhFL plasmid was obtained from Verstraete et al., 2009. Expression constructs for FL_{L27D} was generated using overlap extension PCR (Heckman and Pease 2007) allowing the PCR for generation of AD fragments to first run 10 cycles without primers. Recombinant FL_{WT} and FL_{L27D} were produced according to published methods (Verstraete et al. 2009). Briefly, both proteins were expressed by a Rosetta-gami(DE3) bacterial strain (Novagen) as inclusion bodies. Harvested cell pellets were resuspended in lysis buffer (50 mM Tris pH 8.0, 100 mM NaCl, 1% Triton X-100 and 1 mM EDTA) and lysed by sonication. Inclusion bodies were isolated, washed and solubilized in guanidine buffer (6 M guanidine hydrochloride, 100 mM NaH₂PO₄, 10 mM Tris, 10 mM 2-ME, pH 8.0) by gentle stirring at 40°C, after which the protocol of Verstraete and colleagues was followed to the letter. Endotoxins were removed by washing the nickel-immobilized refolded FLT3 ligands with 5 column volumes of 0.1% ampicin (Sigma) in phosphate buffer, prior to elution.

Expression constructs.

cDNA sequences coding for FLT3_{FL} residues Met1 to Ser993 was obtained from Verstraete et al., 2011. Constructs for transient mammalian expression of FLT3 carrying a C-terminal thrombin-cleavable AviTag, followed by a hexahistidine sequence, were generated in the pHLsec vector (Aricescu, Lu, and Jones 2006). Expression constructs for FLT3_{D835Y} was generated using overlap extension PCR (Heckman and Pease 2007) allowing the PCR for generation of AD fragments to first run 10 cycles without primers.

FL-mediated FLT3 internalization assay.

Suspension-adapted HEK293 S cells were seeded, grown and transfected according to proprietary protocols (Nico Callewaert Lab, VIB - UGent Center for Medical Biotechnology). Forty-eight hours post transfection, 24 well plates (24-well suspension plate TC, Sarstedt) were seeded with 500 µl of each cell culture. Where indicated, midostaurin (PKC-412 - Midostaurin hydrate, Sigma Aldrich) was added to the wells. Plates were overnight incubated in orbital shaker at 37 °C, 8% CO₂. Next day, cells were stimulated with indicated FL concentrations. After 15 minutes incubation, cells were harvested, washed and stained for 20 min at 4°C in the dark with APC rat anti-mouse CD135 (A2F10.1; BD Pharmingen; used 1/100). To be able to remove dead cells from our analysis, we used Fixable Viability Dye eFluor506 (eBioscience; used 1/200). The stained samples were acquired on an LSR Fortessa cytometer (BD Biosciences), analysis and graphical output were performed using FlowJo software (Tree

Star, Inc.). Living cells were selected from the non-debris as eFluor506-negative cells, and 10k events in this gate was used as a stopping gate.

Median APC signal from living cells was used to quantify FLT3 membrane detection. The following data was collected into a single dataset:

- 3 experiments with 2 biological replicates each for FLT3_{WT}. In one experiment, treatment with midostaurin was not tested. The two other experiments had conditions with and without midostaurin treatment
- 2 experiments with 2 biological replicates each for FLT3_{D835Y}. Each of those experiments had conditions with and without midostaurin treatment
- 3 experiments with 2 biological replicates each for mock transfected cells. In one experiment, treatment with midostaurin was not tested. The two other experiments had conditions with and without midostaurin treatment

A Hierarchical Generalized Linear Mixed Model (HGLMM) as implemented in Genstat v19 (Baird, Murray, Payne, & Soutar, 2017) was fitted to the data. The linear predictor vector of the median R670 counts can be written as follows: $\eta = \mathbf{X}\beta + \mathbf{Z}\mathbf{v}$, where η represents the link function, the matrix \mathbf{X} is the design matrix for the fixed terms RECEPTOR, CONCENTRATION and INHIBITOR and their interaction, β is their vector of regression coefficients, \mathbf{Z} is the design matrix for the random replicate terms with technical replicates nested into the biological replicates, and \mathbf{v} is the corresponding vector of random replicate effects. A Poisson distribution with log link was considered for the fixed terms, and a gamma distribution with log link for the random effects. Inspection of residual plots revealed no departures from normality or homogeneity of variance. T statistics were used to assess the significance of the fixed main and interaction effects estimated as differences to the reference level. Estimated mean values were obtained as predictions from the HGLMM, formed on the scale of the response variable and under the assumption of Normal distribution of residuals at the 1% confidence level. Receptor identity, concentration and inhibitor presence were chosen as explanatory factors for the median R670 signal. Technical replicates were considered nested into the biological ones, and together added to the model as random terms. Added random terms assumed to be following a Normal distribution. The means and standard errors of the mean R670 signal were predicted for each concentration and the t-value for each estimated parameter in the mean HGLM model was converted to a probability, allowing to estimate the significance of the effect on the response variate upon changing explanatory factors, for a given reference condition.

6. Author contributions

All experiments were performed by Erwin Pannecoucke with experimental and intellectual input from Kim Deswarte and Steven De Munck for the flow cytometry studies, and from Marnik Vuylsteke for the statistical analysis.

7. References

- Aricescu, A Radu, Weixian Lu, and E Yvonne Jones. 2006. "A Time- and Cost-Efficient System for High-Level Protein Production in Mammalian Cells." *Acta crystallographica. Section D, Biological crystallography* 62(Pt 10): 1243–50. <http://www.ncbi.nlm.nih.gov/pubmed/17001101> (July 18, 2012).
- Bojko, P. et al. 2002. "Flt3 Ligand and Thrombopoietin Serum Levels during Peripheral Blood Stem Cell Mobilization with Chemotherapy and Recombinant Human Glycosylated Granulocyte Colony-Stimulating Factor (Rhu-G-CSF, Lenograstim) and after High-Dose Chemotherapy." *Annals of Hematology* 81(9): 522–28.
- Brunet, Salut et al. 2012. "Impact of FLT3 Internal Tandem Duplication on the Outcome of Related and Unrelated Hematopoietic Transplantation for Adult Acute Myeloid Leukemia in First Remission: A Retrospective Analysis." *Journal of Clinical Oncology* 30(7): 735–41.
- Chihara, T et al. 2010. "IL-34 and M-CSF Share the Receptor Fms but Are Not Identical in Biological Activity and Signal Activation." *Cell Death and Differentiation* 17(12): 1917–27. <http://www.ncbi.nlm.nih.gov/pubmed/20489731>.
- Choudhary, Chunaram et al. 2009. "Mislocalized Activation of Oncogenic RTKs Switches Downstream Signaling Outcomes." *Molecular Cell* 36(2): 326–39.
- Deschler, Barbara et al. 2013. "Parameters Detected by Geriatric and Quality of Life Assessment in 195 Older Patients with Myelodysplastic Syndromes and Acute Myeloid Leukemia Are Highly Predictive for Outcome." *Haematologica*.
- Deschler, Barbara, and Michael Lübbert. 2006. "Acute Myeloid Leukemia: Epidemiology and Etiology." *Cancer* 107(9): 2099–2107.
- Djuretic, Ivana et al. "Poster Abstract: A Novel Full Length Anti-FLT3 CD3 Bispecific Antibody for the Treatment of Acute Myeloid Leukemia." *ASH Annual Meeting*: Abstract 1445 Session 616.
- Forbes, S A et al. 2008. "The Catalogue of Somatic Mutations in Cancer (COSMIC)." eds. Jonathan L Haines et al. *Current protocols in human genetics editorial board Jonathan L Haines et al* Chapter 10(March): Unit 10.11. <http://www.pubmedcentral.nih.gov/articlerender.fcgi?artid=2705836&tool=pmcentrez&render type=abstract>.
- Fröhling, Stefan et al. 2002. "Prognostic Significance of Activating FLT3 Mutations in Younger Adults (16 to 60 Years) with Acute Myeloid Leukemia and Normal Cytogenetics: A Study of the AML Study Group Ulm." *Blood* 100(13): 4372–80.
- Goh, Lai Kuan, and Alexander Sorokin. 2013. "Endocytosis of Receptor Tyrosine Kinases." *Cold Spring Harb Perspect Biol* (5): a017459.
- Goldstein, Rebecca et al. 2017. "Abstract: Evaluation of a FLT3 Bite for Acute Myeloid Leukemia." *Blood* 130(Suppl 1): 1354.
- Griffith, James et al. 2004. "The Structural Basis for Autoinhibition of FLT3 by the Juxtamembrane Domain." *Molecular Cell* 13(2): 169–78.
- Heckman, Karin L, and Larry R Pease. 2007. "Gene Splicing and Mutagenesis by PCR-Driven Overlap Extension." *Nature protocols* 2(4): 924–32. <http://www.ncbi.nlm.nih.gov/pubmed/17446874> (August 20, 2013).

- Hu, Bei, Praveen Vikas, Mohamad Mohty, and Bipin N. Savani. 2014. "Allogeneic Stem Cell Transplantation and Targeted Therapy for FLT3/ITD+ Acute Myeloid Leukemia: An Update." *Expert Review of Hematology* 7(2): 301–15. <http://www.expert-reviews.com/loi/ehm?cookieSet=1%5Cnhttp://ovidsp.ovid.com/ovidweb.cgi?T=JS&PAGE=reference&D=emed11&NEWS=N&AN=2014189787>.
- Jetani, Hardikkumar et al. 2018. "CAR T-Cells Targeting FLT3 Have Potent Activity against FLT3-ITD+AML and Act Synergistically with the FLT3-Inhibitor Crenolanib." *Leukemia* 32(5): 1168–79. <http://dx.doi.org/10.1038/s41375-018-0009-0>.
- Kiyoi, H et al. 1998. "Internal Tandem Duplication of the FLT3 Gene Is a Novel Modality of Elongation Mutation Which Causes Constitutive Activation of the Product." *Leukemia : official journal of the Leukemia Society of America, Leukemia Research Fund, U.K* 12(9): 1333–37.
- Knapper, Steven et al. 2017. "A Randomized Assessment of Adding the Kinase Inhibitor Lestaurtinib to First-Line Chemotherapy for FLT3-Mutated AML." *Blood* 129(9): 1143–54.
- Kottaridis, Panagiotis D. et al. 2002. "Studies of FLT3 Mutations in Paired Presentation and Relapse Samples from Patients with Acute Myeloid Leukemia: Implications for the Role of FLT3 Mutations in Leukemogenesis, Minimal Residual Disease Detection, and Possible Therapy with FLT3 Inhibitors." *Blood* 100(7): 2393–98.
- Lau, Colleen M. et al. 2016. "Leukemia-Associated Activating Mutation of Flt3 Expands Dendritic Cells and Alters T Cell Responses." *The Journal of Experimental Medicine* 213(3): 415–31. <http://www.jem.org/lookup/doi/10.1084/jem.20150642>.
- Lee, Pierre S W et al. 1999. "The Cbl Protooncprotein Stimulates CSF-1 Receptor Multiubiquitination and Endocytosis, and Attenuates Macrophage Proliferation." *EMBO Journal* 18(13): 3616–28.
- Lemmon, Mark A, and Joseph Schlessinger. 2010. "Cell Signaling by Receptor-Tyrosine Kinases." *Cell* 141(7): 1117–34.
- Levis, Mark. 2011. "FLT3/ITD AML and the Law of Unintended Consequences." *Blood* 117(26): 6987–90.
- . 2011. "Results from a Randomized Trial of Salvage Chemotherapy Followed by Lestaurtinib for Patients with FLT3 Mutant AML in First Relapse." *Blood* 117(12): 3294–3301.
- . 2017. "Midostaurin Approved for FLT3-Mutated AML." *Blood* 129(26): 3403–6.
- Lupher, Mark L. et al. 1997. "The Cbl Phosphotyrosine-Binding Domain Selects a D(N/D)XpY Motif and Binds to the Tyr292 Negative Regulatory Phosphorylation Site of ZAP-70." *Journal of Biological Chemistry* 272(52): 33140–44.
- Lyman, By Stewart D et al. 1995. "Plasma/Serum Levels of Flt3 Ligand Are Low in Normal Individuals and Highly Elevated in Patients With Fanconi Anemia and Acquired Aplastic Anemia." *Blood* 86(11): 4091–96.
- Mazzarella, Luca. 2016. "Orlando Magic: Report from the 57th Meeting of the American Society of Haematology, 5–7 December 2015, Orlando, USA." *Ecancermedalscience* 10(December): 5–7. <http://www.ecancer.org/journal/10/full/612-orlando-magic-report-from-the-57th-meeting-of-the-american-society-of-haematology-5-7-december-2015-orlando-usa.php>.
- Nakano, Yasuyuki et al. 1999. "Molecular Evolution of Acute Myeloid Leukaemia in Relapse: Unstable N- Ras and FLT3 Genes Compared with P53 Gene." *British Journal of Haematology* 104(4): 659–

64.

- Nguyen, Bao et al. 2017. "FLT3 Activating Mutations Display Differential Sensitivity to Multiple Tyrosine Kinase Inhibitors." *Oncotarget*.
<http://www.oncotarget.com/abstract/14539%0Ahttp://www.ncbi.nlm.nih.gov/pubmed/28077790>.
- NIH, National Cancer Institute. "Cancer Stat Facts: Leukemia - Acute Myeloid Leukemia (AML)." <https://seer.cancer.gov/statfacts/html/amyl.html> (November 21, 2018).
- Opatowsky, Yarden et al. 2014. "Structure, Domain Organization, and Different Conformational States of Stem Cell Factor-Induced Intact KIT Dimers." *Proceedings of the National Academy of Sciences of the United States of America* 111(5): 1772–77.
<http://www.ncbi.nlm.nih.gov/pubmed/24449920>.
- Piloto, Obdulio et al. 2005. "Inhibitory Anti-FLT3 Antibodies Are Capable of Mediating Antibody-Dependent Cell-Mediated Cytotoxicity and Reducing Engraftment of Acute Myelogenous Leukemia Blasts in Nonobese Diabetic/Severe Combined Immunodeficient Mice." *Cancer Research* 65(4): 1514–22.
- Raum, Tobias; DE et al. 2017. "Antibody Constructs for FL T3 and CD3." : 1–185.
- Reiter, K. et al. 2018. "Tyrosine Kinase Inhibition Increases the Cell Surface Localization of FLT3-ITD and Enhances FLT3-Directed Immunotherapy of Acute Myeloid Leukemia." *Leukemia* 32(2): 313–22.
<http://dx.doi.org/10.1038/leu.2017.257>.
- Rivat, Cyril et al. 2018. "Inhibition of Neuronal FLT3 Receptor Tyrosine Kinase Alleviates Peripheral Neuropathic Pain in Mice." *Nature Communications* 9(1): 1042.
<http://www.nature.com/articles/s41467-018-03496-2>.
- Sargin, Bülent et al. 2007. "Flt3-Dependent Transformation by Inactivating c-Cbl Mutations in AML." *Blood* 110(3): 1004–12.
- Sato, Takashi et al. 2011a. "FLT3 Ligand Impedes the Efficacy of FLT3 Inhibitors in Vitro and in Vivo." *Blood* 117(12): 3286–93.
- . 2011b. "FLT3 Ligand Impedes the Efficacy of FLT3 Inhibitors in Vitro and in Vivo." *Blood* 117(12): 3286–93.
- Schmidt-Arras, D.E. et al. 2005. "Tyrosine Phosphorylation Regulates Maturation of Receptor Tyrosine Kinases." *Molecular and cellular biology* 25(9): 3690.
<http://mcb.asm.org/cgi/content/abstract/25/9/3690>.
- Serve, Hubert et al. 2013. "Sorafenib in Combination with Intensive Chemotherapy in Elderly Patients with Acute Myeloid Leukemia: Results from a Randomized, Placebo-Controlled Trial." *Journal of Clinical Oncology* 31(25): 3110–18.
- Sheridan, Cormac. 2017. "First New Drug Approval for AML in 15 Years." *Nature Biotechnology* 35(8): 696–98. <http://www.nature.com/doifinder/10.1038/nbt0817-696>.
- Shih, Lee Yung et al. 2002. "Internal Tandem Duplication of FLT3 in Relapsed Acute Myeloid Leukemia: A Comparative Analysis of Bone Marrow Samples from 108 Adult Patients at Diagnosis and Relapse." *Blood* 100(7): 2387–92.
- Smith, C C et al. 2015. "FLT3 D835 Mutations Confer Differential Resistance to Type II FLT3 Inhibitors." *Leukemia* (April): 1–3. <http://www.nature.com/doifinder/10.1038/leu.2015.165>.

- Stone, Richard M. et al. 2017. "Midostaurin plus Chemotherapy for Acute Myeloid Leukemia with a *FLT3* Mutation." *New England Journal of Medicine*: NEJMoa1614359. <http://www.nejm.org/doi/10.1056/NEJMoa1614359>.
- Synimmune. "Synimmune GmbH: Flysyn." <https://www.synimmune.de/products/flysyn/> (November 25, 2018).
- Thiede, C et al. 2002. "Analysis of *FLT3*-Activating Mutations in 979 Patients with Acute Myelogenous Leukemia: Association with FAB Subtypes and Identification of Subgroups with Poor Prognosis." *Blood* 99(12): 4326–35.
- Turner, By Anne M et al. 1996. "*FLT3* Receptor Expression on the Surface of Normal and Malignant Human Hematopoietic Cells." *Blood*.
- Verstraete, Kenneth et al. 2009. "Efficient Production of Bioactive Recombinant Human *Flt3* Ligand in *E. Coli*." *Protein Journal* 28(2): 57–65. <http://www.ncbi.nlm.nih.gov/pubmed/19184382> (August 30, 2012).
- . 2011. "Structural Insights into the Extracellular Assembly of the Hematopoietic *Flt3* Signaling Complex." *Blood* 118(1): 60–68.
- Verstraete, Kenneth, and Savvas N Savvides. 2012. "Extracellular Assembly and Activation Principles of Oncogenic Class III Receptor Tyrosine Kinases." *Nature reviews. Cancer* 12(11): 753–66. <http://www.ncbi.nlm.nih.gov/pubmed/23076159> (March 6, 2013).
- Whitman, S. P. et al. 2001. "Absence of the Wild-Type Allele Predicts Poor Prognosis in Adult de Novo Acute Myeloid Leukemia with Normal Cytogenetics and the Internal Tandem Duplication of *FLT3*: A Cancer and Leukemia Group B Study." *Cancer Research*.
- Wodnar-Filipowicz, Aleksandra et al. 1996. "*Flt3* Ligand Level Reflects Hematopoietic Progenitor Cell Function in Aplastic Anemia and Chemotherapy-Induced Bone Marrow Aplasia." *Blood* 88(12): 4493–99. <http://www.ncbi.nlm.nih.gov/pubmed/8977241>.
- Yamamoto, Y. et al. 2001. "Activating Mutation of D835 within the Activation Loop of *FLT3* in Human Hematologic Malignancies." *Blood* 97(8): 2434–39.
- Yanada, M et al. 2005. "Prognostic Significance of *FLT3* Internal Tandem Duplication and Tyrosine Kinase Domain Mutations for Acute Myeloid Leukemia: A Meta-Analysis." *Leukemia* 19(8): 1345–49. <http://www.ncbi.nlm.nih.gov/pubmed/15959528> (April 12, 2013).
- Yee, Nelson S et al. 1994. "Mechanism of Down-Regulation of c-Kit Receptor." *The Journal of biological chemistry* 269(50): 31991–98.
- Yousoufian, Hagop, Eric K. Rowinsky, James Tonra, and Yiwen Li. 2010. "Targeting FMS-Related Tyrosine Kinase Receptor 3 with the Human Immunoglobulin G1 Monoclonal Antibody IMC-EB10." *Cancer* 116(SUPPL. 4): 1013–17.
- Zeng, Shan, Xu Zhiheng, Stan Lipkowitz, and Jack B. Longley. 2004. "Regulation of Stem Cell Factor Receptor Signaling by *Cbl* Family Proteins (*Cbl-b/c-Cbl*)." *blood* 105(1): 226–32.

Curriculum vitae

Personal information

Erwin Pannecoucke
Engelstraat 87
9040 Sint-Amandsberg
0484/92.57.89
erwin.pannecoucke@gmail.com
Date of birth: 12 May 1989

Academic education

2012 – present

Pre-doctoral researcher at the Unit for Structural Biology, Department of Biochemistry and Microbiology, Faculty of Sciences, Ghent University, VIB Center for Inflammation Research, Ghent, Belgium.

Promotor: Prof. Dr. Savvas N. Savvides

Thesis title: *An integrative approach towards unraveling the activation of oncogenic FLT3*

Research interests: X-ray protein crystallography, macromolecular structure-function relationships, hematopoietic cytokine-receptor interactions, structure-based drug design, microcalorimetry

2010 – 2012

Master of Science in the Biochemistry and Biotechnology, Major Biochemistry and Structural Biology, Ghent University, Ghent, Belgium.

Masters dissertation at The Laboratory for Protein Biochemistry and Biomolecular Engineering, Department of Biochemistry and Microbiology, Faculty of Sciences, Ghent University, Ghent, Belgium.

Promotor: Prof. Dr. Savvas N. Savvides

Thesis title: *Structural characterization of the novel cytokine Interleukin 34 in complex with its cognate receptor CSF-1R.*

2007 - 2010

Bachelor in Biochemistry and Biotechnology, Ghent University, Ghent, Belgium.

Academic grants

2014 IWT pre-doctoral Fellowship

Competencies

Languages Dutch: native
 English: fluent
 French: intermediate

Computer knowledge:

Windows OS, Linux-based OS, MacOS, Android
Microsoft Office, Adobe Photoshop, Adobe Illustrator

Publications

Felix J., Elegheert J., Gutsche I., Shkumatov A.V., Wen Y., Bracke N., Pannecoucke E., Vandenberghe I., Devreese B., Svergun D.I., Pauwels E., Vergauwen B. and Savvides S.N. (2013). Human IL-34 and CSF-1 establish structurally similar complexes with their common hematopoietic receptor. *Structure* 21(4): 528-539.

Workshops and conferences

- VIB Structural Dynamics in Cellular Communication Meeting
20-21/09/2018, Brussels, Belgium
- Belgian Biophysical Society School on X-ray and neutron diffraction techniques,
28-30/05/2018, Zwijnaarde, Belgium
- Malvern Panalytical Bioscience Days
15-16/05/2018, Etten-Leur, The Netherlands
Invited speaker: *Thermodynamic dissection of the cooperativity of a cytokine-receptor assembly*
- VIB Conference Next-Generation antibodies and protein analysis - 2nd edition
21/10/2018, Ghent, Belgium
- Masterclass Presentatietechnieken ter voorbereiding van De Wetenschapsbattle
21/02/2018, Ghent, Belgium
- VIB Tech transfer course
22-26/08/2016, Ghent, Belgium
- MicroCal Users meeting
24-25/11/2015, Munich, Germany
- VIB Structural Dynamics in Cellular Communication
09-10/02/2018, Brussels, Belgium (**Poster presentation**)
- BioCrys 2014 FEBS Practical & Lecture Course – Fundamental of Modern Methods of BioCrystallography
20-27/09/2014, Oeiras, Portugal
- Crystallography workshop: Getting the best from your structural data: beyond black boxes.
18-21/09/2013, Strasbourg, France
- DGK-AK1-Workshop - Diffraction Data Collection Using Synchrotron Radiation
12-16/06/2013, Berlin, Germany (**Poster presentation**)
- Netherlands Society on Biomolecular Modelling – Fall meeting
26/11/2012, Utrecht, The Netherlands (**Poster presentation**)